

UNIVERSITY OF MODENA AND REGGIO EMILIA

PhD Programme: Clinical and Experimental Medicine

Curriculum: Translational Medicine

XXXVI Doctorate Cycle

Director of the PhD Programme: Prof. Marco Vinceti

SARS-CoV-2 specific immune response after infection and vaccination

Supervisor:

Prof. Andrea Cossarizza

PhD Candidate:

Annamaria Paolini

Co-Supervisor:

Dr. Sara De Biasi

Academic year 2022/2023

Table of contents

ABSTRACT (ENGLISH VERSION)	4
ABSTRACT (ITALIAN VERSION)	6
ABBREVIATION INDEX	8
1. INTRODUCTION	10
1.1 SEVERE ACUTE RESPIRATORY SYNDROME CORONA VIRUS 2 (SARS-CoV-2): ORIGIN OF THE PANDEMIC.....	10
1.2 COVID-19 ANCESTORS: SARS AND MERS	10
1.3 GENERAL CHARACTERISTICS OF SARS-CoV-2, SARS-CoV AND MERS-CoV	11
1.4 SARS-CoV-2 TRANSMISSION AND SYMPTOMATOLOGY	13
1.4 PATHOGENESIS OF COVID-19	15
1.5 HOST RESPONSE TO SARS-CoV-2: CYTOKINE STORM, INNATE AND ADAPTIVE IMMUNE RESPONSE.	16
1.5.1 <i>Cytokine storm</i>	17
1.5.2 <i>Innate immune response</i>	19
1.5.3 <i>Adaptive immune response</i>	23
1.6 VACCINES AGAINST SARS-CoV-2 INFECTION.....	27
1.7 IMMUNOCOMPROMISED PATIENTS LIVING THE PANDEMIC.....	28
1.8 SARS-CoV-2 VACCINATION AND MULTIPLE SCLEROSIS	29
1.8 METHOD FOR THE IDENTIFICATION AND CHARACTERIZATION OF SARS-CoV-2 ANTIGEN- SPECIFIC CELLS	29
1.9 POLYCHROMATIC FLOW-CYTOMETRY AND DATA ANALYSIS	31
2. AIM OF THE THESIS	34
2.1 CHARACTERIZATION OF THE POLYFUNCTIONAL PROFILE OF SARS-CoV-2-SPECIFIC CD4 ⁺ AND CD8 ⁺ T CELLS IN PATIENTS EXPERIENCING OR RECOVERING FROM COVID-19.....	34
2.2 CHARACTERIZATION OF SARS-CoV-2-SPECIFIC T AND B CELLS AFTER INFECTION OR HETEROLOGOUS VACCINATION	35
2.3 CHARACTERIZATION OF SARS-CoV-2-SPECIFIC T AND B CELLS IN MULTIPLE SCLEROSIS PATIENTS ON DIFFERENT IMMUNOMODULATORY DRUGS.....	37
3. METHODS	39
3.1 CD4 ⁺ AND CD8 ⁺ T CELLS POLYFUNCTIONALITY IN PATIENTS EXPERIENCING OR RECOVERING FROM COVID-19 ..	39
3.1.1 <i>Patients' selection</i>	39
3.1.2 <i>Blood Processing</i>	39
3.1.3 <i>In Vitro Stimulation and Intracellular Cytokine Staining (ICS)</i>	40
3.1.4 <i>Statistical Analysis</i>	40
3.2 SARS-CoV-2 SPECIFIC T AND B CELLS AFTER INFECTION OR HETEROLOGOUS VACCINATION	42
3.2.1 <i>Blood collection and isolation of mononuclear cells</i>	42
3.2.2 <i>Activation-induced cell marker assay and T-cell phenotype</i>	42
3.2.3 <i>Detection of SARS-CoV-2-specific B cells</i>	43
3.2.4 <i>Computational analysis of flow cytometry data</i>	43
3.2.5 <i>Measuring anti-SARS-CoV-2 anti-spike and anti-RBD IgG antibodies</i>	44
3.2.6 <i>Principal component analysis and correlation plot</i>	45
3.2.7 <i>Statistical analysis</i>	45
3.3 SARS-CoV-2 SPECIFIC T AND B CELLS IN MS PATIENTS ON DIFFERENT DMTs.....	54
3.3.1 <i>Blood collection and isolation of mononuclear cells</i>	54
3.3.2 <i>Activation induced cell marker assay (AIM) and T cell phenotype</i>	54
3.3.3 <i>Detection of SARS-CoV-2-specific B cells</i>	55
3.3.4 <i>Intracellular cytokine staining (ICS)</i>	55
3.3.5 <i>Computational analysis of flow cytometry data</i>	56
3.3.6 <i>Statistical analysis</i>	57
3.3.7 <i>Principal Component Analysis</i>	57
TABLE	59
4. RESULTS	66
4.1 POLYFUNCTIONAL CD4 ⁺ AND CD8 ⁺ T CELLS ANALYSIS IN COVID-19 INFECTED OR RECOVERED PATIENTS	66
4.1.1 <i>Characteristics of the Patients</i>	66

4.1.2 Recovered Patients Who Experienced a Severe Disease Display High Percentage of Antigen-Specific CD4 ⁺ T Cells Producing Th1 and Th17 Cytokines.....	66
4.1.3 Recovered Patients Who Experienced a Severe Disease Are Characterized by Polyfunctional SARS-CoV-2 Antigen-Specific CD4 ⁺ T cells.....	67
4.2 CHARACTERIZATION OF SARS-COV-2-SPECIFIC T AND B CELLS AFTER INFECTION OR HETEROLOGOUS VACCINATION	79
4.2.1 Study design	79
4.2.2 MIX showed a skewed Th1 Ag-specific CD4 ⁺ T-cell polarization compared to that of recovered ones	79
4.2.3 Vaccinated individuals showed a higher percentage of Tc1-like Ag-specific CD8 ⁺ T cells compared to that of recovered subjects.....	81
4.2.4 Patients who recovered from COVID-19 display more polyfunctional antigen-specific CD4 ⁺ T cells compared to those in vaccinated donors.....	82
4.2.5 Vaccinated donors showed a higher percentage of antigen-specific and activated memory B cells expressing IgG compared to that in REC.....	83
4.2.6 Recovered patients show different immunological profiles compared to those of vaccinated donors	84
4.3 INVESTIGATION OF SARS-COV-2 SPECIFIC RESPONSE IN MULTIPLE SCLEROSIS PATIENTS UNDER DIFFERENT DISEASE MODIFYING THERAPIES	109
4.3.1 Demographic and clinical characteristics of the patients	109
4.3.2 MS patients treated with different DMT develop similar percentages of Ag ⁺ CD4 ⁺ T cells, but these cells display a different phenotype compared to healthy donors.....	109
4.3.3 Patients treated with teriflunomide develop higher percentage of Ag ⁺ CD8 ⁺ T cells if compared to healthy donors	111
4.3.4 MS patients treated with different DTM reveal polyfunctional profiles	112
4.3.5 Fingolimod- or anti-CD20 treated-patients displayed low or undetectable levels of Ag ⁺ B cells	113
4.3.6 FTY- and natalizumab-treated patients develop a different antigen-specific immune response	114
5. DISCUSSION	127
5.1 PATIENTS RECOVERING FROM SEVERE COVID-19 DEVELOP A POLYFUNCTIONAL ANTIGEN-SPECIFIC CD4 ⁺ T CELL RESPONSE.....	127
5.2 DETAILED CHARACTERIZATION OF SARS-COV-2-SPECIFIC T AND B CELLS AFTER INFECTION OR HETEROLOGOUS VACCINATION	130
5.3 RELAPSING-REMITTING MS PATIENTS TREATED WITH FTY OR NATALIZUMAB PRESENT A DIFFERENT VACCINE-SPECIFIC RESPONSE COMPARED TO PATIENTS ON OTHER DMTs.....	133
6. CONCLUSION	136
7. REFERENCES	139
ACKNOWLEDGEMENTS	160

Abstract (english version)

Immunological memory, conferred by the cells of the adaptive immune system, such as B and T cells, is crucial for protecting the host against pathogens, and indeed vaccines base their efficacy on the induction of a long-term memory response. The duration of the protection is related to the quantity and quality of this response. More than the antibody production, the quantity and quality of T cells (*i.e.* the percentage, absolute number and the polyfunctionality of antigen (Ag)-specific cells) are likely correlated with immune protection. For this reason, we deeply characterize the SARS-CoV-2 Ag-specific response during infection, COVID-19 recovery and after SARS-CoV-2 vaccination in different categories of patients. The phenotype and functionality of SARS-CoV-2 specific CD4⁺, CD8⁺ T cells and B cells have been investigated by state of the art flow cytometry and data analysis.

Firstly, we studied patients with moderate or severe COVID-19 pneumonia, compared to patients recovering from moderate or severe infection. We assessed the polyfunctionality of virus-specific CD4⁺ and CD8⁺ T cells by quantifying cytokine production after *in vitro* stimulation with different SARS-CoV-2 peptide pools. By using polychromatic flow cytometry, we quantified the percentage of CD4⁺ and CD8⁺ T cells simultaneously producing different cytokines. We observed that, compared to patients experiencing severe COVID-19, those recovering from a severe disease display high proportions of Ag-specific CD4⁺ T cells producing Th1 and Th17 cytokines and are characterized by polyfunctional SARS-CoV-2-specific CD4⁺ T cells. This suggests that the impaired immune response of patients experiencing severe infection turns into a high quality CD4⁺ T cells response during recovery.

Then, we focused on the effects of different vaccine combinations. We investigated the SARS-CoV-2-specific immune response developed in two groups of healthy donors after vaccination compared to a group of subjects who recovered from the infection. We observed that vaccinated individuals display a skewed Th1 Ag-specific T cell polarization and a higher percentage of Ag-specific and activated memory B cells compared to those of patients who recovered from severe COVID-19. In addition, recovered individuals show higher percentages of CD4⁺ T cells producing one or two cytokines simultaneously, while the vaccinated are distinguished by highly polyfunctional populations. These data suggest that functional and phenotypic properties of SARS-CoV-2 adaptive immunity differ in recovered COVID-19 individuals and vaccinated ones.

Finally, we characterized the immune response developed after SARS-CoV-2 vaccination by Multiple Sclerosis (MS) patients on different disease modifying therapies (DMT). We find that almost all patients develop a detectable and functional SARS-CoV-2 immune response. Among the studied DMTs, only fingolimod and natalizumab significantly modify SARS-CoV-2-specific B and T cell

composition after vaccination. These data contribute to highlight the importance of a good vaccine administration and its effectiveness, even in patients on immunomodulatory therapies.

The investigation of the quality and the quantity of the memory response is important to gain feedback on the presence and duration of the protection. This could support treatment decisions and help in making sensible choices about re-vaccination schemes in the future.

Keywords: SARS-CoV-2, antigen-specific, T cells, B cells, flow cytometry.

Abstract (italian version)

La memoria immunologica, conferita dai linfociti B e T appartenenti al sistema immunitario acquisito, è fondamentale per la protezione contro patogeni. I vaccini, infatti, basano la loro efficacia sull'induzione di una risposta di memoria a lungo termine. La durata della protezione è correlata alla quantità ed alla qualità della risposta immunitaria. Più che la produzione di anticorpi, è la risposta dei linfociti T (*i.e.* la percentuale, il numero assoluto e polifunzionalità delle cellule antigene (Ag)-specifiche) ad essere correlata con la protezione. Per questi motivi, in questi studi abbiamo caratterizzato la risposta Ag-specifica a SARS-CoV-2 durante infezione, guarigione da COVID-19, e successivamente alla vaccinazione, in varie categorie di pazienti. Il fenotipo e la funzionalità dei linfociti T CD4⁺, CD8⁺ e dei linfociti B sono stati studiati utilizzando tecniche di ultima generazione di citometria a flusso e data analisi.

Nel primo studio abbiamo incluso pazienti con polmonite moderata o severa da COVID-19, confrontati con pazienti guariti da queste due forme di infezione. Abbiamo caratterizzato la polifunzionalità dei linfociti CD4⁺ e CD8⁺ attraverso la quantificazione delle citochine prodotte in vitro successivamente alla stimolazione con pool di peptidi di SARS-CoV-2. Utilizzando la tecnica di citometria a flusso policromatica, abbiamo quantificato la percentuale di cellule CD4⁺ e CD8⁺ polifunzionali. Abbiamo quindi osservato che, rispetto a pazienti con infezione severa, quelli guariti da una forma severa presentano cellule CD4⁺ che producono citochine di tipo Th1 e Th17 e sono caratterizzati da una risposta CD4⁺ polifunzionale. Questo suggerisce che la risposta immunitaria compromessa osservata nei pazienti con infezione severa si trasforma in una risposta di alta qualità durante la fase di guarigione.

Successivamente, ci siamo focalizzati sull'effetto di diverse combinazioni di vaccini. In particolare, abbiamo analizzato la risposta specifica a SARS-CoV-2 sviluppata in due gruppi di donatori sani in seguito a vaccinazione, confrontati con un gruppo di pazienti guariti dall'infezione. Abbiamo quindi osservato che i soggetti vaccinati presentano cellule T Ag-specifiche del tipo Th1 ed un'alta percentuale di cellule B Ag-specifiche attivate e di memoria, se paragonati con quelle dei pazienti guariti da una forma severa di COVID-19. In aggiunta, i pazienti guariti presentano un'alta percentuale di cellule CD4⁺ in grado di produrre una o due citochine simultaneamente, mentre i vaccinati si distinguono per popolazioni di cellule altamente polifunzionali. Questi dati suggeriscono che il fenotipo e la funzionalità della risposta Ag-specifica a SARS-CoV-2 sono diversi se sviluppati in seguito a vaccinazione o ad infezione.

Infine, abbiamo caratterizzato la risposta immunitaria sviluppata in seguito a vaccinazione in pazienti con Sclerosi Multipla (SM) in trattamento con diversi farmaci. Abbiamo potuto notare che

la maggior parte dei pazienti sviluppa una risposta immunitaria a SARS-CoV-2 rilevabile e funzionale. All'interno delle categorie di farmaci analizzati, abbiamo osservato che solo fingolimod e natalizumab modificano significativamente la composizione delle cellule B e T Ag-specifiche. Questi risultati contribuiscono a mettere in evidenza l'importanza e l'efficacia di una buona somministrazione dei vaccini , anche in pazienti in cura con terapie immunomodulanti.

Lo studio della qualità e la quantificazione della risposta di memoria è importante per ottenere informazioni riguardo la presenza e la durata della protezione. Questi dati potrebbero supportare decisioni riguardo trattamenti terapeutici ed aiutare in una scelta oculata riguardo futuri richiami o specifici schemi vaccinali.

Parole chiave: SARS-CoV-2, antigene-specifiche, cellule T, cellule B, citometria a flusso.

ABBREVIATION INDEX

ACE2: angiotensin-converting enzyme-2; **Ag⁺**: antigen-specific; **Ag⁻**: antigen non-specific; **AICD**: activation induced cell death; **AIM**: activation-induced marker assay; **APCs**: antigen presenting cells; **ARDS**: acute respiratory distress syndrome; **aTBCs**: atypical B cells; **CoVs**: coronaviruses; **COVID-19**: coronavirus disease 2019; **CCL2**: chemokines C–C motif chemokine ligand 2; **CCR2**: C-C chemokine receptor type 2; **CMIA**: chemiluminescent microparticle immunoassay; **CNS**: central nervous system; **CRP**: c-reactive protein; **cTfh**: circulating T follicular helper; **CTLA4**: cytotoxic T-lymphocyte-associated protein 4; **DAMPs**: damage-associated molecular patterns; **DCs**: dendritic cells; **DMF**: dimethylfumarate; **DMTs**: disease-modifying therapies; **DPP4**: dipeptidyl Peptidase 4; **EL**: elastase; **FasL**: Fas ligand; **FDR**: false discovery rate; **FP**: fusion peptide; **GCs**: germinal centers; **GLMM**: generalized linear mixed model; **GMCSF**: granulocyte-macrophage colony-stimulating factor; **gp130**: glycoprotein 130; **GRZB**: granzyme B; **HD**: healthy donor; **HIV**: human immunodeficiency virus; **HLA-DR**: human leukocyte antigen-DR isotype; **HSCT**: hematopoietic stem cell transplant; **ICPs**: immune checkpoint inhibitors; **ICS**: intracellular cytokine staining; **ICU**: intensive care unit; **IFN γ** : interferon- γ ; **Ig**: immunoglobulin; **IL**: interleukin; **IL-6R**: interleukin-6 receptor; **IMV**: invasive mechanical ventilation; **IP-10**: IFN- γ -inducible protein 10; **JAK**: janus kinase; **KLH**: keyhole limpet hemocyanin; **LLPCs**: long-lived plasma cells; **M**: membrane; **MCP-1**: monocyte chemoattractant protein-1; **MEA**: European Medicines Agency; **MERS**: middle east respiratory syndrome; **MERS-CoV**: middle east respiratory syndrome coronavirus; **MHC**: major histocompatibility complex; **MPO**: myeloperoxidase; **MS**: multiple sclerosis; **N**: nucleocapsid; **NETs**: neutrophil extracellular traps; **NK**: natural killer; **NLR**: neutrophil-to-lymphocyte ratio; **NSPs**: non-structural proteins; **ORFs**: open reading frames; **OPN**: osteopontin; **OXPHOS**: oxidative phosphorylation; **PaO₂/FiO₂**: ratio of arterial partial pressure of oxygen to fraction of inspired oxygen; **PB**: plasmablast; **PBS**: phosphate buffer saline; **PD-1**: programmed cell death protein 1; **PD-L1**: programmed cell death ligand 1; **Pre-GC MBCs**: pre-germinal center memory B cells; **RAAS**: renin-angiotensin-aldosterone system; **RBD**: receptor binding domain; **RLU**: relative light unit; **ROS**: reactive oxygen species; **RR**: relapsing-remitting; **RRMS**: relapsing-remitting multiple sclerosis; **RT**: room temperature; **S**: spike; **SARS**: severe acute respiratory syndrome; **SARS-CoV-2**: severe acute respiratory syndrome coronavirus 2; **SE**: spreading error; **SLPCs**: short-lived plasma cells; **STAT**: signal transducer and activator of transcription; **SpO₂**: saturation of peripheral oxygen; **TCR**: T cell receptor; **Tfh**: T follicular helper; **TGF- β** : transforming growth factor beta; **Th**: T helper; **TIGIT**: T cell immunoreceptor with immunoglobulin and ITIM domain; **TIM3**: T cell immunoglobulin and mucin domain-containing protein 3; **TLR**: Toll-like receptors; **TNF**: tumor necrosis factor; **TrB**: transitional B cells; **Treg**: regulatory T cell; **VOC**: variant of concern; **WHO**: world health organization.

1. INTRODUCTION

1.1 Severe Acute Respiratory Syndrome Corona Virus 2 (SARS-CoV-2): origin of the pandemic

On December 2019, news reported cases of pneumonia in Wuhan, China [1]. The infection was caused by an unknown virus. Evidences linked the cases to the Seafood Market in Wuhan, a wholesale fish and live animal market selling different animal species [2,3]). Soon after, at the beginning of January 2020, a new human-infecting coronavirus was identified. It was first named “2019 novel Coronavirus” (2019-nCoV) by the World Health Organization (WHO). Subsequently, as a genetic relation with the coronavirus responsible for the epidemic occurred in 2003, the virus was renamed as severe acute respiratory syndrome coronavirus 2 (SARS-CoV-2) [4,5]. The disease caused by this virus was then called Coronavirus Disease 2019 (COVID-19). On March, the evidence of a rapid human to human transmission became strong. This evidence led the WHO, on March 2020, to declare COVID-19 a pandemic [6]. In fact, in that period the WHO noted that in 2 weeks there has been a 13-fold increase in the number of cases outside China and the number of countries with cases increased threefold. The virus spreading was incredibly fast and due to characteristics as incubation period (period in which a person is infected but does not show symptoms yet), it was not possible to stop its spreading all over the world [6]. In Italy, the first patient diagnosed for COVID-19 was in Lombardy, dated February 21, 2020 [7]. At the end of March 2020, the city of Modena was facing more than 1,500 cases of which about one-fifth were hospitalized [8].

After more than three years from the first identified cases, we can state that each country faced an unprecedented emergency. Different strategies were put in place to contain the spreading of the virus and to save lives. Despite that, now, as of August 2023, it has been registered 768 million cases worldwide and almost 7 million deaths (<https://covid19.who.int/>).

1.2 COVID-19 ancestors: SARS and MERS

SARS-CoV-2 belong to the Coronaviridae family, in particular to the β -coronavirus together with its ancestors Severe Acute Respiratory Syndrome (SARS) and Middle East Respiratory Syndrome (MERS) [9].

SARS first case was registered in November 2002 in the Guangdong Province of China. From that moment the virus spread from continent to continent, resulting in more than 8,000 infection with a mortality rate of 10%, considered at that time as the most severe disease caused by a coronavirus

[10,11]. The median incubation period of this virus were 4 days [12]. The outbreak was mostly contained because of the relative inefficient SARS-CoV transmission due to its low infectivity index [13,14]. However, SARS pandemic not only caused a public health issue, but its effects had a socio-economic impact in China [15].

The first case of MERS was identified in a patient showing acute pneumonia and renal failure in Jeddah, Kingdom of Saudi Arabia in June, 2012 [16,17]. The medium incubation period was from 5.5 to 6.5 days [18,19]. The case fatality rate of MERS is, among the cited coronavirus, the highest as of 34.4% [20]. A so high mortality rate had for sure a negative impact on the transmission of the virus.

SARS-CoV-2 presented a low case fatality rate (2.13%) compared to SARS-CoV and MERS-CoV. However, it rampantly spread throughout the world impacting health, lifestyle and socio-economic aspect of the involved countries [20].

1.3 General characteristics of SARS-CoV-2, SARS-CoV and MERS-CoV

SARS-CoV-2 is an enveloped virus with a positive single-stranded RNA genome. Coronaviruses (CoVs) present the largest viral genome, ranging from 26 to 36 kb in length [4]. Their viral envelope is derived from the host cell, it has glycoprotein spikes and the genome is protected by the nucleocapsid [11]. SARS-CoV-2 shares about the 82% of the genome identity with SARS-CoV and MERS-CoV. More than 90% of these sequences encode for essential enzyme and structural proteins. This high level of identity correlates with similar pathogenic mechanisms [21]. SARS-CoV-2 is constituted by 4 structural proteins as Spike (S), Envelope (E), Membrane (M) and Nucleocapsid (N), and 16 non-structural proteins (nsp1-16). CoVs share the use of the S protein to bind host cell-surface receptors [21]. Spike is a transmembrane protein constitute of homotrimers that protrude from the viral surface enabling for a binding action. After this viral-host contact, by using a host protease, Spike undergoes a cleavage that activates the two subunits of the protein: S1 and S2. S1 contains the Receptor Binding Domain (RBD) to bind the host receptor, while S2 contains the Fusion Peptide (FP) essential for the fusion of the two membranes, an event that complete the entry process [22]. Once in the host cell, SARS-CoV-2 replicates its genome that will be included in viral particles and will exit the host cell to disseminate in the organism [23].

The target receptor of CoVs is not always the same. SARS-CoV and SARS-CoV-2 bind to the Angiotensin-Converting Enzyme-2 (ACE2), while MERS-CoV recognizes the Dipeptidyl Peptidase 4 (DPP4) receptor [21]. This difference suggests changes in the residual composition of the Spike protein among CoVs, that correlates with different cell targets. ACE2 is widely express on the

surface of different type of cells. First of all, it is the homologue of the angiotensin-converting enzyme involved in the renin-angiotensin-aldosterone system (RAAS); thus, it is involved in the regulation of blood pressure and fluid balance. Moreover, it is expressed at the lung levels, where it inhibits vasodilation and elevation of vascular permeability. ACE2 is also expressed at the gastrointestinal level where it is involved in the regulation of the local innate immunity or the gut microbial ecology. Thus, this receptor is expressed on various tissues such as heart, lung, gut, kidney, brain and others [24]. In addition, the expression of ACE2 change during the life of an individual, decreasing with age but also specific pathologies such as hypertension, diabetes or cardiovascular diseases are related with ACE2 deficiency [24]. Thus, it could be hypothesized a correlation between ACE2 expression, disease severity and categories of infected individuals; however, this hypothesis has not been verified yet [24]. SARS-CoV-2 primarily targets lung epithelial cells; however, intestinal and other epithelia can be infected with active virus replication [25].

Despite binding the same receptor, SARS-CoV and SARS-CoV-2 binding domain present some differences. First of all, amino acids substitutions have been identified. In particular SARS-CoV-2 RBD present some substitutions that favors a stronger interaction with ACE2, while other substitutions reduce this affinity if compared to SARS-CoV [26]. Regarding the overall structure of the two proteins, SARS-CoV-2 Spike resembles that of SARS-CoV. One difference has been identified in the position of the RBD. The former present a RBD region closer to the central cavity of the trimer, while the latter present the RBD region packed near the N-terminal domain of the neighboring protomer (a structural unit of an oligomeric protein composed by at least two different protein chains that forms a larger hetero-oligomer by the association of two or more copies of this unit) [27]. However, when the two proteins are aligned, they still reflect an high degree of structural homology. To gain a deeper understanding of the binding mechanism despite the structural differences above cited, it has been quantified the kinetics of the Spike protein and ACE2 interaction by plasmon resonance. ACE2 binding to SARS-CoV-2 RBD is 10-20 fold higher than for SARS-CoV. Thus, even minor changes in the protein structure and amino acids sequence may have contributed to a new characteristic of this virus, as its incredible human to human spreading [27].

Due to differences in host-cell targets, MERS-CoV showed a much broader cell tropism. In particular, a part from respiratory epithelial cells, MERS-CoV infects also different human immune cell lines such as monocytes and T lymphocytes. Moreover, as the wide distribution of DPP4, MERS-CoV infects also dendritic cells (DCs), which are important Antigen Presenting Cells (APCs), with the role to link the innate and adaptive immune response [28]. DCs are also susceptible to SARS-CoV infection but in this case the infection was mostly abortive and when it was successful, it failed to trigger an interferon response but resulted in an up-regulation of cytokines and chemokines thus

being counterproductive [29]. SARS-CoV-2, on the other side, can bind and infect monocytes/macrophages but not T lymphocytes [30]. Moreover, only SARS-CoV-2 can replicate in in the upper respiratory tract during both pre and post symptomatic phases. These characteristics may increase its transmissibility [31]. The main characteristics of MERS-CoV, SARS-CoV, and SARS-CoV-2 are reported in **Table 1**.

All these cited features, characterize the ability of a virus to infect and reproduce itself. Surely, the aggressiveness of MERS-CoV was a negative trait for its survival. In fact, its mortality rate was really high and the spread of the virus was limited by it. SARS-CoV-2 shows a very high transmissibility compared to the other two CoVs and this was surely related to some conformational changes that helped in a higher affinity with its target receptor, its replication in the upper respiratory tract and also the non-symptomatic phases that delayed the identification and traceability of the infected individuals.

	SARS-CoV	MERS-CoV	SARS-CoV-2
Date of outbreak	November 2002	June 2012	December 2019
Origin	China	Saudi Arabia	China
Mortality rate [%]	10	34.4	2.13
Median incubation period [days]	4	5.5-6.5	5.1-6.5
Spreading	Low infectivity index → contained outbreak	High fatality rate → low transmission	Period of incubation, asymptomatic patients → fast spreading worldwide
Target receptor	ACE2	DPP4	ACE2

Table.1 Summary of MERS-CoV, SARS-CoV and SARS-CoV-2 characteristics.

1.4 SARS-CoV-2 transmission and symptomatology

SARS-CoV-2 infection happens mostly via fomites and droplets of respiratory fluid released from an infected individual when in contact with another individual. A so called “direct” infection happens through a real contact between two individuals in situation of coughing, breathing, talking, sneezing. The “indirect” infection happens through the contact of surfaces or objectives that previously came in contact with an infected individual [23]. The strengths of this virus are the period of incubation and the possibility to infect through asymptomatic individuals. The period of incubation is defined as the time between the event of the infection and the manifestation of symptoms. The period of incubation has been estimated to be between 5.1 to 6.5 days [32,33]. During this period, infected people do not know about their status and are able to infect other people. People during the

incubation phase and asymptomatic individuals are the carriers of the virus. Although people from all age can be infected, older adults with comorbidities are at higher risk [11]. Comorbidities can be asthma, cancer, cardiovascular disease, obesity, diabetes, the use of immunosuppressive therapy or being a transplant patient. Moreover, the severity of symptoms is really different. In fact the infection can range from asymptomatic to severe [32]. The most common symptoms are fever, cough, sore throat, headache, myalgia, fatigue and dyspnea. Other observed symptoms are loss of taste or smell and gastrointestinal disorder [34,35]. In critical patient, the infection can lead to hospitalization, to ventilatory support or even invasive mechanical ventilation (IMV). The clinical spectrum has been described as follows (for up-to-date information: <https://www.covid19treatmentguidelines.nih.gov/>):

- Asymptomatic or presymptomatic infection: individuals who tested positive for SARS-CoV-2 but present no symptoms related to COVID-19. However, in some cases objective radiographic findings related to COVID-19 pneumonia have been reported [36,37].
- Mild illness: patients that shows different symptoms but do not have shortness of breath, dyspnea on exertion or abnormal imaging. These patients can be managed through ambulatory visits or also telemedicine. No particular exams are needed in these cases. However, patients with comorbidities showing mild COVID-19 are at higher risk of disease progression, thus they need to be monitored.
- Moderate illness: patients who exhibit evidence of lower respiratory disease during clinical assessment or imaging. These patients present a saturation of peripheral oxygen (SpO_2) $\geq 94\%$ on room air at sea level. These patients need to be constantly monitored as the disease can rapidly worsen.
- Severe illness: patients presenting $SpO_2 < 94\%$ on room air at sea level, a ratio of arterial partial pressure of oxygen to fraction of inspired oxygen (PaO_2/FiO_2) < 300 mm Hg, a respiratory rate > 30 breaths/min, or lung infiltrates $> 50\%$. These patients need to be hospitalized and given oxygen therapy.
- Critical illness: patients presenting complication as acute respiratory distress syndrome (ARDS), septic shock, multiple organ dysfunction, cardiac shock and an uncontrolled inflammatory response.

SARS-CoV-2 structural and infective characteristics are listed in **Table 2**.

SARS-CoV-2	
Genome	Positive single-stranded RNA (26-36 kb)
Genome identity with previous CoVs	~ 82%
Structural proteins	4 (S, M, N, E)
Non-structural proteins	16 (nsp1-16)
Target receptor	ACE2
Strength of interaction with target receptor	10-20 fold higher than SARS-CoV
Target cells	Monocytes/macrophages
Transmission	Fomites and droplets of respiratory fluid
Period of incubation	5.1-6.5 days
Most common symptoms	Fever, cough, sore throat, headache, myalgia, fatigue, dyspnea
Clinical spectrum	<ul style="list-style-type: none"> • Asymptomatic or presymptomatic infection • Mild illness • Moderate illness • Severe illness • Critical illness

Table 2. Structural and infective characteristics of SARS-CoV-2.

1.4 Pathogenesis of COVID-19

The leading manifestation of COVID-19 is hypoxemia (low levels of oxygen in the blood), that can worsen to various stages of ARDS, defined as an impairment of oxygenation [38]. SARS-CoV-2 infection can also cause an unusual phenomenon as the so-called silent hypoxemia. In this condition, patient present low PaO₂ but only mild respiratory discomfort and dyspnea [39,40]. In fact, not all the patients experiencing low PaO₂/FiO₂ ratio present symptoms as shortness of breath [41]. However, when PaO₂ < 60 mmHg, the physiological response is to increase the respiratory drive, that is the intensity of the neural stimulus to breathe, regulating so the respiratory rate and depth. This condition can worsen lung function leading to a deterioration of patient condition [42,43]. During the infection, sustained pulmonary inflammation and also fibrosis can cause progressive lung edema that alter lung mechanics worsening tissue hypoxia [38]. COVID-19 deceased patients, present increased average lung weight characterized by edema while alveoli are typically filled with fluid and fibrin [44,45]. Regarding cells, type II pneumocytes frequently present disrupted membranes contributing to lung parenchyma remodeling. Microangiopathy is a predominant feature, causing a dissemination of platelet-fibrin microthrombi in alveolar capillaries. Thus, several marker of angiogenesis are upregulated. Moreover, cellular infiltration is common especially in relation to leukocyte such as T lymphocyte, macrophages, monocytes and neutrophils [46-48].

ARDS related to COVID-19 present specific characteristics. Firstly, it is often associated with normal respiratory system compliance. The increased respiratory drive is probably lower to that of non-COVID-19 ARDS, potentially masking the true extent of hypoxemia [49,50]. Secondly, lung fibrosis is a deleterious consequence of COVID-19 ARDS. It leads to the deterioration of lung function and respiratory failure. This condition is irreversible and correlates with poor prognosis [51].

Lung fibrosis is driven by the release of pro-fibrotic factors among which transforming growth factor- β (TGF- β). The secretion of this factor from injured lung cells, promotes repair and resolution of the damage. However, in COVID-19 the release can be excessive leading to epithelial-to-mesenchymal and endothelial-to-mesenchymal transition [52-54]. Once in recovery, most of the patient that experienced a severe COVID-19 with an important inflammatory response, present pulmonary fibrosis. In critical condition, a transplant is needed [55].

Coagulopathy and endothelial damage are other key features of COVID-19, rising the risk of arterial and venous thromboembolism [56]. The prevalence of thrombosis in COVID-19 is higher than in influenza [57]. Hypercoagulability in SARS-CoV-2 infected patients can be identified by higher concentration of circulating D-dimer (a product of fibrin degradation) if compared to general Intensive Care Unit (ICU) patients or those experiencing severe pneumonia not related to COVID-19 [58]. Severe COVID-19 can present the following characteristics: hypercoagulability, increased fibrinogen, thrombocytopenia, elevated prothrombin time and elevated activated partial thromboplastin time [42,59,60]. Studies suggest an association between deranged coagulation and severity of lung failure and mortality [61-64]. Hypercoagulability in COVID-19 can be influenced by direct virus-induced endothelial damage and consequent inflammation [65]. The hypothesis that pulmonary circulation thrombosis can be induced by endothelial injury is supported by the evidence that alveolar damage in COVID-19 is frequently associated with thrombotic microangiopathy [66], [67]. This phenomenon can be explained as a dysfunctional cross-talk between leukocyte and endothelial cells that aggravates hypoxemia [68]. The combination of pulmonary vascular dysfunction and thrombosis is a case of high risk mortality for patients with COVID-19 and ARDS [69-71].

1.5 Host response to SARS-CoV-2: cytokine storm, innate and adaptive immune response.

After recognizing the presence of a pathogen, the host immune system mounts a response to fight the intruder. The first line of defense are innate immune cells that start their action by both signaling the presence of a pathogen and releasing pro-inflammatory molecules. After some time and the release of a huge quantity of soluble mediators, cells from the adaptive immunity are recalled on the site of the infection.

1.5.1 Cytokine storm

A hallmark of SARS-CoV-2 infection is the phenomenon of the “cytokine storm”. This definition is representative of a situation in which a large and various amount of cytokines, both pro-inflammatory and anti-inflammatory, are produced in a way that, based on patient conditions, can be uncontrolled and can lead to multi-organ failure and death [72]. ARDS, in fact, is mainly caused by an excessive immune response rather than an high viral load [73]. Thus, virus-induced hyperinflammatory syndrome can be associated with disease severity [74-75]. Cytokines are essential to maintain and accomplish all the immune system functions. These soluble molecules are involved in a variety of pathways, such as inflammation, coagulation, tissue repair and fibrosis. However, when produced in a dysregulated manner, cytokines may become harmful for the organism. Pro-inflammatory cytokines plays a major role in the up-regulations of inflammatory response, in case of both infectious or non-infectious disease. Inflammation is a local process aimed to restrict pathogen spreading [76].

One of the principal cause of cytokine storm caused by COVID-19 is the infection of lung cells, in particular type II pneumocytes, that lead to the recall of immune cells among which neutrophils, macrophages, monocytes and lymphocytes that in response produce a large quantity of cytokines [77]. Increased neutrophil-to-lymphocyte ratio (NLR) in COVID-19 patients is a marker of cytokine storm. Many studies demonstrated the presence of inflammatory infiltrates within different tissues in patients diagnosed for COVID-19 [78]. Numerous inflammatory cytokines contribute to this process, such as Interleukin (IL) -1 β , -2, -6, -10, Interferon (IFN) - γ , Tumor Necrosis Factor (TNF) - α , IFN- γ -inducible protein 10 (IP-10), granulocyte macrophage-colony stimulating factor (GM-CSF), and monocyte chemoattractant protein-1 (MCP-1) and the plasma concentration of these molecules also correlate with disease severity [79,80]. These cytokines are produced and released as a cascade by different cell types. Different are the pathway of activation:

- Direct viral recognition: activation via pattern recognition receptors (primarily by virus-specific Toll-like receptors as TLR3, TLR7, TLR8 and TLR9);
- Indirect recognition: cytokine production in response to cell damage such as when epithelial cells damaged by SARS-CoV-2 infection release damage-associated molecular patterns (DAMPs).

The first cytokines to be produced and released are TNF- α and IL-1 β : these molecules then stimulate the production of others [81]. In a condition in which the patient is able to cope with the infection, T lymphocyte exhaustion and production of suppressive cytokines such as IL-10 can take part in re-

establishing homeostasis in the lung. This balance of immune activation and suppression is crucial for the host to fight the infection.

“Cytokine storm” is a definition already used for different viral infections such as influenza, MERS-Cov and Ebola. However, this term have been used also to describe sepsis of various etiology or other non-infectious pathologies such as severe traumas and burns, acute pancreatitis, macrophage activating syndrome. [81]. Among all cytokines, IL-6 was a protagonist in scientific discussion during COVID-19 pandemic. IL-6 is one of the main pro-inflammatory cytokines that is involved in different aspects of both innate and adaptive immunity. IL-6 promotes the differentiation of monocyte to macrophages rather than to Dendritic Cells (DCs), thus controlling the antigen presenting cell development and favoring the presence of cells able to fight pathogens [82]. Regarding adaptive immunity, IL-6 is a growth factor for B cells and inducer of plasma cell differentiation, thus impacting on antibodies production. In addition, IL-6 is a co-stimulatory molecule for T cell activation enhancing proliferation and also protecting CD4⁺ T cells from activation induced cell death (AICD), downregulating Fas ligand (FasL) expression [83]. It can also inhibit TGF- β induced regulatory T cell (Treg) differentiation, reinforcing inflammation. IL-6 stimulates hepatocytes to produce inflammation proteins such as C-reactive protein (CRP) and fibrinogen. All these actions, when taken to the excess, cause damage to the organism [84]. IL-6 as well as its receptor can be found both as soluble and membrane-bound molecules. IL-6 binds to its receptor, IL-6 receptor (IL-6R or CD126) and to Glycoprotein 130 (gp130). When bound, it forms a hexameric complex that transduces the signal through the Janus kinase (JAK) and signal transducer and activator of transcription (STAT) pathway [85]. The complex IL-6/IL-6R/gp130 can activate classic signaling and trans-signaling. When the combination is composed of membrane-bound IL-6, the classic signaling is activated, while when it is involved the soluble molecule, the trans-signaling pathway is then turned on. When the serum levels of IL-6 are low, then the classic pathway is activated playing an anti-inflammatory role. On the other hand, when IL-6 concentration increases, trans-signaling is activated and pro-inflammatory reactions occurs in a wide cell population [86].

IL-6 is typically found in blood of healthy individuals at low concentration (1-5 pg/ml). The association between IL-6 > 80 pg/ml and respiratory failure or death was observed in different studies and was the fuse that led to the use of IL-6 blockers in the management of severe COVID-19 patients [85]. Tocilizumab is a humanized monoclonal antibody that by binding to IL-6R (both soluble and membrane-bound) can inhibit the interaction with the ligand, interfering with IL-6 signaling and opposing to inflammation. This new drug is largely used by rheumatologist in the treatment of rheumatoid arthritis. Regarding COVID-19, tocilizumab is effective in patients with hypoxemia and in need for oxygen therapy. It improves survival and lower the chances of progressing to mechanical

ventilation in critical patients in ICUs. However, as usually occurs, not all the patients can benefit from this therapy [87-89]. Thus, studies tried to identify markers to distinguish responder from non-responder patients and highlighted that, at the time of treatment initiation, COVID-19 patients who responded to tocilizumab presented higher concentrations of pro-inflammatory cytokines such as IL-1 β , IL-1 α and IFN- β [90]. Where IL-6 was high, the early administration of tocilizumab determined improvement in oxygenation, defined as the ratio between arterial oxygen tension and fraction of inspired oxygen [91]. In non-responders, IL-6 has been seen to increase its levels even after the administration of tocilizumab [90].

The mode of action of tocilizumab affects B cell growth, B cell differentiation, survival of plasma cells and, more in general, B cell homeostasis in all COVID-19 patients, both responding or non-responding to therapy. In particular, B cells increase in number after tocilizumab treatment even in non-responders [92]. Responder patients, after therapy, present also higher number of CD4⁺ and CD8⁺ T cells, with a particular increase in naïve and recently activated memory T cells. In inflammation caused by rheumatoid arthritis, tocilizumab contributes to the increase of protective Treg and to inhibit T helper (Th) 17 phenotype [93-95]. Regarding tocilizumab therapy, responding patients before treatment seem to be characterized by higher levels of inflammation, B and T cells if compared to non-responders which present leukopenia [90].

1.5.2 Innate immune response

The innate immune response is fundamental for a fast action against the pathogen. It has three main and pivotal role:

- The restriction of viral replication within infected cells;
- The creation of an antiviral state as well as the recruitment of effector cells of the innate immune system;
- The priming of the adaptive immune response.

The first two activities slow down the viral replication and spreading, while the third is critical for a clearance of the infection [96]. The first barriers that SARS-CoV-2 encounter when infecting the host are the physical barriers, as skin and mucosa lining in the respiratory tract. Then cells of the innate branch of immunity are recalled. Innate immune cells are dendritic cells, macrophages, monocytes and granulocytes (eosinophil, basophil, neutrophils), each one with a different function and activating pathways that lead to different outcomes. The intensity of the response depends on the activation of these cells [97].

The majority of cells infiltrating lungs are monocytes and macrophages. These cells together with multinucleated giant cells were observed in lungs during autopsy from COVID-19 death patients and were associated with alveolar injury [97].

Monocytes are a heterogeneous population of APC that constitute the 5-10% of peripheral-blood leukocyte. On the basis of surface marker expression, monocytes can be subdivided in:

- Classical monocytes: expressing high levels of CD14 but no CD16 (CD14^{bright}, CD16⁻); during the infection these monocytes can home to the site of inflammation, recognize and phagocytose the pathogen, secrete pro-inflammatory cytokines and recruit immune cells [98].
- Intermediate monocytes: expressing high levels of both CD14 and CD16 (CD14^{bright}, CD16^{bright}); these cells are the main source of pro-inflammatory cytokines, such as IL-6, TNF, IL-1 β and IL-8 [99].
- Non-classical monocytes: expressing medium levels of CD14 but high levels of CD16 (CD14^{dim}, CD16^{bright}); these innate immune cells can move along the vasculature and are considered surveilling monocytes.

These subsets differ for the expression of homing receptors, for the production of pro-inflammatory cytokines and for the ability to present antigens [98].

In a physiological situation, monocytes produce adenosine triphosphate (ATP) to exert their functions by both oxidative phosphorylation (OXPHOS) and glycolysis. During a situation of inflammation or hypoxia, monocytes preferentially activate one of the two pathways changing their metabolism to face the danger. However, during COVID-19 infection, monocyte metabolic conditions are profoundly compromised. In particular, both the pathways were found to be defective, reminding of a condition seen in patients with sepsis that was called “metabolic paralysis” [100]. Monocyte metabolism impacts their functionality; the quantification of reactive oxygen species (ROS), produced during respiratory (or oxidative) burst, is a direct measure of the activation and phagocytic function of the cell. This capacity of respiratory burst together with microbial killing, phagocytosis and cytokine production are hallmarks of monocyte function and are influenced by their metabolism [101-102]. From a metabolic point of view, COVID-19 patient monocytes are less efficient and more dysfunctional if compared to healthy controls. These cells during the infection present low glycolysis levels and reduced ability to perform oxidative burst. In addition, mitochondria were depolarized and presented abnormal ultrastructure [103].

SARS-CoV-2 infection induces a change in the redistribution of the three subpopulations of monocytes. In particular, intermediate monocytes are more present in COVID-19 patients than

healthy individual, at the expense of classical and non-classical monocytes that are less present if compared to controls. An important reduction in the number of non-classical monocytes has been observed in the peripheral blood of severe patients compared to mild or control ones, together with a reduction in Human Leukocyte Antigen-DR isotype (HLA-DR) reduced expression on CD14^{bright} monocytes. IL-6 is responsible for the inhibition of HLA-DR expression, thus the over production of IL-6 related to the cytokine storm could be responsible for this phenomenon. Indeed, when IL-6R antibodies are used, the restoration of normal levels of HLA-DR and non-classical monocytes have been observed. The decrease of non-classical monocytes is not related to other pathologies, thus representing a specific characteristic of SARS-CoV-2 infection [104-106]. However, this subset modification could be partially explained by the recruitment of non-classical monocytes to the site of the infection [107].

Monocytes can express C-C chemokine receptor type 2 (CCR2⁺), a marker that induce chemotaxis to the site of the infection. CCR2⁺ monocytes can migrate to the site of inflammation, differentiate into inflammatory macrophages and activate Natural Killer (NK) lymphocytes as well as memory CD8⁺ T cells which are involved in the antiviral response [103,108,109]. SARS-CoV-2 can also impact monocyte asset of surface antigen expression. Indeed, monocytes can express exhaustion markers, as antigens that are expressed after long stimuli and that inhibit the effector function of the cells. Among those, Programmed Cell Death Protein -1 (PD-1) is one of the most famous and cited. PD-1 binds to its ligand Programmed Death-Ligand 1 (PD-L1). PD-1/PD-L1 pathway is also involved in the pathogenesis of sepsis, where the increased expression of the two markers on monocytes is associated with increased mortality [110-112]. Regarding COVID-19 patients, PD-1 and PD-L1 were increased on all the three subpopulations of monocytes, indicating possible bad prognosis [103].

Despite their metabolic dysfunction and expression of marker of exhaustion, monocytes still produce cytokines. Inflammatory chemokines involved in monocyte regulation and migration such as C-C motif chemokine ligand (CCL2 , ligand of CCR2), CCL11, CXCL10 (ligand of CXCR3), osteopontin (OPN) are more abundant in COVID-19 patients compared to healthy controls. Another important molecules increased in COVID-19 patients is GM-CSF, indicating the activation of emergency myelopoiesis during the infection, a process defined by the mobilization of immature myeloid cells in the attempt to restore immune functions. IFN- γ , in addition, is increased in plasma of patients with the function of stimulating macrophages to produce pro-inflammatory cytokines in an uncontrolled way [103,104].

Granulocytes can be distinguished in eosinophil, basophil and neutrophil, named after their cytoplasmic granules staining characteristics. Neutrophil, for example, present neutrally stained

granules. Among innate immune cells, neutrophils are the most abundant effector cells, characterized by an important role in the response against pathogens. Neutrophils can phagocytose cells, produce different types of chemokines and cytokines, release huge amount of ROS during respiratory burst, degranulate and release granules of lytic enzyme and neutrophil extracellular traps (NETs). In addition, these cell can release anti-inflammatory molecules and cytokines such as resolvins, IL-4 and IL-10, helping ending the inflammation [113,114]. Neutrophil also have chemoattractant properties: through the release of CCL2 and CXCL10 or CCL2 and CCL20 these cells can attract Th1 and Th17 to the site of inflammation [113,115]. Regarding their metabolism, neutrophils are highly glycolytic cells. The formation of NETs depends on glucose and on glycolysis-derived ATP. In patients with severe COVID-19, neutrophils remodel their metabolism, enhancing glycolysis, storage and mobility of glycogen to perform NETs. Neutrophils release extracellular fibers mostly composed of DNA and globular proteins with antimicrobial properties that disarm and kill the pathogen [116-118]. These formations allow neutrophils to kill the pathogen while minimizing damage to the host cells as the release of enzymes happens in a very concentrated space without spreading. However, when NETs are released in huge quantity as in severe COVID-19 patients, the phenomenon leads to organ damage. Elevated levels of NETs markers, such as myeloperoxidase (MPO)/DNA complexes, have been found in circulation and in pulmonary vessel of patients [119-122]. MPO is an oxidative enzyme and elastase (EL) is the enzyme that breaks down elastin, a protein that imparts elasticity to connective tissue as in the lung. However, when upregulated, EL damages the function of the lung permeability barrier and induce the release of pro-inflammatory cytokines [123]. The antibacterial activity of MPO involves the release of ROS and reactive nitrogen species, so the control of MPO release at the site of infection is of prime importance. An uncontrolled release of MPO could lead to tissue damage [124]. Evidences reported that during autopsies of patients who died from COVID-19, neutrophils and NETs were identified in different tissues and organs such as lungs, heart, kidneys, liver and brain [125]. Even *in vitro* experiments reported data of this important neutrophil activation. Plasma of SARS-CoV-2 infected patients presented high concentration of MPO and EL [126], thus isolated neutrophils from healthy donors, when exposed to serum from COVID-19 patients, start to form NETs, suggesting the presence of NET-inducing molecules. In addition, isolated neutrophils from COVID-19 patients, in the absence of exogenous stimuli are more prone to produce NETs *in vitro* compared to healthy controls, indicating high activation [122,124,127].

Plasmacytoid dendritic cells (pDCs) are important protagonist of the fight against pathogen. During the infection, pDCs migrate from peripheral blood to the site of infection where they can sense the virus even if they do not present virus-specific receptors. In response to the pathogen these cells produce pro-inflammatory cytokines and IFNs, especially type I IFN that restrict SARS-CoV-2

spreading during the acute phase of the infection. However, pDCs decrease in absolute number in COVID-19 patients admitted to ICU, compromising the development of a protective anti-viral T cell response. In addition, the remaining pDCs seems to exert a pro-inflammatory function more than an anti-viral one [128].

1.5.3 Adaptive immune response

The adaptive immune system is composed of three major cell types: CD4⁺ T cells, CD8⁺ T cells and B cells. The latter, produce antibodies against the pathogen, CD4⁺ T cell action can range from helper to effector while CD8⁺ are cytotoxic T cells [96]. Adaptive immune response has two major role: (1) the control and clearance of almost all the virus that cause diseases in humans and (2) the memory preservation of the processed antigens in order to mount a faster response in case of a second infection. The adaptive immune system is primed by the innate immune system.

The input for CD4⁺ T cell differentiation is the antigenic stimulation. The interaction between T Cell Receptor (TCR) present on CD4⁺ T cell surface and antigen- major hystocompatibility complex (MHC) II complex on APCs, induce a signaling pathway that eventually lead to naïve cell proliferation and differentiation into effector cells. CD4⁺ T cells can differentiate into various cells type. The lineage-specific differentiation depends on the surrounding cytokine milieu, the antigen concentration, the type of APCs and the presence of costimulatory molecules [129,130]. Virus-specific CD4⁺ T cells mainly differentiate into Th1 and T follicular helper (Tfh) cells. Th1 differentiation is induced by IL-2 and IFN γ . IL-2 is secreted by APCs after their activation; IL-2 then induces NK cells to produce IFN γ . Th1 exert an antiviral activity through the production and release of cytokines. However, if their function is not well organized and cytokine storm starts to hit, the prolonged production of anti-viral cytokine induces Th2 response. Th2 cells secrete various cytokines among which IL-4 and IL-10 that have an anti-inflammatory action. In addition, activation of Th2 can also inhibit the antimicrobial activity of Th1. Thus, in an ideal situation, a balance between Th1 and Th2 would be the best solution to eradicate the pathogen. Th cell activation plays an essential role in determining the severity of the infection [130].

Tfh differentiation is primarily induced by IL-6 and IL-21. These cells are located in the follicular areas of the lymphoid tissues, where they take part in the development of antigen (Ag) - specific B cells and neutralizing antibody response [130,131]. Circulating Tfh (cTfh) are generated during the acute phase of SARS-CoV-2 infection and their frequency has been associated with reduced disease severity. Moreover, an important fraction of cTfh express CCR6, a molecule involved

in homing processes, indicating that these cells may be directed towards mucosal airway as it was already seen for human coronavirus HKU1 [132].

Another important T cell lineages are Th17 and Treg. Th17 have both a protective and pathogenic role, associated with chronic inflammation and autoimmune disease. These cells produce a wide array of cytokines such as IL-17A, IL-21, GM-CSF, IL-10 and IFN γ . IL-17A, in particular, attracts neutrophils and monocytes to the site of infection promoting innate immune cell recruitment [133]. Tregs are responsible for immune system homeostasis, negatively modulating proliferation, activation and effector functions of different immune cells. These cells are the first line of defense against uncontrolled inflammation with the suppression of CD4⁺ and CD8⁺ T cell response and NK, eosinophil and neutrophil cell infiltration into the site of infection. Therefore, Tregs produce anti-inflammatory cytokines such as IL-10 and IL-35 [134].

During viral infection, CD8⁺ T cells that recognize the antigen presented through MHC-I complex, are activated, undergo clonal expansion and differentiate into effector cells. Effector CD8⁺ T cells are responsible for a killer action against the pathogen. The presence of CD8⁺ T cells during the infection correlates with better prognosis. These cells are characterized by the expression and release of granules containing cytotoxic molecules such as CD107a, granzyme B (GRZB), perforin and IFN γ [135]. CD107a is a marker of NK degranulation and activated CD8⁺ T cells. When exerting the cytotoxic function, CD8⁺ T cells release pre-formed lytic granules located within the cytoplasm. These granules contain various proteins and on their surface express CD107a. During the process of degranulation, the membrane of the secretory vesicles fuses with the activated CD8⁺ T cell and release all the content in the immunological synapse between T cell and its target. Among the proteins inside the vesicles there are perforin and GRZB: the first one forms a pore-like structure on the membrane of the target cells, allowing the latter to enter and mediate cell death [136].

Lymphopenia is a key marker of severe COVID-19. In most patients the proportion between CD4⁺ and CD8⁺ T cells remain stable but a decrease in CD4⁺ and CD8⁺ count as well as CD4⁺/CD8⁺ ratio can be observed. Patients with COVID-19 also present the expression of marker of senescence or exhaustion. CD8⁺ T cells, for example, were found expressing CD57, a marker of aging or prolonged chronic infection; PD-1 was also expressed by T cells. Exhaustion is a state of functional unresponsiveness necessary to prevent massive immune activation and excessive tissue damage. PD-1 together with its ligand, PD-L1 mediates a potent inhibitory signal to block proliferation and function of T effector cells [137]. Immune Checkpoint inhibitors (ICPs) are a family of receptors that are responsible for the establishment of an exhaustion state. PD-1 belongs to this family as well as T-cell immunoglobulin mucin 3 (TIM3), Lymphocyte-activation gene 3, T cell immunoreceptor with

Ig and ITIM domains (TIGIT) and cytotoxic T-lymphocyte-associated antigen 4 (CTLA-4) and many other molecules.

B cells play a role of control and clearance during viral infection. These cells exert their function through cytokine production, antigen presentation and antibody secretion, thus presenting a wide-range of functionalities [138]. After the interaction between naïve B cells and Tfh cells in germinal centers (GCs), B cells go through a process of proliferation and differentiation, producing pre-germinal center memory B cells (pre-GC MBCs) and short-lived plasma cells (SLPCs). These cells secrete antibodies with low affinity. Other B cells entering GCs, can increase their antibody affinity by clonal expansion, somatic hypermutation and class-switching recombination, resulting in long-lived plasma cells (LLPCs) and MBCs. These cells produce high affinity antibodies. With a second stimulation (same virus or vaccination), pre-GC MBCs and SLPCs generate plasma cells to produce high affinity antibodies. B cells and antibodies, then, enter blood circulation and peripheral tissue to fight the pathogen [132]. Patients with severe COVID-19 face a profound impairment of B cell compartment. In these patients, B cell response usually arises 7-10 days after onset of symptoms and in 3 weeks most but not all the patients develop neutralizing antibodies [139]. In normal conditions, MBCs are supposed to remain stable in number or slightly increase in people from 20 to 80 years old [140]. In patients with severe COVID-19 these cells are lower than what observed in controls that were also younger. A hallmark of severe COVID-19 is the number of plasmablasts (or SLPCs): these cells increase in number in severe patients, indicating the production of antibodies by immature cells [141]. B cells exhibit a rapid clonal expansion and diversification following SARS-CoV-2 infection. The quality of this response defines the course of the infection. In fact, lymphopenia of T and B cells was found in patients in need for intensive care support [142].

A schematic representation of COVID-19 immunopathology is reported in **Figure 1**.

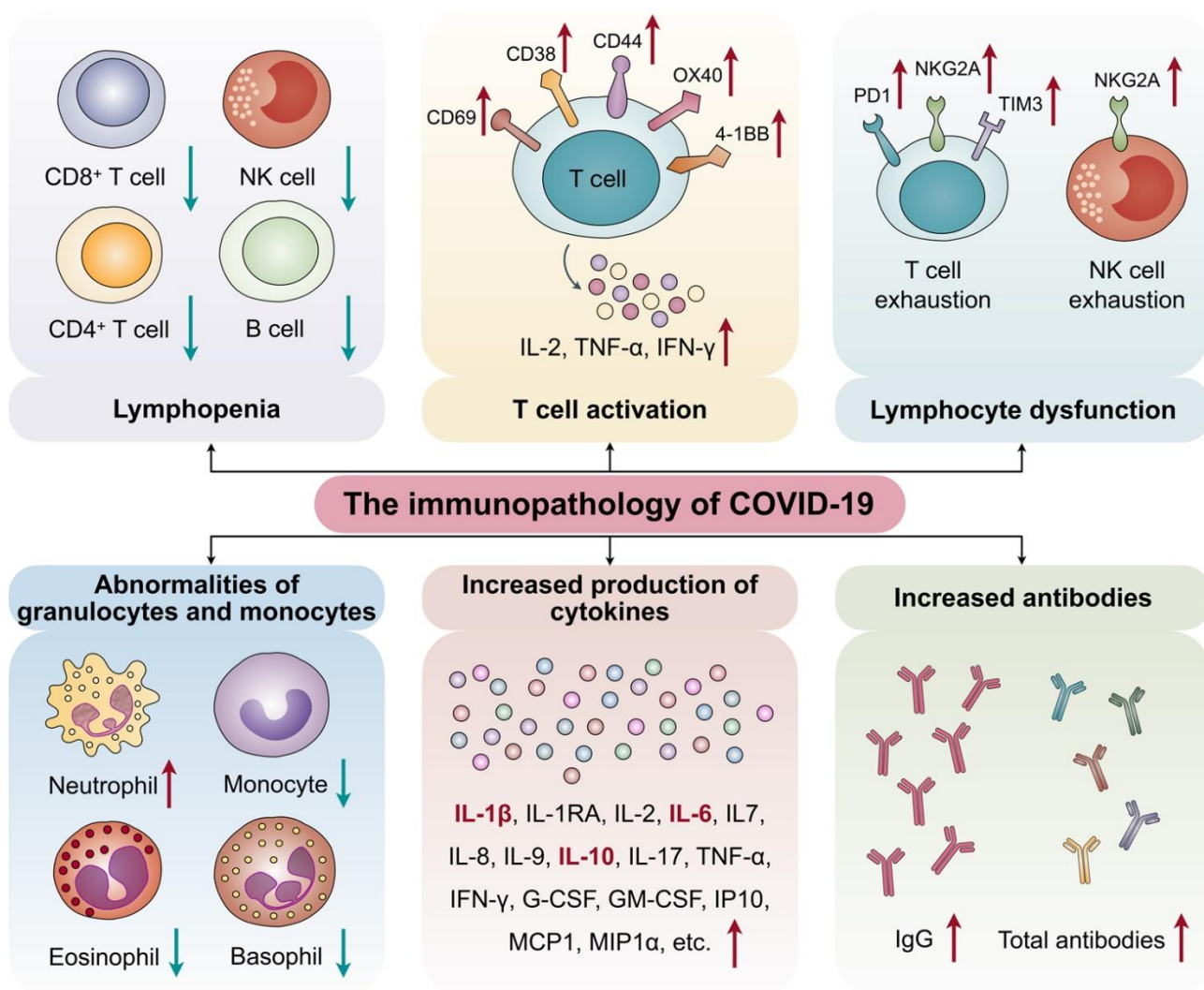


Figure 1. The immunopathology of COVID-19. The main features of COVID-19 include lymphopenia, activation and dysfunction of lymphocytes, abnormalities of granulocytes and monocytes, enhanced cytokine production and increased antibody levels. Lymphopenia is a hallmark of SARS-CoV-2 infection, especially among patients experiencing severe illness. Patients' CD4⁺ and CD8⁺ T cells highly express CD69, CD38 and CD44 but also markers of exhaustion such as programmed cell death protein-1 (PD1), T cell immunoglobulin domain and mucin domain-3 (TIM3), and killer cell lectin-like receptor subfamily C member 1 (NKG2A) upregulation. Virus-specific T cells from severe patients mostly exhibit a central memory phenotype and release high levels of IFN- γ , TNF- α , and IL-2. Severe patients also display high levels of neutrophils together with reduced percentages of eosinophils, basophils, and monocytes. Uncontrolled cytokine production is another main feature of SARS-CoV-2 infection. High levels of IL-1 β , IL-6, and IL-10 are found in plasma of severely infected patients. IgG levels increase as well as the total antibody titer (Figure from: Yang, L., *et al.* COVID-19: immunopathogenesis and immunotherapeutics. *Sig Transduct Target Ther* **5**, 128 (2020).

1.6 Vaccines against SARS-CoV-2 infection

The introduction of vaccines in the fight against SARS-CoV-2 has been a crucial step for public health and a triumph of biomedical research. At the beginning of 2021, after little more than one year from the first cases of COVID-19, vaccines become available in Italy. Vaccination resulted to be an unevaluable tool to fight severe cases of COVID-19 reducing hospitalization and deaths. The first approved vaccine by the European Medicines Agency (MEA) was the m-RNA based vaccine BNT162b2 (Comirnaty). After few months, many vaccines were approved such as a second mRNA vaccine, the mRNA-1273 vaccine (Spikevax), and two viral vector vaccines, the AZD1222 vaccine (Vaxzevria) and Ad26.COVS vaccine (Jcovden). The introduction of all this vaccines allowed to rapidly expand the target population, achieving a high vaccination coverage. In December 2021, an adjuvanted recombinant vaccine, NVX-CoV2373 (Nuvaxovid), was also approved and included in the vaccination campaign [143]. Results from randomized clinical trials (RCTs) indicated a decrease in symptomatic COVID-19 cases after completion of the intended vaccination cycle by more than 90% for mRNA vaccines (95% Comirnaty, 94.1% Spikevax), ~60–70% for viral vector vaccines (59.5% Vaxzevria; 67% Jcovden) and ~90% for the adjuvanted recombinant vaccine Nuvaxovid [144-149]. The technology proposed with mRNA vaccines was not unknown, but the BNT162b2 and mRNA-1273 were the first authorized mRNA vaccines. This new technology proposes a mRNA delivery by liposomal vesicles that fuse with the cell membrane and release mRNA in the cytoplasm. Then mRNA reaches ribosomes and use them for the synthesis of Spike protein. Spike is finally expressed on cell membrane to induce an immune response [150]. AZD1222 consists of a replication-deficient chimpanzee adenoviral vector ChAdOx1, containing the SARS-CoV-2 Spike protein gene. Ad26.COVS vaccine presents the same technology as the previous one, but using an human adenoviral vector called Ad26. Using an adenovirus as viral vector is advantageous as it is a double-stranded non-enveloped DNA virus with more than 300 different serotypes of adenovirus, which can target a wide array of parallel tissues for cell infection, opening up different strategies in vaccine design. Regarding the mechanism of action of this type of vaccines, after injection, adenovirus latches to the host cells and release its DNA into the cytoplasm. It then migrates into the cell nucleus where it uses host enzymes to get converted into mRNA. At this point it can be translated by ribosomes and further expressed on the cell surface as for mRNA based vaccine. This is a safe system, as the DNA portions coding for adenovirus replication is deleted from the vector, and consequently, it cannot be replicated in human cells [150]. NVX-CoV2373 is a protein-based vaccine created with the use of recombinant technology to obtain vaccine nanoparticles to be delivered. It is composed of recombinant full-length, stabilized spike protein homotrimers that form approximately 30-nm

nanoparticles based on hydrophobic interactions. The vaccine formulation comprise the antigen and Matrix-M adjuvant, necessary to better activate the immune response. As it is released after the injection, its presence as a non-self-protein recalls immune system cells [151].

At the end of 2021, a SARS-CoV-2 variant of concern (VOC) called Omicron, started spreading all over the world. With this, also the hypothesis of a reduced protection and effectiveness of natural and vaccine-induced immunity [152]. Virus mutations, in fact, are usually advantageous for its spreading, increasing transmissibility, infectivity, leading to a new rise in hospitalizations and deaths. Omicron, for example, presented numerous mutations in the Spike region, maintaining a robust ACE2 binding together with an increased ability in antibody escape [153]. However, the administration of a booster dose of vaccine showed to be effective in preventing Omicron infection, although with reduced effectiveness compared to other variant of the virus [154]. Due to different vaccine availability and instances of vaccine recalls from the market, heterologous vaccination was taken into consideration. It was observed that boosting with a heterologous vaccine might provide greater immunity and protection against VOCs. A randomized controlled trial conducted in the UK showed an increase in systemic reactogenicity in the context of heterologous vaccination compared to homologous vaccination [155].

1.7 Immunocompromised patients living the pandemic

The pandemic was a challenge for immunocompromised patients. This group represent the 2-3% of the overall population, including people presenting Human Immunodeficiency Virus (HIV) infection, cancers, transplants, primary immune-deficiencies and those treated with immunosuppressive drugs. In these patients, the response to infection is impaired, with fewer possibilities to recover and with the chance to develop complications [156,157]. Transplant recipients, people with metastatic cancer, hematologic malignancies and those receiving cancer chemotherapy present the higher risk for complications. Lung transplant recipients, hematopoietic stem cell transplant (HSCT) recipients and patients receiving anti-CD20 therapies are more subjected to severe and persistent infection and prolonged viral shedding. In particular, patients presenting hematologic malignancies or being transplant recipients can shed viable virus for approximately 4 weeks [158,159]. Thus, when vaccine became available, the WHO pointed to immunocompromised patients as the highest priority category to be vaccinated. However, there was concern about the immune response, particularly for the categories of transplants recipients, hematologic malignancies and patients treated with immunosuppressant or anti-CD20 [160]. The possibility of a missing

immune stimulation and response was taken into account and vaccination schedule was adjusted for immunocompromised [159].

1.8 SARS-CoV-2 vaccination and Multiple Sclerosis

Multiple Sclerosis (MS) is an autoimmune-mediated neurodegenerative disease of the central nervous system (CNS). Due to still unknown processes, the immune system deliberately attacks the nerve cells in the brain and spinal cord causing damage to myelin, the protective layer insulating nerve fibers, leading to signaling deficiencies. Life expectancy is lower than general population (75.9 vs 83.4 years) and MS more commonly affects women. Diagnosis is made based on a combination of signs and symptoms, radiographic and laboratory findings. MS patients need then to be treated with immunosuppressive and immunomodulatory drugs [161]. Disease-modifying therapies (DMTs) used for this clinical condition, act by using different strategies: teriflunomide inhibits the expansion of stimulated lymphocytes; natalizumab and fingolimod keep away immune cells from the CNS; ocrelizumab and cladribine deplete B and T cells respectively. Clearly, due to the strong impact on the immune system, these drugs can be the cause for increased infection risk, reduced vaccine effectiveness or reduced duration of immunity [162]. Among DMTs, other drugs with a less strong impact on the immune system are available: IFN- β acts in shifting the pro-inflammatory response in MS patients to an anti-inflammatory response, reducing T cell activation and the number of inflammatory cells capable to cross the blood-brain barrier [163]; glatiramer acetate simulates the myelin basic protein, blocking myelin-damaging T-cells through a mechanism that is not completely understood; dimethylfumarate (DMF) stimulates the Nrf2-pathways with consequent anti-oxidative, anti-inflammatory and cytoprotective effects. These drugs are not expected to compromise vaccine efficacy; however, some mechanisms of action are still to be clarified [164].

1.8 Method for the identification and characterization of SARS-CoV-2 Antigen-specific cells

Natural infection and vaccination induce the formation and subsequent expansion of Ag-specific cell that can point in a very specific way to the target of infection or vaccination. This is a precious pool of long-living memory cells responsible for future response to a second stimulus. During SARS-CoV-2 infection, after a couple of weeks, Ag-specific CD4⁺ and CD8⁺ T cells reach their peak around 0.5% and 0.2% of the repertoire, respectively [165]. These are considered as “rare events”. Due to their importance in the response against the pathogen, many researcher have focused

on the identification and characterization of these cells using different approaches. Most of these methods are based on flow cytometry.

Ag-specific T cells can be detected by direct analysis of the TCR. One approach is the use of MHC molecule that present a peptide of interest (i.e., SARS-CoV-2 antigen), tagged with a fluorescent molecule. As fluorescent-tagged monomer of MHC molecule would have a weak binding activity as it will bind and then immediately detach, while multimers have been found as a strong solution. By creating multimer, the complex can bind to different TCR on the same cell and the signal is better enhanced. With the help of a fluorophore cells can be identified and deeply characterized by using flow cytometry or even sorted for further analysis (i.e., RNA signature, *in vitro* cell culture). In addition, by combining different color-coded tetramers, it is possible to identify different antigens at the same time [166,167].

Ag-specific T cells can also be identified after *in vitro* stimulation using peptide pools that specifically activate the cells of interest. Peptide pools can be distinguished for the design method: they can be MHC restricted or fragments of a defined number of residues that bind with high selectivity the HLA molecule of interest. In addition, peptide pools can be designed for covering the whole sequence of the genome of the pathogen under investigation or for just covering the sequence of one protein. Thus, it can be investigated both the capacity of cells to respond to a specific protein stimulus or simulate a condition of infection. After stimulation, different approaches can be chosen for the identification and characterization of Ag-specific T cells [168].

Activation-induced marker assay (AIMs) is a method based on the up-regulation of specific markers of activation on the surface of Ag-specific cells. The identification is better done by selecting a pair of markers, such as CD69 plus CD154 (formerly CD40L), OX40 plus CD25, or OX40 plus PD-L1 (CD274) or 4-1BB (CD137) [169,170]. This approach has been used to characterize virus or vaccine Ag-specific response in a large number of studies. While the combination of two marker could be efficient for the identification of virus stimulated cells, when studying response induced by vaccine, it is suggested to use more than two markers as the magnitude of T cell activation may provide high baseline signals due to cross-reactive activation. In fact, it has been noted that also SARS-CoV-2 specific response is biased by the activation of cells specific for seasonal CoVs. It is for this reason that when Ag-specific response was studied comparing unexposed individuals and COVID-19 recovered patients, a little number of SARS-CoV-2 specific cells was found in controls [171]. Another important factor to be considered is the kinetics of markers up-regulation. CD69, CD154, and IFN- γ are detectable after 6 to 9 hours of stimulation; CD137 and OX40 reach their maximum expression after 12 to 24 hours of stimulation, while CD25 and HLA-DR need few days before right up-regulation [172].

Intracellular Cytokine Staining (ICS) is another approach to study activated or Ag-specific T cells. This method allows for the characterization of T cell lineage by the identification of cytokines released after *in vitro* peptide stimulation. 12 hours is the kinetics of cytokine release when studying IFN- γ , TNF, IL-2, IL-17, GRZB and CD107a [173]. With this method, it is also possible to study polyfunctional profile of CD4⁺ and CD8⁺ T cells. Polyfunctional cells are able to produce different cytokines at the same time. Thus, the information that can be obtained after this assay is multiple: it can be qu the percentage of cells producing a specific cytokine or expressing a desired marker, or by using the software Prism 6.0 (GraphPad Software Inc., La Jolla, CA, USA) it can be possible to study polyfunctionality.

The setting up of these assays is sophisticated as different factors are to be considered: (1) peptides have to be chosen based on the endpoint of the analysis as well as co-stimuli (i.e. CD28 for a correct TCR stimulation); (2) the use of appropriate inhibitors to avoid non-specific stimulation (i.e., CD40 blocking: this marker is expressed on APCs and binds CD154; this interaction is blocked in order to avoid non-specific activation of T cells [174]; (3) the setting of the adequate timing for stimulation depending on the choice of markers to identify Ag-specific cells [168].

The identification of Ag-specific B cells requires different protocols and setting up procedures. In order to have a specific binding, soluble SARS-CoV-2 antigen needs to be conjugated with biotin and subsequently added with fluorochrome-conjugated streptavidin. In this way the antigen will bind the specific receptors and Ag-specific B cells can be identified. However, to increase the reliability of the assay, the biotinylated antigen can be separately incubated with two different fluorochrome-conjugated streptavidin. B cells resulting positive for both the fluorescence will be considered as true Ag-specific B cells. However, contaminant needs to be considered. In fact, streptavidin specific B cells could alter the signal. To avoid this problem, a specific staining with fluorochrome-conjugated streptavidin can be implemented before adding the mix containing SARS-CoV-2 antigen. Contaminant cells will be excluded from the analysis in the first steps [175,176].

1.9 Polychromatic flow-cytometry and data analysis

Flow-cytometry is an unevaluable tool to characterize cellular lineage, specific features (i.e., exhaustion, activation, degranulation, senescence) as well as metabolism. Thanks to the progress of technology, more than 40 markers can now be analyzed simultaneously using this technique. This approach combines fast analysis and high throughput results, two fundamental elements in research. However, a multi-color flow cytometry panel needs to be set correctly and many phenomena have to be taken into account. When working with multi-parameter flow cytometry, there will be

fluorochromes with overlapping emission spectra, leading to unwanted fluorescence spilling into a secondary detector. This will create a signal in this secondary detector that will not be specific. By correctly apply the spillover correction, called “compensation”, this phenomenon can be avoided. Moreover, flow-cytometry is a technique that suffers from cell autofluorescence and spreading error (SE) due to errors in the measurements of photons, particularly at the red and far-red wavelengths where limited number of photons are emitted. SE affects signal in the secondary detector: double positive cells could be obscured by the signal spread from the primary detector. Thus, SE is a major determinant for a flow-cytometry panel success. Even with high overlap in panel spectra, if the SE is low, the result will be successful [177].

Two are the main approaches to analyze flow-cytometry data: by manual gating or using an unsupervised method. Manual gating was the first method used in this field; even though it is ideal to identify subpopulations and to quantify them, it is hard to reproduce and is a major source of variability. Nonetheless, populations of rare cells sometimes cannot be identified. Thus, an unsupervised approach overcomes most of these problems. For a successful unsupervised data analysis, three steps need to be followed: 1) manual pre-processing, 2) computation and 3) validation. During the manual pre-processing, compensation is checked and doublets, dead cells and fluorochrome aggregates are excluded. Then cells of interested are selected (i.e., CD4⁺, CD8⁺ T cells) and samples can be down-sampled if necessary to reduce computational time. During the computation step, all files are uploaded in the R or Python environment and desired parameters selected. Parameters that do not give information for subset separation should be excluded (i.e., live/dead, time, lineage). Then, data need to be transformed using specific algorithm (i.e., biexponential, arcsinh, and HyperLog transformation) to improve the output of the automated gating strategy. Then clustering and dimensionality reduction can be performed [168].

Flow cytometry allows to analyze each cells in a multi-dimensional way, as lot of parameters can be used. To visualize these parameters in a low-dimensional way, different approaches have been implemented: linear and non-linear transformation. The first, includes for example the principal component analysis (PCA), a method that was the firstly applied to immunology to study T cell subpopulations [178]. The second is the preferred one as nowadays analysis mostly involve complex dataset. An example of this approach is the t-distributed stochastic neighbor embedding (t-SNE) or Uniform Manifold Approximation and Projection (UMAP) [179]. Both approaches favor an informative visualization of the heterogeneity of data. Regarding the quality of visualization, distances between data points and clusters is comparable between t-SNE and UMAP, while the distance between clusters is correctly preserved only by UMAP. This means that distances among clusters correlates with their similarities [180].

The last step is validation, a manual inspection of files to confirm what obtained using unsupervised methods.

Thanks to these methods, cells can be deeply characterized and visualization will help in defining the cellular profile of the analyzed sample.

2. AIM OF THE THESIS

2.1 Characterization of the polyfunctional profile of SARS-CoV-2-specific CD4⁺ and CD8⁺ T cells in patients experiencing or recovering from COVID-19

The characterization of the immune response mounted against SARS-CoV-2 is crucial to understand and predict short- and long-term protection. Developing SARS-CoV-2 Ag-specific CD4⁺ and CD8⁺ T cells besides antibodies is fundamental to prevent severe outcomes and protect against reinfections [135]. This explains, at least in part, why: (i) immunocompromised patients with reduced humoral response and deficient B cells can develop a SARS-CoV-2 specific T cell response [181]; (ii) patients experiencing mild COVID-19 can successfully control the virus thanks to a robust SARS-CoV-2 T cell response even in the absence of antibodies [135,182-185]. SARS-CoV-2 T cell response in patients recovered from COVID-19 is multi-specific as T cells recognize several epitopes, by using a heterogenous TCR [171,186-188]. Functional studies using peptide pools covering most of SARS-CoV-2 encoded proteome demonstrated that T cell response to structural proteins such as M, S or N is co-dominant and that a significant reactivity is also developed against other targets, such as Open Reading Frames (ORFs) and nonstructural proteins (NSPs) [171,186,189]. However, whether this multi-specificity is the key to long-term protection is still uncertain.

CD4⁺ and CD8⁺ T cell polyfunctionality indicate the ability of cells to simultaneously produce more than one cytokine and to exert multiple functions. This is a crucial feature in Ag-specific responses as, in some cases, the quality of the response can be more important than the quantity in conferring protection against reinfection or pathogen reactivation [190,191]. In this scenario, CD4⁺ Th1 and Th17 are fundamental in inducing CD8⁺ T and B cells activity and promoting a pro-inflammatory response [192,193]. For example, Th1 and Th17 CD4⁺ T and CD8⁺ T cells dominate the influenza A virus-specific response, so inducing both a highly inflammatory environment and viral clearance [194-196].

For these reasons, given the role and capability of these cells, the aim of the study is to characterize the polyfunctional profile of SARS-CoV-2-specific T cells. Moreover, we aimed to investigate possible differences in the specific response between patients experiencing and recovering from moderate or severe infection, deepening at the same time the immunogenic capacity of M, N and S SARS-CoV-2 structural proteins.

2.2 Characterization of SARS-CoV-2-specific T and B cells after infection or heterologous vaccination

Memory is the main characteristic of the immune system, being at the basis of its efficacy and functionality, and indeed the activation of secondary response is the crucial strategy utilized by vaccination. Natural infection and vaccines induce the formation and subsequent expansion of Ag-specific cells that can block pathogens as soon as they try to invade the host. The creation of a pool of long-living memory T and B cells able to respond to future stimuli is crucial for vaccine efficacy, as well as the plasma level of antibodies [165].

During natural infection, CD4⁺ T cells display a memory profile (including a specific subset formed by stem cell memory) and are able to produce high levels of both IL-2 and Th1 cytokines [197-199]. CD4⁺ T-cell response is greater than the CD8⁺ counterpart [200]. Robust immunity is certainly maintained by more than 6 months, but the duration of SARS-CoV-2-specific T cells could depend also on the clinical severity of the initial infection [201]. Long-lived T-cell responses and efficient response to SARS-CoV-2 are characterized by a CD45RA⁺ effector-memory phenotype and a potent activation of the IFN transcriptomic signature whose magnitude is largely due to the genetic background of the host [202,203]. B-cell response is highly altered during COVID-19: in the plasma of most individuals, anti-SARS-CoV-2 antibodies (Abs) persist for more than 6 months after primary infection, but some patients rapidly lose their specific Abs [141,182,201,204]. However, specific MBCs predominantly express immunoglobulin (Ig)M⁺ or IgG1⁺ and rise until 150 days after infection, regardless of age. Receptor-binding domain (RBD)-specific IgG⁺ MBCs are predominantly CD27⁺, and their number significantly correlates with cTfh cell numbers [205,206].

Vaccination against SARS-CoV-2 induces a robust specific immune response. CD8⁺ T-cell response can be detected as early as 11 days after the first vaccination, and such cells can recognize immunodominant peptides from ORF1ab [207,189]. Two-dose vaccination with BNT162b2 leads to strong generation of virus-specific CD4⁺ T-cell responses with a Th1 profile, and it is detectable 6 months after vaccination [208-211]. Spike-specific antibodies peak after 7 days, and titers and ACE2/RBD binding-inhibiting activity is still observed after 6 months, despite a progressive decline over time. Concomitant to antibody reduction, spike-specific MBCs, mostly switched to IgG, increase and persist 6 months after vaccination [212]. T-cell responses after vaccination are of similar magnitude to those seen after natural infection, although they seem to be more differentiated with the presence of T stem cell memory (T_{SCM}) subsets [213]. An adenovirus-based vaccine generates a higher magnitude of spike-specific T cells, while mRNA vaccines develop higher antibody titers. For this reason, heterologous vaccines have been used in clinical practice [214-217].

As vaccination and natural infection increase across the world, there is growing interest in predicting the risk of primary infection or reinfection. Observational and limited comparison between natural and vaccine-induced immunity showed that the protection against SARS-CoV-2 infection was significantly higher in COVID-19 recovered individuals if compared to that of those vaccinated who additionally received a booster vaccine [218]. Antibodies decline more rapidly following vaccination in naive individuals than those in individuals who have recovered from COVID-19, but they display the same frequencies of spike-specific B and CD4⁺ T cells at 8 months after vaccination [219]. However, besides the magnitude of the spike-specific antibody response or neutralizing titer, the percentage, phenotypic identity, and functional profile of specific cellular immune responses have not been taken into account as immune correlates of protection.

Here, by using high-parameter polychromatic flow cytometry and sophisticated data analyses, we deeply investigated the magnitude, phenotype, and functionality of SARS-CoV-2-specific immune memory in two groups of healthy subjects after heterologous vaccination compared to those of subjects who recovered from SARS-CoV-2 infection.

2.3 Characterization of SARS-CoV-2-specific T and B cells in multiple sclerosis patients on different immunomodulatory drugs

The immunosuppressive and immunomodulatory DMTs used for MS act at different levels, *i.e.*, inhibiting the expansion of activated lymphocytes (teriflunomide), redirecting pathological immune cells away from the central nervous system [natalizumab, fingolimod (FTY)] or depleting immune cell subsets (B and T cells; anti-CD20, cladribine) [162]. In treated patient, DMT can introduce potential risk for increased infections, reduced vaccine effectiveness or reduce the duration of specific immunity. Clearly, these aspects have a critical importance, especially in the course of a pandemic like that due to SARS-CoV-2, where the host immune response is crucial, and that was effectively fought by several different vaccines [7,8,90,118,137, 141,199,220-223].

As far as DMT in MS patients are concerned, IFN- β , glatiramer acetate and DMF are not expected to compromise vaccine efficacy [164], although the effect of DMF-induced lymphopenia on vaccine efficacy is unknown, and attenuated vaccine responses in patients with moderate or severe lymphopenia is conceivable [224]. A modestly diminished rate of immune response to vaccines was described in patients treated with teriflunomide, even if this did not compromise the achievement of seroprotective antibody levels [225]. Valid immune response to diphtheria-tetanus toxoid and to Keyhole limpet hemocyanin (KLH) was found in natalizumab-treated patients [226], while H1N1 and seasonal influenza vaccination provided evidence that an adequate response to the immunization may not occur in some patients [227,228]. Adequate immune responses to seasonal influenza vaccine and tetanus toxoid booster were detected in patients receiving FTY [229]. On the other hand, MS patients treated with cell-depleting agents (such as ocrelizumab, rituximab, ofatumumab, alemtuzumab, and cladribine) displayed attenuated vaccine responses, especially if they were vaccinated during the maximum cell depletion period. Peripherally B cell-depleted ocrelizumab recipients mounted attenuated humoral responses to clinically relevant vaccines and the neoantigen KLH, suggesting that use of standard non-living vaccines while on ocrelizumab treatment requires careful considerations [230]. In any case, it is nevertheless recommended to vaccinate patients for seasonal influenza because a potentially protective humoral response, even if attenuated, can be expected [231].

How different DTM affect vaccination effectiveness and safety in patients with MS was highlighted during the outbreak of COVID-19. In particular, therapies with anti-CD20 (aCD20) monoclonal antibodies or with the sphingosine-phosphate receptor modulator (FTY) have been shown to weaken the formation of immune response after SARS-CoV-2 vaccination [232-240]. MS patients treated with teriflunomide or alemtuzumab achieved effective humoral and cellular immune

responses up to 6 months following the second COVID-19 vaccination. Immune responses were reinforced following the third vaccine booster [241]. However, the response to vaccination was mainly measured by humoral responses (in term of antibody titers in plasma) and or production of IFN- γ by T cells as correlate for a protective response. However, the protective capacity of the adaptive immune response to SARS-CoV-2 depends not only on virus-specific antibodies, but also on the cellular response [242]. The phenotype of antigen-specific (Ag⁺) T cells of patients treated with aCD20 displayed a skewed response, mostly compromising cTfh cell responses and augmenting the induction of CD8⁺ T cell [242]. Moreover, when compared to healthy donors (HD), MS patients showed lower percentages in Ag-specific cells able to produce IFN- γ , IL-2 and TNF [243].

A detailed overview of different functional and metabolic features of the long-term immune response after vaccination in relapsing-remitting (RR) MS patients treated with different DMT is still missing. For this reason we broadly interrogated SARS-CoV-2 specific T and B cells 6 months after the third dose of mRNA vaccine in a cohort of 106 MS patients treated with different DMT such as cladribine, DMF, FTY, IFN- β , natalizumab, teriflunomide or aCD20. By using 21-parameter flow cytometry, we have investigated the phenotype and function of Ag-specific T and B cells. We find that almost all patients develop a detectable and functional SARS-CoV-2 immune response. Finally, using a novel approach of prediction analysis, we identify a SARS-CoV-2 specific immunological signature that could likely predict protection from breakthrough SARS-CoV-2 infection.

3. METHODS

3.1 CD4⁺ and CD8⁺ T cells polyfunctionality in patients experiencing or recovering from COVID-19

3.1.1 Patients' selection

Four groups of patients were enrolled in this study, along with a group of healthy donors (HD). We enrolled 13 COVID-19 patients admitted into the Infectious Diseases Clinics or ICU of the University Hospital in Modena between March and May 2020. Patients tested positive for the SARS-CoV-2 PCR test. Within this group, 7 patients (median age: 55.0 years) were classified as moderate and 6 (63.0 years) as severe, according to World Health Organization guidelines [244]. We also studied 15 COVID-19 recovered patients, enrolled during follow-up visits between June and August 2020. Within this group, 9 patients (56.0 years) were classified as moderate and 6 (56.5 years) as severe. COVID-19 and recovered patients were subdivided for the analysis according to disease severity. Moreover, 10 HD (49.5 years) were included in this study. HD presented neither symptoms nor prior diagnosis of SARS-CoV-2 and had negative serology. Informed consent, according to Helsinki Declaration, was provided by each participant. All uses of human material have been approved by the local Ethical Committee (Comitato Etico dell'Area Vasta Emilia Nord, protocol number 177/2020, 11 March 2020) and by the University Hospital Committee (Direzione Sanitaria dell'Azienda Ospedaliero-Universitaria di Modena, protocol number 7531, 11 March 2020).

3.1.2 Blood Processing

Blood samples were obtained after informed consent. For COVID-19 patients, blood was obtained after diagnosis of SARS-CoV-2 infection during hospitalization. For recovered patients, blood was collected during a follow-up visit within 120–128 days after hospital admission and SARS-CoV-2 diagnosis. Up to 20 mL of blood were collected from each patient in vacuettes containing ethylenediamine-tetraacetic acid. Peripheral blood mononuclear cells (PBMCs) were isolated according to standard procedures and stored in liquid nitrogen until use [245].

Plasma was collected and stored at -80°C until the quantification of IgM and IgG, performed according to standard methods by SARS-CoV-2 IgM or IgG Quant Reagent Kit for use with Alinity (Abbott, Abbott Park, IL, USA).

3.1.3 In Vitro Stimulation and Intracellular Cytokine Staining (ICS)

For functional assays on cytokine production by T cells, isolated PBMCs were thawed and rested for 6 h. PBMCs were cultured in the presence of 15-mer peptides with 11-amino acids overlap, covering the sequence of different proteins of SARS-CoV-2: Nucleocapsid phosphoprotein (“N”) (PepTivator SARS-CoV-2 Prot_N), Membrane glycoprotein (“M”) (PepTivator SARS-CoV-2 Prot_M) and Spike glycoprotein (PepTivator SARS-CoV-2 Prot_S) (Miltenyi Biotec, Bergisch Gladbach, Germany). Each peptide was tested separately and 1 µg/mL of anti-CD28 (Miltenyi Biotec, Bergisch Gladbach, Germany) was added to each condition. PBMCs were stimulated for 16 h at 37 °C in a 5% CO₂ atmosphere in a complete culture medium (RPMI 1640 supplemented with 10% fetal bovine serum and 1% each of l-glutamine, sodium pyruvate, nonessential amino acids, antibiotics, 0.1 M HEPES, 55 µM β-mercaptoethanol). A negative control with unstimulated cells was included in the experimental conditions. All samples were incubated with a protein transport inhibitor containing brefeldin A (Golgi Plug, BD Biosciences Pharmingen, San Diego, CA, USA), a protein transport inhibitor containing monensin (Golgi Stop, BD Biosciences Pharmingen, San Diego, CA, USA) and mAb CD107a-PE (Biolegend, San Diego, CA, USA) at a previously defined concentration. After stimulation, cells were stained with LIVE-DEAD Aqua (ThermoFisher Scientific, Eugene, OR, USA) and surface mAbs recognizing CD3 PE-Cy5, CD4⁺ AF700, and CD8⁺ APC-Cy7 (Biolegend, San Diego, CA, USA). Cells were washed with stain buffer, fixed and permeabilized with the Cytotfix/Cytoperm buffer set (BD Biosciences Pharmingen, San Diego, CA, USA) for cytokine detection [220]. Cells were stained with previously titrated directly conjugated mAbs: IL-17A-PE-Cy7, TNF-BV605, IFN-γ-FITC, IL-2-APC and GRZB-BV421 (all mAbs from Biolegend, San Diego, CA, USA). Cells were analyzed by an Attune NxT acoustic cytometer (ThermoFisher Scientific, Eugene, OR, USA). **Table 3** reports mAb titers, producer, clone, catalog number, lot number and type of fluorochrome used in the panel.

3.1.4 Statistical Analysis

Quantitative variables were compared using the Kruskal–Wallis non-parametric test corrected for multiple comparisons by controlling the False Discovery Rate (FDR), method of Benjamini and Hochberg. Statistically significant *q* values are represented (* *q* < 0.05; ** *q* < 0.01; *** *q* < 0.001). T cell polyfunctionality was defined by using Simplified Presentation of Incredibly Complex Evaluation (SPICE) software (version 6, kindly provided by Dr. Mario Roederer, Vaccine Research Center, NIAID, NIH, Bethesda, MD, USA) [246]. Data from the total cytokine production are

represented as individual values, means, and standard errors of the mean. Regarding polyfunctionality, data in pie charts are represented as median values; statistical analysis was performed using permutation test (* $p < 0.05$; ** $p < 0.01$; *** $p < 0.001$). Data in graphs are reported as individual values, means and standard errors of the mean. Statistical analyses were carried out using Prism 6.0 (GraphPad Software Inc., La Jolla, CA, USA). Background was subtracted from each sample.

Target	Dye	Clone	Producer	Catalog Number	Lot Number	Titer (μL)/100 μL
LIVE DEAD	AQUA	N/A	ThermoFisher	L34966	2268307	1.25
CD3	PE-Cy5	UCHT1	BioLegend	300410	B270168	0.6
CD4	AF700	RPA-T4	BioLegend	300526	B336913	0.6
CD8a	APC-Cy7	RPA-T8	BioLegend	301016	B300873	0.6
IFN- γ	FITC	B27	BioLegend	506504	B286029	2.5
IL-2	APC	MQ1-17H12	BioLegend	500310	B313276	2.5
Granzyme B	BV421	QA18A28	BioLegend	396414	B311965	2.5
IL-17A	PE-Cy7	BL168	BioLegend	512315	B325831	3.75
TNF	BV605	MAb11	BioLegend	502936	B327946	3.75
CD107a	PE	H4A3	BioLegend	328608	B321484	0.3

Table 3. List of antibodies used in the Intracellular Cytokine Staining (ICS) panel (Paolini A., et al., 2022).

3.2 SARS-CoV-2 specific T and B cells after infection or heterologous vaccination

3.2.1 Blood collection and isolation of mononuclear cells

Up to 30 ml of blood was collected from each patient in vacuettes containing ethylenediaminetetraacetic acid (EDTA). Blood was immediately processed. Isolation of PBMCs was performed using Ficoll-Hypaque according to standard procedures [245]. PBMCs were stored in liquid nitrogen in fetal bovine serum (FBS) supplemented with 10% dimethyl sulfoxide (DMSO). Plasma was stored at -80°C until use.

3.2.2 Activation-induced cell marker assay and T-cell phenotype

Isolated PBMCs were thawed and rested for 6 h. After resting, CD4+0-blocking antibody (0.5 µg/ml final concentration) (Miltenyi Biotec, Bergisch Gladbach, Germany) was added to the cultures 15 min before stimulation. PBMCs were cultured in a 96-well plate in the presence of 15-mer peptides with 11-amino acid overlap, covering the complete sequence of Wuhan SARS-CoV-2 spike glycoprotein (PepTivator SARS-CoV-2 Prot_S complete, Miltenyi Biotec, Bergisch Gladbach, Germany) together with 1 µg/ml of anti- CD28 (Miltenyi Biotec, Germany). PBMCs were stimulated for 18 h at 37°C in a 5% CO₂ atmosphere in complete culture medium (RPMI 1640 supplemented with 10% FBS and 1% each of L-glutamine, sodium pyruvate, nonessential amino acids, antibiotics, 0.1 M 4-(2-hydroxyethyl)-1-piperazineethanesulfonic acid (HEPES), and 55 mM β-mercaptoethanol) [171,168]. For each stimulated sample, an unstimulated one was prepared as a negative control. After stimulation, cells were washed with Phosphate buffer saline (PBS) and stained with PromoFluor IR-840 (Promokine, PromoCell, Heidelberg, Germany) for 20 min at room temperature (RT). Next, cells were washed with FACS buffer (PBS added with 2% FBS) and stained with the following fluorochrome-labeled monoclonal antibodies (mAbs) for 30 min at 37°C: CXCR5-BUV661, CCR6-BUV496, and CXCR3-BV785. Finally, cells were washed with FACS buffer and stained for 20 min at RT with Duraclone IM T-cell panel (Beckman Coulter, Brea, CA, USA) containing CD45-Krome Orange, CD3-APC-A750, CD4-APC, CD8-AF700, CD27-PC7, CD57-Pacific Blue, CD279 (PD-1)-PC5.5, CD28-ECD, CCR7-PE, and CD45RA-FITC and added with three other fluorescent mAbs, i.e., CD69-BV650, CD137-BUV395, and CD95-BV605. Samples were acquired on a CytoFLEX LX flow cytometer (Beckman Coulter). All reagents used for T-cell phenotype are reported in **Table 4**. All mAbs added to DuraClone IM T cells were previously titrated on human PBMCs and used at the concentration giving the best signal- to-noise ratio. The gating strategy used to identify CD4⁺ and CD8⁺ T cells is reported in **Figure 2**.

3.2.3 Detection of SARS-CoV-2-specific B cells

Thawed PBMCs were washed twice with RPMI 1640 supplemented with 10% FBS and 1% each of L-glutamine, sodium pyruvate, nonessential amino acids, antibiotics, 0.1 M HEPES, 55 mM β -mercaptoethanol, and 0.02 mg/ml DNase. PBMCs were washed with PBS and stained using viability marker PromoFluor IR-840 (Promokine, PromoCell, Heidelberg, Germany) for 20 min at RT in PBS. Next, cells were washed with PBS and stained for 15 min at RT with streptavidin-AF700 (decoy channel; ThermoFisher Scientific, USA) to remove false-positive SARS-CoV-2-specific B cells. After washing with FACS buffer, cells were stained with biotinylated full-length SARS-CoV-2 spike protein (R&D Systems, Minneapolis, USA) labeled with different streptavidin-fluorophore conjugates. Full-length biotinylated spike protein was mixed and incubated with streptavidin-BUV661 (Becton Dickinson) or streptavidin-BV650 (BioLegend) at a 6:1 mass ratio for 15 min at RT. All samples were stained with both fluorescent and biotinylated spike protein for 1 hour at 4°C. Then, cells were washed with FACS buffer and stained for 20 min at RT with DuraClone IM B cells (Beckman Coulter, Brea, CA, USA) containing the following lyophilized directly conjugated mAbs: anti-IgD-FITC, CD21-PE, CD19-ECD, CD27-PC7, CD24-APC, CD38-AF750, anti-IgM-PB, and CD45-KrO to which the following drop-in antibodies were added: CD71-BUV395, CD20-BV785, anti-IgG-BUV496, and anti-IgA-PerCP-Vio700. Samples were acquired on a CytoFLEX LX flow cytometer (Beckman Coulter). A minimum of 1,000,000 cells per sample were acquired. All reagents used for B-cell phenotype are reported in **Table 4**. All mAbs added to DuraClone IM B cells were previously titrated on human PBMCs and used at the concentration giving the best signal-to-noise ratio. The gating strategy used to identify Ag⁻ and Ag⁺ B cells is reported in **Figure 3**.

3.2.4 Computational analysis of flow cytometry data

T cell analysis

Compensated Flow Cytometry Standard (FCS) 3.0 files were imported into FlowJo software version v10.7.1 and analyzed by standard gating to remove doublets, aggregates, and dead cells. For ex vivo immunophenotyping of non-antigen-specific (Ag⁻) and antigen-specific (Ag⁺) T cells of both CD4⁺ and CD8⁺, we analyzed only the data of stimulated samples. For each sample, we therefore selected data from all living CD4⁺ or CD8⁺ T cells and imported them in R using flowCore package v2.4.0 for a total of 8,436,275 CD4⁺ T cells (of which 89,400 were SARS-CoV-2-specific) and 3,723,899 CD8⁺ T cells (of which 20,413 were SARS-CoV-2-specific) [247]. Further analysis was performed using CATALYST v1.17.3 [248]. All data obtained by flow cytometry were transformed in R using hyperbolic arcsine “arcsinh (x/ cofactor)” applying manually defined cofactors (where x is the

fluorescence-measured intensity value). Clustering and dimensional reduction were performed using FlowSOM (version 2.4.0) and Uniform Manifold Approximation and Projection (UMAP) (version 0.2.8.0) algorithms, respectively. The Ag⁺CD4⁺ and CD8⁺T-cell clusters have been reanalyzed more in-depth by performing a new step of clustering using the following markers: CD45RA, CCR7, CD27, CD28, PD-1, CCR6, CXCR3, CXCR5, and CD95. Starting from 15 clusters of either CD4⁺T cells or CD8⁺T cells, reclustering gave origin to 10 clusters of CD4⁺T cells and 11 of CD8⁺T lymphocytes. The quality control (QC) of clustering for CD4⁺ and CD8⁺T cells is reported in **Figure 4** and **Figure 5**, respectively.

B cell analysis

Compensated FCS 3.0 files were imported into FlowJo software version v10.7.1 and analyzed by standard gating to remove doublets, aggregates, and dead cells and identify CD19 B cells. Then, from the total CD19 B cells, we excluded decoy-positive B cells to remove false-positive SARS-CoV-2 specific B cells. For each sample, we selected the SARS-CoV-2 specific B cells as positive cells for both Spike_streptavidin-BUV661 and Spike_streptavidin-BV650 (we referred to as Ag⁺ B cells). The remaining double-negative cells were non-SARS-CoV-2-specific B cells (we referred to as Ag⁻ B cells). Then, we exported for each sample separately both Ag⁺ and Ag⁻ B cells and imported them in R using flowCore package v2.4.0 for a total of 3,057,659 CD19 B cells (of which 9,898 were SARS-CoV-2-specific). The unsupervised analysis was performed using CATALYST v1.17.3. All data were transformed in R using hyperbolic arcsin (arcsinh x/cofactor) applying manually defined cofactors (where x is the fluorescence-measured intensity value). Clustering and dimensional reduction were performed using FlowSOM and UMAP algorithms, respectively. The QC of clustering for B cells is reported in **Figure 6**.

3.2.5 Measuring anti-SARS-CoV-2 anti-spike and anti-RBD IgG antibodies

Anti-spike antibody levels were measured by qualitative and semiquantitative chemiluminescent microparticle immunoassay (CMIA). AdviseDx SARS-CoV-2 IgG II assay (Abbott) was used to detect plasmatic IgG antibodies able to bind the RBD of the S1 subunit of the spike protein. Plasma, SARS-CoV-2 Ag-coated paramagnetic microparticles, and assay diluent are combined and incubated. The anti-spike IgG antibodies present in the sample bind to the SARS-CoV-2 Ag-coated paramagnetic microparticles. The mixture was then washed. Anti-human IgG acridinium-labeled conjugate was added and incubated to create a reaction mixture. The resulting chemiluminescent reaction was measured as a relative light unit (RLU). There is a direct relationship between the

amount of IgG antibodies to SARS-CoV-2 in the sample and the RLU detected by the system optics. Results from the anti-spike AdviseDx SARS- CoV-2 IgG II assay are reported as arbitrary units per milliliter (AU/ ml). As recommended, we applied a cutoff of 50 AU/ml as a positive threshold. Every measurement was performed on Abbott “Alinity I” platform. The level of anti-RBD IgG antibodies was calculated by using NAB Neutralizing Antibody kit (SGM Italia).

3.2.6 Principal component analysis and correlation plot

PCA was performed and visualized in R using prcomp and pca3d package. To perform PCA, we used a matrix containing the level of plasmatic anti-SARS-CoV-2 IgG antibodies, Ag-specific T, B cell percentages, and the fraction of polyfunctional CD4⁺ T cells. The total contribution of a given variable retained by PC1 and PC2 is equal to $[(C1 * Eig1) + (C2 * Eig2)] / (Eig1 + Eig2)$, where C1 and C2 are the contributions of the variable on PC1 and PC2; Eig1 and Eig2 are the eigenvalues of PC1 and PC2. Correlation analysis was performed on the same parameters used to run the PCA (see above) except the following features that were not used for the correlation analysis of REC donors because they were not available: PB IgA, PB, and CD107a⁺IFN-g⁺IL2⁺TNF⁺IL17⁻. Pairwise correlations between variables were calculated and visualized as a correlogram using R packages stats (version 3.6.2) and corrplot (version 0.90). Spearman’s rank correlation coefficient (r) was indicated by color scale; significance was indicated by asterisks (* P < 0.05; ** P < 0.005; *** P < 0.0005).

3.2.7 Statistical analysis

Differential cell population abundance analysis was performed using generalized linear mixed model (GLMM) implemented within diffcyt package [249] applying FDR cutoff = 0.05; each P-value was reported in the figure. Quantitative variables were compared using Kruskal–Wallis nonparametric test corrected for multiple comparisons by controlling the false discovery rate (FDR), method of Benjamini and Hochberg. Statistically significant adjusted P-values are represented. Statistical analysis of cytokine production was performed using GraphPad Prism version 8 (GraphPad Software Inc., La Jolla, USA). The total percentage of Ag-specific (Ag⁺CD4⁺ and Ag⁺CD8⁺) T cell data has been calculated as background subtracted data. SPICE software (version 6, kindly provided by Dr. Mario Roederer, Vaccine Research Center, NIAID, NIH, Bethesda, MD, USA) was used to analyze flow cytometry data on T-cell polyfunctionality [246]. Data from the total cytokine production are represented as individual values, means, and standard errors of the mean. Regarding polyfunctionality, data in pie charts are represented as median values, and statistical analysis was

performed using the permutation test. Data in graphs are represented as individual values, means, and standard errors of the mean.

Target	Dye	Clone	Producer	Catalog Number	Lot Number	Titer (μL)/100μL	Panel
PromoFluor840	Maleimide	N/A	Promocell	PK-PF840-3-01		0.3	AIM assay and B
CD45RA	FITC	2H4	Beckman Coulter (DuraClone IM T)	B53328		-	AIM assay
CCR7	PE	G043H7	Beckman Coulter (DuraClone IM T)	B53328		-	AIM assay
CD28	ECD	CD28.2	Beckman Coulter (DuraClone IM T)	B53328		-	AIM assay
PD-1	PC5.5	PD1.3.5	Beckman Coulter (DuraClone IM T)	B53328		-	AIM assay
CD27	PC7	1A4.CD27	Beckman Coulter (DuraClone IM T)	B53328		-	AIM assay
CD4	APC	13B8.2	Beckman Coulter (DuraClone IM T)	B53328		-	AIM assay
CD8	A700	B9.11	Beckman Coulter (DuraClone IM T)	B53328		-	AIM assay
CD3	APC-A750	UCHT-1	Beckman Coulter (DuraClone IM T)	B53328		-	AIM assay
CD57	Pacific Blue	NC1	Beckman Coulter (DuraClone IM T)	B53328		-	AIM assay
CD45	Krome Orange	J33	Beckman Coulter (DuraClone IM T)	B53328		-	AIM assay
CXCR3	BV785	G025H7	BioLegend	353738	B302668	1.25	AIM assay
CCR6	BUV496	11A9	Becton Dickinson	612948	1114714	1.25	AIM assay
CXCR5	BUV661	RF8B2	Becton Dickinson	741559	1298915	0.6	AIM assay
CD69	BV650	FN50	BioLegend	310934	B346313	2.5	AIM assay
CD137	BUV395	4B4-1	Becton Dickinson	745737	1298922	1.25	AIM assay
CD95	BV605	DX2	BioLegend	305628	B344380	2.5	AIM assay
LIVE DEAD	AQUA	N/A	ThermoFisher	L34966	2268307	1.25	ICS
CD3	PE-Cy5	UCHT1	BioLegend	300410	B270168	0.6	ICS
CD4	AF700	RPA-T4	BioLegend	300526	B336913	0.6	ICS
CD8a	APC-Cy7	RPA-T8	BioLegend	301016	B300873	0.6	ICS
IFN-γ	FITC	B27	BioLegend	506504	B286029	2.5	ICS
IL-2	APC	MQ1-17H12	BioLegend	500310	B313276	2.5	ICS
Granzyme B	BV421	QA18A28	BioLegend	396414	B311965	2.5	ICS
IL-17A	PE-Cy7	BL168	BioLegend	512315	B325831	3.75	ICS
TNF	BV605	MAb11	BioLegend	502936	B327946	3.75	ICS
CD107a	PE	H4A3	BioLegend	328608	B321484	0.3	ICS
IgD	FITC	IA6-2	Beckman Coulter (DuraClone IM B)	B53318		-	B
CD21	PE	BL13	Beckman Coulter (DuraClone IM B)	B53318		-	B

CD19	ECD	J3-119	Beckman Coulter (DuraClone IM B)	B53318		-	B
CD27	PC7	1A4CD27	Beckman Coulter (DuraClone IM B)	B53318		-	B
CD24	APC	ALB9	Beckman Coulter (DuraClone IM B)	B53318		-	B
CD38	APC-A750	LS198-4-3	Beckman Coulter (DuraClone IM B)	B53318		-	B
IgM	Pacific Blue	SA-DA4	Beckman Coulter (DuraClone IM B)	B53318		-	B
CD45	Krome Orange	J33	Beckman Coulter (DuraClone IM B)	B53318		-	B
Streptavidin	BV650	-	BioLegend	405231	B347044	0.3	B
Streptavidin	BUV661	-	Becton Dickinson	612979	1188291	0.3	B
Streptavidin	AF700	-	ThermoFisher	S21383	2286302	0.1	B
S-protein	Biotin	DOJH0421071	R&D	Bt10549	-	4.5	B
IgG	BUV496	G18-154	Becton Dickinson	741172	1341490	1.25	B
IgA	PerCP-Vio700	1S11-8E10	Miltenyi Biotec	130-113-478	5211109889	0.5	B
CD71	BUV395	M-A712	Becton Dickinson	743308	1298918	1.25	B
CD20	BV785	2H7	BioLegend	302356	B337363	0.6	B

Table 4. List of antibodies used in flow cytometry panels to identify antigen-specific T and B cells. AIM assay: Activation Induced Marker assay. ICS: Intracellular Cytokine Staining. B: Ag⁺ B cell phenotype (Lo Tartaro D., et al., 2023).

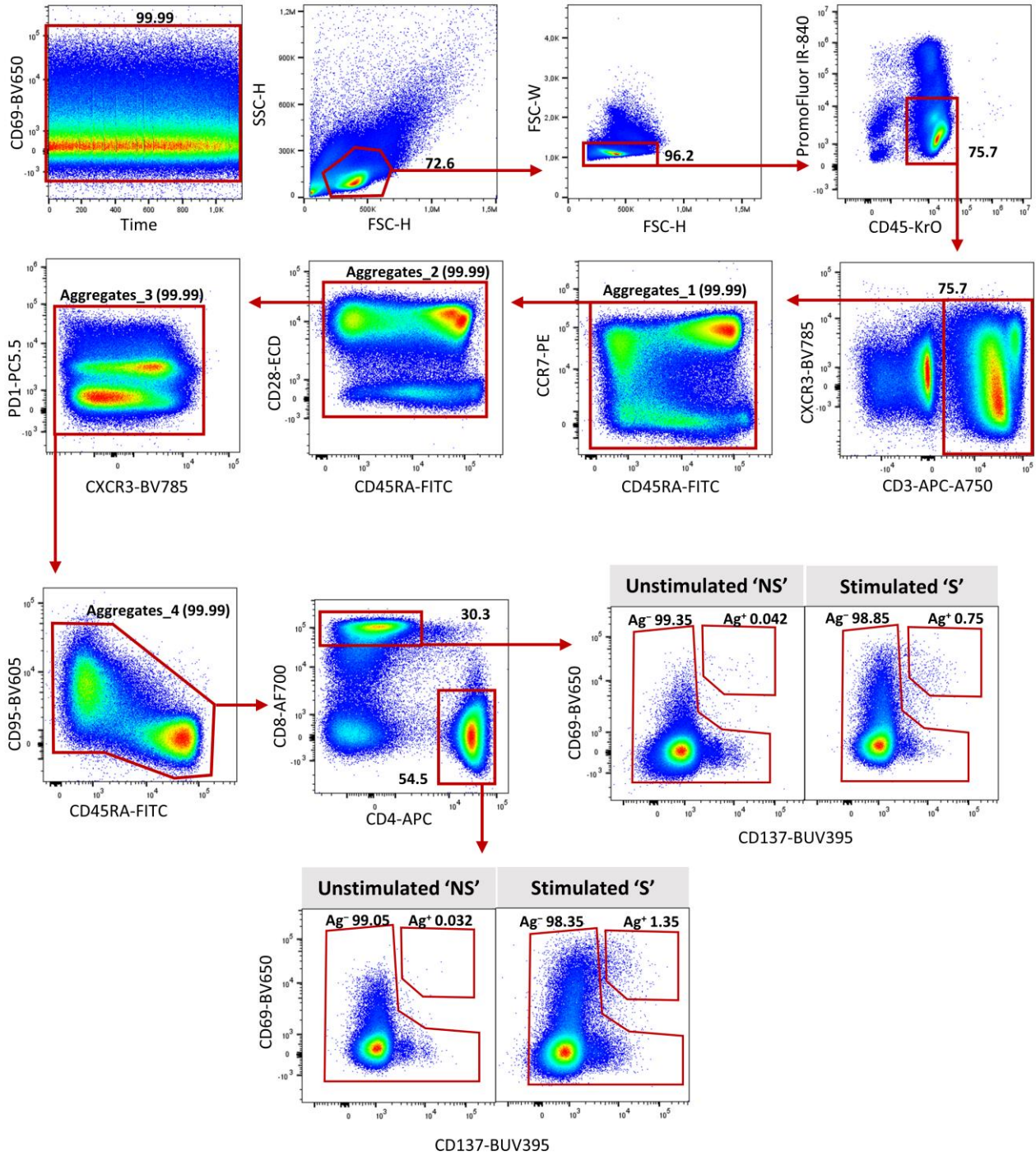


Fig. 2 Data processing performed before unsupervised computational analysis of CD4+ and CD8+ T cells. For *ex vivo* immunophenotyping of non-antigen-specific (Ag⁻) and antigen-specific (Ag⁺) T cells of both CD4⁺ and CD8⁺ we analyzed only the data of stimulated 'S' samples (Lo Tartaro D., et al., 2023).

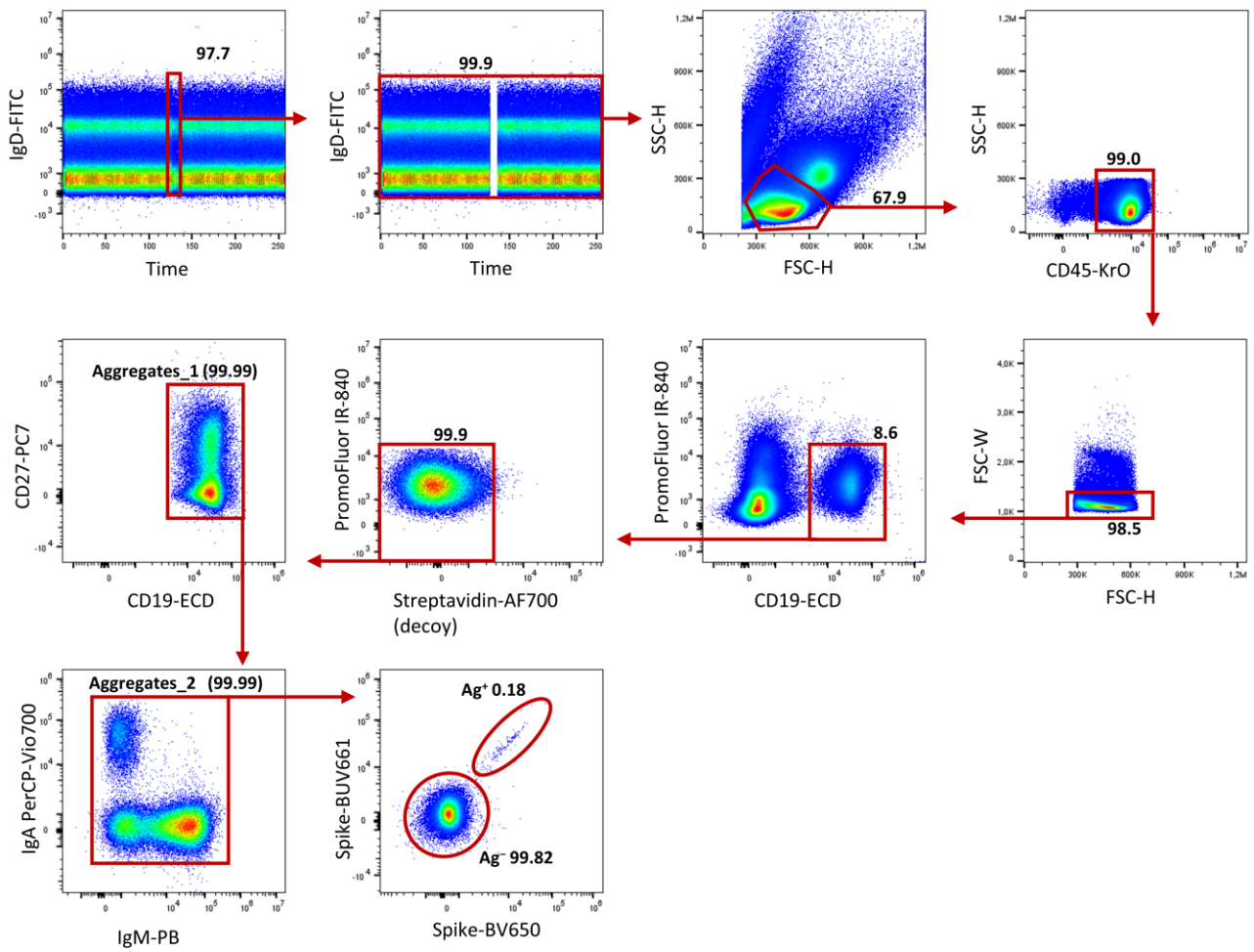


Figure 3. Data processing performed before unsupervised computational analysis of Ag⁺ and Ag⁻ B cells. The time vs IgD-FITC gate was used to exclude unstable flow cells (Lo Tartaro D., et al., 2023).

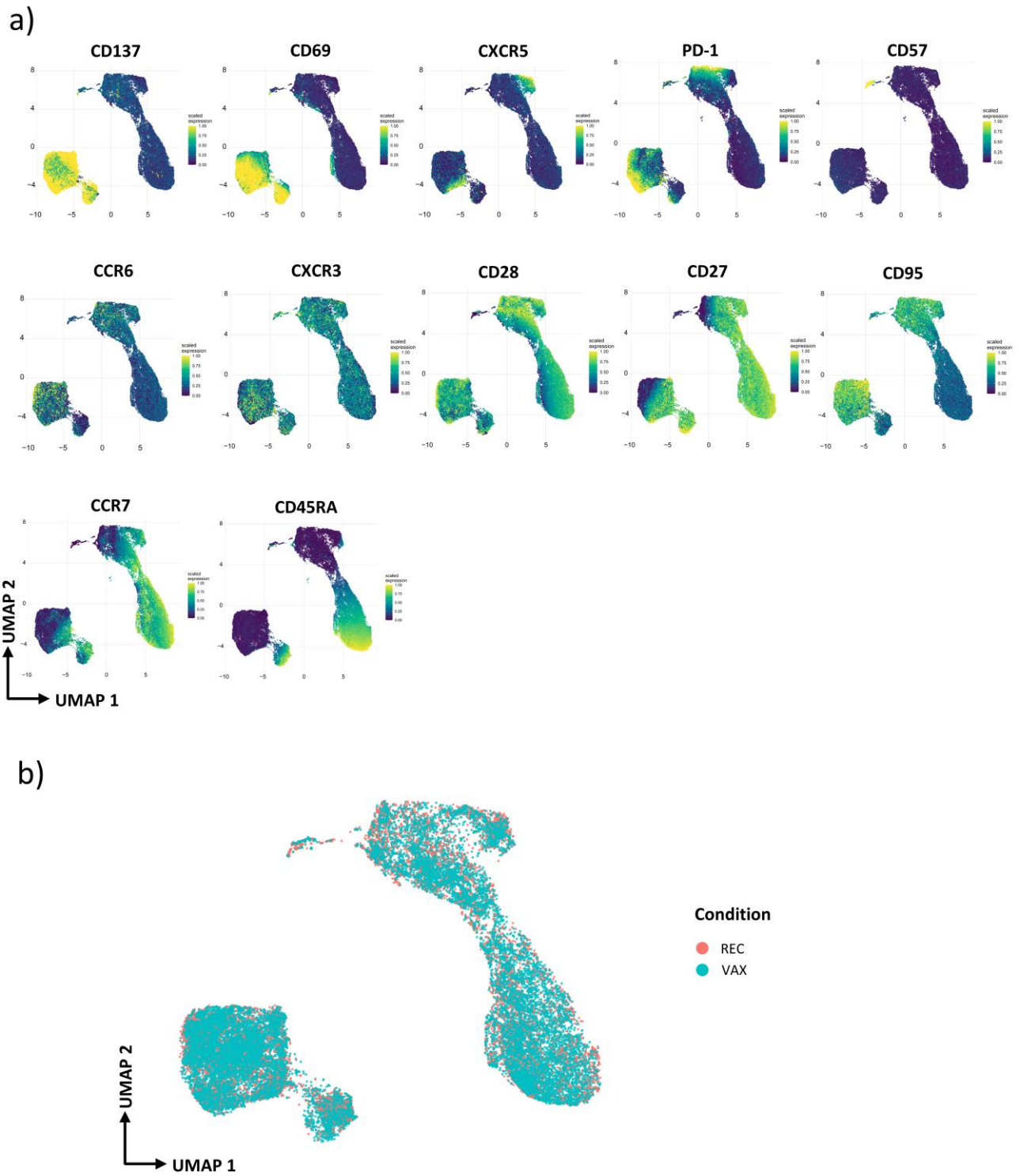


Figure 4. a) UMAP graphs colored by the expression of 12 markers used for CD4⁺ T cell phenotyping. b) Projection of UMAP graph stratified by condition. The condition levels are referred to: recovered (REC) and vaccinated subjects (VAX; MIX+RNA) (Lo Tartaro D., et al., 2023).

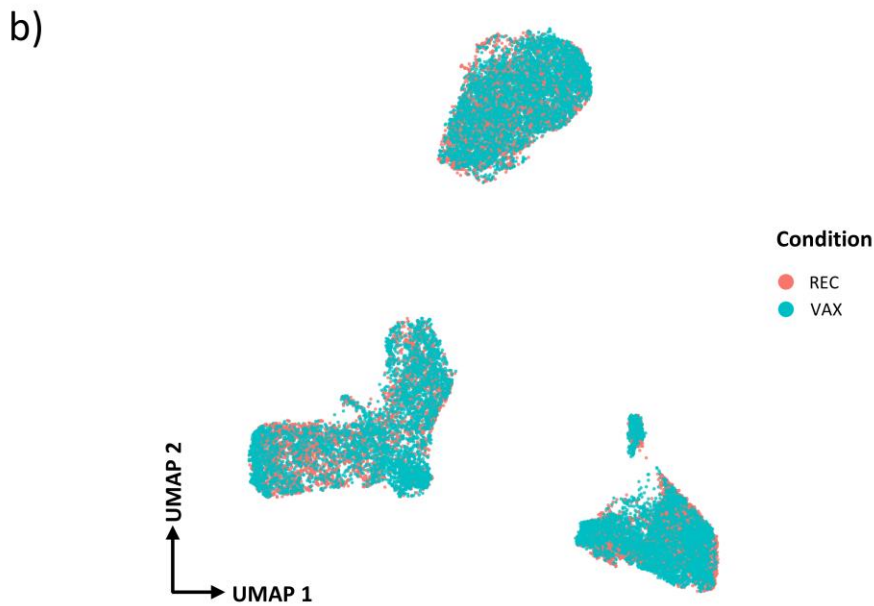
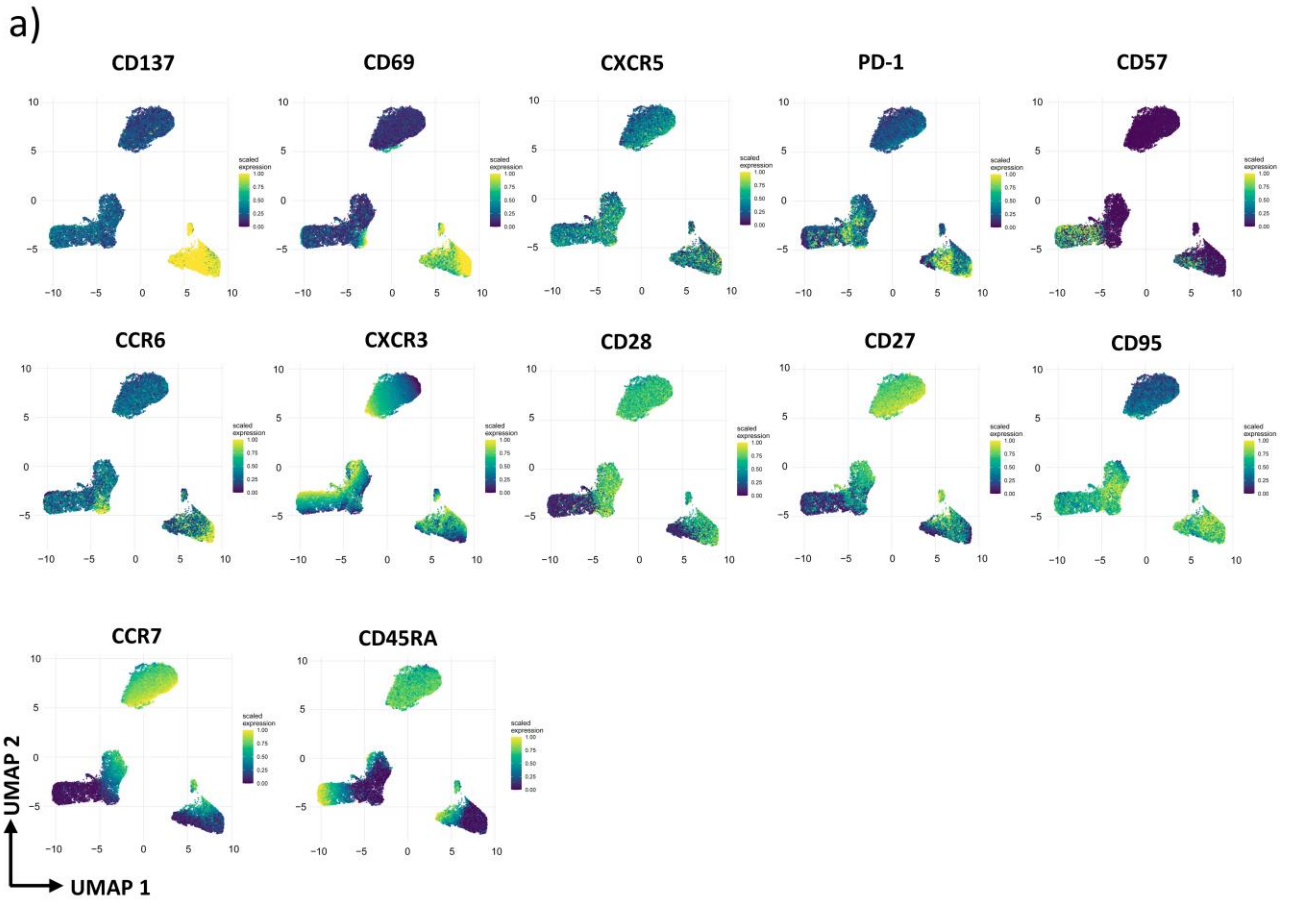
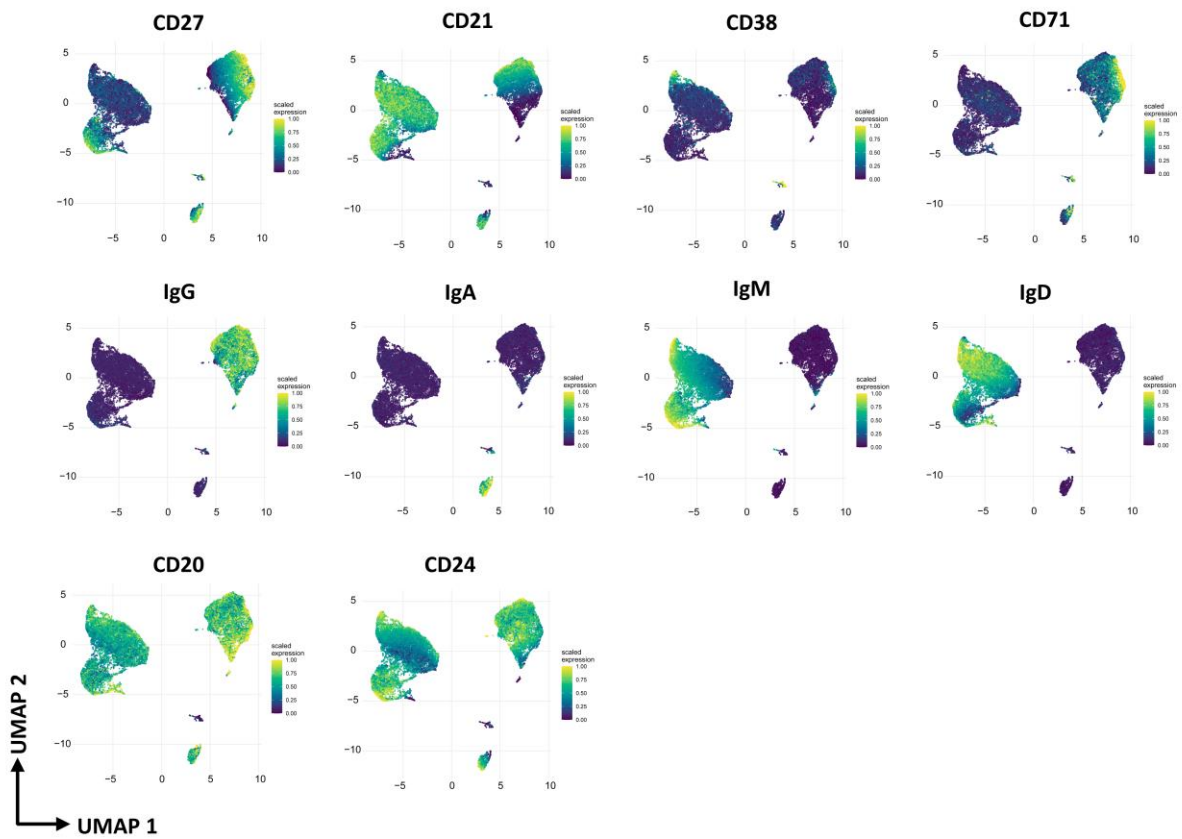


Figure 5. a) UMAP graphs colored by the expression of 12 markers used for CD8⁺ T cell phenotyping. b) Projection of UMAP graph stratified by condition. The condition levels are referred to: recovered (REC) and vaccinated subjects (VAX; MIX+RNA) (Lo Tartaro D., et al., 2023).

a)



b)

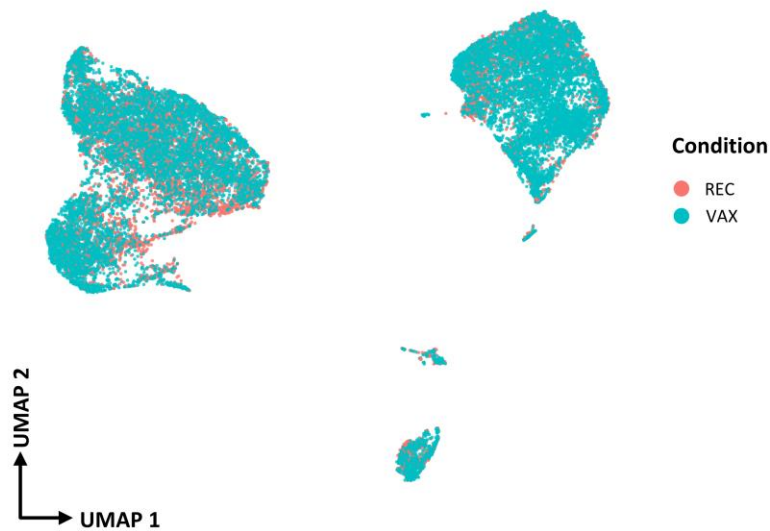


Figure 6. a) UMAP graphs colored by the expression of 12 markers used for CD19⁺ B cell phenotyping. b) Projection of UMAP graph stratified by condition. The condition levels are referred to: recovered (REC) and vaccinated subjects (VAX; MIX+RNA) (Lo Tartaro D., et al., 2023).

3.3 SARS-CoV-2 specific T and B cells in MS patients on different DMTs

3.3.1 Blood collection and isolation of mononuclear cells

Up to 30 mL of blood were collected from each patient in vacuettes containing ethylenediamine-tetraacetic acid (EDTA). Blood was immediately processed. Isolation of peripheral blood mononuclear cells (PBMC) was performed using ficoll-hypaque according to standard procedures. For all experiments PBMC were stored in liquid nitrogen in fetal bovine serum (FBS) supplemented with 10% dimethyl sulfoxide (DMSO). Plasma was stored at -80°C until use. The study was reviewed and approved by each participant, including healthy donors, provided informed consent according to Helsinki Declaration, and all uses of human material have been approved by the local Ethical Committee (Comitato Etico dell'Area Vasta Emilia Nord, protocol number 199/ 2022, May 24th, 2020) and by the University Hospital Committee (Direzione Sanitaria dell'Azienda Ospedaliero Universitaria di Modena, protocol number 5974, February 24th, 2023). The patients/participants provided their written informed consent to participate in this study.

3.3.2 Activation induced cell marker assay (AIM) and T cell phenotype

Isolated PBMCs were thawed and rested for 6 hours. After resting, CD40-blocking antibody (0.5 mg/ml final concentration) (Miltenyi Biotec, Bergisch Gladbach, Germany) was added to the cultures 15 min before stimulation. PBMCs were cultured in 96-well plate in the presence of 15-mer peptides with 11-amino acids overlap, covering the complete sequence of Wuhan SARS-CoV-2 Spike glycoprotein (PepTivator SARS-CoV-2 Prot_S complete, Miltenyi Biotec, Bergisch Gladbach, Germany) together with 1 $\mu\text{g}/\text{mL}$ of anti-CD28 (Miltenyi Biotec, Germany). PBMCs were stimulated for 18 h at 37°C in a 5% CO_2 atmosphere in complete culture medium (RPMI 1640 supplemented with 10% fetal bovine serum and 1% each of L-glutamine, sodium pyruvate, nonessential amino acids, antibiotics, 0.1M HEPES, 55 μM β -mercaptoethanol). For each stimulated sample, an unstimulated one was prepared, as negative control. After stimulation, cells were washed with PBS and stained with PromoFluor IR-840 (Promokine, PromoCell, Heidelberg, Germany) for 20 minutes at room temperature (RT). Next, cells were washed with FACS buffer (PBS supplemented with 2% FBS) and stained with the following fluorochrome-labeled mAbs: CXCR5-BUV661, CCR6-BUV496, CXCR3-BV785 for 30 minutes at 37°C . Finally, cells were washed with FACS buffer and stained for 20 minutes at RT with Duraclone IM T cell panel (Beckman Coulter, Brea, CA) containing CD45-Krome Orange, CD3-APC-A750, CD4-APC, CD8-AF700, CD27-PC7, CD57-Pacific Blue, CD279 (PD-1)-PC5.5, CD28-ECD, CCR7-PE, CD45RA-FITC and added with other three fluorescent mAbs i.e., CD69-BV650, CD137-BUV395 and CD95-BV605. Samples were acquired on

a CytoFLEX LX flow cytometer (Beckman Coulter). All reagents used for T cell phenotyping are listed in **Table 5**. All mAbs added to DuraClone IM T cells were previously titrated on human PBMCs and used at the concentration giving the best signal-to-noise ratio. The gating strategies used to identify CD4⁺ and CD8⁺ T cells are reported in the **Figures 7, 8**.

3.3.3 Detection of SARS-CoV-2-specific B cells

Thawed PBMC were washed twice with RPMI 1640 supplemented with 10% fetal bovine serum and 1% each of L-glutamine, sodium pyruvate, nonessential amino acids, antibiotics, 0.1M HEPES, 55µM β-mercaptoethanol and 0.02 mg/ml DNase. PBMC were washed with PBS and stained using viability marker PromoFluor IR-840 (Promokine, PromoCell, Heidelberg, Germany) for 20 min at RT in PBS. Next, cells were washed with PBS and stained for 15 min at RT with streptavidin-AF700 (decoy channel; ThermoFisher Scientific, USA) to remove false positive SARS-CoV-2-specific B cells. After washing with FACS buffer, cells were stained with biotinylated full-length SARS-CoV-2 spike protein (R&D Systems, Minneapolis) labelled with different streptavidin-fluorophore conjugates. Full-length biotinylated spike protein was mixed and incubated with streptavidin-BUV661 (Becton Dickinson) or streptavidin-BV650 (BioLegend) at a 6:1 mass ratio for 15 min at RT. All samples were stained with both biotinylated streptavidin for 1h at 4°C. Then, cells were washed with FACS buffer and stained for 20 min at RT with DuraClone IM B cells (Beckman Coulter, Brea, CA) containing the following lyophilized directly conjugated mAbs: anti-IgD-FITC, CD21-PE, CD19-ECD, CD27-PC7, CD24-APC, CD38-AF750, anti-IgM-PB, CD45-KrO to which following drop-in antibodies were added: CD71-BUV395, CD20-BV785, anti-IgG-BUV496 and anti-IgA-PerCP-Vio700. Samples were acquired on a CytoFLEX LX flow cytometer (Beckman Coulter). A minimum of 1,000,000 cells per sample were acquired. All reagents used for B cell phenotype are reported in **Table 6**. All mAbs added to DuraClone IM B cells were previously titrated on human PBMCs and used at the concentration giving the best signal-to-noise ratio. The gating strategy used to identify Ag⁻ and Ag⁺ B cells is reported in the **Figure 9**.

3.3.4 Intracellular cytokine staining (ICS)

Isolated PBMCs were thawed and rested for 6 h. PBMCs were stimulated in the presence of a pool of lyophilized peptides covering the complete protein coding sequence (aa 5–1273) of spike glycoprotein ("S") of SARS-CoV-2 (PepTivator SARS-CoV-2 Prot_S Complete Miltenyi Biotec, Bergisch Gladbach, Germany) together with 1 µg/ml of anti-CD28/49d (Becton Dickinson). PBMCs

were stimulated for 16 h at 37°C in a 5% CO₂ atmosphere in complete culture medium (RPMI 1640 supplemented with 10% FBS and 1% each of L-glutamine, sodium pyruvate, non-essential amino acids, antibiotics, 0.1 M HEPES, 55 mM β-mercaptoethanol, and 0.02 mg/mL DNase I). For each stimulated sample, an unstimulated one was prepared as a negative control. All samples were incubated with protein transport inhibitors brefeldin A (Golgi Plug, Becton Dickinson Bioscience, San Jose, CA, USA) and monensin (Golgi Stop, Becton Dickinson Bioscience, San Jose, CA, USA) and previously titrated concentration of CD107a-PE (BioLegend, San Diego, CA, USA). After stimulation, cells were washed with PBS and stained with LIVE/DEAD fixable Aqua (ThermoFisher Scientific, USA) for 20 min at RT. Next, cells were washed with FACS buffer and stained with surface mAbs recognizing CD3-PE.Cy5, CD4-AF700, and CD8-APC.Cy7 (BioLegend, San Diego, CA, USA). Cells were washed with FACS buffer and fixed and permeabilized with the Cytotfix/Cytoperm buffer set (Becton Dickinson Bioscience, San Jose, CA, USA) for cytokine detection. Then, cells were stained with previously titrated mAbs recognizing IL-17-PE-Cy7, TNF-BV605, IFN-γ-FITC, IL-2-APC, and GRZMB BV421 (all mAbs from BioLegend, San Diego, CA, USA). Samples were acquired on an Attune NxT acoustic cytometer (ThermoFisher Scientific, USA). **Table 7** reports mAb titers, clones, catalog numbers, and type of fluorochrome used in the panel. Gating strategy used to identify and analyze the intracellular cytokine production of CD4⁺ and CD8⁺ T lymphocytes is reported in **Figure 10**.

3.3.5 Computational analysis of flow cytometry data

T cells analysis

Compensated Flow Cytometry Standard (FCS) 3.0 files were imported into FlowJo software version v10.7.1 and analyzed by standard gating to remove doublets, aggregates and dead cells. For ex vivo immunophenotyping of non-antigen-specific (Ag⁻) and antigen-specific (Ag⁺) T cells of both CD4⁺ and CD8⁺ we analyzed only the data of stimulated samples. For each sample, we therefore selected data from all living CD4⁺ or CD8⁺ T cells and imported them in R using flowCore package v2.4.0 for a total of 37,397,203 CD4⁺ T cells (of which 465,729 were SARS-CoV-2 specific) and 12,758,008 CD8⁺ T cells (of which 180,267 were SARS-CoV-2 specific). The further analysis was performed using CATALYST v1.17.3. All data obtained by flow cytometry were transformed in R using hyperbolic arcsine “arcsinh (x/cofactor)” applying manually defined cofactors (where x is the fluorescence measured intensity value). Clustering and dimensional reduction were performed using FlowSOM (version 2.4.0) and UMAP (version 0.2.8.0) algorithms, respectively. The Ag⁺ CD4⁺ and CD8⁺ T cell clusters have been analyzed using the following markers: CD45RA, CCR7, CD27,

CD28, PD-1, CCR6, CXCR3, CXCR5 and CD95. The quality control (QC) of clustering for CD4⁺ and CD8⁺ T cells is reported in the respective **Figures 11, 12**.

B cell analysis

Compensated Flow Cytometry Standard (FCS) 3.0 files were imported into FlowJo software version v10.7.1 and analyzed by standard gating to remove doublets, aggregates, dead cells, and identify CD19⁺ B cells. From total CD19⁺ B cells, to remove false positive SARS-CoV-2-specific B cells we eliminated decoy-positive B cells. For each sample, we selected the SARS-CoV-2-specific B cells as positive cells for both Spike_streptavidin-BUV661 and Spike_streptavidin-BV650 and now referred to as Ag⁺ B cells. The remaining double negative cells were non-SARS-CoV-2-specific B cells and mentioned to as Ag⁻ B cells. Then, we exported for each sample separately both Ag⁺ and Ag⁻ B cells and imported them in R using flowCore package v2.4.0. The unsupervised analysis was performed using CATALYST v1.17.3. All data were transformed in R using hyperbolic arcsin (arcsinh x/cofactor) applying manually defined cofactors. Clustering and dimensional reduction were performed using FlowSOM and UMAP algorithms, respectively. For each day of acquisition at CytoFLEX LX, we had a sample used as quality control (QC).

3.3.6 Statistical analysis

Quantitative variables were compared using Kruskal-Wallis non-parametric test corrected for multiple comparisons by controlling the False Discovery Rate (FDR), method of Benjamini and Hochberg. Statistically significant q-values are represented. Statistical analysis of cytokines production was performed using GraphPad Prism version 8 (GraphPad Software Inc., La Jolla, USA). Total percentage of antigen-specific (Ag⁺CD4⁺ and Ag⁺CD8⁺) T cell data have been calculated as background subtracted data. Simplified Presentation of Incredibly Complex Evaluation (SPICE) software (version 6, Vaccine Research Center, NIAID, NIH, Bethesda, MD, USA) was used to analyze flow cytometry data on T cell polyfunctionality. Data from the total cytokine production are represented as individual values, means, and standard errors of the mean. Regarding polyfunctionality, data in pie charts are represented as median values and statistical analysis was performed using permutation test; data in graphs are represented as individual values, means, and standard errors of the mean.

3.3.7 Principal Component Analysis

Principal Component Analysis (PCA) was executed and visualized in R using the precomp function (stats v3.6.2) and the pca3d package v0.1. The data used included the proportions and absolute

number of Ag⁺ CD19⁺ B cells, CD4⁺, CD8⁺ T cells along with clinical parameters (reported in results section). Missing values of dataset were imputed using missMDA package v1.18. The total impact of a specific variable retained by PC1 and PC2 was computed as $[(C1 * Eig1) + (C2 * Eig2)] / (Eig1 + Eig2)$, where C1 and C2 represent the contributions of the variable to PC1 and PC2, and Eig1 and Eig2 denote the eigenvalues of PC1 and PC2, respectively. The Euclidean distance of MS-treated groups to HD in PCA space was calculated using the phenoptr v.0.3.2 package.

Target	Dye	Clone	Producer	Catalog number	Lot number	Titer (uL)/100uL
PromoFluor840	Maleimide	N/A	Promocell	PK-PF840-3-01		0.3
CD45RA	FITC	2H4	Beckman Coulter (DuraClone IM T)	B53328		-
CCR7	PE	G043H7	Beckman Coulter (DuraClone IM T)	B53328		-
CD28	ECD	CD28.2	Beckman Coulter (DuraClone IM T)	B53328		-
PD-1	PC5.5	PD1.3.5	Beckman Coulter (DuraClone IM T)	B53328		-
CD27	PC7	1A4.CD2 7	Beckman Coulter (DuraClone IM T)	B53328		-
CD4	APC	13B8.2	Beckman Coulter (DuraClone IM T)	B53328		-
CD8	A700	B9.11	Beckman Coulter (DuraClone IM T)	B53328		-
CD3	APC-A750	UCHT-1	Beckman Coulter (DuraClone IM T)	B53328		-
CD57	Pacific Blue	NC1	Beckman Coulter (DuraClone IM T)	B53328		-
CD45	Krome Orange	J33	Beckman Coulter (DuraClone IM T)	B53328		-
CXCR3	BV785	G025H7	BioLegend	353738	B302668	1.25
CCR6	BUV496	11A9	Becton Dickinson	612948	1114714	1.25
CXCR5	BUV661	RF8B2	Becton Dickinson	741559	1298915	0.6
CD69	BV650	FN50	BioLegend	310934	B346313	2.5
CD137	BUV395	4B4-1	Becton Dickinson	745737	1298922	1.25
CD95	BV605	DX2	BioLegend	305628	B344380	2.5

Table 5. List of monoclonal antibodies used in the AIM assay (De Biasi S., et al., 2024).

Target	Dye	Clone	Producer	Catalog Number	Lot Number	Titer (mL)/100mL
PromoFluor840	Maleimide	N/A	Promocell	PK-PF840-3- 01		0.3
CD45	Krome Orange	J33	Beckman Coulter (DuraClone IM B)	B53318		-
CD19	ECD	J3-119	Beckman Coulter (DuraClone IM B)	B53318		-
CD21	PE	BL13	Beckman Coulter (DuraClone IM B)	B53318		-
CD27	PC7	1A4CD27	Beckman Coulter (DuraClone IM B)	B53318		-
CD24	APC	ALB9	Beckman Coulter (DuraClone IM B)	B53318		-
CD38	APC-A750	LS198-4-3	Beckman Coulter (DuraClone IM B)	B53318		-
IgD	FITC	IA6-2	Beckman Coulter (DuraClone IM B)	B53318		-
IgM	Pacific Blue	SA-DA4	Beckman Coulter (DuraClone IM B)	B53318		-
Streptavidin	BV650	-	BioLegend	405231	B347044	0.3
Streptavidin	BUV661	-	Becton Dickinson	612979	1188291	0.3
Streptavidin	AF700	-	ThermoFisher	S21383	2286302	0.1
S-protein	Biotin	-	R&D	BT10549	DOJH042107 1	4.5
CD20	BV785	2H7	BioLegend	302356	B337363	0.6
CD71	BUV395	M-A712	Becton Dickinson	743308	1341511	1.25
IgG	BUV496	G18-154	Becton Dickinson	741172	1341490	1.25
IgA	PerCP-Vio700	1S11-8E10	Miltenyi Biotec	130-113-478	5211109889	0.5

Table 6. List of monoclonal antibodies used in B cell panel (De Biasi S., et al., 2024).

Target	Dye	Clone	Producer	Catalog number	Lot Number	Titer (uL)/100uL
LIVE/DEAD	AQUA	N/A	ThermoFisher	L34966	2268307	1.25
CD4	AF700	RPA-T4	Biolegend	300526	B336913	0.6
CD8	APC-Cy7	RPA-T8	Biolegend	301016	B300873	0.6
CD3	PE-Cy5	UCHT1	Biolegend	301016	B300873	0.6
IFN γ	FITC	B27	Biolegend	506504	B286029	2.5
TNF	BV605	MAb11	Biolegend	502936	B327946	3.75
IL-2	APC	MQ1-17H12	Biolegend	500310	B313276	2.5
IL-17a	PE-Cy7	BL168	Biolegend	512315	B325831	3.75
GRZB	BV421	QA18A28	Biolegend	396414	B311965	2.5
CD107a	PE	H4A3	Biolegend	328608	B321484	0.3

Table 7. List of monoclonal antibodies used in the ICS assay (De Biasi S., et al., 2024).

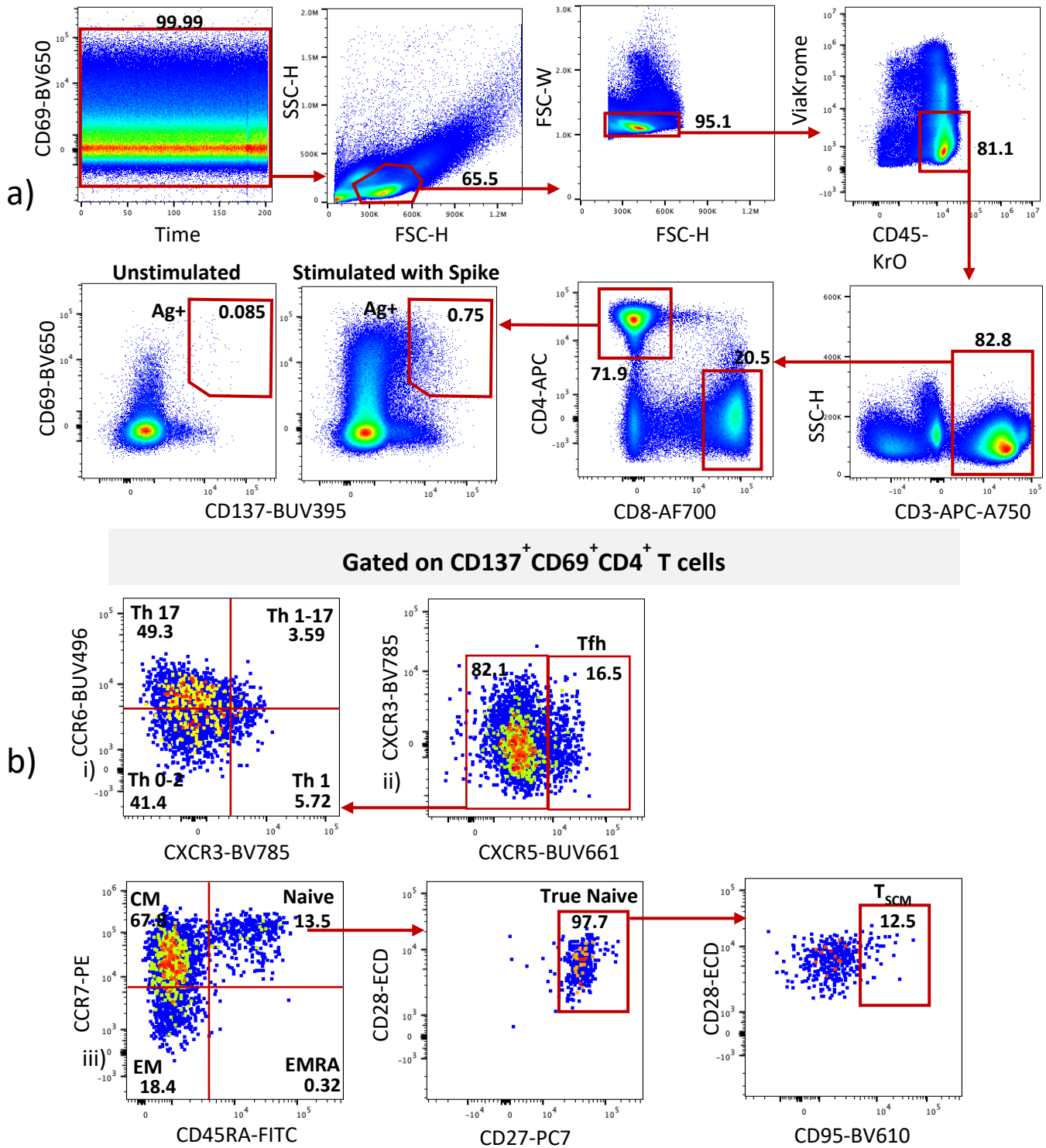


Figure 7. Gating strategy for the identification and characterization of antigen-specific CD4⁺ T cells (AIM assay). **(a)** A gate was set on CD69 vs TIME plot, then in this population, a gate was set according to physical parameter (FSC and SSC. Further gating is done in an FSC-H and FSC-Width dot plot to eliminate doublets. On a bivariate plot of CD45 vs. ViaKrome (viability) select CD45⁺, ViaKrome⁻ cells (viable cells). On a bivariate plot of CD3 vs SSC-H select CD3 T lymphocytes. CD4⁺ T cells was selected and the percentage of Antigen-Specific (CD69⁺ CD137⁺) T cells was quantified. **(b)** Gating strategy to identify and characterize i) T helper (Th), ii) circulating T follicular helper (cTfh), iii) Naive, true naive and T_{SCM} among Ag⁺ CD4⁺ T cell populations. EM, effector memory; CM central memory; EMRA, terminally differentiated effector memory; T_{SCM} stem memory cell (De Biasi S., et al., 2024).

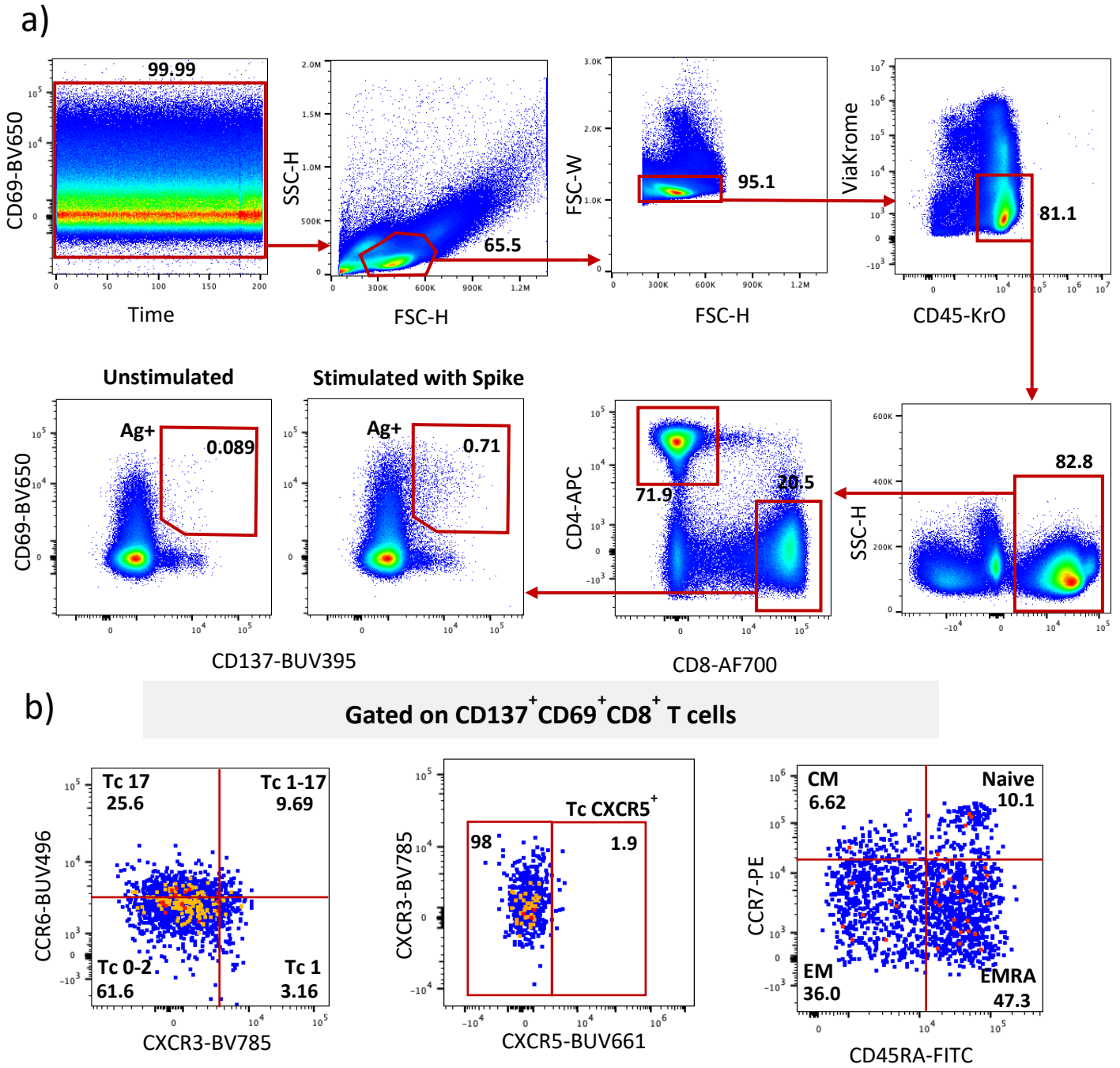


Figure 8. Gating strategy for the identification and characterization of antigen-specific CD8⁺ T cells (AIM assay). **(a)** A gate was set on CD69 vs TIME plot, then in this population, a gate was set according to physical parameter (FSC and SSC). Further gating is done in an FSC-H and FSC-Width dot plot to eliminate doublets. On a bivariate plot of CD45 vs. ViaKrome (viability) select CD45⁺, ViaKrome⁻ cells (viable cells). On a bivariate plot of CD3 vs SSC-H select CD3 T lymphocytes. CD4⁺ T cells was selected and the percentage of Antigen-Specific (CD69⁺ CD137⁺) T cells was quantified. **(b)** Gating strategy to identify and characterize i) T cytotoxic (Tc), ii) Tc CXCR5⁺, iii) Naive, true naive and T_{SCM} among Ag⁺CD4⁺ T cell populations. EM, effector memory; CM central memory; EMRA, terminally differentiated effector memory; T_{SCM} stem memory cell (De Biasi S., et al., 2024).

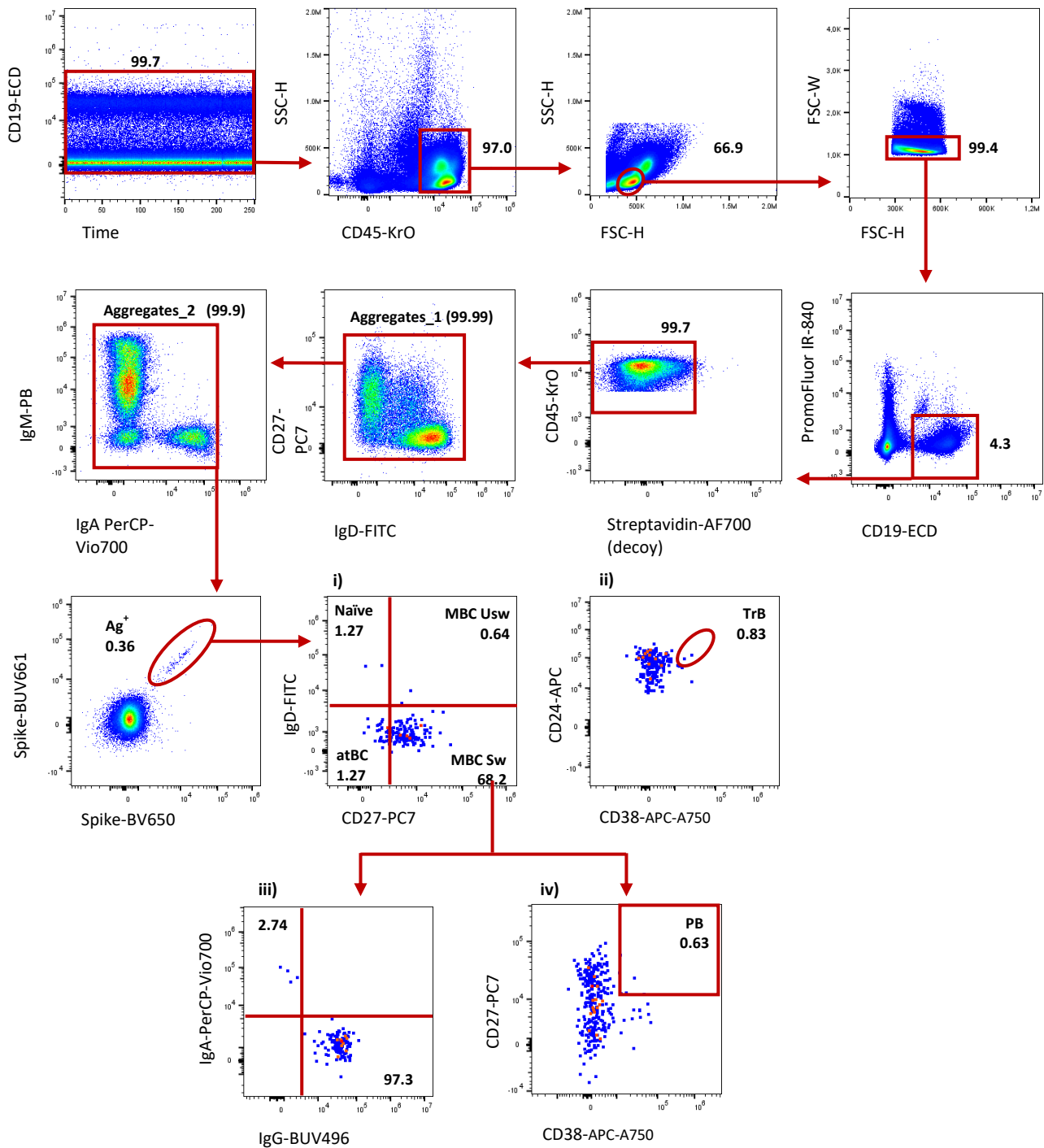


Figure 9. Gating strategy before computational analysis of Ag^+ B cells. The Time vs CD19-ECD gate was used to exclude unstable flow during acquisition. Leukocytes were selected as CD45⁺ cells. Next, lymphocytes were selected based on their physical characteristics, and doublets were excluded from the analysis by utilizing forward scatter height (FSC-H) and forward scatter width (FSC-W) parameters. Living B cells were selected as PromoFluor⁻ and CD19⁺. Aggregates were removed and Ag^+ (Spike-BUV661⁺ and Spike-BV650⁺) and Ag^- ((Spike-BUV661⁻ and Spike-BV650⁻) B cells were displayed. Inside Ag^+ B cells, we identified **i)** Naïve cells. Memory Unswitched B cells (MBC Usw). Memory Switched B cells (MBC Sw), and atypical B cells (atBC); **ii)** transitional B cells (TrB). Within MBC Sw gate, **iii)** the quadrant plots reported the different percentages of IgA⁺ IgG⁺ cells while **iv)** the dot plots plasmablast (PB) percentage (De Biasi S., et al., 2024).

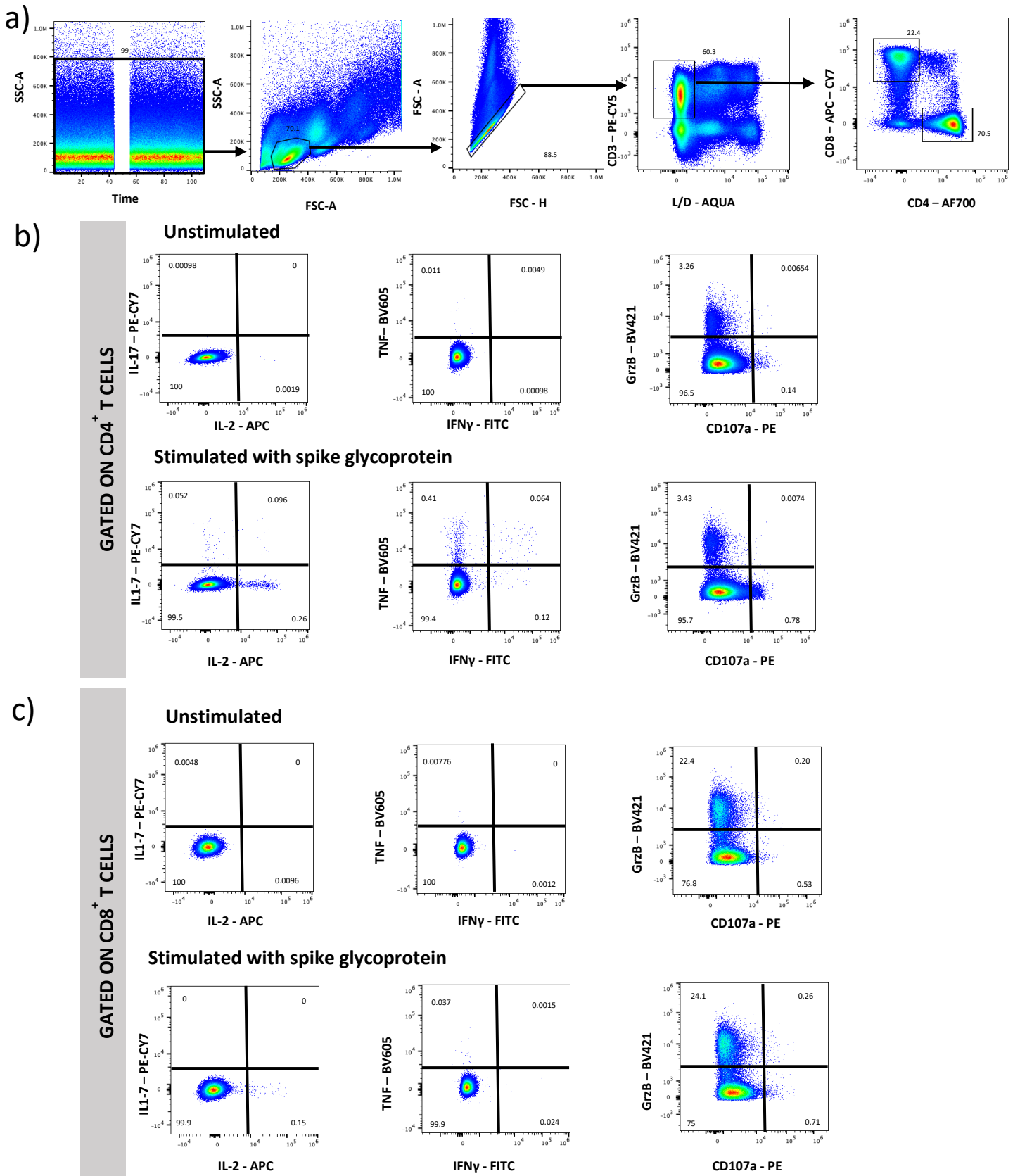


Figure 10. Gating strategy and representative plots of intracellular staining analysis of cytokine producing cells (ICS) after overnight stimulation with spike protein compared to unstimulated control. Cytokine production and polyfunctionality of antigen-specific CD4⁺ T cells (**panel b**) and CD8⁺ T cells (**panel c**). Numbers in the dot plots indicate the percentage of CD4⁺ and CD8⁺ cells identified by the gates. Comparison between the total production of IFN-g, TNF, IL-17, IL-2, CD107a, and GZMB (De Biasi S., et al., 2024).

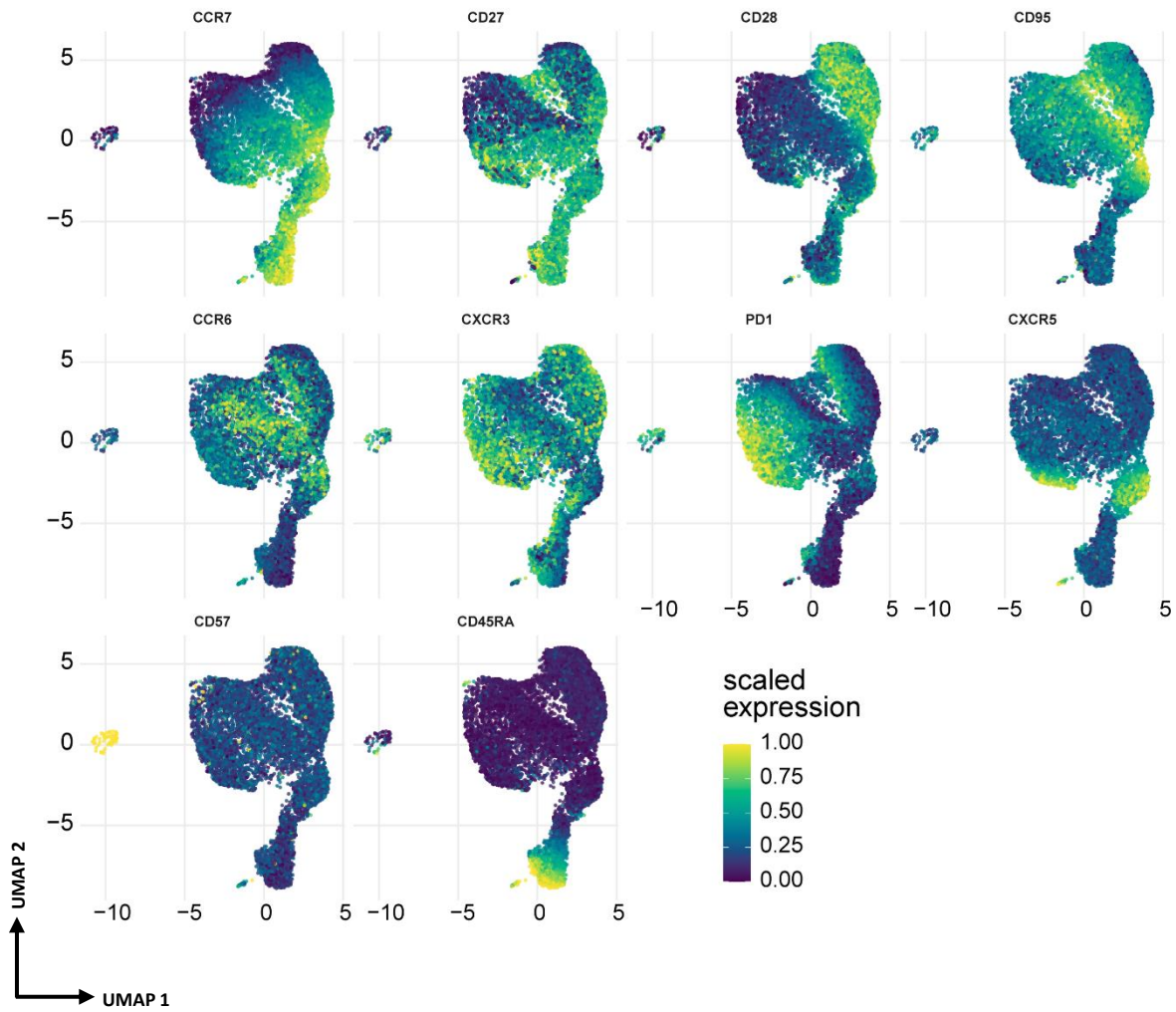


Figure 11. Uniform Manifold Approximation and Projection (UMAP) plot shows the 2D spatial distribution of cells from 28 healthy donors (HD) vaccinated against SARS-CoV2 and 106 patients with multiple sclerosis undergoing different disease-modifying therapies (DMT) and vaccinated against COVID-19. UMAP graphs are colored by the expression of ten different markers used for unsupervised analysis of CD4⁺ antigen specific T cells. Yellow: high expression. Dark blue: low expression (De Biasi S., et al., 2024).

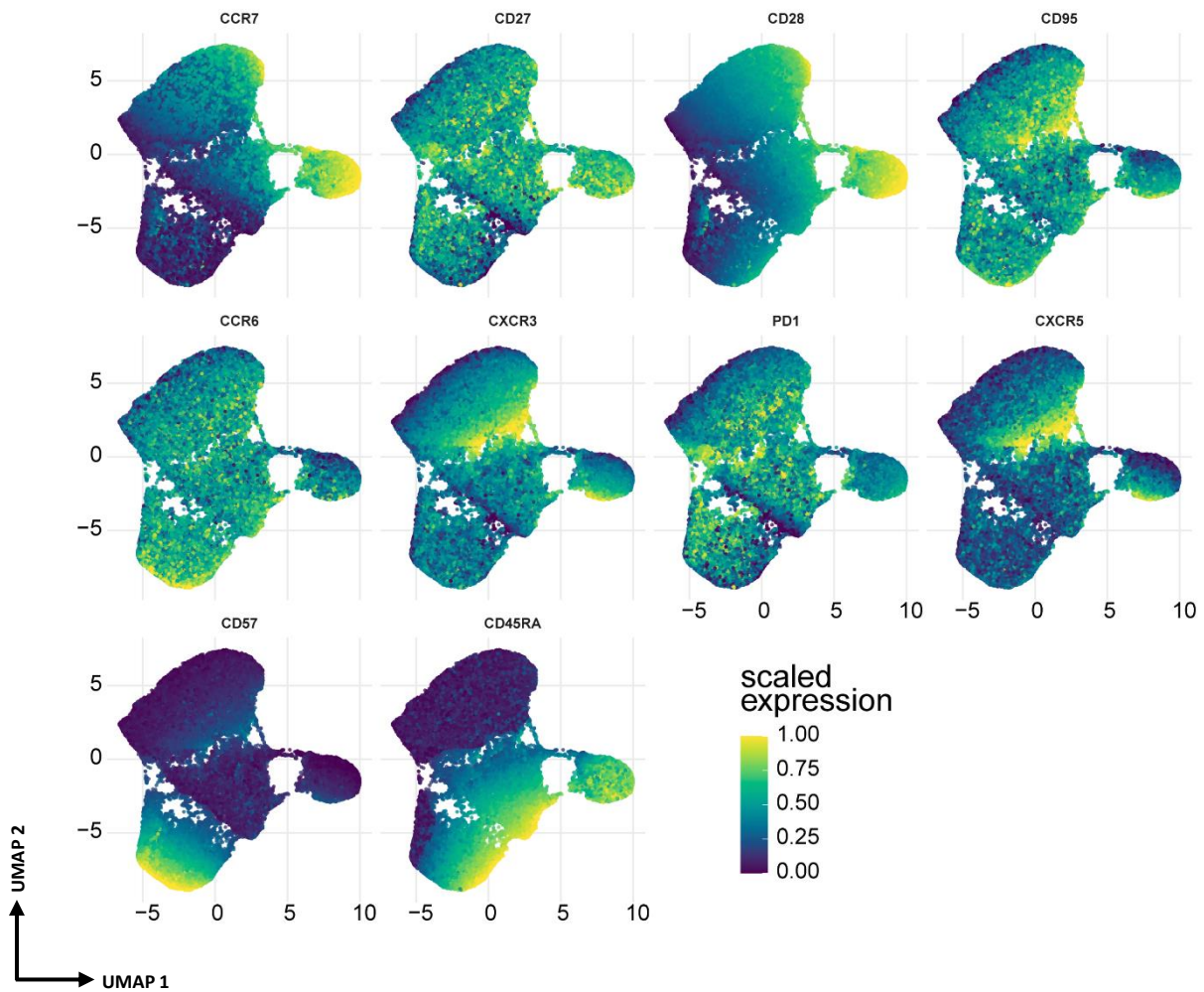


Figure 12. Uniform Manifold Approximation and Projection (UMAP) plot shows the 2D spatial distribution of cells from 28 healthy donors vaccinated against SARS-CoV2 and 106 patients with multiple sclerosis undergoing different disease-modifying therapies (DMT) and vaccinated against COVID-19. UMAP graphs colored by the expression of 10 markers used for CD8⁺ antigen specific T cell. Blue represents lower expression while yellow represent higher expression (De Biasi S., et al., 2024).

4. RESULTS

4.1 Polyfunctional CD4⁺ and CD8⁺ T cells analysis in COVID-19 infected or recovered patients

4.1.1 Characteristics of the Patients

We studied a total of 28 patients with COVID-19 pneumonia admitted into the Infectious Diseases Clinics or to the Intensive Care Unit (ICU) of the University Hospital in Modena over the period of March 2020–May 2020, and 10 healthy donors.

Characteristics of patients are reported in **Table 8**. COVID-19 moderate and COVID- severe presented higher levels of LDH when compared to recovered moderate and recovered severe, respectively. Regarding SARS-CoV-2 specific IgM and IgG, even if IgM were more represented among patients with moderate disease, no statistically significant differences were found between those with COVID-19 and the recovered, while HD tested negative for both assays. One patient from the COVID-19 severe group and one from the recovered severe group presented type 2 diabetes. Recovered moderate and recovered severe were hospitalized and diagnosed with SARS-CoV-2 infection 120 ± 18 (mean \pm SD) days and 128 ± 3 (mean \pm SD) days, respectively, before blood withdrawal.

An example of the gating strategy for the identification of cells able to exert one or more functions is reported in **Figure 13**. Peripheral blood mononuclear cells (PBMCs) were stimulated or not with M, N or S peptide pool, cultured and stained. PBMCs were first gated according to their physical parameters, and the aggregates were electronically removed from the analysis by using a gate designed for singlets. Living (Live/Dead, L/D-) cells and CD3⁺ T cells were identified. Among CD3⁺ cells, CD4⁺ and CD8⁺ T cell subpopulations were identified. In each subpopulation, the percentage of cells producing interferon IFN- γ , TNF, IL-2, IL-17, and GRZB, as well as expression of CD107a, was then quantified.

4.1.2 Recovered Patients Who Experienced a Severe Disease Display High Percentage of Antigen-Specific CD4⁺ T Cells Producing Th1 and Th17 Cytokines

Cytokine production was assessed following 16 h of in vitro stimulation with SARS- CoV-2 peptide pools covering the sequence of different proteins (N, M or S). The percentage of CD4⁺ and CD8⁺ T cells producing IFN- γ , TNF, IL-2, IL-17, and GRZB was quantified along with the

percentage of cells able to express CD107a. The identification of these cytokines allows us to recognize different subsets of helper CD4⁺ and CD8⁺ T cells, such as: (i) Th1, defined as cells producing IFN- γ , TNF, IL-2; (ii) Th17 identified as cells producing IL-17; (iii) cytotoxic T cells, which are positive for GRZB and CD107a [250,136].

Individuals who recovered from a severe form of COVID-19 disease showed a higher percentage of CD4⁺ T cells responding to N and S compared to healthy donors (HD) (**Figure 14a**). Moreover, taking into consideration all the stimuli used, patients who recovered from a severe disease exhibited a higher percentage of CD4⁺ T cells producing IFN- γ , TNF and IL-2 compared to either HD or individuals who recovered from moderate disease (**Figure 14b**). This was also observed when COVID-19 patients with a moderate disease were compared to HD. Furthermore, recovered individuals who experienced a severe disease also displayed a higher percentage of CD4⁺ T cells producing IL-17 compared to recovered moderate, regardless of the stimulus used (**Figure 14b**). On the other hand, COVID-19 patients with severe infection were characterized by higher proportions of cells expressing CD107a compared to HD after M and S stimulation, indicating a more enhanced cytotoxic phenotype (**Figure 14b**).

Regarding CD8⁺ T cell response, the percentage of CD8⁺ T cells responding to peptide pool stimulation was higher in COVID-19 patients with a moderate disease compared to either HD or recovered individuals who experienced a moderate infection. In addition, COVID-19 patients with severe form exhibited a higher percentage of responding CD8⁺ T cells compared to those who recovered from a severe form (**Figure 15a**). Furthermore, after in vitro stimulation with M, COVID-19 severe patients displayed a higher percentage of CD8⁺ T cells expressing CD107a compared to individuals who recovered from severe infection (**Figure 15b**). Thus, antigen-specific CD8⁺ T cells are more abundant among COVID-19 patients and present a more pronounced cytotoxic phenotype in line with their role in mediating clearance during viral infections [251].

4.1.3 Recovered Patients Who Experienced a Severe Disease Are Characterized by Polyfunctional SARS-CoV-2 Antigen-Specific CD4⁺ T cells

In vitro stimulation with the M peptide pool induced a different polyfunctional profile between COVID-19 moderate and severe patients, COVID-19 severe patients and those who recovered from severe disease. Moreover, the polyfunctional response was different when compared to HD in either patients with moderate COVID-19 or those who recovered from severe disease. In particular, COVID-19 moderate patients and recovered individuals from severe disease, when compared to HD, reported higher percentages of IFN- γ +IL-2+TNF⁺, IFN- γ +TNF⁺ and IL-2+TNF⁺ within CD4⁺ T

cells. Patients experiencing COVID-19 moderate also displayed a high percentage of IFN- γ +IL-2+ within CD4⁺ T cells. The percentage of the latest population was higher in COVID-19 severe and recovered moderate if compared to recovered severe and HD (**Figure 16a**).

Stimulation with N induced differences in the overall polyfunctionality of CD4⁺ T cells between patients who recovered (moderate vs. severe) and between COVID-19 severe patients and those who recovered from severe disease. Finally, COVID-19 moderate patients and recovered displayed a different cytokine profile when compared to HD. Regarding the subsets of polyfunctional CD4⁺ T cells, individuals who recovered from the severe disease exhibited the same cytokine production as seen with M stimulation. In addition, this group of patients presented a small population of TNF⁺, IL-17⁺ cells. COVID-19 moderate patients, compared to HD, also presented a high percentage of IFN- γ +IL-2+TNF⁺ and IL-2+TNF⁺ (**Figure 16b**). Finally, after stimulation with S, individuals who recovered from different disease severity showed a different polyfunctionality as well as COVID-19 moderate patients and recovered from the moderate disease. In addition, recovered from severe disease displayed a distinct polyfunctional asset compared to COVID-19 severe and HD. Individuals who recovered from severe disease presented almost overlapping results as those observed after stimulation with N and M. Moreover, they also displayed a higher percentage of TNF+IL-17+ within CD4⁺ T cells if compared to COVID-19 severe and HD. Regarding COVID-19 moderate, the cell distribution after stimulation is the same as the one measured after N stimulation (**Figure 16c**). For clarity, **Figure 16d** shows the legend of the colors and symbols of the previous **Figure 16** panels.

The polyfunctional profile of CD8⁺ T cells after in vitro stimulation with M or N was similar among the groups. Only the S peptide pool induced a slightly different profile in COVID-19 moderate patients when compared to HD (**Figure 17**).

Table 8. Demographic and clinical characteristics of healthy donors (HD), COVID-19 and recovered patients (Paolini A., et al., 2022)

Variable	HEALTHY DONOR (N=10)	COVID-19 MODERATE (N=7)	COVID-19 SEVERE (N=6)	RECOVERED MODERATE (N=9)	RECOVERED SEVERE (N=6)	p-value COVID-19 MODERATE E vs COVID-19 SEVERE	p-value COVID-19 MODERATE E vs RECOVERED MODERATE	p-value RECOVERED MODERATE vs RECOVERED SEVERE	p-value COVID-19 SEVERE vs RECOVERED SEVERE
Demographic characteristics									
Age (median years, range) ¹	49.5 (37-70)	55.0 (43-65)	63.0 (53-68)	56.0 (36-63)	56.5 (43-61)	ns	ns	ns	ns
Sex (M, %) ²	5 (50)	6 (85.7)	6 (100)	5 (55.6)	4 (66.7)	ns	ns	ns	ns
Clinical characteristics									
<i>Coexisting conditions</i>									
Type 2 diabetes, N (%) ²	/	0 (0)	1 (16.7)	0 (0)	1 (16.7)	ns	ns	ns	ns
Cardiovascular Dis., N (%) ²	/	0 (0)	0 (0)	0 (0)	0 (0)	NA	NA	NA	NA
Chronic Kidney Dis., N (%) ²	/	0 (0)	0 (0)	0 (0)	0 (0)	NA	NA	NA	NA
Cancer., N (%) ²	/	0 (0)	0 (0)	0 (0)	0 (0)	NA	NA	NA	NA
Clinical Blood parameters									
Total bilirubin, mg/dL (median, range) ¹	/	1.0 (0.6-1.4)	0.8 (0.3-0.9)	0.7 (0.3-0.9)	0.4 (0.3-0.8)	ns	ns	ns	ns
CK, U/L (median, range) ¹	/	81.0 (56-154)	34.5 (23-259)	102.0 (87-139)	139.0 (12-282)	ns	ns	ns	ns
Creatinine, mg/dL (median, range) ¹	/	0.8 (0.6-1.0)	0.6 (0.5-0.8)	0.9 (0.7-1.1)	0.9 (0.8-1.2)	ns	ns	ns	ns
D-dimer, ng/mL (median, range) ¹	/	495 (230-7,810)	750 (190-5,820)	180 (100-340)	255 (140-780)	ns	ns	ns	ns
LDH, U/L (median, range) ¹	/	591 (580-886)	581 (507-1,521)	361 (244-450)	384 (337-430)	ns	0.0272	ns	0.0272
CRP, mg/dL (median, range) ¹	/	0.3 (0.2-0.9)	0.35 (0.2-12.1)	0.2 (0.2-0.3)	0.2 (0.2-0.4)	ns	ns	ns	ns
Blood cell count									
White blood cells, N/uL (median, range) ¹	/	7,500 (2,888-10,880)	6,305 (4,800-15,300)	6,480 (4,420-7,160)	6,985 (6,340-7,680)	ns	ns	ns	ns
Lymphocytes, N/uL (median, range) ¹	/	2,898 (2,698-3,098)	1,642 (629-2,460)	2,240 (1,600-7,160)	2,615 (2,120-3,740)	ns	ns	ns	ns
Neutrophils, N/uL (median, range) ¹	/	6,390 (5,545-7,235)	3,818 (1,906-14,560)	3,120 (2,430-2,980)	3,755 (3,060-3,900)	ns	ns	ns	ns
Detection of SARS-CoV-2 IgM, IgG									
IgM, Index (median, range) ¹	0.0	28.7 (5.7-59.1)	6.4 (1.2-66.3)	4.7 (0.3-28.6)	4.5 (0.5-20.0)	ns	ns	ns	ns
IgG, Index (median, range) ¹	0.0	7.3 (6.3-9.0)	6.2 (1.5-8.6)	6.1 (2.0-9.4)	3.9 (1.2-7.0)	ns	ns	ns	ns

NA; not applicable

¹Kruskal-Wallis test with original FDR method of Benjamini and Hochberg

²Chi-square test

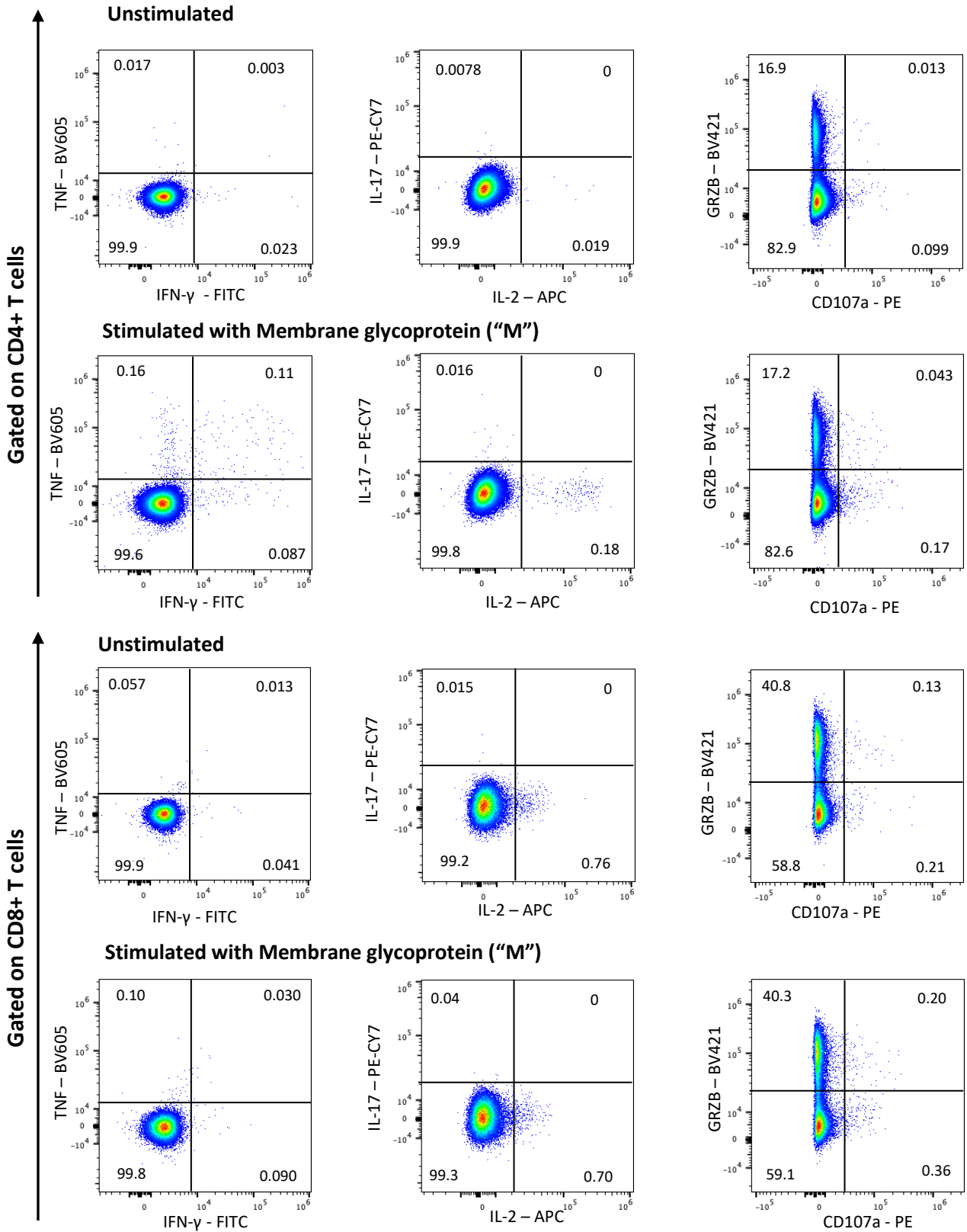
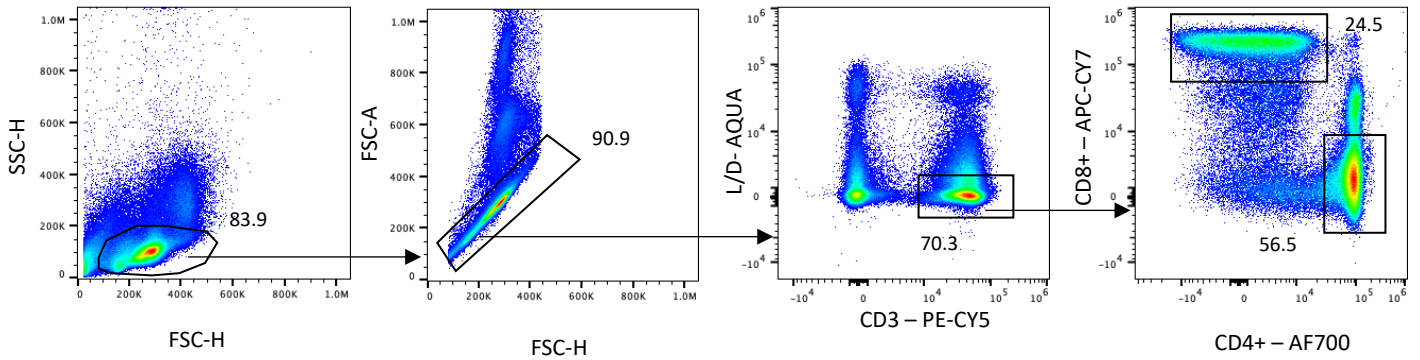


Figure 13. Gating strategy for the identification of CD4⁺ and CD8⁺ T lymphocytes for the analysis of intracellular cytokines. PBMCs were gated according to physical parameters and aggregates were removed from the analysis. Living (Live/Dead, L/D-) cells and CD3 T cells were identified; among CD3 cells, CD4⁺ and CD8⁺ T cell subpopulations were identified. In the quadrants the percentages of CD3⁺, CD4⁺ or CD8⁺ T cells are shown, along with the percentages of cells producing IFN- γ , TNF, IL-2, IL-17, GRZB as well as expression of CD107a (Paolini A., et al., 2022).

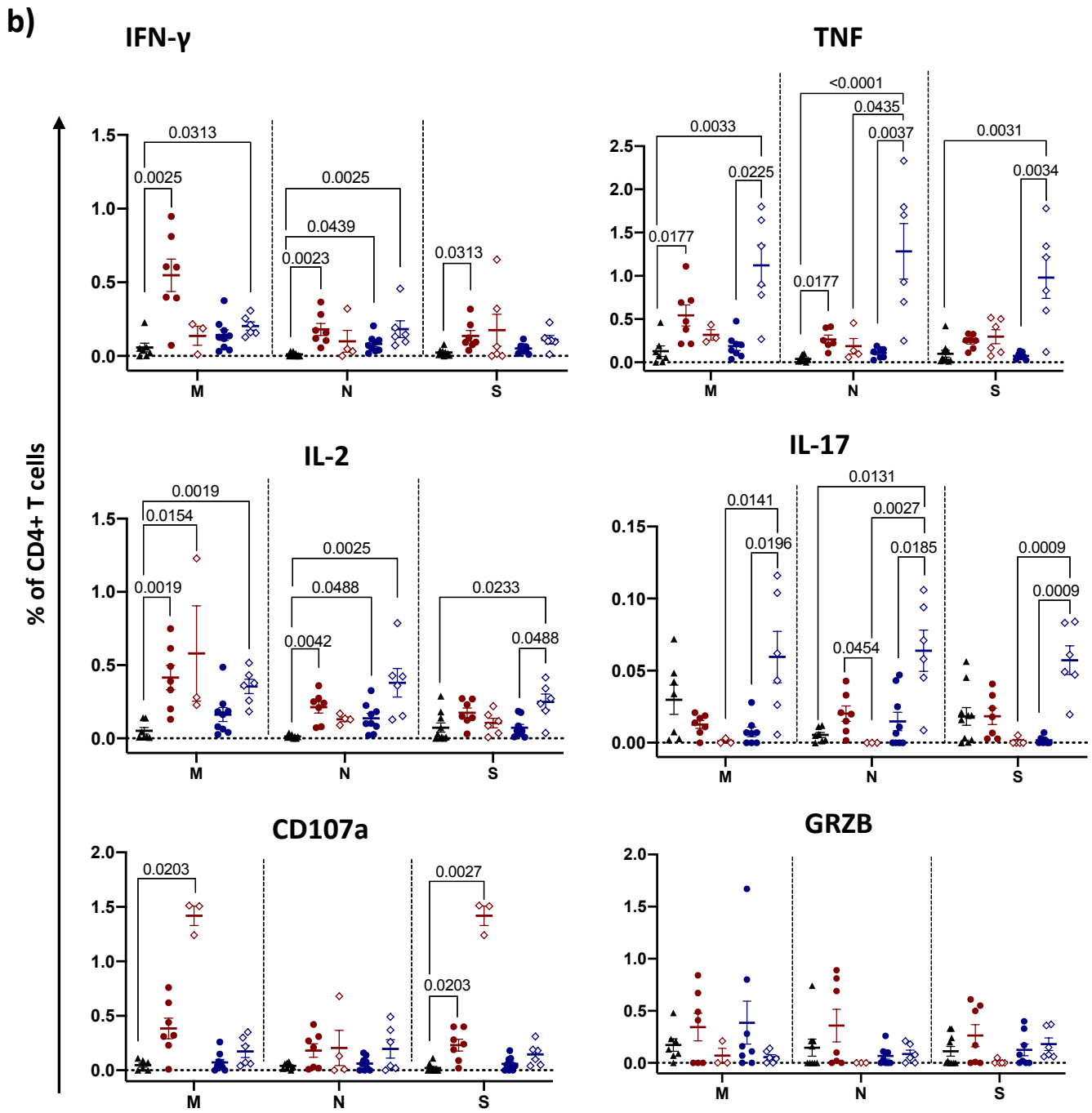
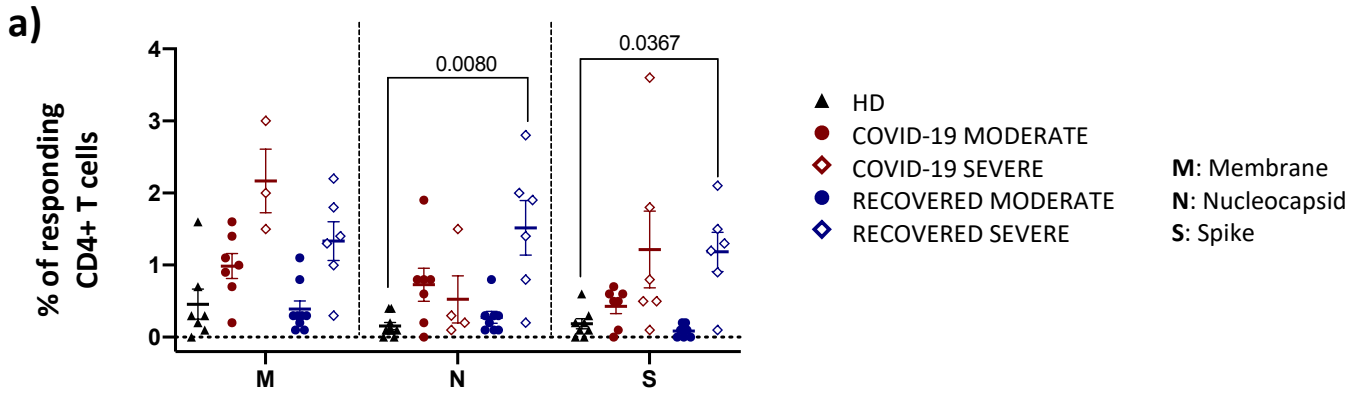
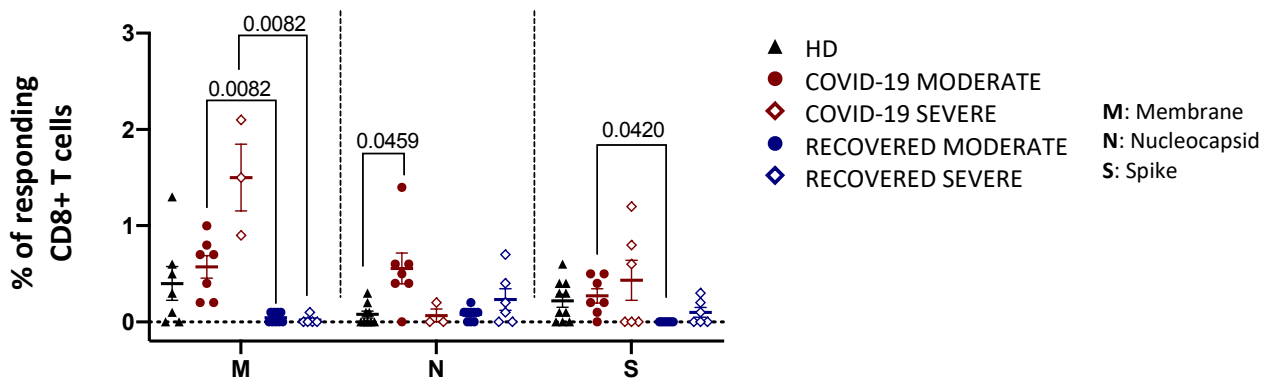


Figure 14. Total cytokine production by CD4⁺ T cells after *in vitro* stimulation. a) Percentage of responding CD4⁺ T cells after stimulation with M, N or S. Data represent individual values from healthy donors (HD, n=10), COVID-19 moderate (n=7), COVID-19 severe (n=6), recovered moderate (n=9) and recovered severe (n=6). Mean (center bar) ± standard error of the mean (SEM, upper and lower bars) is represented. Statistical analysis was performed using Kruskal-Wallis non-parametric test corrected for multiple comparisons by controlling the False Discovery Rate (FDR), method of Benjamini and Hochberg. Statistically significant q values are represented. Background was subtracted from each sample. b) Representation of the total production of each cytokine after stimulation of CD4⁺ T cells. We evaluated the percentage of CD4⁺ T cells producing IFN-γ, TNF, IL-2, IL-17, GRZB as well as expressing CD107a among HD (n=10), COVID-19 moderate (n=7), COVID-19 severe (n=6), recovered moderate (n=9) and recovered severe (n=6). Data are represented as individual values, mean (center bar) ± standard error of the mean (SEM, upper and lower bars) is represented. Statistical analysis was performed using Kruskal-Wallis non-parametric test corrected for multiple comparisons by controlling the False Discovery Rate (FDR), method of Benjamini and Hochberg. Statistically significant q values are represented. Background (i.e., the value determined in unstimulated controls) was subtracted from each sample (Paolini A., et al., 2022).

a)



b)

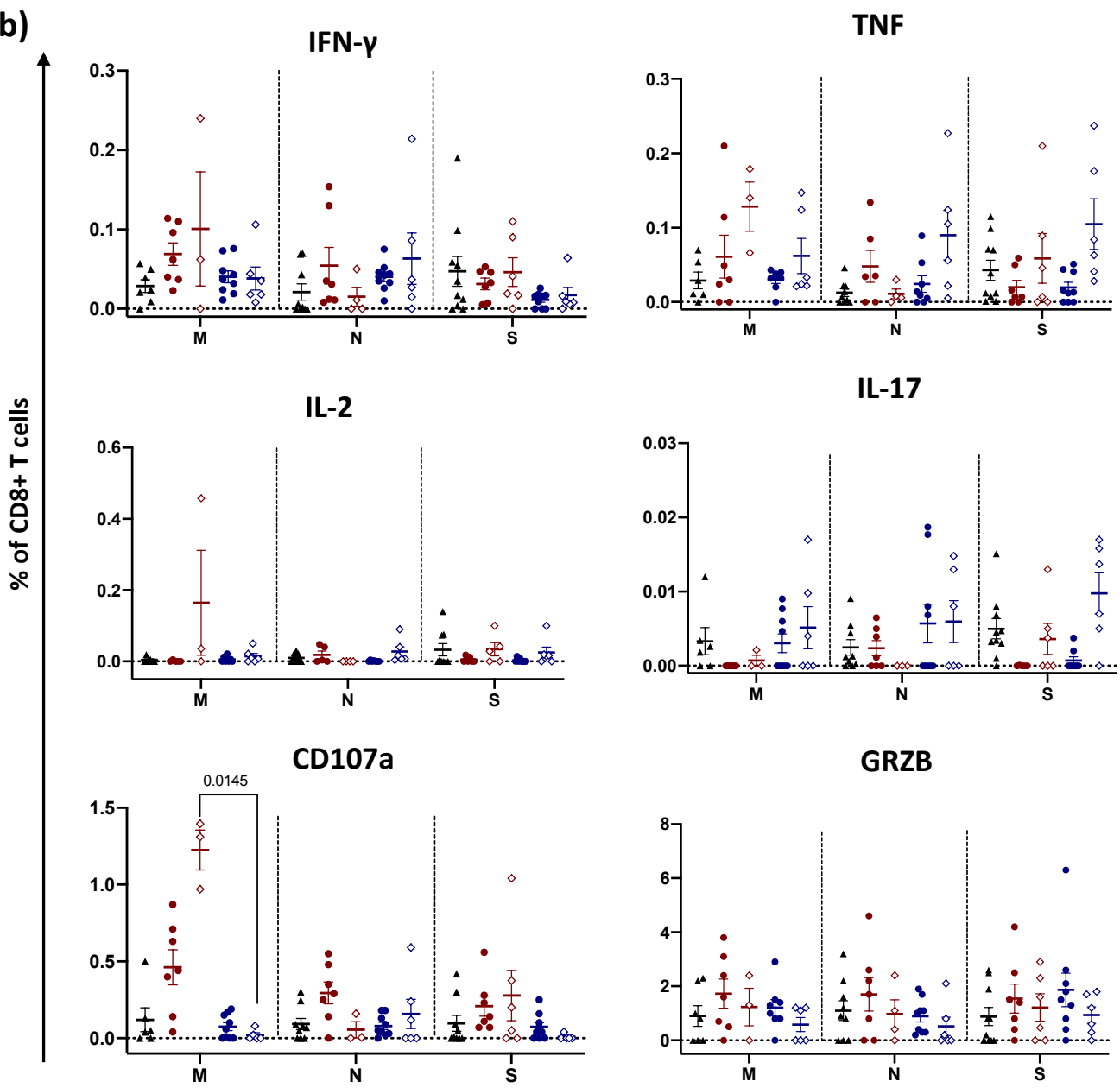
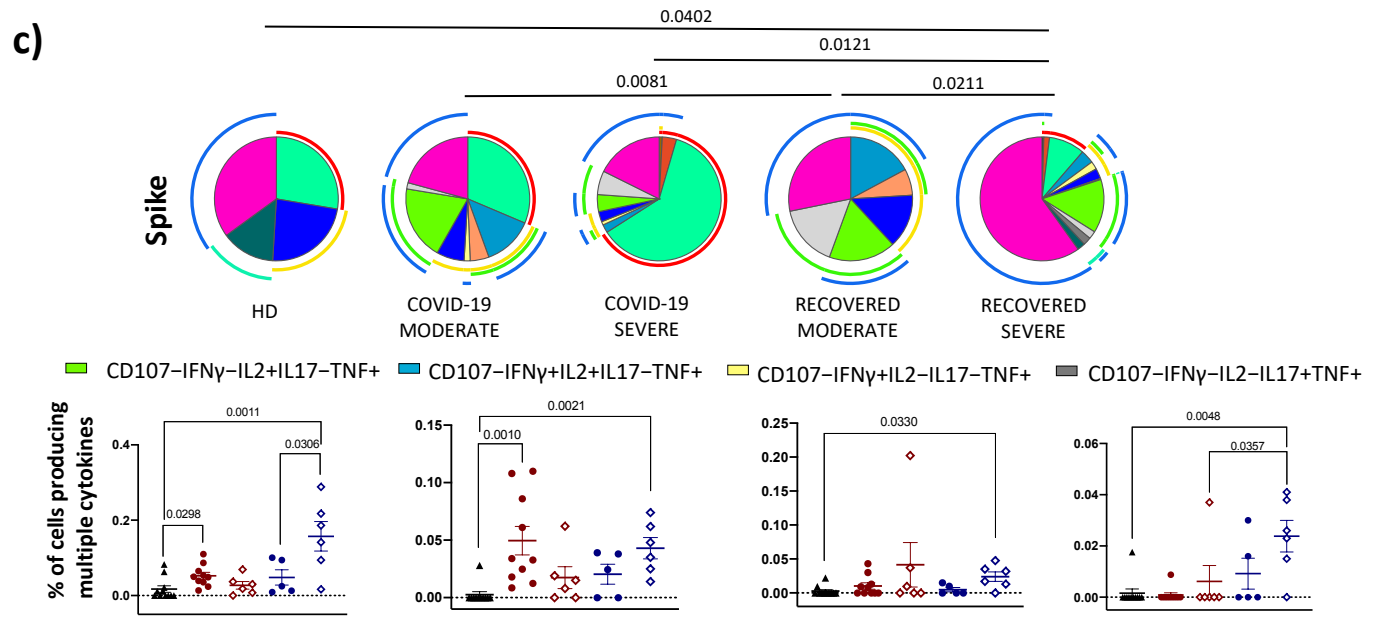
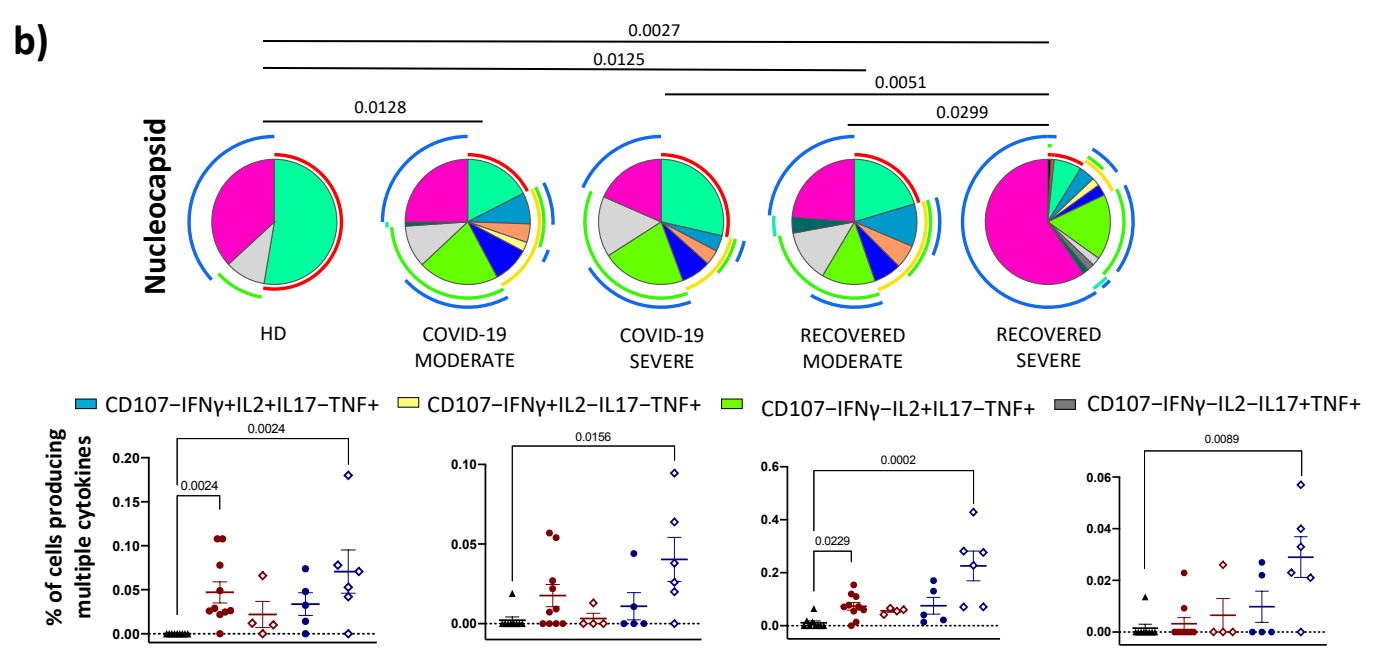
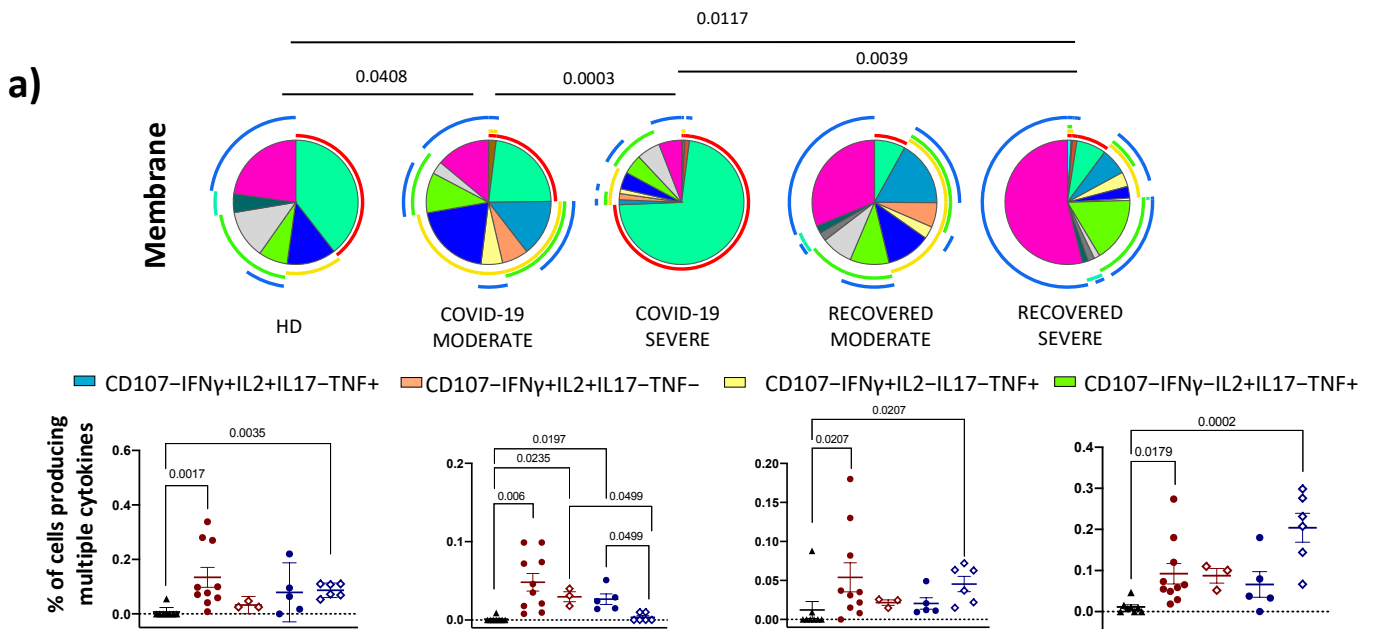


Figure 15. Total cytokine production by CD8⁺ T cells after *in vitro* stimulation. a) Percentage of responding CD8⁺ T cells after stimulation with M, N or S. Data represent individual values from HD (n=10), COVID-19 moderate (n=7), COVID-19 severe (n=6), recovered moderate (n=9) and recovered severe (n=6). Mean (center bar) ± standard error of the mean (SEM, upper and lower bars) is represented. Statistical analysis was performed using Kruskal-Wallis non-parametric test corrected for multiple comparisons by controlling the False Discovery Rate (FDR), method of Benjamini and Hochberg. Statistically significant q values are represented. Background was subtracted from each sample. b) Representation of the total production of cytokines after stimulation of CD8⁺ T cells. We evaluated the percentage of CD8⁺ T cells producing IFN- γ , TNF, IL-2, IL-17, GRZB as well as expressing CD107a among HD (n=10), COVID-19 moderate (n=7), COVID-19 severe (n=6), recovered moderate (n=9) and recovered severe (n=6). Data are represented as individual values, mean (center bar) ± standard error of the mean (SEM, upper and lower bars) is represented. Statistical analysis was performed using Kruskal-Wallis non-parametric test corrected for multiple comparisons by controlling the False Discovery Rate (FDR), method of Benjamini and Hochberg. Statistically significant q values are represented. Background (i.e., the value determined in unstimulated controls) was subtracted from each sample (Paolini A., et al., 2022).



d)

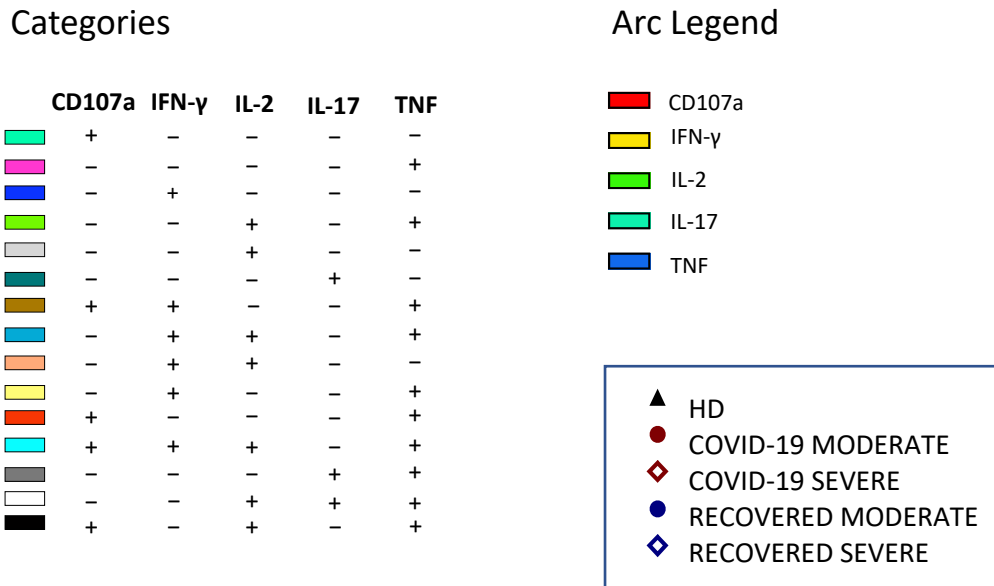


Figure 16. Polyfunctionality of CD4⁺ T cells after *in vitro* stimulation. Pie charts representing the proportion of CD4⁺ T cells producing different combinations of IFN- γ TNF, IL-2, IL-17, GRZB as well as expressing CD107a after stimulation with a) M; b) N; or c) S peptide pools from HD (n=10), COVID-19 moderate (n=7), COVID-19 severe (n=6), recovered moderate (n=9) and recovered severe (n=6) patients. For clarity, panel d reports the legend for the colours and the symbols used in panels a, b and c. Data in pie charts are represented as median values. Frequencies were corrected by background subtraction as determined in non-stimulated controls using SPICE software. Statistical analysis between pie charts was performed using permutation test. Pie arches represent the total production of different cytokines. Comparison between the production of different combinations of cytokines by CD4⁺ T cells is represented. Data are represented as individual values, mean (center bar) \pm standard error of the mean (SEM, upper and lower bars) is represented. Statistical analysis was performed using Kruskal-Wallis non-parametric test corrected for multiple comparisons by controlling the False Discovery Rate (FDR), method of Benjamini and Hochberg. Statistically significant q values are represented (Paolini A., et al., 2022).

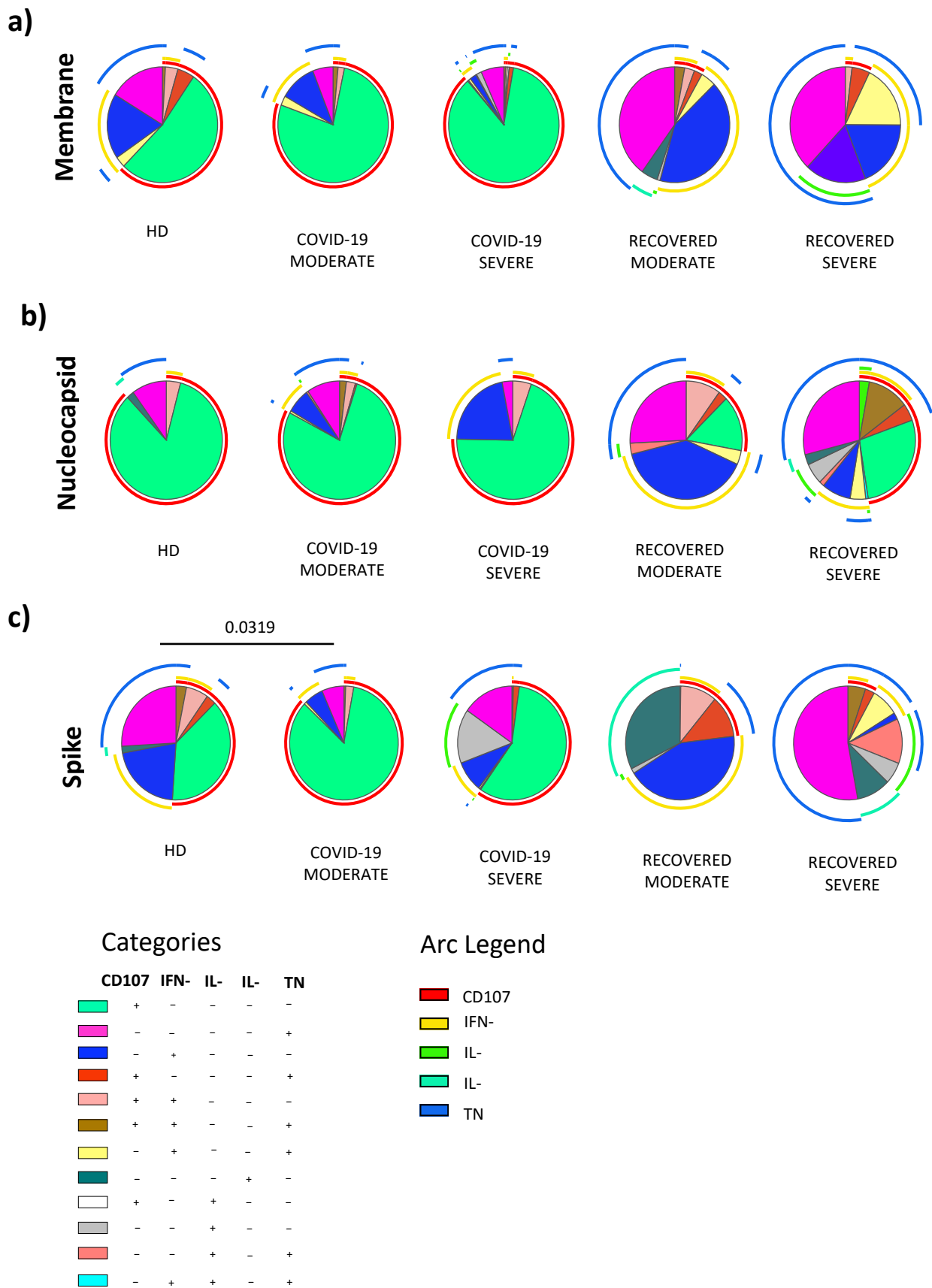


Figure 17. Polyfunctionality of CD8⁺ T cells after *in vitro* stimulation. Pie charts representing the proportion of CD8⁺ T cells producing different combinations of IFN- γ , TNF, IL-2, IL-17, GRZB as well as expressing CD107a after stimulation with a) M; b) N; or c) S peptide pools from HD (n=10), COVID-19 moderate (n=7), COVID-19 severe (n=6), recovered moderate (n=9) and recovered severe (n=6) patients. Data in pie charts are represented as median values. Frequencies were corrected by background subtraction as determined in non-stimulated controls using SPICE software. Statistical analysis between pie charts was performed using permutation test. Pie arches represent the total production of different cytokines (Paolini A., et al., 2022).

4.2 Characterization of SARS-CoV-2-specific T and B cells after infection or heterologous vaccination

4.2.1 Study design

Three groups of donors were enrolled in this study. The first one was composed of nine COVID-19 recovered patients (hereafter called REC; mean age of 35.1 ± 11.1 years), with a mean of 131.1 days (range 64–165 days) from last infection during follow-up visits at the Infectious Diseases Clinics of the Azienda Ospedaliero-Universitaria Policlinico di Modena. All REC had symptoms consistent with COVID-19 and positive PCR-based testing for SARS-CoV-2 over the period of March 2020–August 2020. Within this group, four patients were classified as severe (35.3 ± 5.68 years) while five patients were moderate (35.0 ± 7.4) according to World Health Organization guidelines [244]. Given that there were no differences between moderate and severe recovered individuals and their low number, they were considered as a unique group for the statistical analysis. Twenty-three vaccinated donors were enrolled in this study, and they were divided into two groups: one was composed of 11 donors with a mean of 31.1 days (range 30–35 days) after the third dose of SARS-CoV-2 vaccine (hereafter defined MIX; 27.0 ± 4.5 years); these subjects were vaccinated with three different vaccines (first dose: ChAdOx1; second dose: BNT162b2; third dose: mRNA-1273). The second group was composed of 12 donors with a mean of 33.9 days (range 26–44 days, hereafter defined RNA; 35.3 ± 11.3 years) after being vaccinated with two different RNA vaccines (first and second doses: BNT162b2; third dose: mRNA-1273). Each participant, including healthy donors, provided informed consent according to the Helsinki Declaration, and all uses of human material have been approved by the local Ethics Committee (Comitato Etico dell'Area Vasta Emilia Nord, protocol number 177/2020, 11 March 2020) and by the University Hospital Committee (Direzione Sanitaria dell'Azienda Ospedaliero Universitaria di Modena, protocol number 7531, 11 March 2020). The clinical characteristics of all participants are reported in **Table 9**.

4.2.2 MIX showed a skewed Th1 Ag-specific CD4⁺ T-cell polarization compared to that of recovered ones

To investigate the percentage of Ag-specific T cells, we used T-cell receptor (TCR)-dependent activation-induced marker (AIM) assays to identify and quantify SARS-CoV-2-specific CD4⁺ T cells. We stimulated peripheral blood mononuclear cells (PBMCs) from nine REC patients and 11 MIX and 12 RNA donors overnight with 15-mer peptides with 11-amino acid overlap, covering the complete sequence of Wuhan SARS-CoV-2 spike glycoprotein (see *Methods* for details).

The phenotype of Ag-specific T cells (i.e., those CD137⁺CD69⁺) within CD4⁺ T cells, hereafter termed Ag⁺CD4⁺T cells, was first analyzed by manual gating and compared with the non-Ag-specific CD4⁺T cell counterparts (CD137⁻CD69⁻, hereafter called Ag⁻CD4⁺). Ag⁺CD4⁺ T cells showed different cell subset distributions (in terms of the expression of differentiation markers such as CD45RA, CCR7, CD28, and CD95) and Th cell polarization (evaluated by the expression of CCR6 and CXCR3). Ag⁺CD4⁺ T displayed a low percentage of naive (N, CD45RA⁺CCR7⁺CD28⁺CD95⁻) and higher frequencies of memory compartment such as central memory (CM; CD45RA⁻CCR7⁺CD28⁺CD95⁺), transitional memory (TM; CD45RA⁻CCR7⁻CD28⁺CD95⁺), effector memory (EM; CD45RA⁻CCR7⁻CD28⁻CD95⁺), and T_{SCM} (CD45RA⁺CCR7⁺CD28⁺CD95⁺) and a similar percentage of terminally differentiated effector memory (EMRA; CD45RA⁺CCR7⁻CD28⁻CD95⁺) (**Figure 18a, b**). Considering T-cell polarization, in comparison with Ag⁻CD4⁺ T cells, those Ag-specific displayed a higher percentage of Th1 (CXCR3⁺CCR6⁻), Th17 (CXCR3⁻CCR6⁺), and Th1/Th17 (CXCR3⁺CCR6⁺) and a lower percentage of Th0/Th2 (CXCR3⁻CCR6⁻) (**Figure 18c**).

To gain a more detailed overview on the differentiation status and Th-polarization, we took advantage of unsupervised FlowSOM clustering. This analysis revealed a total of 19 clusters, and within these, six clusters represented SARS-CoV-2-reactive CD4⁺ T cells expressing CD69 and CD137 (**Figure 19a, b; Figure 4**). The frequencies of the different clusters of T cells within Ag⁻CD4⁺ T cells were similar in the three groups of individuals as shown in **Figure 20**. We focused our attention on Ag⁺CD4⁺ T cells that were selected and reclustered. We obtained 10 clusters, representing different subpopulations of Ag⁺ T cells. We found naive T cells that were defined as CD45RA⁺CCR7⁺CD27⁺CD95⁻, T_{SCM} as CD45RA⁺CCR7⁺CD27⁺CD95⁺, CM Th1 as CCR7⁺CD45RA⁻CCR6⁻CXCR3⁺ (CM Th1), CM Th0/Th2 as CCR7⁺CD45RA⁻CCR6⁻CXCR3⁻, CM Th17 as CCR7⁺CD45RA⁻CCR6⁺CXCR3⁻, CM CXCR5⁺ as CCR7⁺CD45RA⁻CXCR5⁺PD-1⁻, circulating T follicular helper as CCR7⁺CD45RA⁻CXCR5⁺PD-1⁺ (cTfh), TM Th1 as CCR7⁻CD45RA⁻CD28⁺CXCR3⁺ (TM Th1), TM Th0/Th2 as CCR7⁻CD45RA⁻CD28⁺CCR6⁻CXCR3⁻, and TM Th17 as CCR7⁻CD45RA⁻CD28⁺CCR6⁺CXCR3⁻ (**Figure 19c**).

The percentage of total CD4⁺ and Ag⁺ CD4⁺ T cells was similar among the three groups (**Figure 19d**). Despite that, within the latter, we observed a different distribution of the populations among REC and vaccinated groups (both MIX and RNA). RNA displayed higher percentages of CM Th1, CM Th0/Th2, and TM Th1 if compared to those in REC subjects. Moreover, both MIX and RNA showed a lower percentage of cTfh cells (**Figure 19e**). No differences were found between Ag⁺

CD4⁺ T-cell clusters of MIX and RNA. Similar percentages of all other clusters were present in REC, MIX, and RNA subjects (**Figure 21**).

4.2.3 Vaccinated individuals showed a higher percentage of Tc1-like Ag-specific CD8⁺ T cells compared to that of recovered subjects

The AIM assay was used for CD8⁺ T-cell analysis to identify and quantify SARS-CoV-2-specific (see *Methods*). We first manually gated different subpopulations of T cells on the basis of differentiation markers and cytotoxic-polarization markers (Tc-polarization). We observed that Ag⁺CD8⁺ T cells, if compared to Ag⁻CD8⁺ T lymphocytes, displayed lower percentages of N and higher percentages of T_{SCM}, CM, and TM; similar percentages of both EM and EMRA were found (**Figure 22a, b**). In terms of Tc-polarization, similar percentages of Tc1 cells were found within Ag⁺ and Ag⁻CD8⁺ T cells. However, Ag⁺CD8⁺ T cells were characterized by higher percentages of both Tc17 and Tc1/Tc17 and lower percentages of Tc0/Tc2 (**Figure 22c**).

As for CD4⁺ T-cell analysis, we applied unsupervised analysis and found 21 clusters, of which six were SARS-CoV-2-reactive CD8⁺ T cells (**Figure 23a, b; Figure 5a**). Considering Ag⁻CD8⁺ T cells, both MIX and RNA showed increased levels of TM Tc17 CD69⁺, TM Tc0/ Tc2, and TM Th0/Th2 PD-1⁺ CXCR5⁺ if compared to those of REC subjects. Furthermore, RNA showed a higher percentage of TM Tc1 PD-1⁺ CXCR5⁺ compared to those of REC and MIX (**Figure 24**). Ag⁺CD8⁺ T cells were selected and after reclustering, 11 clusters were identified. Besides naive T cells and T_{SCM}, defined as CD45RA⁺CCR7⁺CD27⁺CD28⁺CD95⁻ and CD45RA⁺CCR7⁺CD27⁺CD28⁺CD95⁺, respectively, we found two clusters of CM T cells defined as follows: CM Tc1 PD-1⁻ that were CD45RA⁻CCR7⁺CD28⁺CXCR3⁺PD-1⁻ and CM Tc1 PD-1⁺ that were CD45RA⁻CCR7⁺CD28⁺CXCR3⁺PD-1⁺.

Among effector Ag⁺CD8⁺ T cells, we found five clusters defined as TM Tc1 PD-1⁻ (CCR7⁻CD45RA⁻CD28⁺CXCR3⁺PD-1⁻), TM Tc1 PD-1⁺ (CCR7⁻CD45RA⁻CD28⁺CXCR3⁺PD-1⁺), TM Tc0/Tc2 (CCR7⁻CD45RA⁻CD28⁺CCR6⁻CXCR3⁻), TM Tc17 (CCR7⁻CD45RA⁻CD28⁺CCR6⁺CXCR3⁻), and EM Tc1 CD57⁺ PD-1⁺ (CCR7⁻CD45RA⁻CD28⁻CD57⁺PD-1⁺). Moreover, three populations of effector memory cells re-expressing CD45RA (EMRA) were detected, i.e., EMRA Tc1 CD57⁻ PD-1⁺ (CCR7⁻CD45RA⁺CXCR3⁺CD57⁻PD-1⁺), EMRA Tc1 CD57⁺ PD-1⁺ (CCR7⁻CD45RA⁺CXCR3⁺CD57⁺PD-1⁺), and EMRA Tc1 CD57⁺ PD-1⁻ (CCR7⁻CD45RA⁺CXCR3⁺CD57⁺PD-1⁻) (**Figure 23c**).

Similar percentages of total CD8⁺ and Ag⁺CD8⁺ T cells were found among the three groups (**Figure 15d**). However, within the Ag⁺ population, we observed increased percentages of EM Tc1 CD57⁺ PD-1⁺ in both vaccinated groups if compared to that in the recovered ones (**Figure 23e**). Furthermore, MIX and RNA showed increased levels of EMRA Tc1 CD57⁺ PD-1⁺ terminal effector CD8⁺ T cells compared to that in REC. Finally, we observed that the percentage of EMRA Tc1 CD57⁺PD-1⁻ terminal effector CD8⁺ T cells was higher in MIX compared to those of both REC and RNA (**Figure 23e**). Similar percentages of all other subpopulations were found among REC, MIX, and RNA (**Figure 25**).

4.2.4 Patients who recovered from COVID-19 display more polyfunctional antigen-specific CD4⁺ T cells compared to those in vaccinated donors

Besides Th-polarization, the functional properties of Ag⁺-specific T cells were investigated by measuring the percentages of cells producing IFN- γ , TNF, IL-2, IL-17 and GZMB, along with the expression of the degranulation marker CD107a. The percentages of cells producing cytokines were assessed following 16 h of in vitro stimulation with SARS-CoV-2 peptide pool covering the complete sequence of Wuhan SARS-CoV-2 spike glycoprotein. The gating strategy is reported in **Figure 26**. REC displayed a higher percentage of CD4⁺ T cells producing TNF, IL-2, and IL-17 than that in the MIX group, but not with respect to that of the RNA group. Furthermore, a higher percentage of CD4⁺ T cells producing IL-2 and TNF was observed in RNA compared to that in MIX subjects. Similar percentages of IFN- γ , CD107a, and GZMB were found among the three groups (**Figure 27b**). Polyfunctional properties were investigated in CD4⁺ and CD8⁺ T cells by analyzing the simultaneous production of TNF, CD107a, IFN- γ , IL-2, and IL-17 using the bioinformatic SPICE tool. Among CD4⁺ T cells, REC exhibited a different polyfunctionality profile from those who had been vaccinated (**Figure 27b**). In particular, REC displayed a higher percentage of CD4⁺ T cells simultaneously producing IL-2 and TNF compared to those in MIX and RNA. The percentage of CD4⁺ T cells producing TNF or IL-17 was higher in REC compared to those in both vaccinated groups. Moreover, RNA exhibited higher percentages of CD4⁺ T cells simultaneously producing IL-2 and TNF or IL-2 alone compared to those in MIX. Furthermore, we found that both vaccinated groups displayed higher percentages of cells defined as “highly polyfunctional” as simultaneously producing CD107a, IFN- γ , IL-2, and TNF compared to those in REC (**Figure 27c**). The functional properties of CD8⁺ T were similar between the three groups (**Figure 28**).

4.2.5 Vaccinated donors showed a higher percentage of antigen-specific and activated memory B cells expressing IgG compared to that in REC

SARS-CoV-2 antibodies decline already as early as 21 days after infection or vaccination [201]. However, long-lived MBCs constitute a durable long-term memory and provide a rapid recall response differentiating into high-affinity matured plasma cells [252]. For this reason, we measured the frequencies of circulating SARS-CoV-2 spike-specific B cells (Ag^+ B cells) (see *Methods*). Similar percentages of total B cells were found among the three groups (**Figure 29a**). However, both MIX and RNA showed a higher percentage of Ag^+ B cells (defined as $\text{CD45}^+\text{CD19}^+\text{decoy}^-\text{Spike-BUV661}^+\text{Spike-BV650}^+$) when compared to that in REC (**Figure 29b**). By applying manual gating, we observed that Ag^+ B cells compared to its Ag^- counterpart displayed a lower percentage of naive B cells and an increased percentage of memory switched, memory unswitched and of $\text{CD27}^-\text{IgD}^-$ B cells (**Figure 30a**). Moreover, after vaccination or SARS-CoV-2 infection, $\sim 42\%$ – 96% of Ag^+ B cells were IgG^+ . This percentage decreased to $\sim 5\%$ – 22% in the Ag^- B cells, where $\sim 69\%$ – 90% of cells were IgD^+IgM^+ (**Figure 30b**). Furthermore, the percentage of IgA^+ B cells was higher in the Ag^- compartment (**Figure 30b**). To deeply characterize both Ag^- and Ag^+ B cells, we took advantage of unsupervised clustering. The analysis revealed 15 clusters, spanning from naive to atypical B cells (atBCs; $\text{CD21}^-\text{CD27}^-\text{CD38}^-$) [253] (**Figure 29c, d; Figure 6a**). Besides naive and transitional B cells (TrB), respectively defined as naive: $\text{CD20}^+\text{CD21}^+\text{CD24}^+\text{CD38}^-\text{IgD}^+\text{IgM}^+$ and TrB: $\text{CD20}^+\text{CD21}^+\text{CD24}^+\text{CD38}^+\text{IgD}^+\text{IgM}^+$, we found five clusters of MBCs defined as follows: MBC IgD^+IgM^+ ($\text{CD20}^+\text{CD21}^+\text{CD24}^+\text{CD27}^+\text{IgD}^+\text{IgM}^+$), MBC IgA^+ ($\text{CD20}^+\text{CD21}^+\text{CD24}^+\text{CD27}^+\text{IgA}^+$), MBC IgG^+ ($\text{CD20}^+\text{CD21}^+\text{CD24}^+\text{CD27}^+\text{IgG}^+$), MBC IgA^+ CD71^+ ($\text{CD20}^+\text{CD21}^+\text{CD24}^+\text{CD27}^+\text{IgA}^+\text{CD71}^+$), and MBC IgG^+ CD71^+ ($\text{CD20}^+\text{CD21}^+\text{CD24}^+\text{CD27}^+\text{IgG}^+\text{CD71}^+$). Among plasmablasts (PBs), we found the following three clusters: PB IgA^+ as $\text{CD27}^+\text{CD71}^+\text{CD38}^{++}\text{IgA}^+$, PB IgM^+ as $\text{CD27}^+\text{CD71}^+\text{CD38}^{++}\text{IgM}^+$, and PB IgG^+ as $\text{CD27}^+\text{CD71}^+\text{CD38}^{++}\text{IgG}^+$. Together with naive, TrBs, MBCs, and PBs, we identified five clusters of atBCs, i.e., atBC1 as $\text{CD21}^-\text{CD27}^-\text{CD20}^+\text{IgG}^+$, atBC2 as $\text{CD21}^-\text{CD27}^-\text{CD24}^+\text{CD20}^+\text{IgG}^+$, atBC3 as $\text{CD21}^-\text{CD27}^-\text{CD20}^+\text{IgD}^+$, atBC4 as $\text{CD21}^-\text{CD27}^-\text{CD20}^+\text{IgD}^+\text{IgM}^+$, and atBC5 as $\text{CD21}^-\text{CD27}^-\text{CD20}^+\text{CD24}^+$. Within Ag^- B cells, MIX and RNA showed higher levels of MBC IgD^+IgM^+ and lower levels of atBC5 compared to those in REC (**Figure 31**). Within Ag^+ B cells, MIX and RNA displayed lower percentages of naive, MBC IgA^+ , and atBC4 B cells if compared to those in REC, while the percentages of MBC IgG^+ CD71^+ and atBC2 were significantly higher (**Figure 29e**). Moreover, REC displayed a higher percentage of atBC4 cells if compared to those in MIX and RNA (**Figure 29e**). Similar percentages of all other subpopulations were found among

REC, MIX, and RNA subjects (**Figure 32**). In addition, we measured IgG antibodies able to bind the spike and the RBD of the S1 subunit of the spike protein (the latter known as neutralizing antibodies). We observed that both vaccinated groups had higher levels of anti-spike and anti-RBD-binding IgG compared to those in REC subjects (**Figure 29f**).

4.2.6 Recovered patients show different immunological profiles compared to those of vaccinated donors

The principal component analysis (PCA) computed using the complete phenotype of Ag⁺ B and T cells, CD4⁺ T cell polyfunctionality, plasmatic anti-spike, and anti-RBD antibodies showed that the group of REC clusters in a different position of the two-dimensional PCA space if compared to MIX and RNA, which are almost entirely overlapping (**Figure 33a, left**). Immune features related to the amount of MBC IgA, CD107a⁻IFN- γ ⁻IL2⁻TNF⁺IL17⁻, CD107a⁻IFN- γ ⁻IL2⁺TNF⁺IL17⁻, CD107a⁻IFN- γ ⁻IL2⁻TNF⁻IL17⁺, and naive B cells (more abundant in REC subjects) were the main drivers of the clusterization of samples in two different areas (**Figure 33a, right**). Moreover, the picture of PCA contribution also reveals that both vaccinated groups were characterized by increased levels of MBC IgG CD71⁺, anti-spike, and anti-RBD IgG antibodies (**Figure 33a, right**). By using the same parameters used to perform the PCA, we assessed the existence of immunological correlations between the variables within the REC, MIX, and RNA groups. It is to note that in REC, but not in the MIX and RNA groups, a strong positive correlation was present among the percentages of MBC IgA CD71⁺ and all polyfunctional CD4⁺ T-cell subsets (**Figure 33b, Figure 34**). The percentages of MBC IgD⁺IgM⁺, transitional, and naive B cells inversely correlate with all polyfunctional CD4⁺ T-cell subsets (**Figure 33b, Figure 34**).

Table 9. Demographic and clinical characteristics of COVID-19 recovered patients and vaccinated donors (Lo Tartaro D., et al., 2023).

Variable	RECOVERED (n=9)	AZPM (n=11)	PFZM (n=12)	p-value (RECvsAZPM)	p-value (RECvsPFZM)	p-value (AZPMvsPFZM)
Demographic characteristics						
Age (mean years, range) ¹	35.1 (22-41)	27.0 (22-39)	35.3 (23-62)	0.0177	ns	ns
Sex (Male, %) ²	88.9	27.3	45.5	0.0098	ns	ns
Race/Ethnicity						
White: Non-Hispanic or Latino (%) ³	66.7	100	100	ns	ns	ns
White: Hispanic or Latino (%) ³	11.1	0	0	/	/	/
Black (%) ³	22.2	0	0	/	/	/
Hospitalization status						
Never hospitalized (%)	11.1	/	/	/	/	/
Hospitalized (%)	88.9	/	/	/	/	/
Days of hospitalization (mean days, range)	11.6 (4-17)	/	/	/	/	/
Sample Collection						
Sample Collection Dates	April-December 2020	December 2021- January 2022	December 2021- January 2022	/	/	/
Days post symptom onset or third dose vaccine (mean days, range) ¹	131.1 (64-165)	31.8 (30-35)	33.9 (26-44)	0.0004	0.0009	ns
Disease Severity						
Moderate (%)	55.56% (5/9)	/	/	/	/	/
Severe (%)	44.44% (4/9)	/	/	/	/	/
Vaccine type						
First dose	/	ChAdOx1	BNT162b2	/	/	/
Second dose	/	BNT162b2	BNT162b2	/	/	/
Third dose	/	mRNA-1273	mRNA-1273	/	/	/
Detection of SARS-CoV-2 IgM, IgG						
IgM, Index mean value (± SD) ¹		0.45 (±0.7)	0.18 (±0.2)			
IgG, Index mean value (± SD) ¹		17,151.6 (±10,563.5)	18,284.9 (±11,169.9)			

¹ Kruskal-Wallis test with Original FDR methods of Benjamini and Hochberg

² Fisher's exact test

³ Chi-squared test

ns, not significant

SD, standard deviation

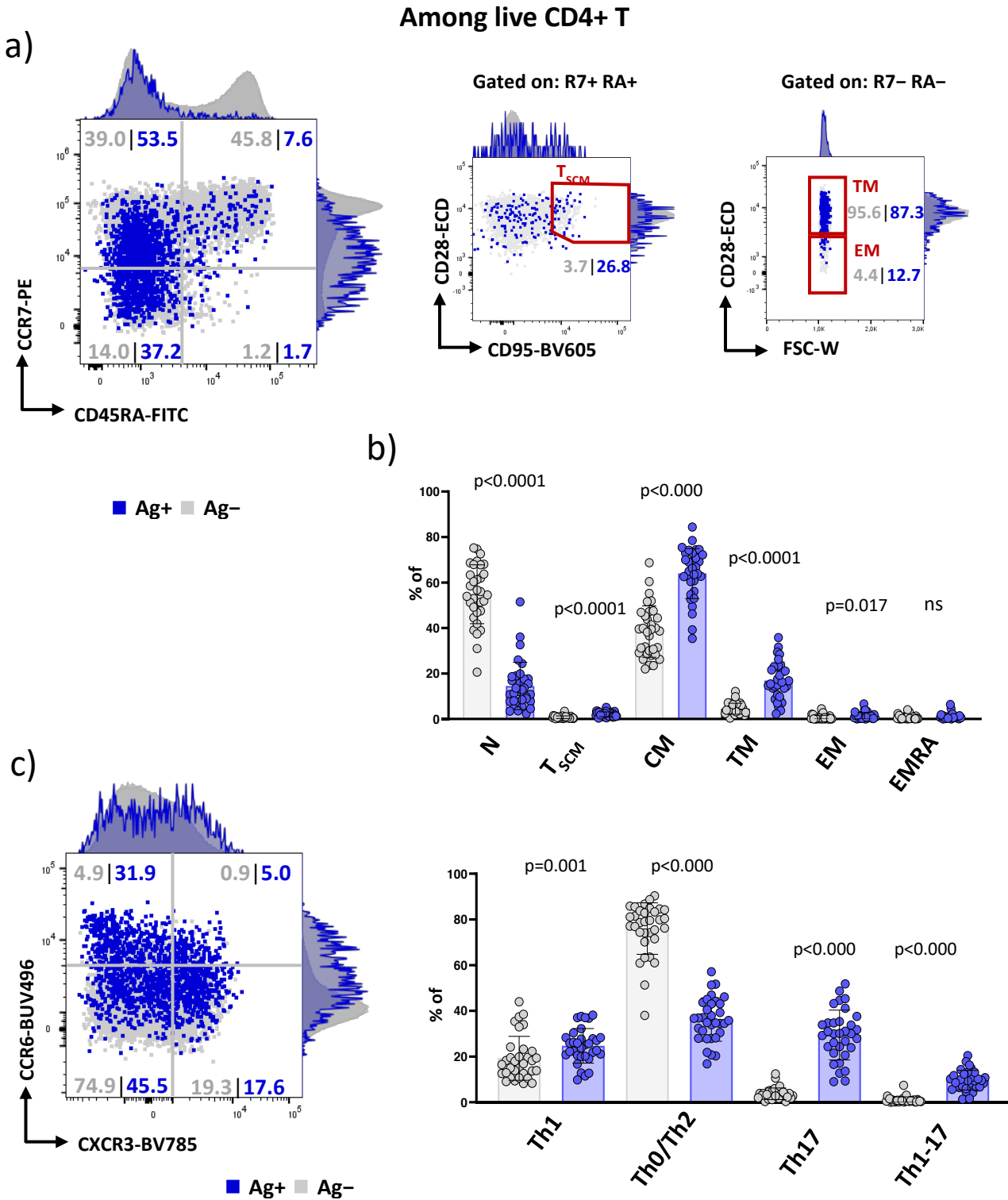


Figure 18 a) Representative dot plots showing manual gating analysis of Ag⁺ (blue dots) and Ag⁻ (grey dots) CD4⁺ T cells from REC, AZPM, and PFZM. Numbers indicate the percentage of cells identified by the gates; **b)** Dot plots show the relative cell percentage of naïve (N, CCR7⁺CD45RA⁺CD28⁺CD95⁻), T stem cell memory (T_{SCM}, CCR7⁺CD45RA⁺CD28⁺CD95⁺), central memory (CM, CCR7⁺CD45RA⁻CD28⁺CD95⁺), transitional memory (TM, CCR7⁻CD45RA⁻CD28⁺CD95⁺), effector memory (EM, CCR7⁻CD45RA⁻CD28⁻CD95⁺) and effector memory re-expressing CD45RA (EMRA, CCR7⁻CD45RA⁺CD28⁻CD95⁺). Numbers indicate the exact p-value obtained by Mann–Whitney test; **c)** (Left) Representative dot plots showing manual gating analysis of Ag⁺ and Ag⁻ CD4⁺ T cells from REC, AZPM, and PFZM. Numbers in the dot plots indicate the percentage of cells identified by the gates; (Right) Dot plots show the relative cell percentage of Th1 (CXCR3⁺CCR6⁻), Th0/Th2 (CXCR3⁻CCR6⁻), Th17 (CXCR3⁻CCR6⁺) and Th1-17 (CXCR3⁺CCR6⁺). Numbers indicate the exact p-value obtained by Mann–Whitney test (Lo Tartaro D., et al., 2023).

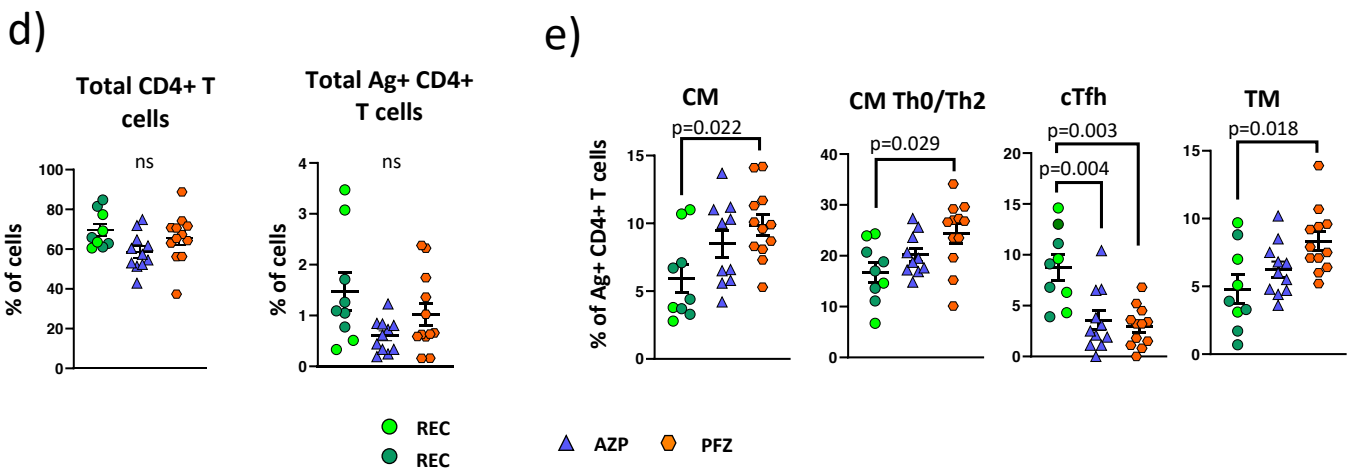
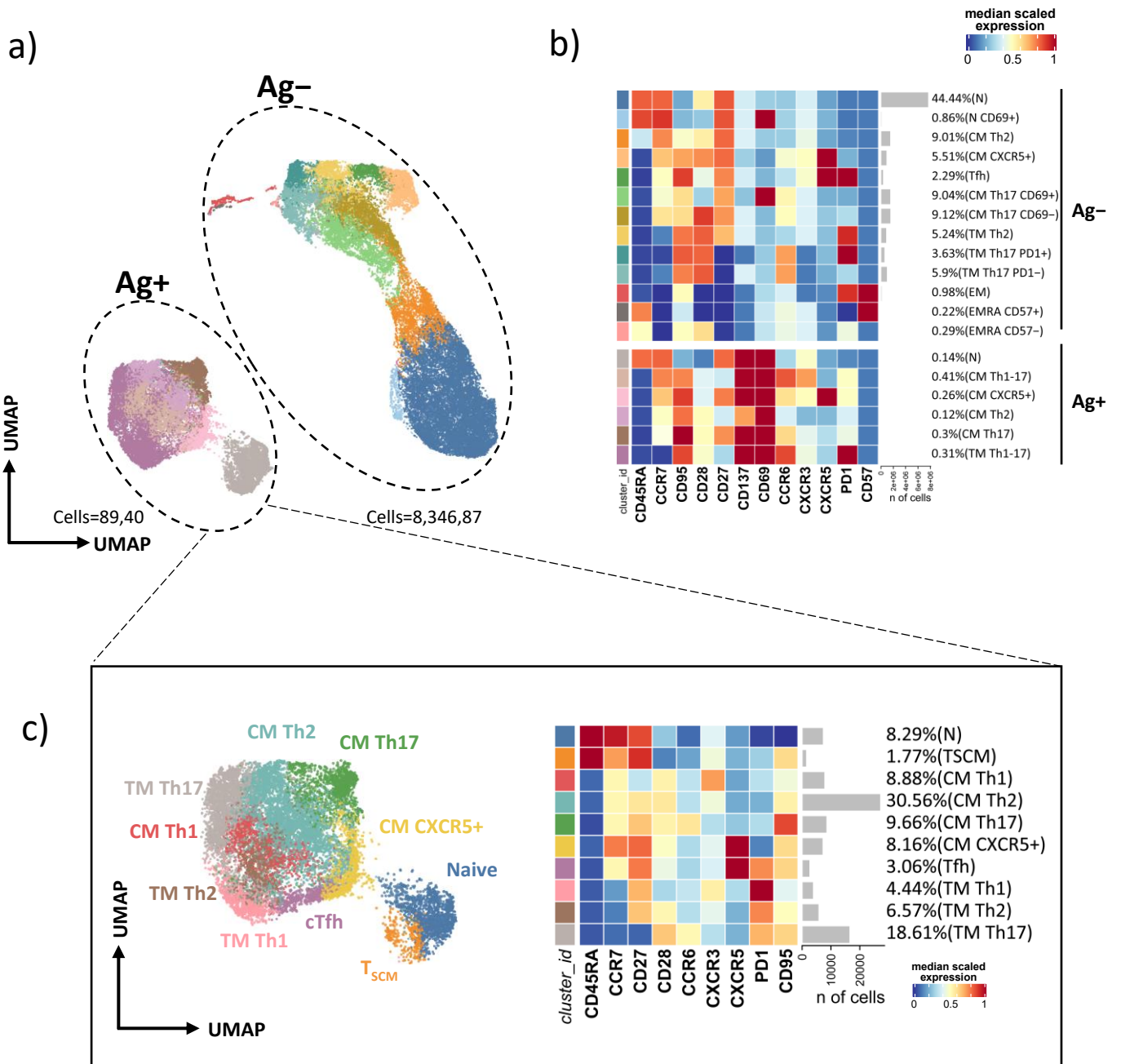


Figure 19. Immune phenotyping of antigen-specific CD4⁺ T cells. (A) Uniform Manifold Approximation and Projection (UMAP) plot shows the 2D spatial distribution of 8,436,275 cells from nine donors who recovered from SARS-CoV-2 infection (REC, severe = 4 and moderate = 5) and 23 vaccinated donors (MIX = 11 and RNA = 12) embedded with FlowSOM clusters. Ag⁺, antigen-specific CD4⁺ T cells; Ag⁻, non-antigen-specific CD4⁺ T cells. (B) Heatmap of the median marker intensities of the 12 lineage markers across the 19 cell populations obtained with FlowSOM algorithm after the manual metacluster merging. The colors of cluster_id column correspond to the colors used to label the UMAP plot clusters. The color in the heatmap is referred to the median of the arcsinh marker expression (0–1 scaled) calculated over cells from all of the samples. Blue represents lower expression, while red represents higher expression. Light gray bar along the rows (clusters) and values in brackets indicate the relative sizes of the clusters. N, naive; T_{SCM}, T stem cell memory; CM, central memory; TM, transitional memory; EM, effector memory; EMRA, effector memory re-expressing the CD45RA; cTfh, circulating T follicular helper cells. The black bar on the right is used to group Ag⁺ or Ag⁻ subpopulations. (C) UMAP and heatmap visualization of 10 manually merged antigen-specific CD4⁺ T-cell clusters. (D) Dot plots show the total percentage of antigen-specific CD4⁺ T cells. Kruskal–Wallis test with Benjamini–Hochberg correction for multiple comparisons was used to test the differences among the three groups. (E) Dot plots show the cell percentage of the antigen-specific CD4⁺ T cells. The central bar represents the mean ± SEM. Generalized linear mixed model (GLMM) test was used for the statistical analysis. Adjusted P-values are reported in the figure. ns, not significant (Lo Tartaro D., et al., 2023).

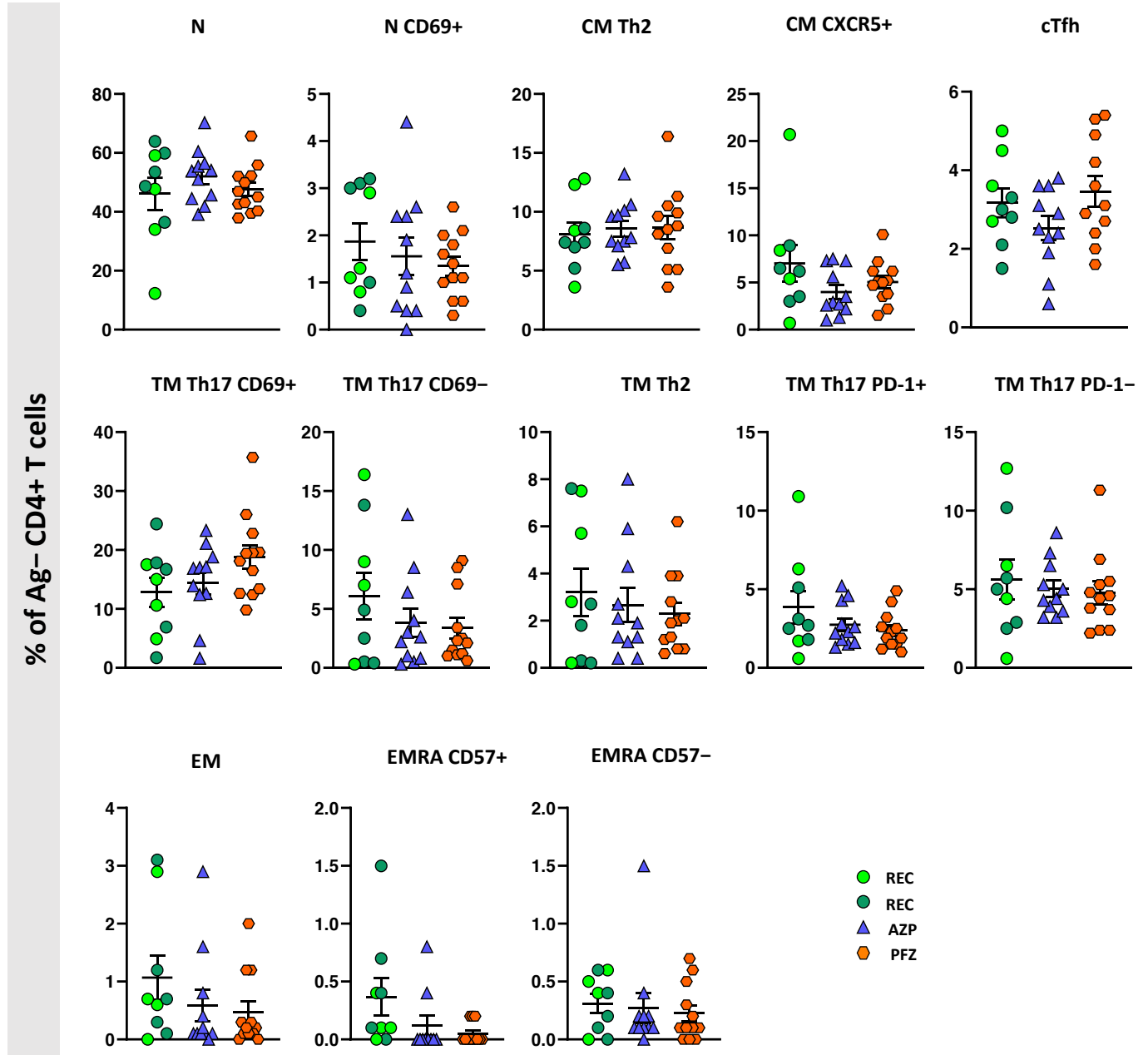


Figure 20. Dot plots show the relative cell percentage of the 13 Ag⁻ CD4⁺ T cell clusters from 9 healthy subjects who recovered from SARS-CoV-2 infection (REC, severe=4 and moderate=5) against 23 vaccinated donors (AZPM=11 and PFMZ=12). The central bar represents the mean ± SEM. Generalized linear mixed model (GLMM) test was used for the statistical analysis. Only significant adjusted p-values are indicated (< 0.05) (Lo Tartaro D., et al., 2023).

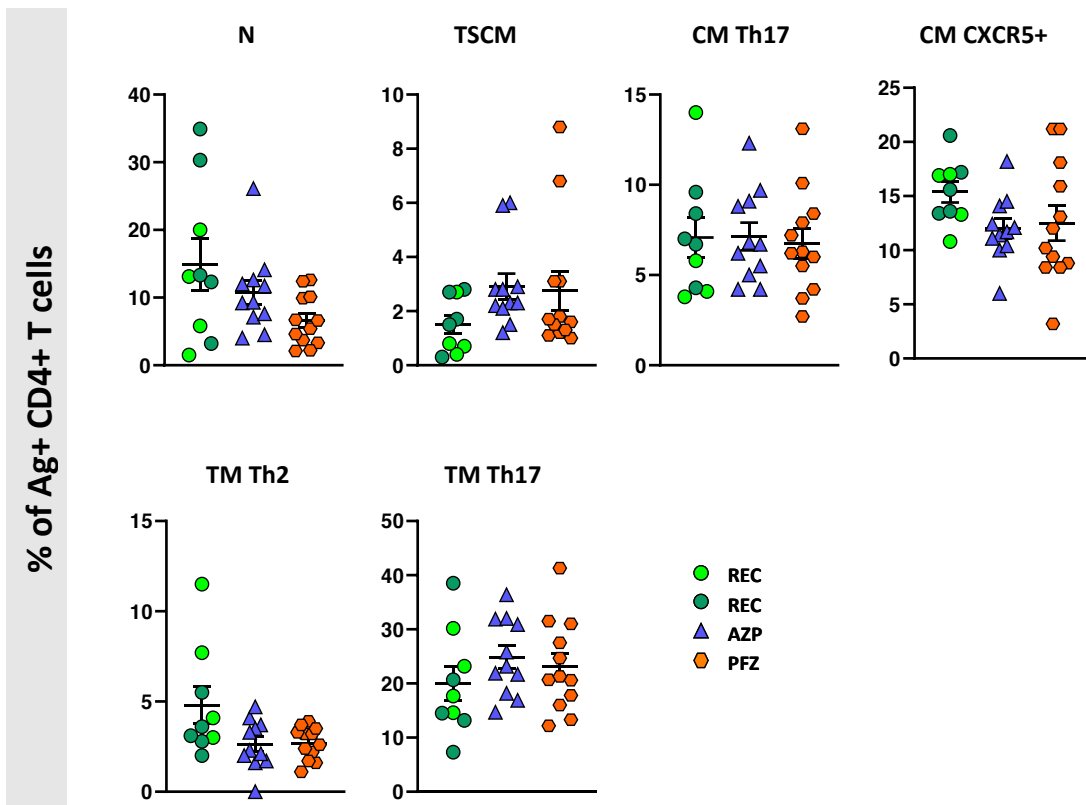


Figure 21. Dot plots show the relative cell percentage of the six Ag⁺ CD4⁺ T cell clusters from 9 healthy subjects who recovered from SARS-CoV-2 infection (REC, severe=4 and moderate=5) against 23 vaccinated donors (AZPM=11 and PFMZ=12). The central bar represents the mean \pm SEM. Generalized linear mixed model (GLMM) test was used for the statistical analysis. Only significant adjusted p-values (< 0.05) (Lo Tartaro D., et al., 2023).

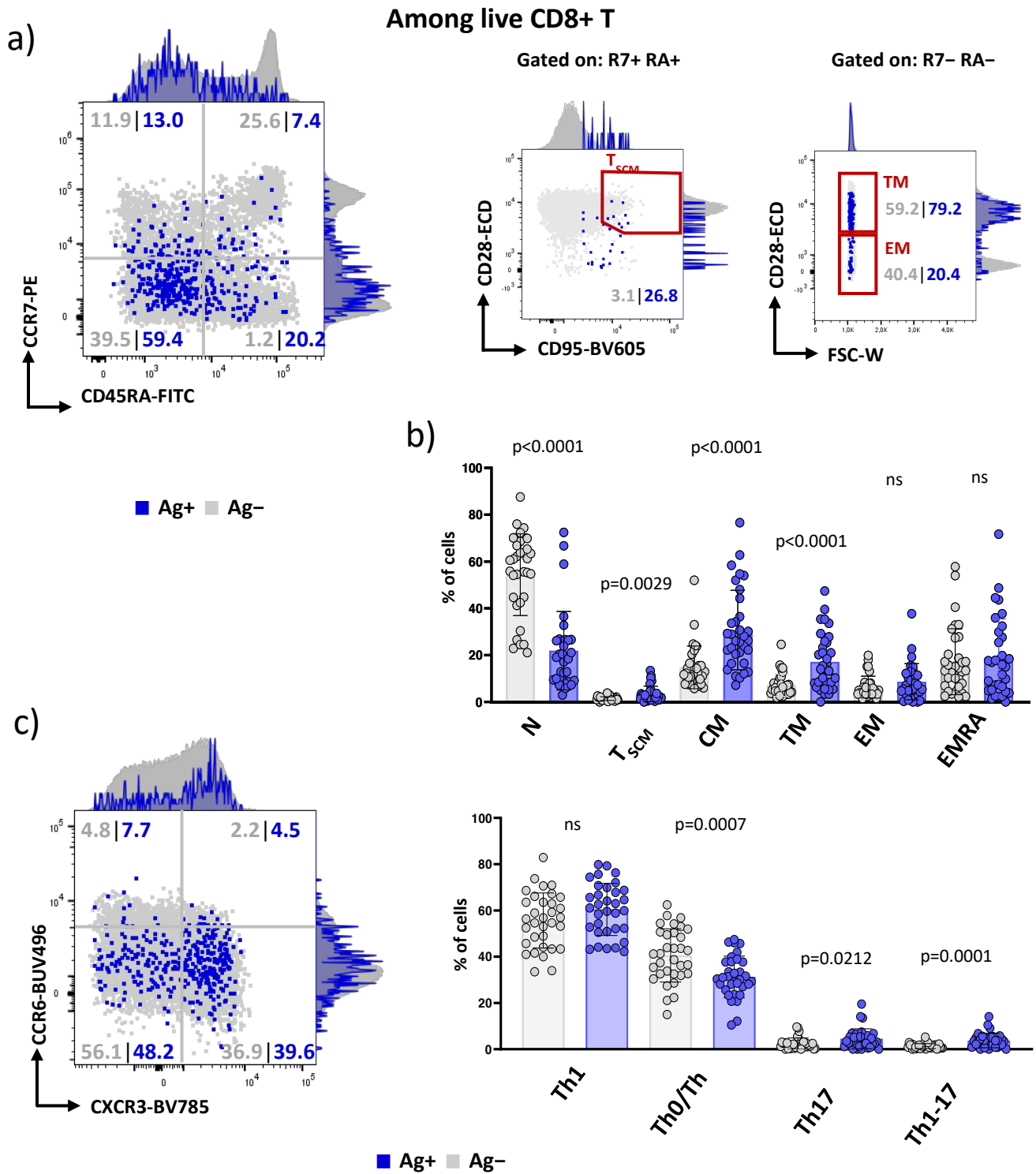


Figure 22. a) Representative dot plots showing manual gating analysis of Ag⁺ (blue dots) and Ag⁻ (grey dots) CD8⁺ T cells from REC, AZPM, and PFZM. Numbers indicate the percentage of cells identified by the gates; **b)** Dot plots show the relative cell percentage of naïve (N, CCR7⁺CD45RA⁺CD28⁺CD95⁻), T stem cell memory (T_{SCM}, CCR7⁺CD45RA⁺CD28⁺CD95⁺), central memory (CM, CCR7⁺CD45RA⁻CD28⁺CD95⁺), transitional memory (TM, CCR7⁻CD45RA⁻CD28⁺CD95⁺), effector memory (EM, CCR7⁻CD45RA⁻CD28⁻CD95⁺) and effector memory re-expressing CD45RA (EMRA, CCR7⁻CD45RA⁺CD28⁻CD95⁺). Numbers indicate the exact p-value obtained by Mann–Whitney test; **c)** (Left) Representative dot plots showing manual gating analysis of Ag⁺ and Ag⁻ CD8⁺ T cells from REC, AZPM, and PFZM. Numbers in the dot plots indicate the percentage of cells identified by the gates; (Right) Dot plots show the relative cell percentage of Th1 (CXCR3⁺CCR6⁻), Th0/Th2 (CXCR3⁻CCR6⁻), Th17 (CXCR3⁻CCR6⁺) and Th1-17 (CXCR3⁺CCR6⁺). Numbers indicate the exact p-value obtained by Mann–Whitney test (Lo Tartaro D., et al., 2023).

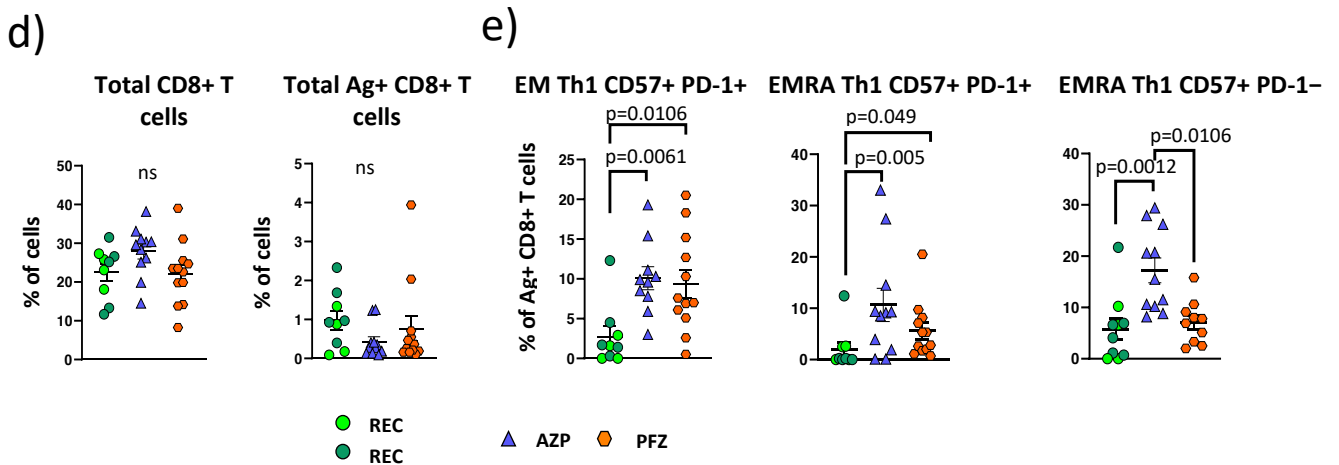
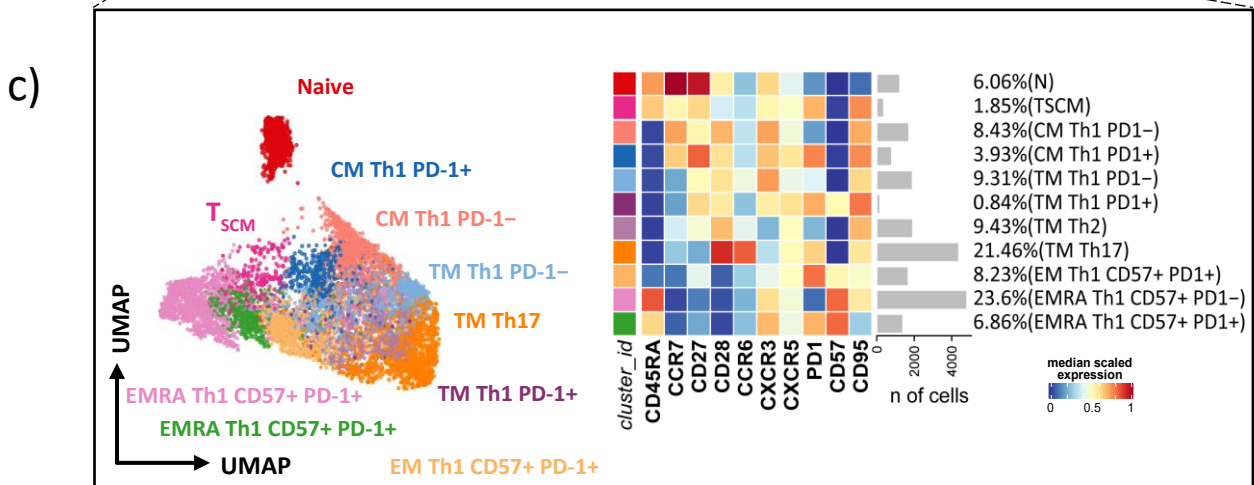
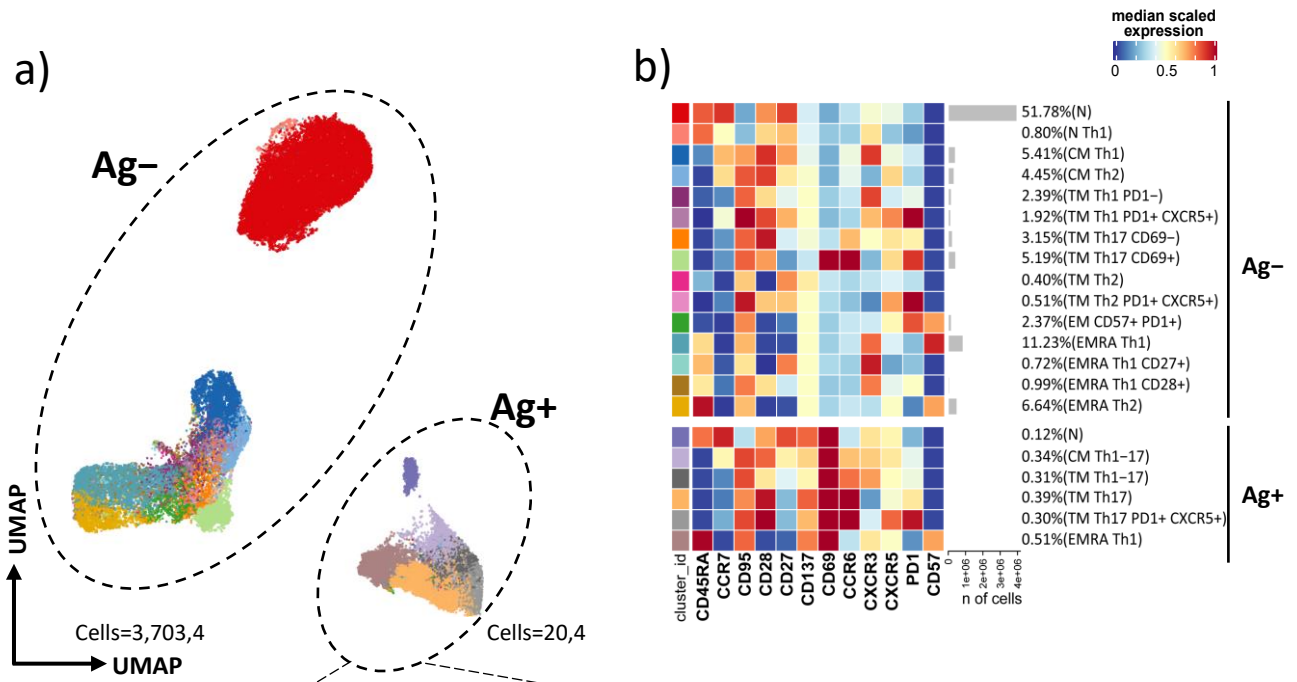


Figure 23. Immune phenotyping of antigen-specific CD8⁺ T cells. (A) UMAP plot shows the 2D spatial distribution of 3,723,899 cells from nine donors who recovered from SARS-CoV-2 infection (REC, severe = 4 and moderate = 5) and 23 vaccinated donors (MIX = 11 and RNA = 12) embedded with FlowSOM clusters. Ag⁺, antigen-specific CD8⁺ T cells; Ag⁻, non-antigen-specific CD8⁺ T cells. (B) Heatmap of the median marker intensities of the 12 lineage markers across the 21 cell populations obtained with FlowSOM algorithm after the manual metacluster merging. The colors of cluster_id column correspond to the colors used to label the UMAP plot clusters. The color in the heatmap is referred to the median of the arcsinh marker expression (0–1 scaled) calculated over cells from all of the samples. Blue represents lower expression, while red represents higher expression. Light gray bar along the rows (clusters) and values in brackets indicate the relative sizes of the clusters. N, naive; CM, central memory; TM, transitional memory; EM, effector memory; EMRA, effector memory re-expressing the CD45RA. The black bar on the right is used to group Ag⁺ or Ag⁻ subpopulations. (C) Uniform Manifold Approximation and Projection UMAP and heatmap visualization of 11 manually merged antigen-specific CD8⁺ T cell clusters. (D) Dot plots show the total percentage of antigen-specific CD8⁺ T cells. Kruskal–Wallis test with Benjamini–Hochberg correction for multiple comparisons was used to test the differences among the three groups. (E) Dot plots show the relative cell percentage of the antigen-specific CD8⁺ T-cell clusters of nine donors who recovered from SARS-CoV-2 infection (REC, severe = 4 and moderate = 5) and 23 vaccinated donors (MIX = 11 and RNA = 12). The central bar represents the mean ± SEM. Generalized linear mixed model GLMM test was used for the statistical analysis. Adjusted P- values are reported in the figure. ns, not significant (Lo Tartaro D., et al., 2023).

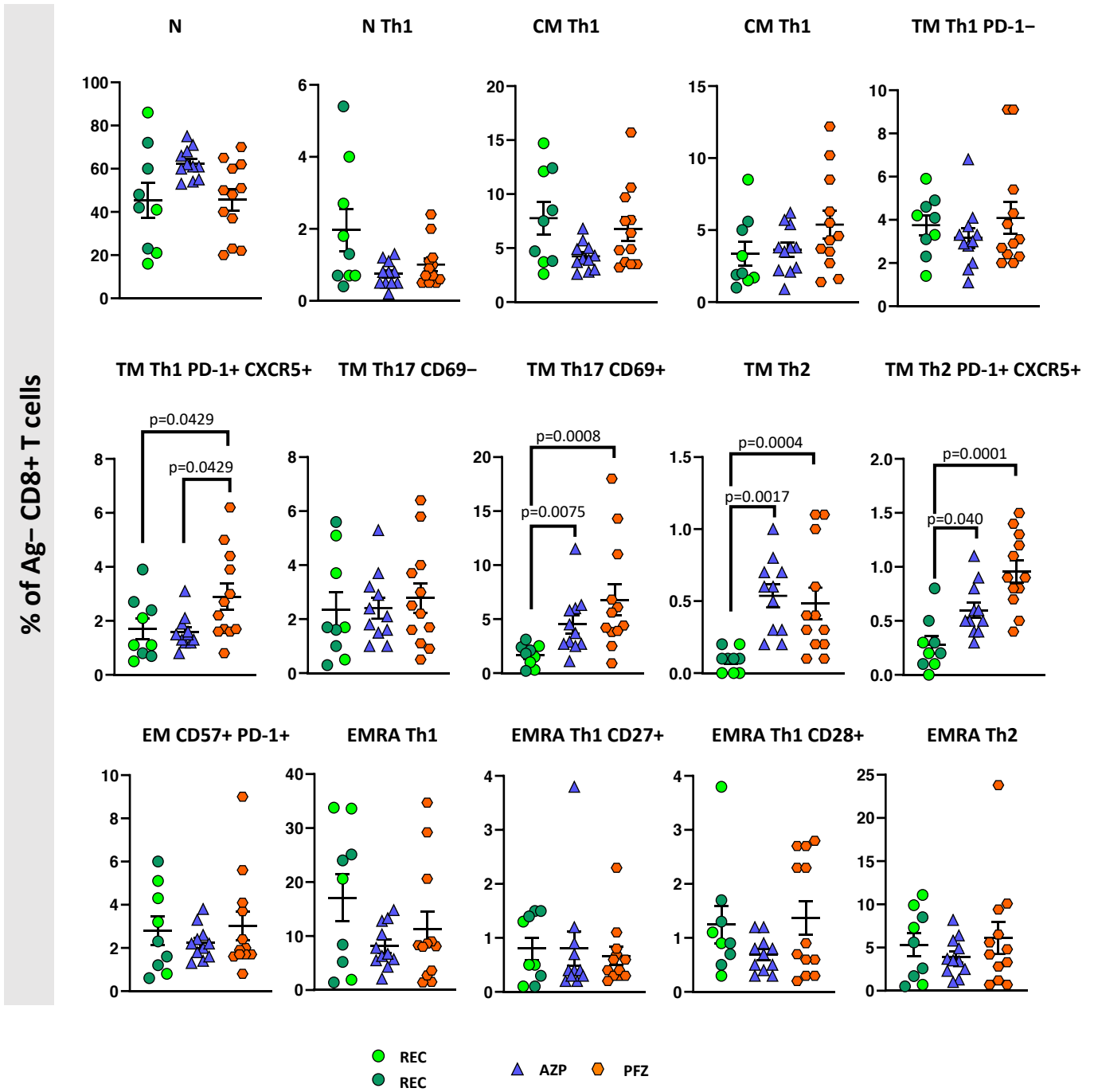


Figure 24. Dot plots show the relative cell percentage of the 16 Ag⁻ CD8⁺ T cell clusters from 9 healthy subjects who recovered from SARS-CoV-2 infection (REC, severe=4 and moderate=5) against 23 vaccinated donors (AZPM=11 and PFMZ=12). The central bar represents the mean ± SEM. Generalized linear mixed mode (GLMM) test was used for the statistical analysis. Only significant adjusted p-values are indicated (< 0.05) (Lo Tartaro D., et al., 2023).

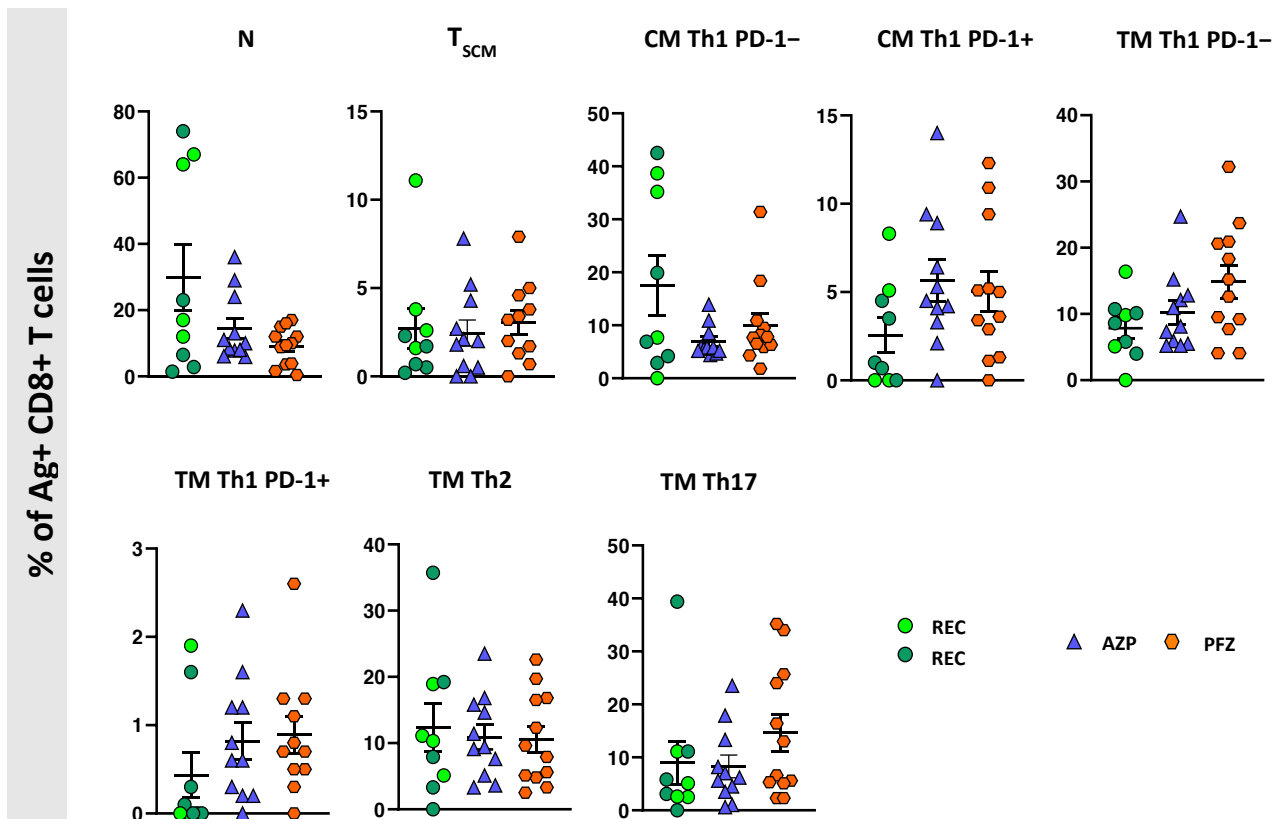


Figure 25. Dot plots show the relative cell percentage of the eight Ag⁺ CD8⁺ T cell clusters from 9 healthy subjects who recovered from SARS-CoV-2 infection (REC, severe=4 and moderate=5) against 23 vaccinated donors (AZPM=11 and PFMZ=12). The central bar represents the mean ± SEM. Generalized linear mixed mode (GLMM) test was used for the statistical analysis. Only significant adjusted p-values are indicated (< 0.05) (Lo Tartaro D., et al., 2023).

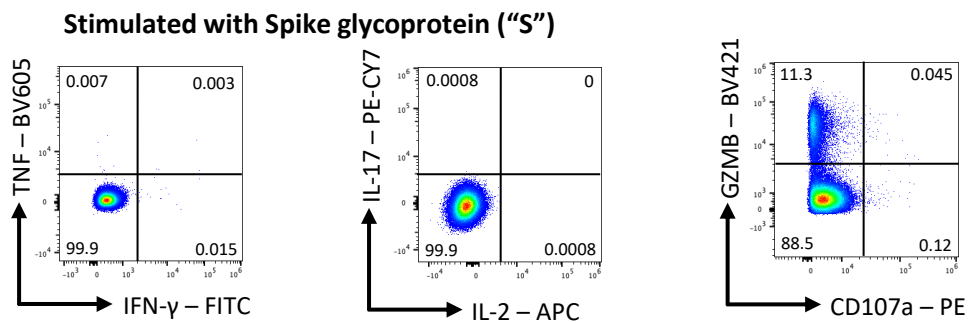
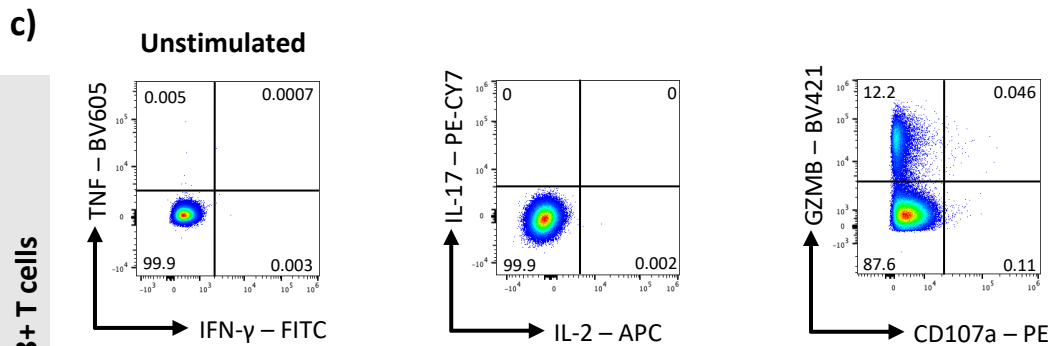
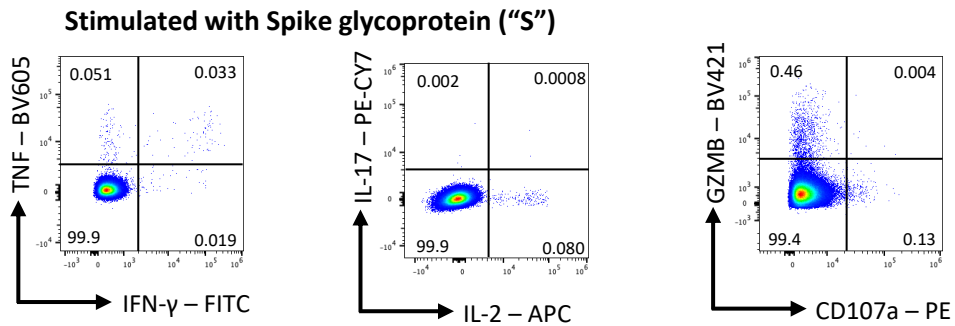
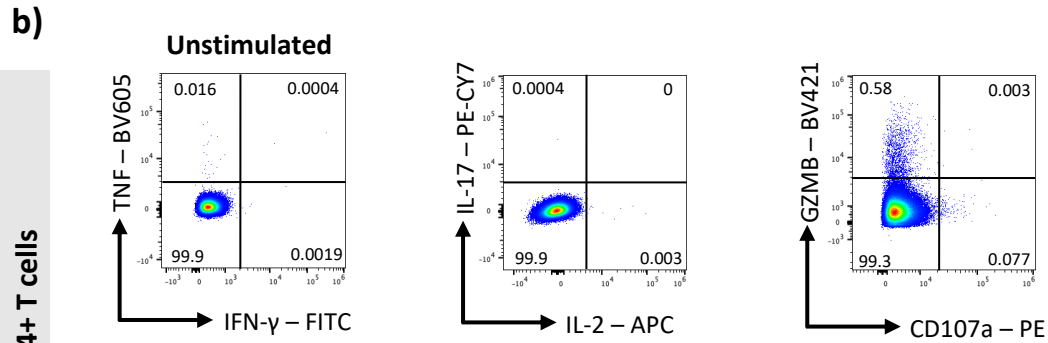
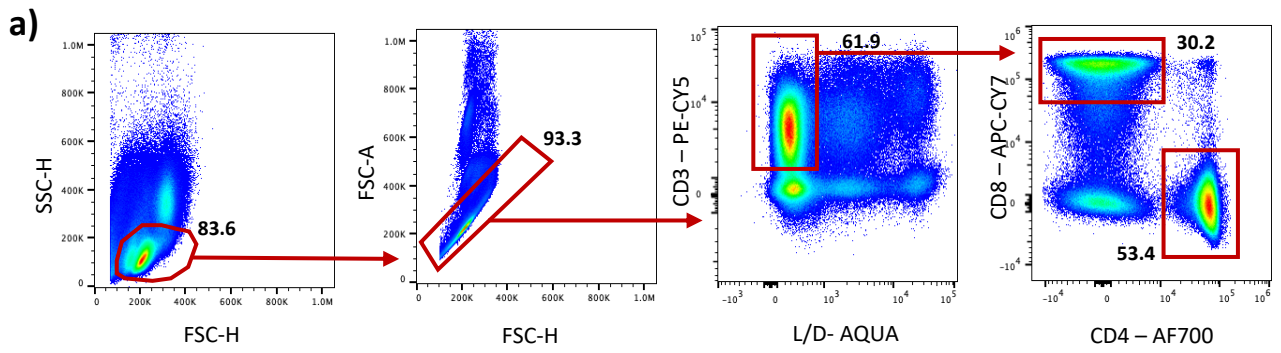


Figure 26. a) Gating strategy used to identify and analyze the intracellular cytokine production of CD4⁺ and CD8⁺ T lymphocytes. Lymphocytes were gated according to physical parameters and doublets were removed from the analysis. Living (Live/Dead negative, L/D-) CD3⁺ T cells were selected; among them, CD4⁺ and CD8⁺ T cell subpopulations were identified. In the quadrant plot is reported the percentages of b) CD4⁺ or c) CD8⁺ T cells producing IFN- γ , TNF, IL-2, IL-17, GZMB as well as the expression of CD107a (Lo Tartaro D., et al., 2023).

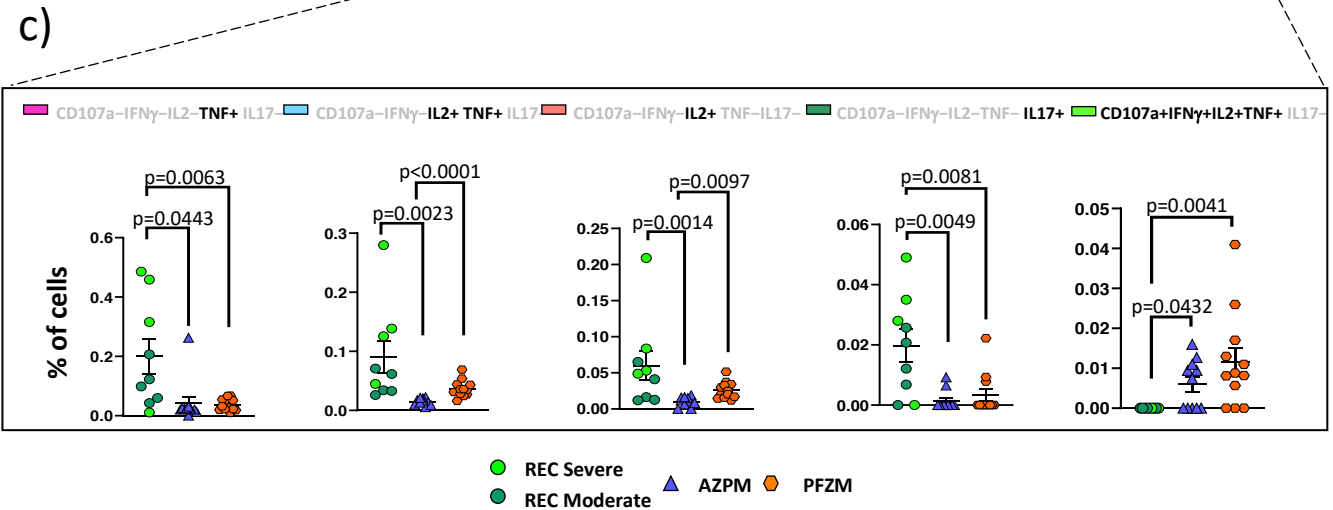
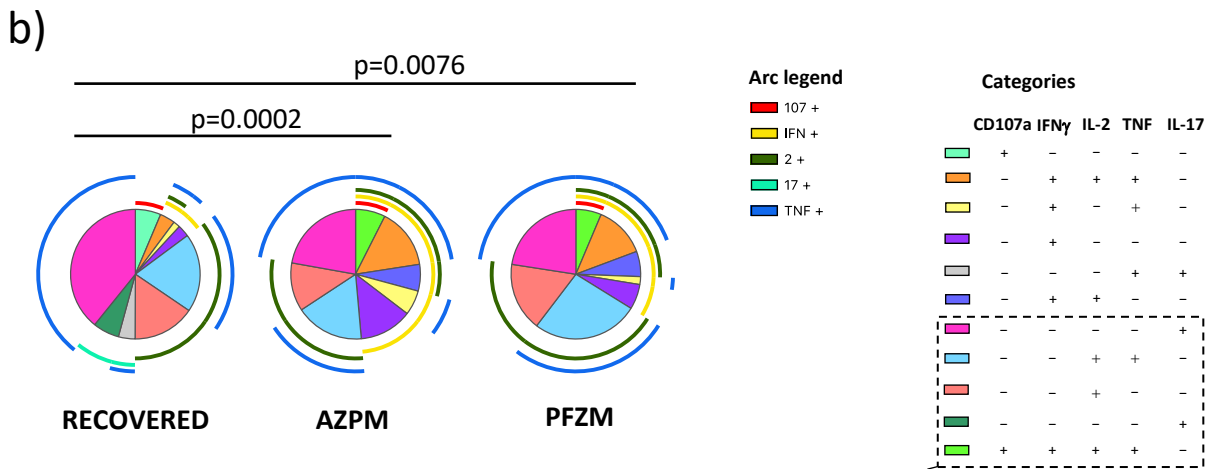
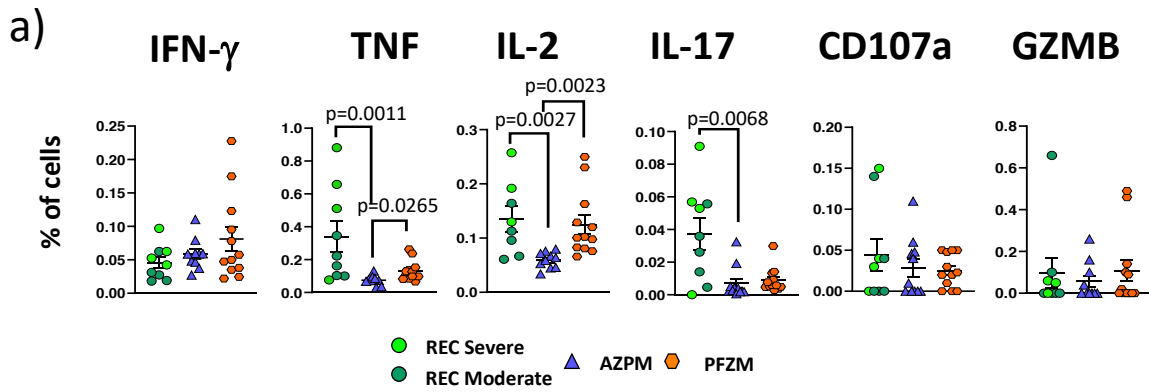
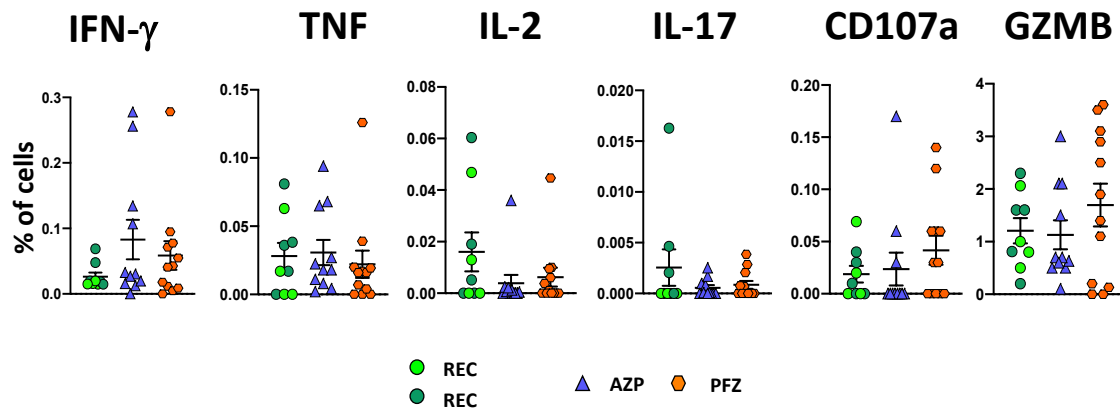


Figure 27. Cytokine production and polyfunctionality of antigen-specific CD4⁺ T cells. (a) Comparison between the total production of IFN-g, TNF, IL-17, IL-2, CD107a, and GZMB by CD4⁺ T cells after in vitro stimulation with 15-mer peptides, covering the complete sequence of Wuhan SARS-CoV-2 spike glycoprotein. Data represent individual values from nine healthy subjects who recovered from SARS-CoV-2 infection (REC, severe = 4 and moderate = 5) and 23 vaccinated donors (MIX= 11 and RNA = 12). Mean (center bar) ± SEM (upper and lower bars). Kruskal–Wallis test with Benjamini–Hochberg correction for multiple comparisons was used to test the differences among the three groups. (b) Pie charts representing the proportion of responding CD4⁺ T cells producing different combinations of CD107a, IL-2, IL-17, IFN-g, and TNF after in vitro stimulation with 15-mer peptides, covering the complete sequence of Wuhan SARS-CoV-2 spike glycoprotein. Frequencies were corrected by background subtraction as determined in non-stimulated controls using SPICE software. Pie arches represent the total production of different cytokines. (c) Percentage of polyfunctional population within CD4⁺ T cells. Kruskal–Wallis test with Benjamini–Hochberg correction for multiple comparisons was used to test the differences among the three groups. Adjusted P-values are indicated in the figure (Lo Tartaro D., et al., 2023).

a)



b)

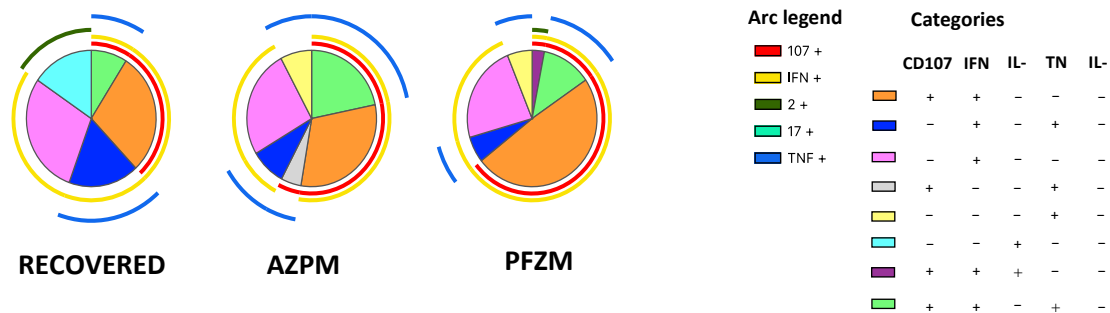


Figure 28. a) Comparison between the total production of IFN- γ , TNF, IL-17, IL-2, CD107a and granzyme-B (GZMB) by CD8⁺T cells after in vitro stimulation with 15-mer peptides, covering the complete sequence of Wuhan SARS-CoV-2 Spike glycoprotein. Data represent individual values from 9 healthy subjects who recovered from SARS-CoV-2 infection (REC, severe=4 and moderate=5) against 23 vaccinated donors (AZPM=11 and PFMZ=12). Mean (central bar) \pm SEM (upper and lower bars). Kruskal-Wallis test with Benjamini-Hochberg correction for multiple comparisons was used to test the differences among the three groups; b) Pie charts representing the proportion of responding CD8⁺ T cells producing different combinations of CD107a, IL-2, IL-17, IFN- γ , and TNF after in vitro stimulation with 15-mer peptides, covering the complete sequence of Wuhan SARS-CoV-2 Spike glycoprotein. Kruskal-Wallis test with Benjamini-Hochberg correction for multiple comparisons was used to test the differences among the three groups (Lo Tartaro D., et al., 2023).

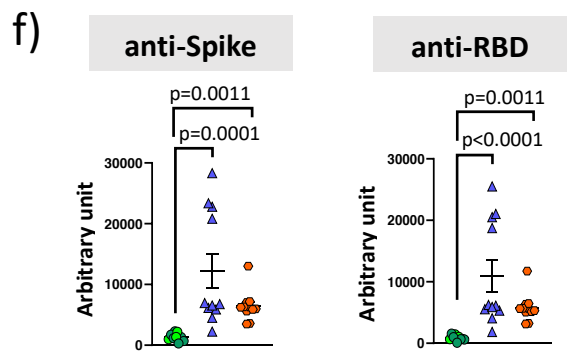
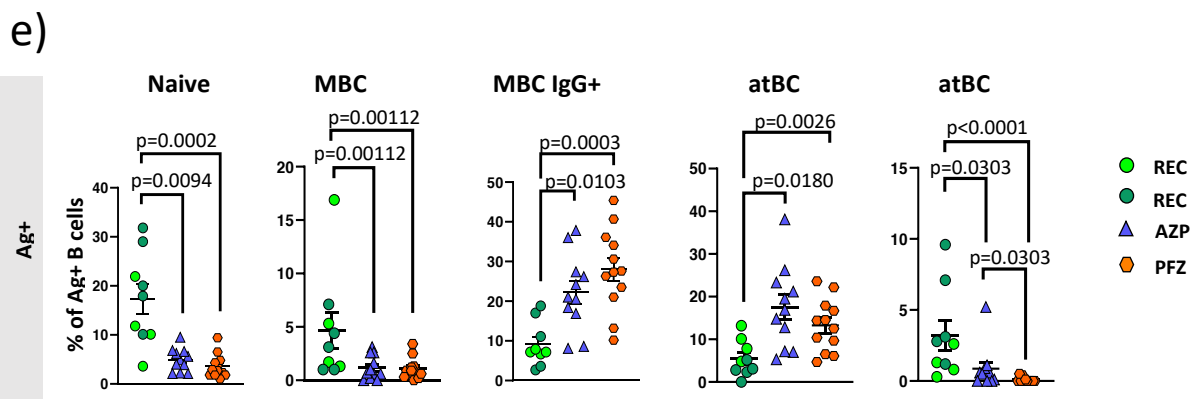
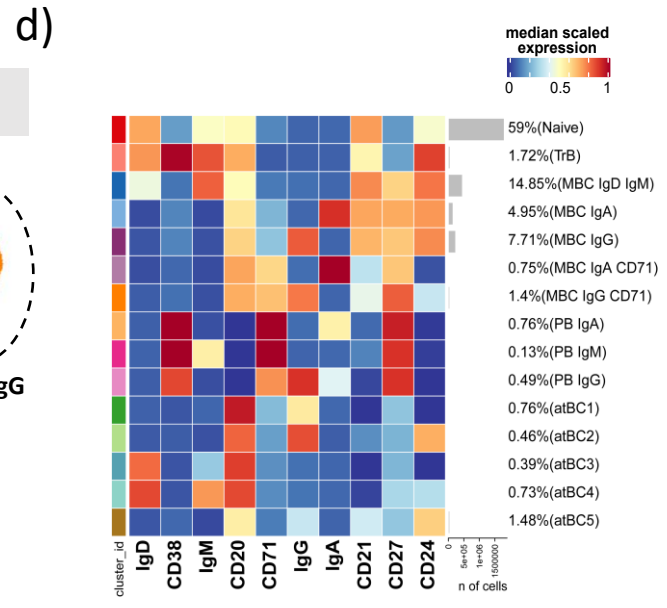
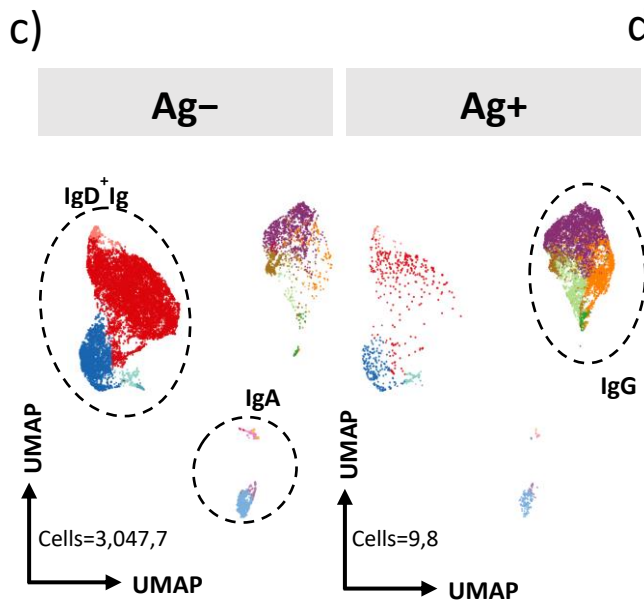
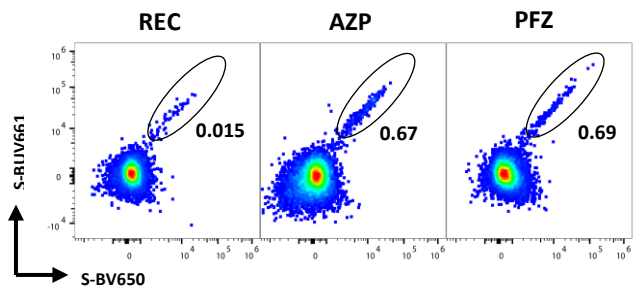
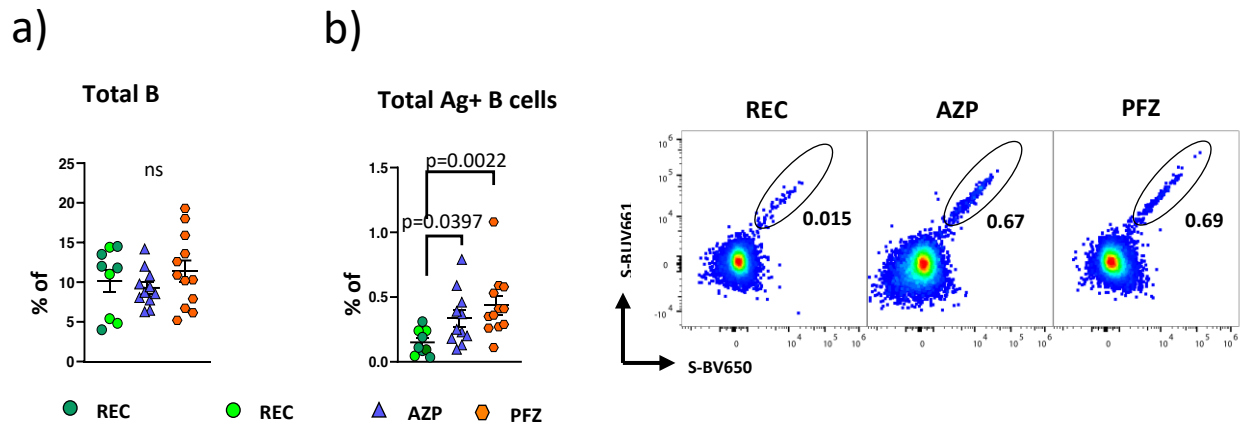


Figure 29. Immune phenotyping of antigen-specific CD19⁺ B cells. (a) Dot plots show the total percentage of CD19⁺ B cells. Kruskal–Wallis test with Benjamini–Hochberg correction for multiple comparisons was used to test the differences among the three groups. (b) Dot plots show the total percentage of antigen-specific CD19⁺ B cells (left); representative dot plots showing manual gating analysis of Ag⁺ B cells from REC, MIX, and RNA. Numbers in the dot plots indicate the percentage of cells identified by the gates (right). Kruskal–Wallis test with Benjamini–Hochberg correction for multiple comparisons was used to test the differences among the three groups. (c) UMAP plot shows the 2D spatial distribution of 3,057,659 cells from nine donors who recovered from SARS-CoV-2 infection (REC, severe = 4 and moderate = 5) and 23 vaccinated donors (MIX = 11 and RNA = 12) embedded with FlowSOM clusters. Ag⁺, antigen-specific CD19⁺ B cells; Ag⁻, non-antigen-specific CD19⁺ B cells. (d) Heatmap of the median marker intensities of the 10 lineage markers across the 15 cell populations obtained with FlowSOM algorithm after the manual metacluster merging. The colors of cluster_id column correspond to the colors used to label the UMAP plot clusters. The color in the heatmap is referred to the median of the arcsinh marker expression (0–1 scaled) calculated over cells from all of the samples. Blue represents lower expression, while red represents higher expression. Light gray bar along the rows (clusters) and values in brackets indicate the relative sizes of the clusters. N, naive; TrB, transitional B cells; MBC, memory B cell; atBC, atypical B cell. (e) Dot plots show the percentage of 15 Ag⁺ B cell clusters among nine donors who recovered from SARS-CoV-2 infection (REC, severe = 4 and moderate = 5) and 23 vaccinated donors (MIX = 11 and RNA = 12). The central bar represents the mean ± SEM. GLMM test was used for the statistical analysis. Adjusted P-values are reported in the figure. (f) Anti-spike and anti-RBD IgG concentrations in plasma samples from REC, MIX, and RNA individuals. Kruskal–Wallis test with Benjamini–Hochberg correction for multiple comparisons was used to test the differences among the three groups. Adjusted P-values are indicated in the figure (Lo Tartaro D., et al., 2023).

Among live CD19+ Decoy- B cells

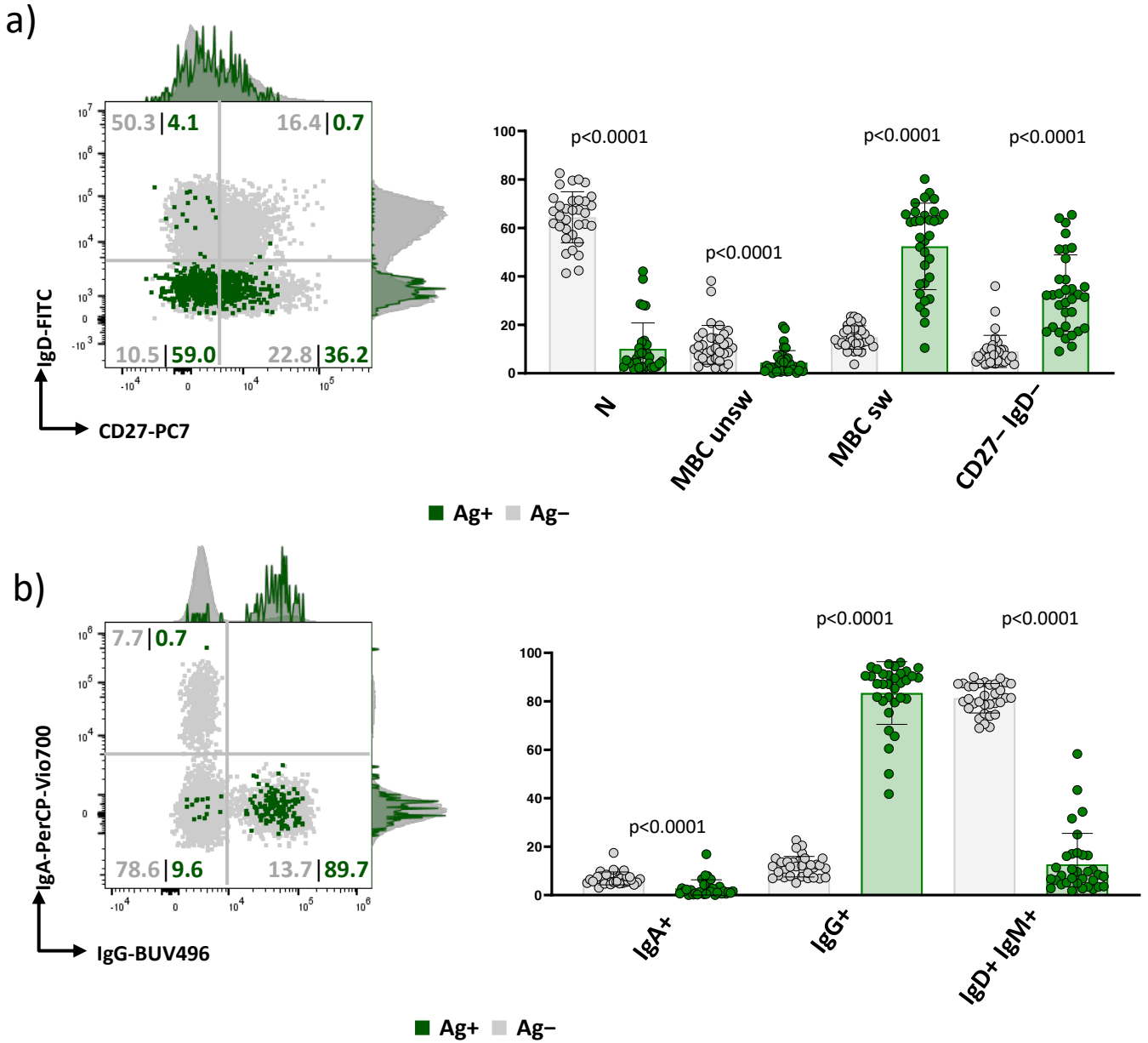


Figure 30. a) (Left) Representative dot plots showing manual gating analysis of Ag⁺ (green dots) and Ag⁻ (grey dots) CD19⁺ B cells from REC, AZPM, and PFZM. Numbers in the dot plots indicate the percentage of cells identified by the gates; (Right) Dot plots show the relative cell percentage of naïve (N, IgD⁺CD27⁻), memory unswitched (MBC unsw, IgD⁺CD27⁺), memory switched (MBC sw, IgD⁻CD27⁺) and IgD⁻CD27⁻. Numbers indicate the exact p-value obtained by Mann–Whitney test; b) (Left) Representative dot plots showing manual gating analysis of Ag⁺ and Ag⁻ CD19⁺ B cells from REC, AZPM, and PFZM. Numbers in the dot plots indicate the percentage of cells identified by the gates; (Right) Dot plots show the relative cells percentage of IgA⁺, IgG⁺ and IgD⁺IgM⁺ (IgA⁻IgG⁻) B cells. Numbers indicate the exact p-value obtained by Mann–Whitney test (Lo Tartaro D., et al., 2023).

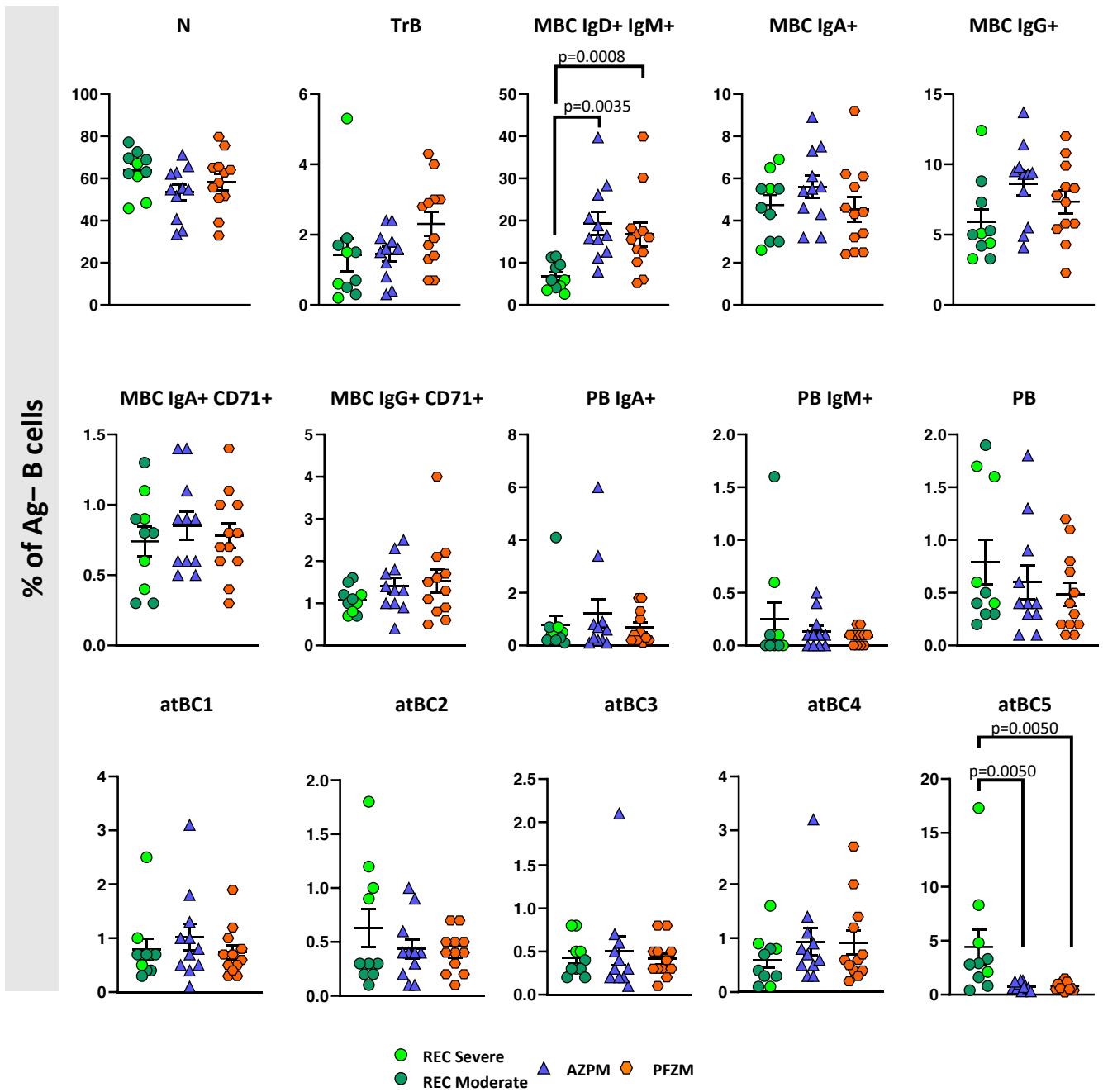


Figure 31. Dot plots show the relative cell percentage of the 15 Ag⁻ CD19⁺ B cell clusters from 9 healthy subjects who recovered from SARS-CoV-2 infection (REC, severe=4 and moderate=5) against 23 vaccinated donors (AZPM=11 and PFMZ=12). The central bar represents the mean ± SEM. Generalized linear mixed mode (GLMM) test was used for the statistical analysis. Only significant adjusted p-values are indicated (< 0.05) (Lo Tartaro D., et al., 2023).

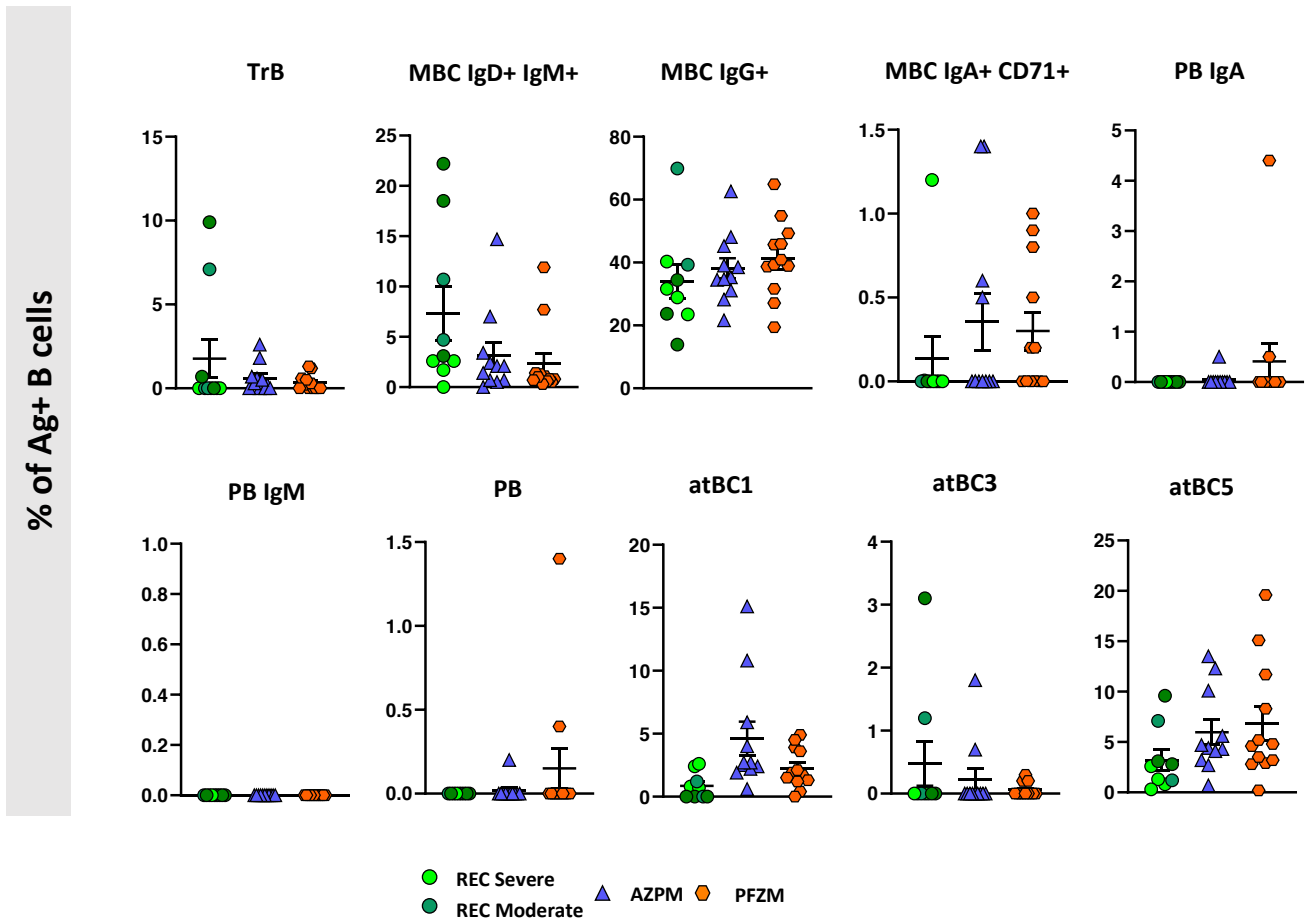
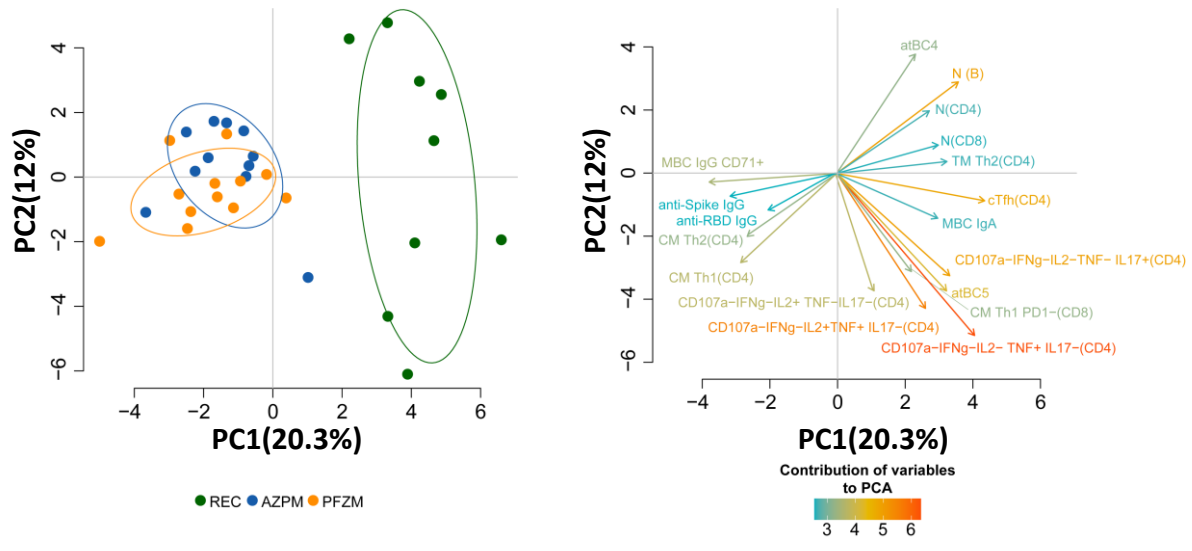


Figure 32. Dot plots show the relative cell percentage of the 10 Ag⁺ CD19⁺ B cell clusters from 9 healthy subjects who recovered from SARS-CoV-2 infection (REC, severe=4 and moderate=5) against 23 vaccinated donors (AZPM=11 and PFMZ=12). The central bar represents the mean ± SEM. Generalized linear mixed mode (GLMM) test was used for the statistical analysis. Only significant adjusted p-values are indicated (< 0.05) (Lo Tartaro D., et al., 2023).

a)



b)

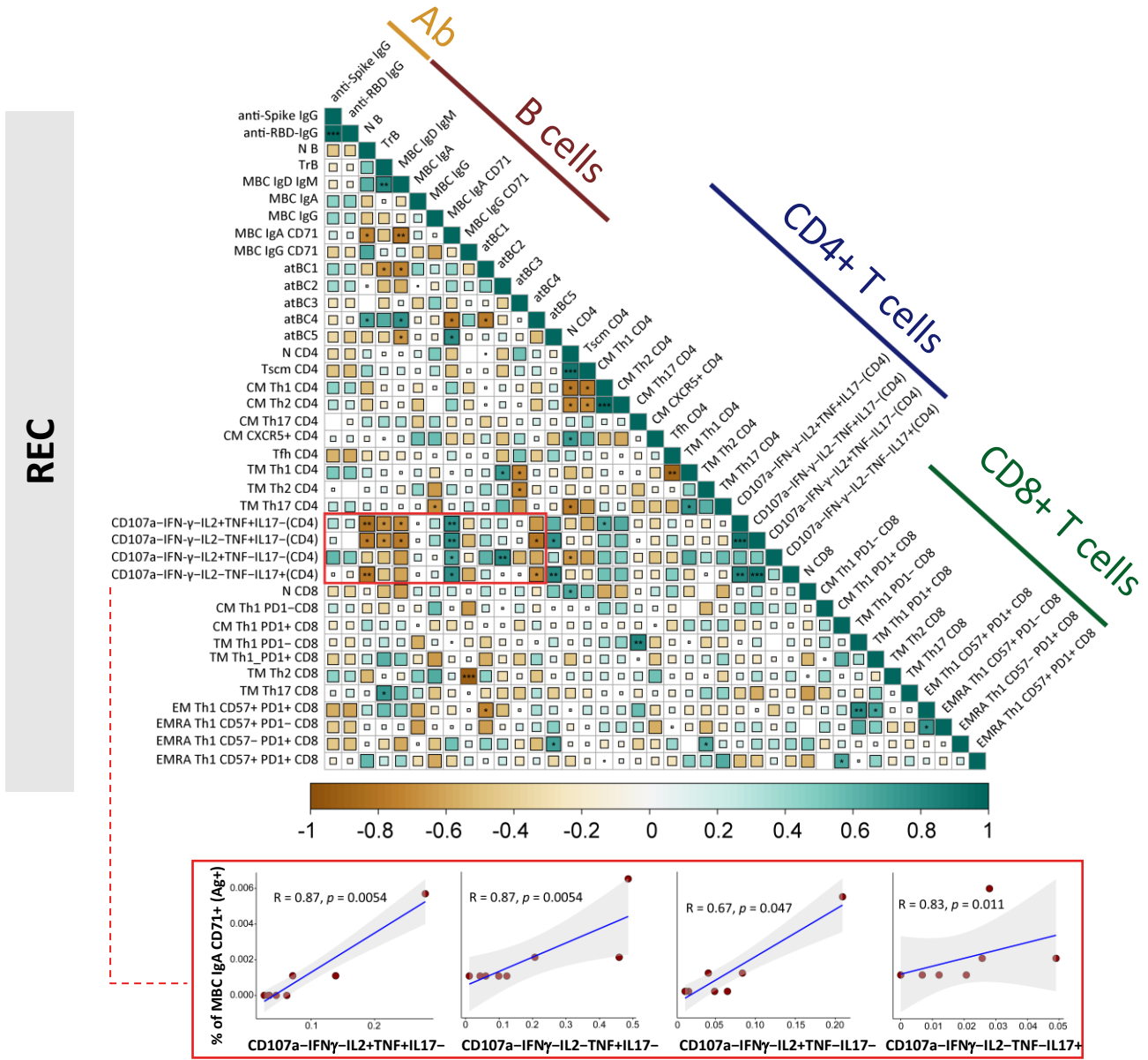
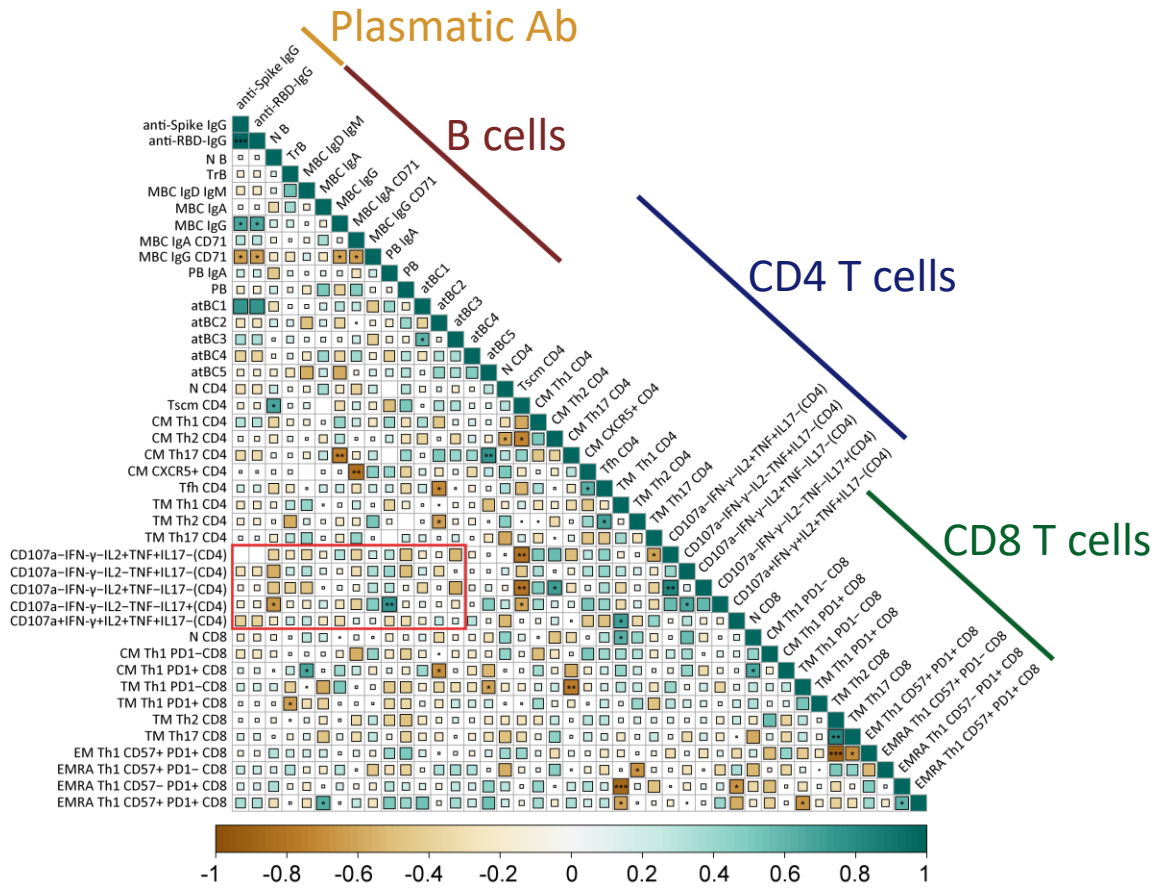


Figure 33. Principal component analysis and correlogram reveal that REC is different from MIX and RNA. (a) (Left) Principal component analysis (PCA) using the plasma level of anti-SARS-CoV-2 IgG antibodies, Ag-specific T, B-cell percentages, and the fraction of polyfunctional CD4⁺ T cells from REC, MIX, and RNA subjects. REC, green circles (n = 9); MIX, blue circles (n = 11); RNA, orange circles (n = 12). (Right) Contribution of the different variables to PCA. The color of the arrows underlines the contribution level, while the position underlines the positive or negative contribution. Negatively correlated variables are positioned on opposite sides of the plot origin (opposed quadrants). (b) Correlogram of REC. Spearman R (r) values are shown from brown (-1.0) to green (1.0); color intensity and areas of square are proportional to correlation coefficients R. Spearman rank two-tailed P-value was indicated by *P < 0.05, **P < 0.01, and ***P < 0.001. Additional XY scatter plots that specifically show the relationship between the variables that are most correlated are displayed. Each scatter plot reports the regression line (blue), the Spearman R (r) value, the exact two-tailed P-value, and the 95% confidence bands (light gray) (Lo Tartaro D., et al., 2023).

a)

AZPM



b)

PFZM

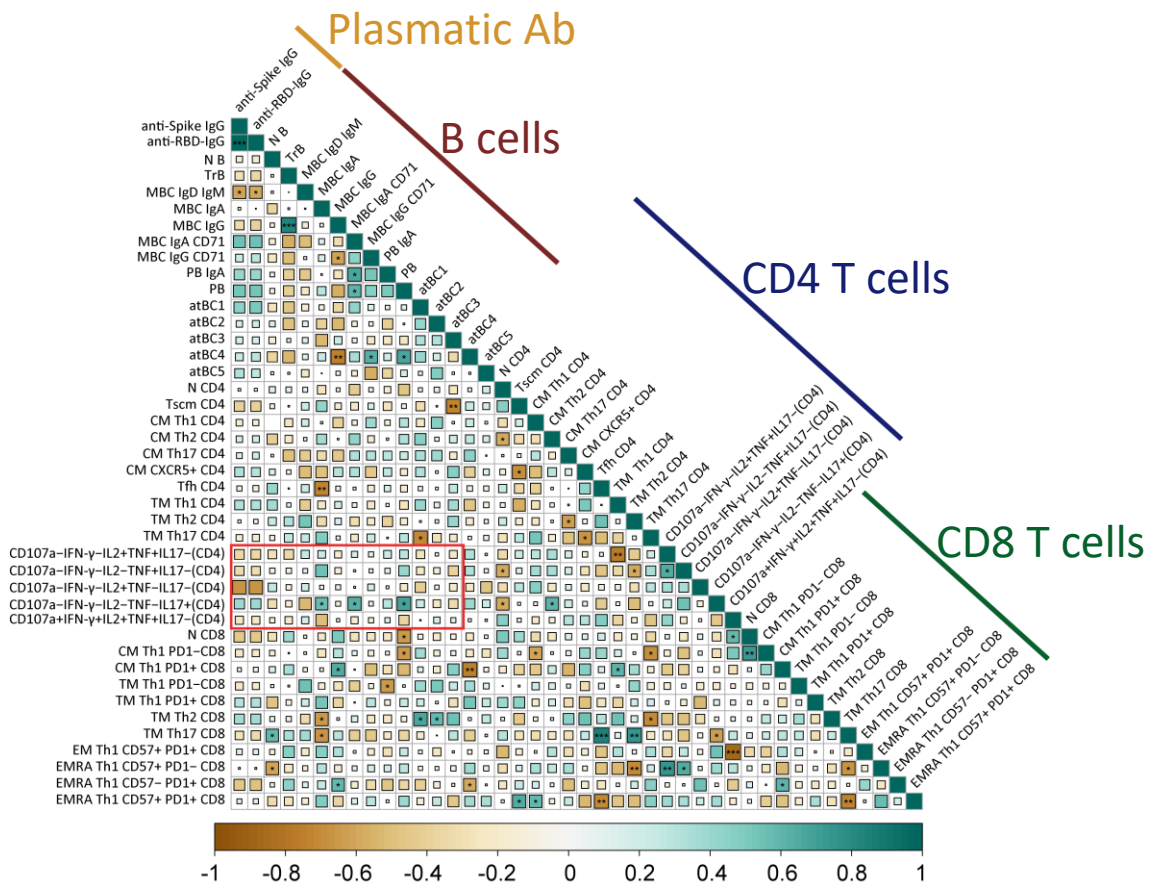


Figure 34. Correlation matrix performed on complete phenotype of Ag⁺ B and T cells, CD4⁺ T cells polyfunctionality, plasmatic anti-Spike and anti-RBD antibodies responses in a) AZPM group and b) PFZM group. Spearman R (ρ) values are shown from brown (-1.0) to green (1.0); color intensity and areas of square are proportional to correlation coefficients R. Spearman rank two-tailed p-value was indicated by *p < 0.05, **p < 0.01, and ***p < 0.001 (Lo Tartaro D., et al., 2023).

4.3 Investigation of SARS-CoV-2 specific response in multiple sclerosis patients under different disease modifying therapies

4.3.1 Demographic and clinical characteristics of the patients

MS patients and healthy donors had a median age of 44.0 (interquartile range, IQR: 41.5-48.5), were mostly female (71.7%), with a median disease duration of 14.3 years (IQR: 10.0-17.1). The most common anti-COVID-19 vaccine used was Pfizer-BioNTech (Comirnaty): 68 persons (64.2%), followed by Moderna (Spikevax): 38 persons (35.8%). Median time from the last dose of vaccine to sample collection was 4.4 months (IQR: 3.8-5.3). Demographic and clinical characteristics of 93 MS patients and 13 healthy donors (HD), the type of DMT at the time of vaccination, the type of third dose vaccine and median range of time to last administration, prior COVID-19 infection status, and relevant comorbidities are shown in **Table 10**. Patients were eligible for inclusion if they met the following criteria: a) a confirmed diagnosis of Relapsing-Remitting Multiple Sclerosis (RRMS), and b) a history of treatment with FTY, dimethyl fumarate, natalizumab, or teriflunomide for a minimum of six months, or having undergone at least two infusional cycles with rituximab/ocrelizumab or completed at least one full cycle of cladribine. Patients on ocrelizumab or rituximab, as per routine clinical practice, underwent SARS-CoV-2 vaccination at least six weeks before subsequent infusion or at least three months after the last infusion. Exclusion criteria comprised treatment with steroids during the preceding six weeks and a history of COVID-19 before vaccination. Patients treated with different DMT were enrolled such as: natalizumab (n=15; 14.2%), DMF (n=18; 17.0%), DMF patients with decreased absolute lymphocyte counts (<800/uL) at the time of sampling, defined “DMF lymphopenic” (n=10; 9.4%), interferon IFN (n=12; 11.3%), FTY (n=14; 11.3%), aCD20 [n=10; 9.4%, which included those treated with ocrelizumab (n=7; 70.0%) or rituximab (n=3; 30.0%)], cladribine (n=6; 5.7%), and teriflunomide (n=8; 7.5%).

4.3.2 MS patients treated with different DMT develop similar percentages of Ag⁺ CD4⁺ T cells, but these cells display a different phenotype compared to healthy donors

First, we investigated by manual gating the percentage of CD4⁺ T cells. **Figure 35A** shows that lymphopenic patients treated with DMF displayed higher percentage of CD4⁺ T cells if compared to HD, while all other MS patients treated with different therapies showed similar percentages of CD4⁺ T cells. The absolute number of CD4⁺ T cells was lower in patients treated with cladribine,

FTY- and lymphopenic-DMF treated patients and higher in those treated with natalizumab if compared to HD.

Then, we identified Ag⁺ T cells, defined as cells expressing CD137 and CD69 after 18 hours of *in vitro* stimulation with SARS-CoV-2 peptides (**Figure 7**) [168, 222]. As shown in **Figure 35B**, the percentage of Ag⁺ T cells within CD4⁺ T cells was similar in all MS patients and HD, confirming that MS patients treated with different drugs mount a detectable specific T cell response. The absolute number of Ag⁺ CD4⁺ T cells was lower in FTY-treated patients if compared to HD and DMF-, IFN-, natalizumab-, teriflunomide- or aCD20-treated patients. Lymphopenic patients treated with DMF displayed lower absolute number of Ag⁺ CD4⁺ T cells if compared to natalizumab-, teriflunomide- or aCD20-treated MS patients. Patients treated with DMF exhibited a higher total number of CD4⁺ Ag⁺ T cells compared to those treated with FTY, but this absolute number was lower in comparison to patients receiving natalizumab treatment. Cladribine-treated patients were characterized by a lower absolute number of these cells if compared to natalizumab- or teriflunomide-treated patients. The highest number of these cells was found in natalizumab-treated patients.

Then, the pool of Ag⁺ CD4⁺ T cells was analyzed by an unsupervised method, *i.e.*, FlowSOM, to better depict their phenotype in terms of differentiation and T helper polarization towards circulating follicular helper (Tfh), Th0/Th2, Th1 or Th17 (**Figure 35C**, **Figure 11**). Cell clustering resulted in 15 different populations that represent the entire differentiation spectrum, from the most undifferentiated cell type (*i.e.*, naïve) to the most differentiated one, such as effector memory T cells (EM). The expression of antigens such as CD45RA, CCR7, CD27, CD28 and CD95 was used to identify the differentiation status to define naïve (CD45RA⁺CCR7⁺CD27⁺CD28⁺CD95⁻), stem memory cell (T_{SCM}, CD45RA⁺CCR7⁺CD27⁺CD28⁺CD95⁺), central memory (CM, CD45RA⁻CCR7⁺CD27⁺CD28⁺CD95⁺), transitional memory (TM, CD45RA⁻CCR7⁻CD27⁺CD28⁺CD95⁺), and effector memory (EM) (CD45RA⁻CCR7⁺CD27⁺CD28⁻CD95⁺). Surface molecules such as CXCR3, CCR6, CXCR5 and PD-1 were used for a classification regarding Th polarization, *i.e.*, Th0/Th2 defined as CXCR3⁻CCR6⁻, Th1 as CXCR3⁺CCR6⁻, Th17 as CXCR3⁻CCR6⁺, Th1/Th17 as CXCR3⁺CCR6⁺ and Tfh as CXCR3⁻CCR6⁻CXCR5⁺PD-1⁺. Senescent T cells were characterized by the expression of CD57 (**Figure 35C**).

Even if MS patients mount a CD4⁺ Ag⁺ T cell response whose frequency was similar among HD and MS patients treated with different drugs, cellular composition was phenotypically different. Differences were evident for the percentage of naïve cells and the Th1 compartment as far as DMF- or teriflunomide-treated patients are concerned (**Figure 35D**), but these differences were lost when

absolute numbers were considered (**Figure 35E**). Indeed, DMF patients displayed higher percentage of naïve Ag⁺ T cells if compared to HD or to patients treated with other therapies, but this difference was not maintained in the absolute numbers. Natalizumab-treated patients displayed the highest percentage of Ag⁺ TM Th0-2 cells if compared to healthy donors or to the other treatments; this difference was maintained also for the absolute numbers. The percentage of CM Th17 Ag⁺ T cells was higher in cladribine- and teriflunomide-treated patients if compared to HD and MS patients, and these differences were maintained only for teriflunomide-treated patients, who also displayed the highest absolute number of this cells. FTY- or aCD20-treated patients displayed lower percentages of Tfh Ag⁺ cells if compared to HD or to other MS patients. This trend was maintained for the absolute number.

4.3.3 Patients treated with teriflunomide develop higher percentage of Ag⁺ CD8⁺ T cells if compared to healthy donors

Next, we aimed to investigate Ag⁺ CD8⁺T cells. **Figure 36A** shows that lymphopenic MS patients treated with DMF showed lower percentage of CD8⁺ T cells if compared to HD. Absolute number of CD8⁺ T cells was lower in cladribine-, DMF- (both groups of patients) or FTY-treated patients if compared to HD. Natalizumab-treated patients displayed the highest absolute number when compared to cladribine-, DMF-, FTY- or IFN-treated patients. Lymphopenic DMF-treated patients showed the lowest absolute number of CD8⁺ T cells when compared to the other treatments. **Figure 36B** indicates that, as far as the percentage of Ag⁺ CD8⁺ T cells is considered (gating strategy is shown in **Figure 8**), teriflunomide-treated patients displayed the highest percentage. DMF- or FTY-treated patients showed the lowest absolute number if compared to HD; moreover, lymphopenic patients treated with DMF were characterized by lower number of Ag⁺ cells if compared to natalizumab-, teriflunomide- or aCD20-treated patients.

Then, we applied the aforementioned unsupervised method of analysis, *i.e.*, FlowSOM, for the identification of the phenotype of Ag⁺ CD8⁺ T cells (**Figure 36C, Figure 12**). We could identify 12 different clusters, spanning from that of naïve Tc0 cells to terminally differentiated effector memory T cells re-expressing CD45RA (EMRA), that were also CD57⁺ and/or PD-1⁺. More in detail, FlowSOM revealed one cluster of CM Tc0/2 (CD45RA⁻CCR7⁺CD27⁺CD28⁺PD-1⁺), one cluster of TM Tc1 expressing CXCR5 (CD45RA⁻CCR7⁻CD27⁺CD28⁺PD-1⁺CXCR5⁺CXCR3⁺), five clusters of EM (mainly Tc0/2, Tc17 or Tc1 expressing or not CD57 and PD-1) and four clusters of EMRA (mainly Tc0/2, Tc17 or Tc1 expressing or not CD57 and PD-1). The phenotype of Ag⁺ CD8⁺ T cells of DMT-treated patients was quite different not only from that of HD, but also among different

therapies (**Figure 36D**). DMF patients (both lymphopenic or not) showed the highest percentage of naïve Tc0 Ag⁺ T cells, natalizumab-treated patients displayed the highest percentage of CM Tc0/2 cells, while FTY-treated patients displayed the lowest percentage of TM Tc1 CXCR5⁺ cells. As for Ag⁺ CD4⁺ T cells, DMF patients displayed the highest percentage of naïve Ag⁺ CD8⁺ T cells if compared to HD and to the other groups, but these differences were not maintained when considering their absolute number. Natalizumab-treated patients showed the highest percentage and absolute numbers of CM Tc0-2 and TM Tc1 CXCR5⁺, while teriflunomide-treated patients were characterized by high percentage and absolute number of cells EM Tc0 PD-1⁻CD57⁻ (**Figure 36E**).

4.3.4 MS patients treated with different DTM reveal polyfunctional profiles

The functional properties of Ag⁺-specific T cells were investigated by measuring the percentages of cells producing IFN- γ , TNF, IL-2, IL-17, and/or GRZB, along with the expression of the degranulation marker CD107a. The percentages of cells producing cytokines were assessed after 16 hours of *in vitro* stimulation with a SARS-CoV-2 peptide pool covering the complete sequence of SARS-CoV-2 spike glycoprotein.

MS patients treated with FTY showed the highest percentage of CD4⁺ T cells producing GRZB and the lowest percentage of CD4⁺ T cells producing IL-2, displaying a more cytotoxic profile, that is typically found in autoimmune diseases and, in particular, during MS (**Figure 37A**). Polyfunctional properties were investigated in CD4⁺ and CD8⁺ T cells by analyzing the simultaneous production of TNF, CD107a, IFN- γ , IL-2, and IL-17 using the bioinformatic Simplified Presentation of Incredibly Complex Evaluation (SPICE) tool. Healthy donors displayed a different polyfunctional profile if compared to FTY-, natalizumab-, teriflunomide- or aCD20-treated MS patients. The polyfunctional profile of natalizumab-treated patients was different from those of IFN-, DMF and DMF-treated lymphopenic patients. These differences were mainly due to the percentage of CD4⁺ T cells producing CD107a+IFN- γ -IL2+IL17-TNF+, CD107a-IFN- γ +IL2+IL17-TNF+ and CD107a-IFN γ -IL2+IL17-TNF+ (**Figure 37B**).

Regarding Ag⁺ CD8⁺ T cell, FTY-treated patients showed a higher percentage of CD8⁺ T cells producing GRZB if compared to those treated with DMF, natalizumab or IFN (**Figure 37C**). The polyfunctional profile of CD8⁺ T cells of HD was then different from those of aCD20-treated patients. The percentage of CD8⁺ T cells that were CD107a-IFN γ -IL2-IL17-TNF+ was higher in teriflunomide-treated patients if compared to those treated with DMF (**Figure 37D**).

4.3.5 Fingolimod- or anti-CD20 treated-patients displayed low or undetectable levels of Ag⁺ B cells

Natalizumab-treated MS patients were characterized by highest percentage and absolute number of B cells if compared to all groups (**Figure 38A**). Consistent with expectations, patients treated with aCD20 exhibited markedly reduced, but detectable levels of circulating B cells. Subsequently, the percentage of Ag⁺ B cells was quantified, revealing that aCD20-treated patients displayed the lowest proportion and absolute count of these cells (**Figure 38B, Figure 9**). Furthermore, patients treated with FTY showed a reduced percentage and absolute count of these cells compared to HD and individuals treated with DMF, IFN, or natalizumab, who displayed the highest proportion and count of Ag⁺ B cells among all other patients on DMTs. Moreover, the phenotype of Ag⁺ B cells was extensively characterized using the aforementioned unsupervised methods (**Figure 39**). Ag⁺ B cells were composed by 11 clusters, such as: naïve (CD20⁺CD21⁺CD24⁺CD38⁻IgD⁺IgM⁺); transitional B cells (TrB; CD20⁺CD21⁺CD27⁻CD24⁺CD38⁺IgD⁺IgM⁺); immature TrB (CD20⁺CD21⁻CD24⁺CD27⁺CD38⁺IgD⁺IgM⁺); six clusters of memory B cell MBCs defined as follows: MBC unswitched (CD20⁺CD21⁺CD24⁺CD27⁺IgD⁺IgM⁺), MBC IgA⁺ (CD20⁺CD21⁺CD24⁺CD27⁺IgD⁺IgM⁺), MBC IgG⁺ CD21^{low} (CD20⁺CD21^{low}CD24⁺CD27⁺IgG⁺), MBC IgG⁺ CD20⁻ (CD21⁺CD24⁺CD27⁺), and MBC IgG⁺ CD71⁺ (CD20⁺CD21⁺CD24⁺CD27⁺IgA⁺) and MBC IgA⁺ (CD20⁺CD21⁺CD24⁺CD27⁺CD71⁺); plasmablasts (PB) were defined as PB CD27⁺CD71⁺CD38⁺⁺; atypical B cells (atBCs) as CD21⁻CD27⁻CD20⁺IgG⁺ (**Figure 38C**). Ag⁺ B cells were phenotypically very similar in all groups except for aCD20 treated patients (**Figure 38D**). The highest percentage of naïve Ag⁺ B cells was found in FTY-treated MS patients and the lowest in aCD20-treated patients, and they both displayed the lowest absolute number of this cell population. However, natalizumab-treated patients displayed the highest absolute number. Moreover FTY-treated patients had the lowest percentage and absolute number of Ag⁺ MBC IgA cells.

Finally, the plasma levels of anti-spike IgG were measured, and nearly all MS patients developed humoral immunity. However, among the patients treated with FTY, 1 out of 14, and among those treated with aCD20, 3 out of 11, did not develop IgG. These groups, along with cladribine-treated patients, showed the lowest IgG concentrations. Additionally, when analyzing the levels of neutralizing antibodies (anti-RBD), 6 out of 8 aCD20-treated patients, 11 out of 13 FTY-treated patients, and 5 out of 6 cladribine-treated patients exhibited positive neutralizing capacity (**Figure 38E**).

4.3.6 FTY- and natalizumab-treated patients develop a different antigen-specific immune response

In order to describe an immunological signature indicating how different DMT could shape Ag-specific immunity and protection against SARS-CoV-2, we took advantage of the use of the principal component analysis (PCA) [90]. Based on the first two PCs, PCA revealed that only FTY- and natalizumab-treated patients develop a clearly different quality of the Ag-specific immune response ($p < 0.05$, **Figure 40A**), forming separate clusters, while all other groups (also including the aCD20 one) displayed similar immunological features even when compared to HD.

As shown in **Figure 40A**, FTY-treated patients form a cluster on the left side of PC1 (whose weight was 13.9%) while natalizumab-treated patients are on the right side. **Figure 40B** reveals that the main responsible of this division were the immunological features more represented in FTY-treated patients, such as: Ag⁺ cytotoxic CD4⁺ and CD8⁺ T cells (expressing CD107a and Granzyme), Ag⁺ T cells expressing of CD57 and PD-1 (indicating senescence and exhaustion/activation). On the contrary, the main features responsible for the clusterization of natalizumab-treated patients were the absolute number of Ag⁺ B and Ag⁺ CD4⁺ T cells, the number of B and CD8⁺ T cells and the marked shift of Ag⁺ T cell towards Th1 phenotype. To better point out the distinctive features of the immune response in patients undergoing treatment with natalizumab or FTY, we employed PCA specifically on these patient groups and confirmed that FTY patients are divided from patients treated with natalizumab according to PC1 (26.5%) (**Figure 40C**).

Table 10. Demographic and clinical characteristics of multiple sclerosis (MS) and healthy donor (HD) patients, type of disease modifying therapy (DMT) at the time of vaccination, type of third dose vaccine and median range of time to last administration, prior COVID-19 infection status and relevant comorbidities ((De Biasi S., et al., 2024).

Study population (N = 106)	HD (N = 13)	CLADRIBINE (N = 6)	DMF (N = 18)	DMF LYMPHO (N = 10)	FTY (N = 14)	IFN (N = 12)	NATALIZUMAB (N = 15)	TERIFLUNOMIDE (N = 8)	aCD20 (N = 10)
Age, median (IQR), y	44.0 (35.0-57.0)	45.0 (43.3-50.5)	41.5 (34.0-46.8)	48.5 (47.0-50.5)	43.0 (40.3-50.1)	50.5 (47.8-54.5)	38.0 (30.0-49.5)	51.5 (47.0-58.0)	34.0 (29.5-38.0)
Females, n (%)	10.0 (76.9)	4.0 (66.7)	13.0 (72.2)	8.0 (80.0)	10.0 (71.4)	8.0 (66.7)	12.0 (80.0)	5.0 (62.5)	6.0 (60.0)
Disease duration, median (IQR), y	–	17.5 (15.0-21.5)	5.5 (3.0-18.5)	7.0 (6.0-17.2)	16.5 (11.3-22.5)	17.5 (11.5-19.0)	12.0 (4.5-19.5)	17.0 (14.5-25.0)	11.0 (10.0-12.5)
Disability by EDSS score, median (IQR)	–	2.0 (0.5-2.8)	1.0 (0.3-2.0)	1.0 (0.0-1.0)	2.0 (1.1-3.3)	1.0 (0.0-1.8)	2.0 (1.0-3.0)	2.0 (1.0-2.7)	2.5 (1.0-4.3)
Time from last treatment starts, median (IQR), y	–	1.3 (1.0-2.7)	2.8 (2.0-4.9)	3.5 (2.5-4.8)	7.4 (6.0-8.0)	6.6 (4.3-9.1)	5.9 (1.4-9.1)	3.1 (2.3-5.9)	2.7 (1.6-4.1)
Time from last infusion to last vaccination, median (IQR), months	–	NA	NA	NA	NA	NA	1.0 (0.5-1.7)	NA	4.9 (4.2-5.2)
Absolute lymphocyte count, median (IQR), 10 ³ cells/mm ³	1.9 (1.6-2.2)	1.1 (0.7-1.7)	1.5 (1.2-1.9)	0.9 (0.8-0.9)	0.8 (0.5-0.9)	1.6 (1.3-1.9)	3.0 (2.6-4.1)	2.1 (1.8-2.2)	1.6 (1.4-2.1)
CD19 B-cell count, median (IQR), n/mm ³	NA	101.0 (97.0-142.0)	NA	NA	36.0 (28.0-40.0)	NA	NA	NA	9.5 (3.8-21.3)
Breakthrough COVID-19 after full vaccination, n (%)	4.0 (13.3)	0 (0.0)	3.0 (16.7)	2.0 (20.0)	3.0 (21.4)	1.0 (8.3)	4.0 (26.7)	0 (0.0)	1.0 (10.0)
SARS-CoV-2 IgGII titer after full vaccination, AU/mL									
Median (IQR)	12,288.5 (5,85.0-28,306.0)	4,666.1 (3,386.2-8,641.6)	14,804.3 (7,892.6-40,000.0)	12,763.2 (4,960.9-17,160.0)	1,958.0 (106.2-7,777.3)	11,277.7 (8,405.0-22,383.9)	6,058.2 (1,163.8-11,091.7)	9,812.0 (1,605.8-19,784.8)	95.5 (31.8-3,973.4)
SARS-CoV-2 RBD IgG titer after full vaccination, AU/mL									
Median (IQR)	8,237.2 (5,275.8-13,011.2)	2,798.8 (1,668.3-4,417.1)	7,160.0 (5,201.2-17,953.5)	10,204.3 (3,967.3-14,666.8)	1,764.2 (63.5-6,542.3)	7,124.1 (4,974.9-20,010.2)	4,964.8 (1,183.1-9,854.2)	4,552.8 (732.3-10,868.5)	65.8 (4.0-3,580.0)
Time from first vaccination to sampling, median (IQR), months	12.0 (9.0-15.1)	13.2 (10.2-15.9)	13.2 (9.6-15.6)	11.5 (10.3-13.0)	11.5 (10.3-13.0)	11.6 (10.3-12.7)	14.1 (9.5-15.5)	12.8 (11.2-14.2)	11.8 (10.0-15.5)
Time from last vaccination to sampling, median (IQR), months	3.5 (1.8-6.1)	4.8 (2.5-8.3)	5.8 (2.1-8.2)	3.9 (2.6-5.0)	3.9 (2.6-5.0)	3.5 (2.1-5.0)	5.5 (1.9-6.7)	5.4 (4.1-6.9)	2.4 (1.7-6.0)
Type of third vaccine dose									
BNT162b2, n (%)	8.0 (61.5)	3.0 (50.0)	11.0 (61.1)	5.0 (50.0)	8.0 (57.1)	6.0 (50.0)	14.0 (93.3)	5.0 (62.5)	8.0 (80.0)
mRNA-1273, n (%)	5.0 (38.5)	3.0 (50.0)	7.0 (38.9)	5.0 (50.0)	6.0 (42.9)	6.0 (50.0)	1.0 (6.7)	3.0 (37.5)	2.0 (20.0)

HD, healthy controls; Cladribine; DMF, Dimethyl Fumarate; DMF Lympho, Dimethyl Fumarate Lymphopenic; FTY, Fingolimod; IFN, interferon; Natalizumab; Teriflunomide; aCD20 (Ocrelizumab; Rituximab); IQR interquartile range; AU, arbitrary unit.

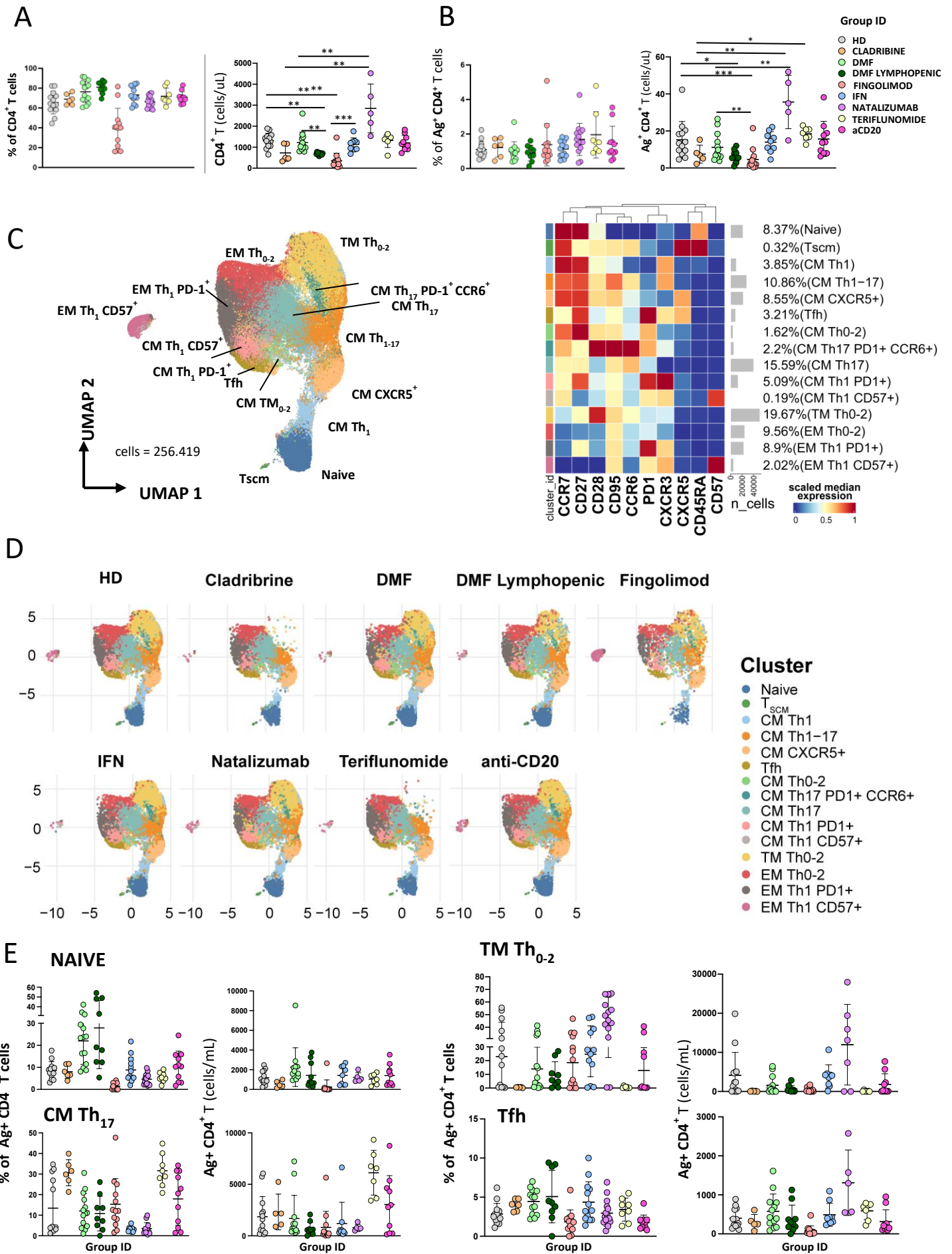


Figure 35. Ag⁺ CD4⁺ T cell landscape. **A) Percentage of Ag⁺ CD4⁺ T cells.** Dot plots show the cell percentage of the antigen-specific (Ag⁺) CD4⁺ T cells. The central bar represents the mean ± SEM. Kruskal–Wallis test with Benjamini–Hochberg correction for multiple comparisons was used to test the differences among the three groups. Significant adjusted q-values are reported in the figure. **B) Absolute number of Ag⁺ CD4⁺ T cells.** Dot plots show the absolute number of the antigen-specific (Ag⁺) CD4⁺ T cells. The central bar represents the mean ± SEM. Kruskal–Wallis test with Benjamini–Hochberg correction for multiple comparisons was used to test the differences among the three groups. Significant adjusted q-values are reported in the figure. **C) Ag⁺ CD4⁺ T cells phenotype UMAP and Heatmap.** Uniform Manifold Approximation and Projection (UMAP) plot shows the 2D spatial distribution of 256,419 cells from 28 healthy donors (HD) and 106 MS patients treated with different DMT embedded with FlowSOM clusters. Ag⁺, antigen-specific CD4⁺ T cells; Heatmap of the median marker intensities of the 10 lineage markers across the 15 cell populations obtained with FlowSOM algorithm after the manual metacluster merging. The colors of cluster_id column correspond to the colors used to label the UMAP plot clusters. The color in the heatmap is referred to the median of the *arcsinh* marker expression (0–1 scaled) calculated over cells from all the samples. Blue represents lower expression, while red represents higher expression. Light gray bar along the rows (clusters) and values in brackets indicate the relative sizes of the clusters. N, naive; T_{SCM}, T stem cell memory; CM, central memory; TM, transitional memory; EM, effector memory; EMRA, effector memory reexpressing the CD45RA; cTfh, circulating T follicular helper cells. **D) UMAP graphs stratified by therapy:** HC, healthy controls; Cladribine, DMF, Dimethyl Fumarate; DMF Lymphopenic, Dimethyl Fumarate Lymphopenic; Fingolimod; IFN, interferon; Natalizumab; Teriflunomide; aCD20. **E) Dot plots of different subpopulation of Ag⁺ T cells in patients treated with different DMT.** Kruskal–Wallis test with Benjamini–Hochberg correction for multiple comparisons was used to test the differences among the three groups (De Biasi S., et al., 2024).

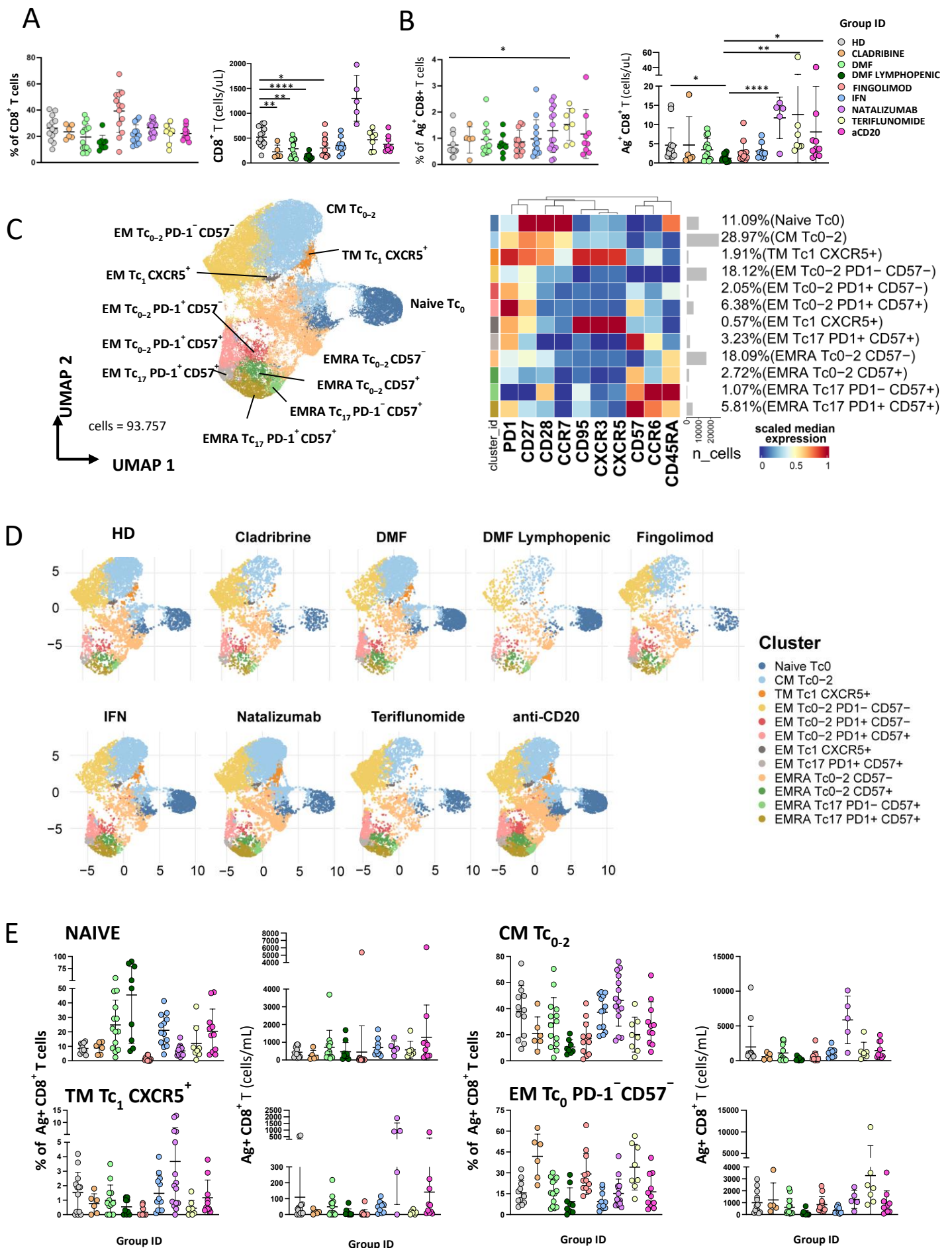


Figure 36. Ag⁺ CD8⁺ T cell landscape. **A) Percentage of Ag⁺ CD8⁺ T cells.** Dot plots show the cell percentage of the antigen-specific (Ag⁺) CD8⁺ T cells. The central bar represents the mean ± SEM. Kruskal–Wallis test with Benjamini–Hochberg correction for multiple comparisons was used to test the differences among the three groups. Significant adjusted q-values are reported in the figure. **B) Absolute number of Ag⁺ CD8⁺ T cells.** Dot plots show the absolute number of the antigen-specific (Ag⁺) CD4⁺ T cells. The central bar represents the mean ± SEM. Kruskal–Wallis test with Benjamini–Hochberg correction for multiple comparisons was used to test the differences among the three groups. Significant adjusted q-values are reported in the figure. **C) Ag⁺ CD8⁺ T cells phenotype UMAP and Heatmap.** Uniform Manifold Approximation and Projection (UMAP) plot shows the 2D spatial distribution of 93,757 cells from 28 healthy donors (HD) and 106 MS patients treated with different DMT embedded with FlowSOM clusters. Ag⁺, antigen-specific CD8⁺ T cells; Heatmap of the median marker intensities of the 10 lineage markers across the 12 cell populations obtained with FlowSOM algorithm after the manual metacluster merging. The colors of cluster_id column correspond to the colors used to label the UMAP plot clusters. The color in the heatmap is referred to the median of the *arcsinh* marker expression (0–1 scaled) calculated over cells from all of the samples. Blue represents lower expression, while red represents higher expression. Light gray bar along the rows (clusters) and values in brackets indicate the relative sizes of the clusters. N, naive; T_{SCM}, T stem cell memory; CM, central memory; TM, transitional memory; EM, effector memory; EMRA, effector memory reexpressing the CD45RA; cTfh, circulating T follicular helper cells. **D) UMAP graphs stratified by therapy:** HC, healthy controls; Cladribine, DMF, Dimethyl Fumarate; DMF Lymphopenic, Dimethyl Fumarate Lymphopenic; Fingolimod; IFN, interferon; Natalizumab; Teriflunomide; aCD20. **E) Dot plots of different subpopulation of Ag⁺ T cells in patients treated with different DMT.** Kruskal–Wallis test with Benjamini–Hochberg correction for multiple comparisons was used to test the differences among the three groups (De Biasi S., et al., 2024).

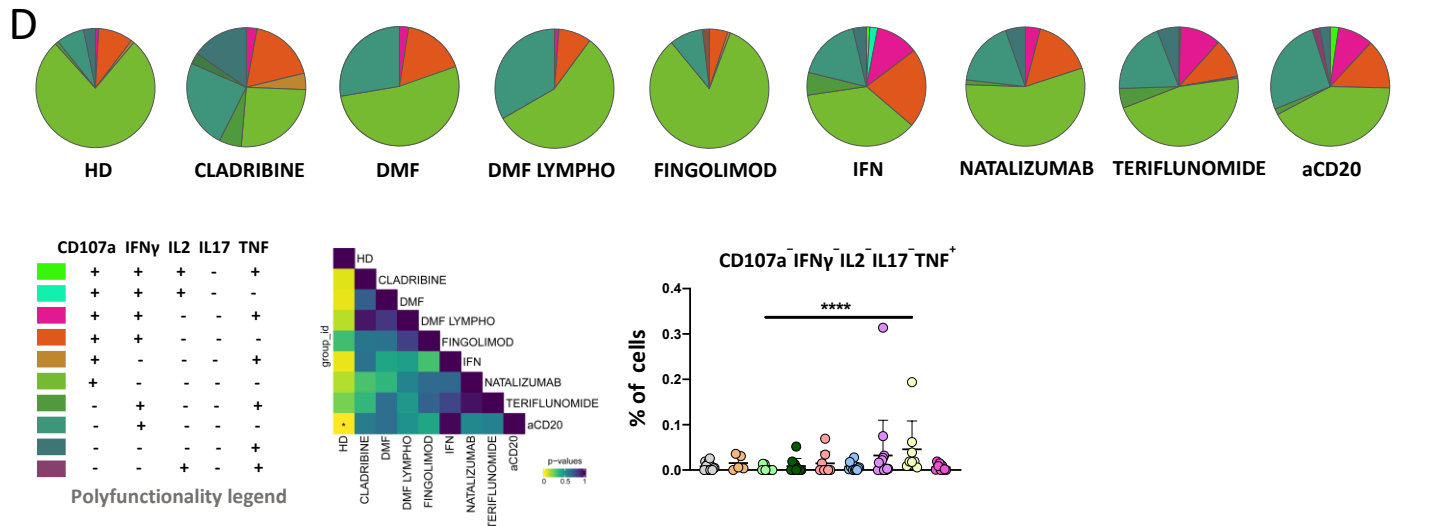
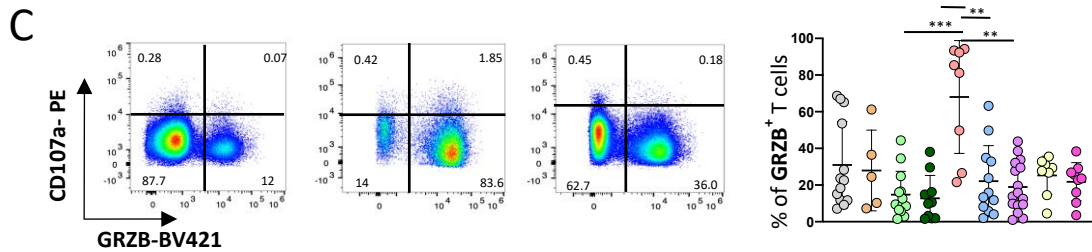
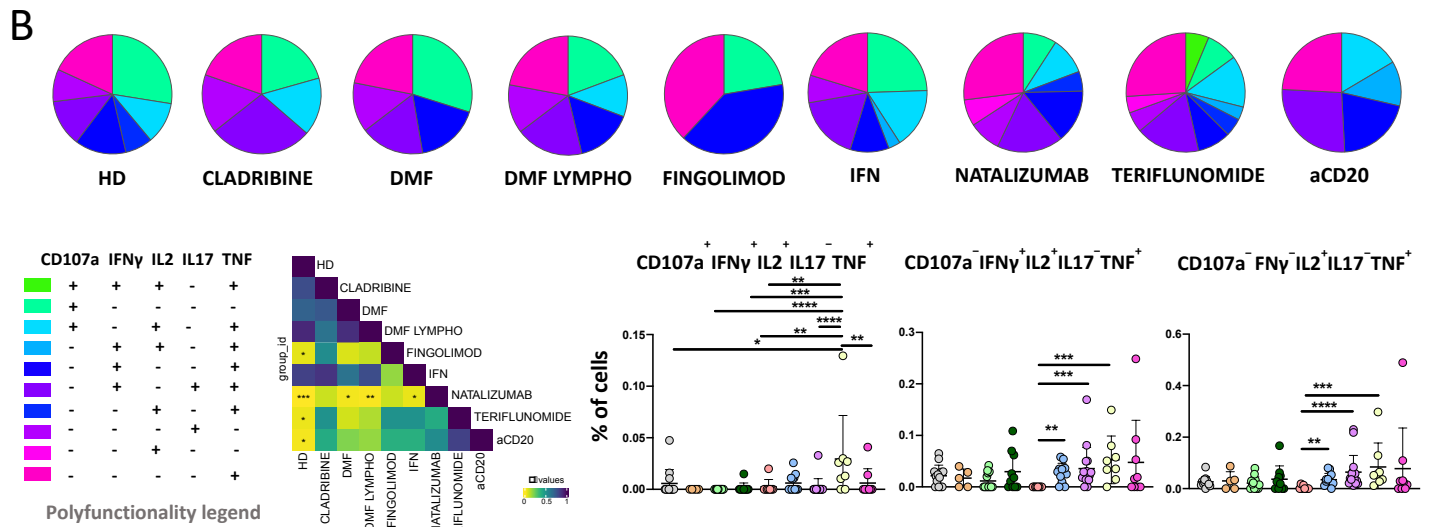
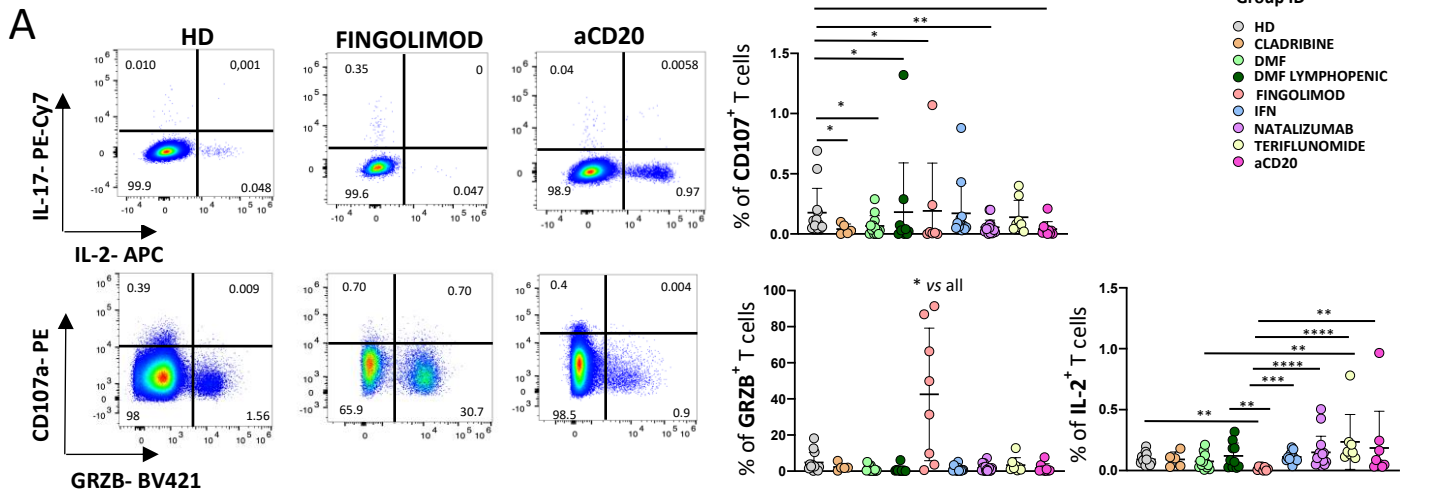


Figure 37. Ag⁺ CD4⁺ and CD8⁺ T cell functionality. A) Total percentage of Ag⁺ CD4⁺ T cells producing different cytokines after *in vitro* stimulation with SARS-CoV-2 peptides. Representative dot plots showing the percentages of CD4⁺ Ag⁺ cells producing IL-2, IL-17, CD107a and granzyme B (GRZB). Pots show mean (centre bar) ± SEM (upper and lower bars). Kruskal-Wallis test with Benjamini-Hochberg correction for multiple comparisons was used to test the differences among the nine groups. **B) Polyfunctional profile of Ag⁺ CD4⁺ T cells.** (Upper) Pie charts representing the proportion of Ag⁺ CD4⁺ T cells producing different combinations of CD107a, IL2, IL17, IFN γ , and TNF after *in vitro* stimulation with SARS-CoV-2 peptides. Each color refers to specific polyfunctional CD4 T subpopulation as reported in the ‘polyfunctionality legend’. The far-left heatmap illustrates the statistical variances among the 9 distinct pie charts; Kruskal-Wallis test with Benjamini-Hochberg correction for multiple comparisons was used to test the differences among the nine groups.. (far-right) Dot plot reporting the percentages of Ag⁺ CD4⁺ CD107a⁺IFN γ ⁺IL2⁺IL17⁻TNF⁺, CD107a⁻IFN γ ⁺IL2⁺IL17⁻TNF⁺ and CD107a⁻IFN γ ⁻IL2⁺IL17⁻TNF⁺ populations are depicted. Kruskal-Wallis test with Benjamini-Hochberg correction for multiple comparisons was used to test the differences among the nine groups. **C) Total percentage of Ag⁺ CD8⁺ T cells producing different cytokines after *in vitro* stimulation with SARS-CoV-2 peptides.** Manual gating strategy of Ag⁺ CD8⁺ cells producing CD107a and GRZB. The numbers displayed on the plot represent the relative percentages of these cells. Dot plot representing the percentage of Ag⁺ CD8⁺ T cells producing GRZB is shown, mean (centre bar) ± SEM (upper and lower bars). Kruskal-Wallis test with Benjamini-Hochberg correction for multiple comparisons was used to test the differences among the nine groups. **D) Polyfunctional profile of Ag⁺ CD8⁺ T cells.** (Upper) Pie charts representing the proportion of Ag⁺ CD8⁺ T cells producing different combinations of CD107a, IL2, IL17, IFN γ , and TNF after *in vitro* stimulation with SARS-CoV-2 peptides. Each color refers to specific polyfunctional CD8 T subpopulation as reported in the ‘polyfunctionality legend’. The far-left heatmap illustrates the statistical variances among the 9 distinct pie charts; Kruskal-Wallis test with Benjamini-Hochberg correction for multiple comparisons was used to test the differences among the nine groups.. (Right) Dot plot reporting the percentages of Ag⁺ CD8⁺ CD107a⁻IFN γ ⁻IL2⁻IL17⁻TNF populations. Kruskal-Wallis test with Benjamini-Hochberg correction for multiple comparisons was used to test the differences among the nine groups (De Biasi S., et al., 2024).

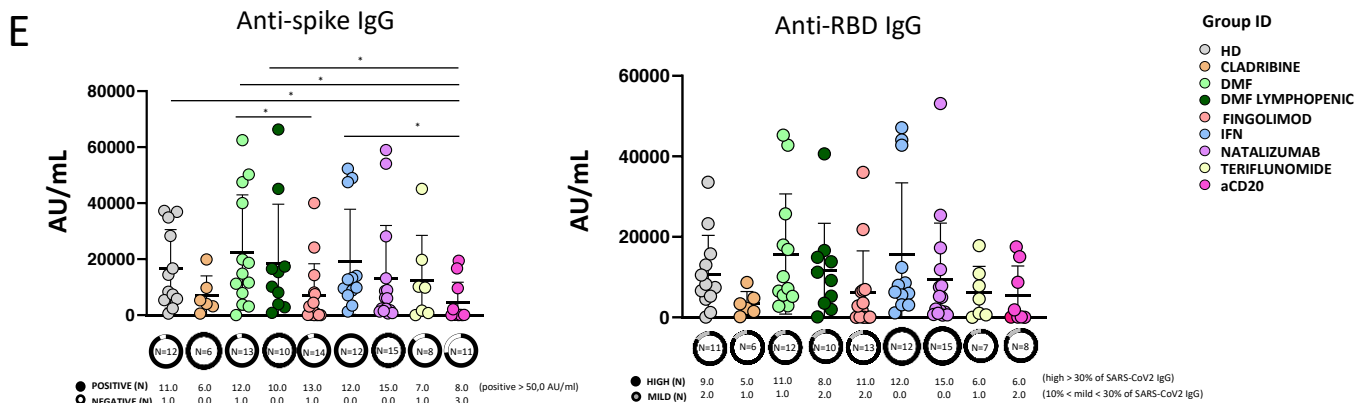
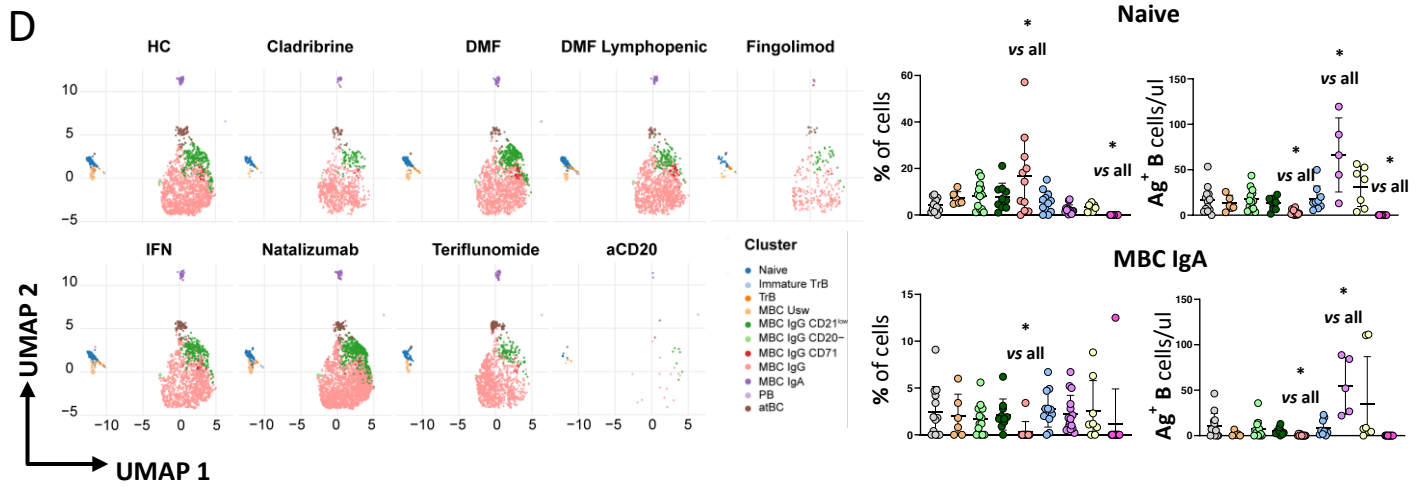
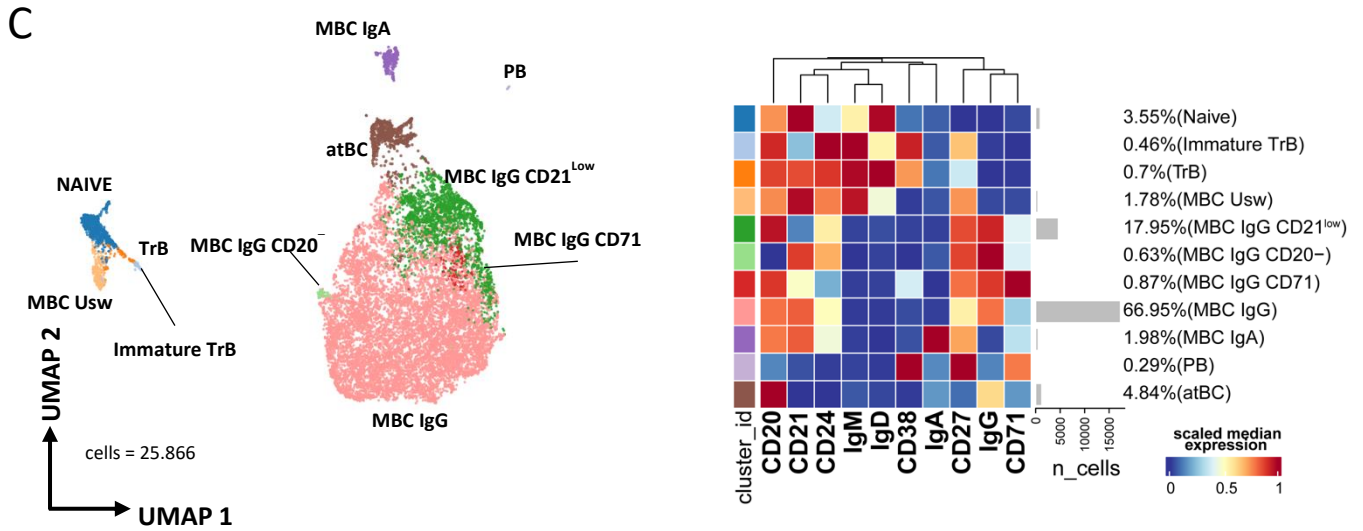
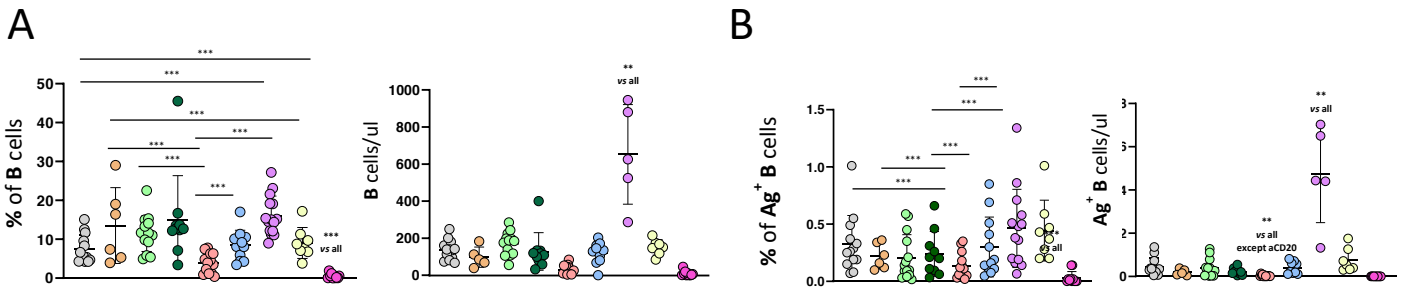


Figure 38. Ag⁺ B cell landscape. **A)** Dot plot shows the total percentage and the absolute number of CD19⁺ B cells. Kruskal–Wallis test with Benjamini–Hochberg correction for multiple comparisons was used to test the differences among the nine groups. **B)** Dot plot shows the percentage and absolute number of antigen-specific CD19⁺ B cells. **C)** UMAP plot shows the 2D spatial distribution of 25,866 antigen-specific B cells from 28 healthy controls (HD) and 106 patients with Multiple Sclerosis embedded with FlowSOM clusters. Heatmap of the median marker intensities of the 10 lineage markers across the 11 cell populations obtained with FlowSOM algorithm after the manual metacluster merging. The colors of cluster_id column on the left correspond to the colors used to label the UMAP plot clusters. Each color in the heatmap is referred to the median of the arcsinh marker expression (0–1 scaled) calculated over cells from samples. Blue represents lower expression, while red represents higher expression. Light gray histogram bar and values indicate the relative sizes of the clusters. Naïve; TrB, transitional B cells; MBC Usw, memory B cell unswitched; MBC, memory B cell; PB, plasmablasts; atBC, atypical B cell. **D)** (Left) UMAP graphs stratified by therapy. (Right) Dot plot showing the percentages and absolute numbers of naïve and MBC IgA B cells. **E)** Anti-spike and anti-RBD IgG concentrations in plasma samples from HD and MS treated groups. Kruskal–Wallis test with Benjamini–Hochberg correction for multiple comparisons was used to test the differences among the three groups. Adjusted P-values are indicated in the figure. HD, healthy donor; Cladribine, DMF, Dimethyl Fumarate; DMF Lymphopenic, Dimethyl Fumarate Lymphopenic; Fingolimod; IFN, interferon; Natalizumab; Teriflunomide; aCD20 (De Biasi S., et al., 2024).

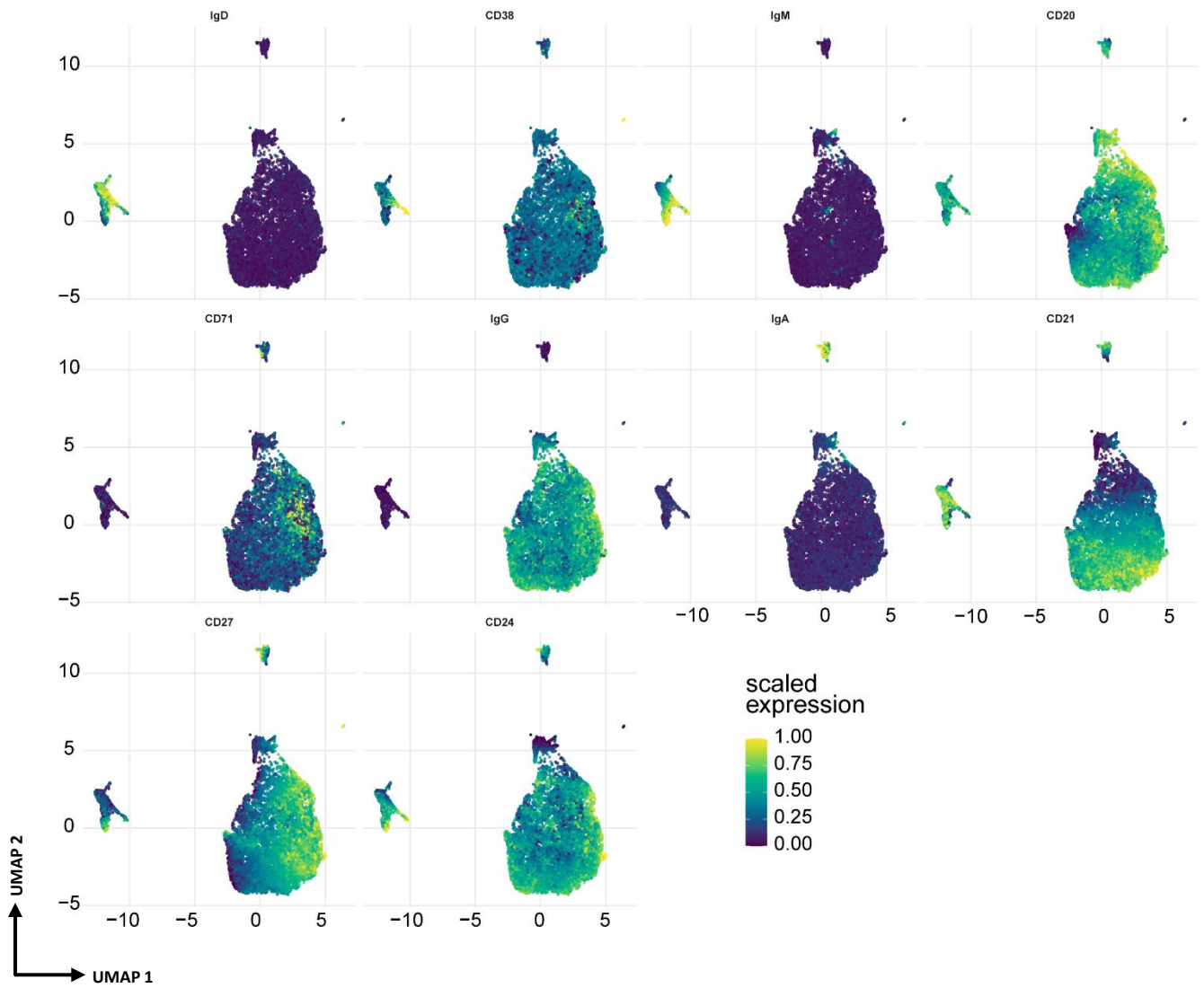
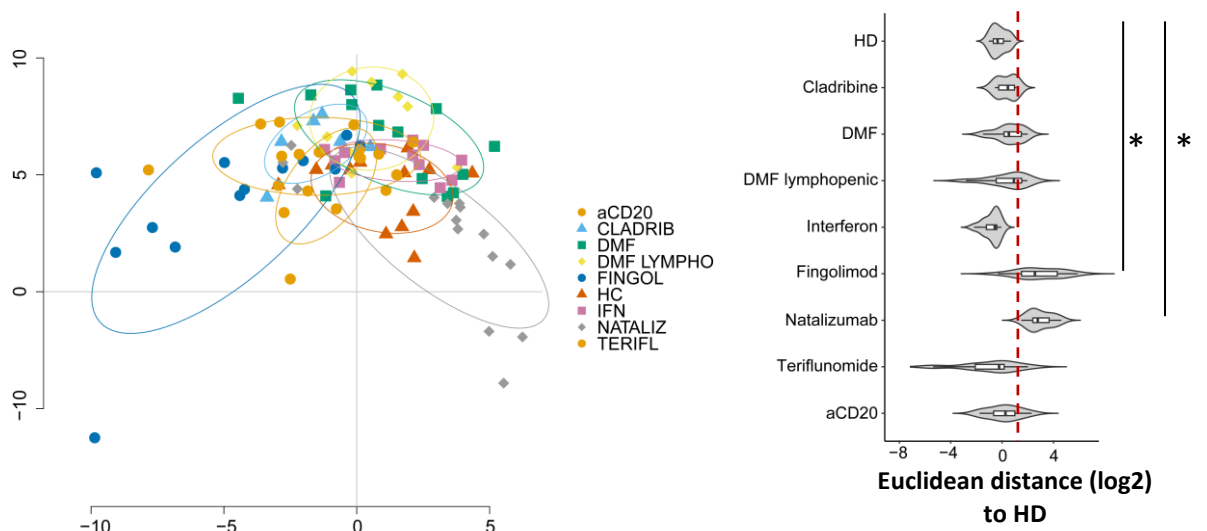
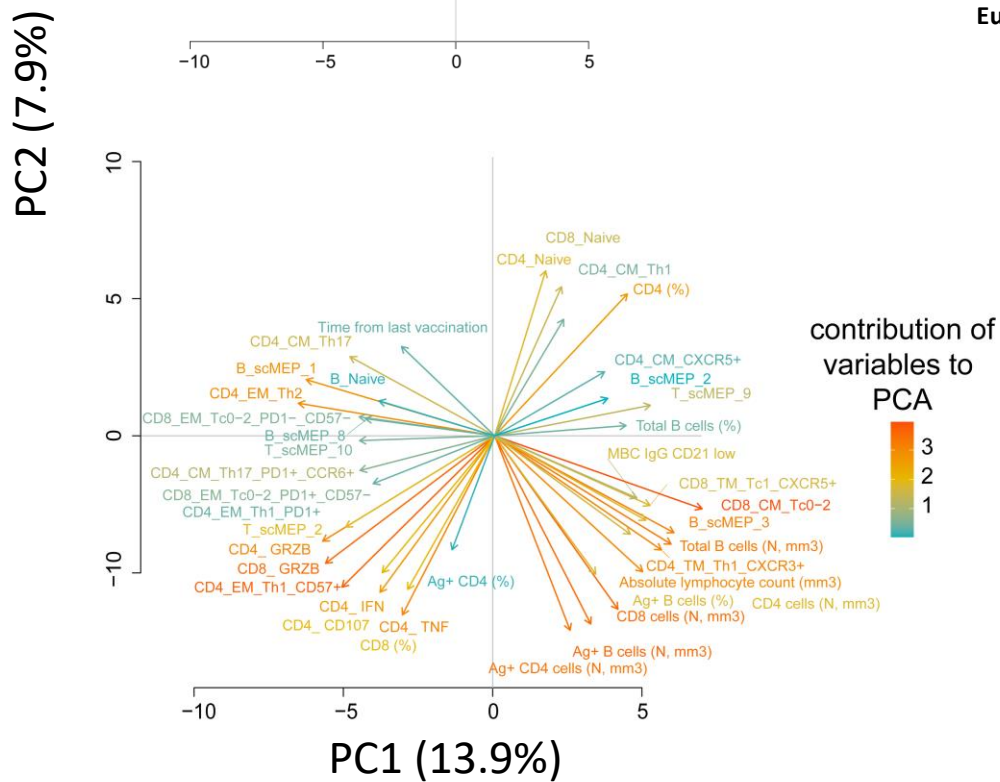


Figure 39. Uniform Manifold Approximation and Projection (UMAP) plot shows the 2D spatial distribution of B cells from 28 healthy donors vaccinated against Sars-CoV-2 and 106 patients with multiple sclerosis undergoing different disease-modifying therapies (DMT) and vaccinated against COVID-19. UMAP graphs colored by the expression of 10 markers used for CD19⁺ antigen specific B cell phenotyping. Blue represents lower expression while yellow represent higher expression (De Biasi S., et al., 2024).

A



B



C

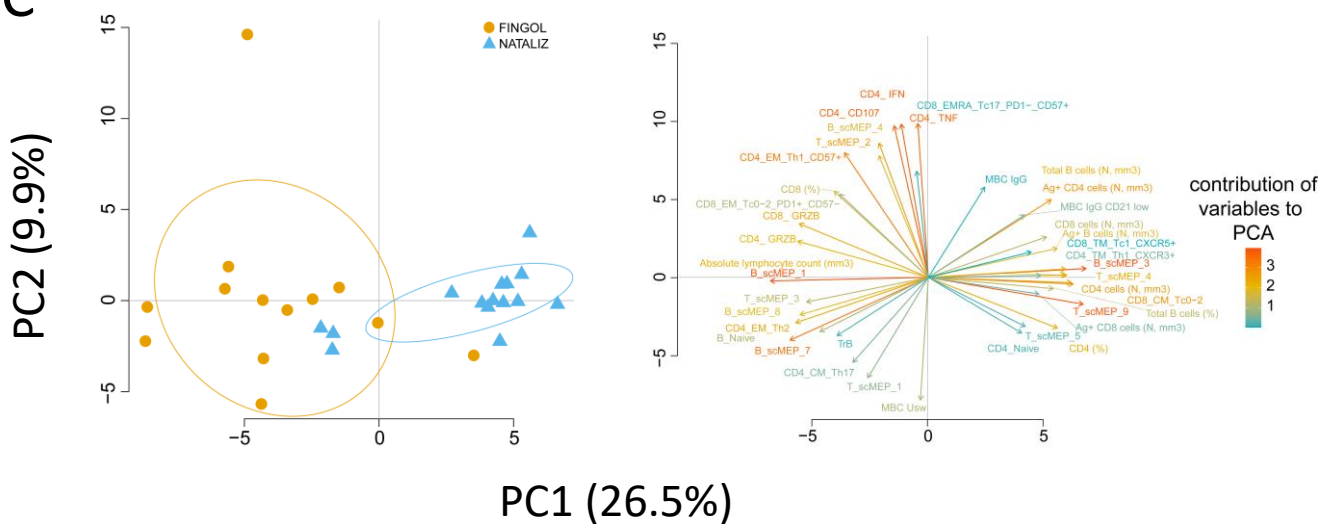


Figure 40. Principal component analysis (PCA) of HD and MS treated groups. **A)** PCA showing the spatial distribution of vaccinated MS patients treated with different DMT and healthy donors. Euclidean distance to HD has been calculated. Kruskal–Wallis test with Benjamini–Hochberg correction for multiple comparisons is used to test the differences among groups, * $p < 0.05$. **B)** Plot displaying the variables as vector, indicating the direction of each variable to overall distribution. The strength of each variable is represented by colors: orange color represents a strong contribution; light blue color represents a milder contribution. Length and direction of the arrows indicate the weight and correlation for each parameter. **C)** (Left) PCA showing the spatial distribution of MS patients treated with fingolimod or natalizumab after SARS-CoV-2 vaccination, (Right) contribution of each immunological variables to PCA (De Biasi S., et al., 2024).

5. DISCUSSION

5.1 Patients Recovering from Severe COVID-19 Develop a Polyfunctional Antigen-Specific CD4⁺ T Cell Response

In this study, we describe the differences in the production of cytokines by SARS-CoV-2-specific T cells from patients with COVID-19 (severe or moderate) and in recovered individuals after *in vitro* stimulation with different peptide pools. Our aim was to measure not only the magnitude but also the characteristics, in qualitative terms, of such antigen-specific response. We found that COVID-19 moderate patients develop polyfunctional CD4⁺ T cells compared to patients experiencing a severe infection, that in turn display a higher percentage of CD107a⁺ cells. Besides their helper capability, CD4⁺ T cells can exert cytotoxicity, and this has been described during persistent infections such as those by Epstein–Barr virus [254], cytomegalovirus [255], and Human Immunodeficiency Virus (HIV) [256]. Cytotoxic potential can be measured, detecting the expression of the degranulation marker CD107a [257]. This result is in line with other studies demonstrating that patients experiencing severe COVID-19 usually mount an impaired SARS-CoV-2 T cell-specific response [135,258]. It is known that the expression of exhaustion markers such as Programmed Death-1 (PD-1) and T-cell immunoglobulin and mucin domain-3 (Tim-3) is associated with disease progression [165,259]. This might reinforce the concept that patients experiencing a more severe infection present impaired CD4⁺ and CD8⁺ T cell functionality due to an exhausted phenotype. However, whether the expression of such markers reflects functional exhaustion rather than ongoing activation is still debated [165].

During the infection, Th1 cytokines such as IFN- γ , IL-2 and TNF are essential for supporting the expansion and maturation of CD8⁺ T lymphocytes and B cells. The loss of CD4⁺ Th1 leads to a progressive CD8⁺ T cell decline and dysfunction with important implications for controlling the infection [260]. In addition, Th17 cells are responsible for the recruitment of several different cell populations at the site of the infection, inducing the inflammatory process necessary for the immediate protective response against a pathogen [192,193]. We found that, if compared to patients experiencing severe COVID-19, those recovering from severe COVID-19 display SARS-CoV-2-specific, highly polyfunctional CD4⁺ T cells with a Th1 and Th17 phenotype. No differences were reported in the CD8⁺ T cell compartment, reflecting the T cell kinetics of the immune response contraction according to which 2 weeks after onset symptoms, when circulating CD8⁺ T cells progressively decline, CD4⁺ T cells remain stable and eventually increase in the initial recovery phase (1–2 months after infection), more than immediately after infection [135,261].

T cells are able to both proliferate and secrete cytokines that in turn can influence other cell functions as well as induce cytolysis of infected cells. Polyfunctionality is the ability of cells to simultaneously perform more than one function, and it can be measured at a single cell level by flow cytometry [262]. In CD4⁺ T cells, such property is a correlate for protection against different pathogens. As an example, comparing the profile (more than the amount) of T cell cytokine production in different groups of HIV-infected individuals such as in those who control the infection to that of patients with a chronic progression of the infection revealed the presence of several key molecules involved in controlling the infection. This approach suggested that in some cases the quality of the T cell response, not the quantity, is correlated with immune protection [191]. During cytomegalovirus (CMV) infection, the development of polyfunctional T cells correlates with a better prognosis and confers an immunological advantage against other pathogens [190]. In addition, polyfunctional CD4⁺ T cells represent a marker for spontaneous control of viral replication in CMV-seropositive patients undergoing liver transplantation [263]. On the whole, this indicates the importance of measuring representative functions of T cells to identify and define correlates of immune protection.

The identification of the most immunogenic epitopes is key to the study and understanding of cellular immune response to gain insights into virus-induced infection mechanisms. An immunogenic peptide is one that is presented by a self-major histocompatibility complex (MHC) and is able to elicit a T cell response [264]. Thus, the identification of such epitopes is also of importance in the context of future therapies.

M, N and S are SARS-CoV-2 structural proteins that constitute different portions of the virus. These proteins have different interactions with the other parts of the virion, and during the infection, they interact differently and in different moments with the host cell. This may define a different level of immunogenicity for each protein. For these reasons, we deepened the SARS-CoV-2 specific response to M, N and S. Overall, in our study we observed that M, N and S induced a similar response among the categories considered, confirming their co-dominance [171,265].

We are aware that this study has a main limitation since the number of individuals that we could study is relatively small, because of the difficulties to obtain biological material from patients admitted to the hospital. However, even if we could study a relatively low number of patients, we could define the polyfunctionality profile of CD4⁺ and CD8⁺ T cells during and after SARS-CoV-2 infection in patients experiencing different severities of COVID-19. Global knowledge of the complex interaction during the cellular response to infection, as well as SARS-CoV-2-induced changes, is helping in understanding mechanisms beyond the immune response toward protective phenotype. In addition, the identification of unique cell subsets involved in immune protection could

allow us to develop and use more and more sophisticated techniques that accurately measure the outcome of new therapies. Thus, the successful use of functional T cell analyses will likely help to significantly advance the field of SARS-CoV-2 therapy as well as vaccine efficacy, and hopefully, aid in reducing the global burden of the pandemic.

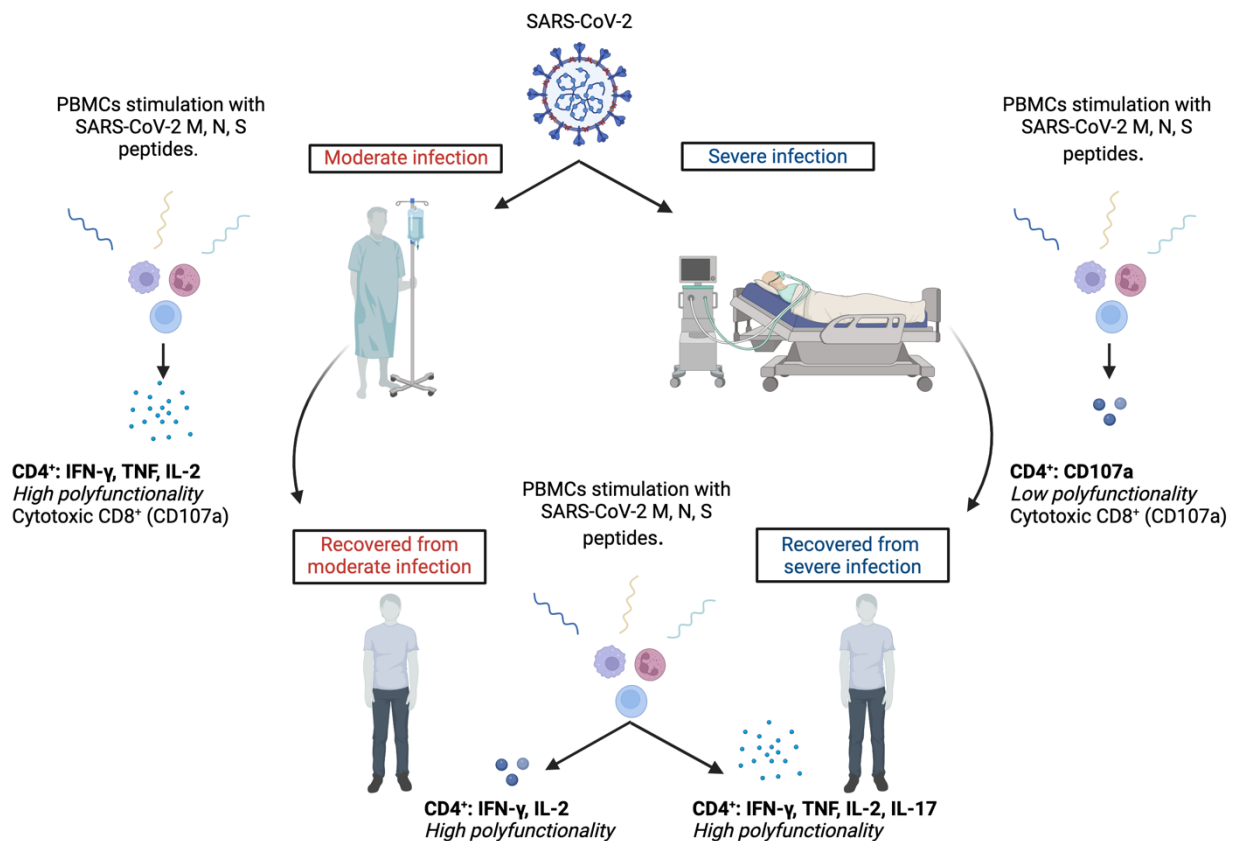


Figure 41. Study of antigen-specific CD4⁺ and CD8⁺ T cell response in patients experiencing and recovering from moderate or severe COVID-19. Blood samples were withdrawn, peripheral blood mononuclear cells (PBMCs) were isolated and separately stimulated with different antigenic peptides of SARS-CoV-2. CD4⁺ T cells producing cytokines were identified using flow cytometry techniques. In cases of moderate infection, a high percentage of CD4⁺ T cells producing various cytokines, including IFN- γ , TNF, and IL-2, were observed. CD8⁺ T cells exhibited a more cytotoxic phenotype characterized by the production of CD107a; high polyfunctionality was a main characteristic of this immune response. On the other hand, patients experiencing severe infection exhibited a more impaired response, with CD4⁺ and CD8⁺ cells mostly producing CD107a (cytotoxic phenotype) and showing low polyfunctionality. However, in the recovery phase, patients presented a different immune response. While patients recovering from moderate infection exhibited a high percentage of CD4⁺ T cells producing IFN- γ and IL-2, those recovering from severe infection showed CD4⁺ T cells producing more cytokines, as IFN- γ , IL-2, IL-17, and TNF. CD4⁺ T cell polyfunctionality was similar for both patient cohorts. The figure was created with *BioRender.com*.

5.2 Detailed characterization of SARS-CoV-2-specific T and B cells after infection or heterologous vaccination

Vaccines are designed to induce a long-term adaptive immune response that confers durable protection. In this study, as revealed by PCA, we report that COVID-19 recovered patients show different long-term immunological profiles compared to those of donors who had been vaccinated with three doses (either with adenovirus or mRNA technologies). Vaccinated individuals display a skewed Th1 Ag-specific T-cell polarization and a higher percentage of Ag-specific and activated MBCs expressing IgG compared to those of patients who recovered from severe COVID-19. Different polyfunctional properties characterize the two groups: recovered individuals show higher percentages of CD4⁺ T cells producing one or two cytokines simultaneously, while vaccinated donors are distinguished by highly polyfunctional populations able to release four molecules such as CD107a, IFN- γ , TNF, and IL-2.

SARS-CoV-2 entry route shapes the innate immune response, as major players such as macrophages and neutrophils contribute to recruit T and B cells that should mount a local specific immune response, with the consequent production of mucosal antibodies. This means that different adaptive mechanisms are involved in the protective immunity generated by the infection or vaccination. Indeed, we found that recovered individuals are characterized by higher percentages of MBCs producing IgA if compared to those of vaccinated ones. However, systemic and mucosal IgA responses are variably induced in response to vaccination and are associated with protection against subsequent infection [266,267].

SARS-CoV-2-specific cells wane more slowly than do antibodies [reviewed in [268]], and T cells able to exert an efficient protection are those capable of exerting many functions simultaneously. Polyfunctional T-cell responses have been documented also in HIV-1 [191], hepatitis B virus vaccine [269], and vaccinia-induced responses [270], indicating that highly functional T-cell responses are commonly found in response to other viral infections and vaccination and are effectively controlled by cellular immunity. The functional population able to produce four cytokines or more is likely of significant immunologic importance because it could directly eliminate virally infected cells (assuming that such cells express or upregulate CD107a) and suppress viral replication while maintaining itself without CD4⁺ T-cell help through autocrine production of IL-2.

We found that vaccinated donors are characterized by MBCs IgG-switched that express CD71. Ag-specific B cells can be divided into antibody-secreting cells (or PBs) and MBCs after infection or vaccination. A particular subset of B cells, called activated B cells, is distinct from

antibody-secreting cells and is committed to the MBC lineage. Activated B cells are characterized by the expression of CD71, which is the transferrin receptor and indicates higher activation status and proliferative capabilities [271]. This population is also typically found in blood after infection with Ebola or influenza virus and also after vaccination [272,273].

As far as vaccination strategy is concerned, the ChAdOx1 vaccine uses a nonreplicating adenovirus as a vector to introduce into the cells of the recipient's DNA coding for the spike protein of SARS-CoV-2. BNT162b2 instead uses messenger RNA (mRNA) coding for spike, which cells take up and use to synthesize the protein. mRNA vaccines are good at inducing antibody responses, and the vector-based vaccines are better at triggering T-cell responses. In a Spanish study, people who received a dose of the Pfizer-BioNTech vaccine 8 weeks after an initial AstraZeneca dose had few side effects and a robust antibody response 2 weeks after the second shot, suggesting that mixing the two types of vaccine may give the immune system multiple ways to recognize a pathogen [274]. However, in our small cohort of vaccinated individuals, the immunological response was not different in the two groups of individuals who received different vaccination strategies likely because the immune response has been investigated after the third dose.

We are well aware that this study has some limitations. First of all, the number of patients studied is low, but the B- and T-cell compartments were investigated in-depth in terms of phenotype and functionality. Second, the number of days post symptom onset (for recovered individuals) or after the third dose of the vaccine (for vaccinated ones) is different. This could be relevant when interpreting the results regarding SARS-CoV-2-specific antibodies or the percentage of Ag-specific B cells and cTfh cells in recovered patients. Third, a group of donors who developed hybrid immunity characterized by immunity developed by natural infection and vaccination.

However, our study can provide a novel characterization of the humoral and cellular immune responses upon COVID-19 vaccination or infection by including the fine phenotypic and functional analysis of Ag-specific B and T cells together with the comparison between different vaccination strategies (after the third dose of vaccination) and natural infection.

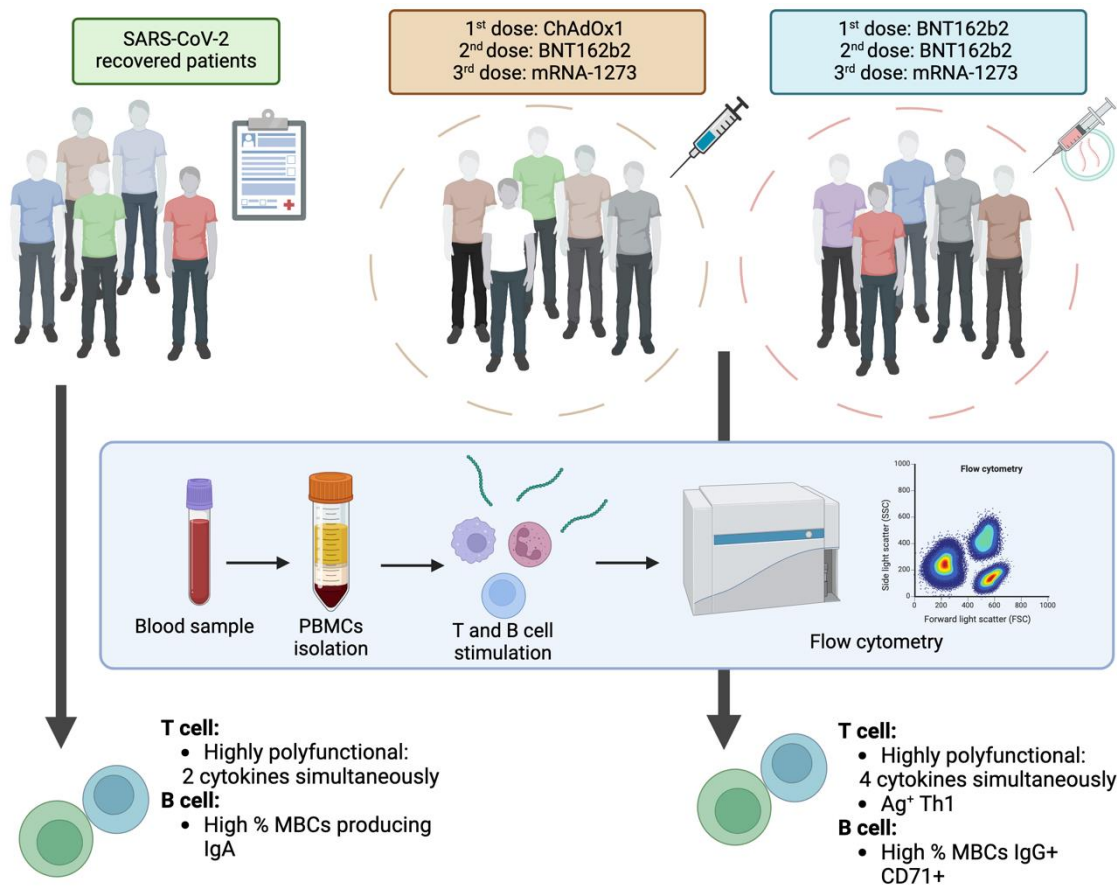


Figure 42. Characterization of SARS-CoV-2 specific T and B cells after infection or heterologous vaccination. Three cohorts of patients were studied: those recovering from SARS-CoV-2 infection and two groups of donors vaccinated with different vaccine combinations. Blood samples were collected from each group, and peripheral blood mononuclear cells (PBMCs) were isolated. T and B cells were then separately analyzed to characterize their phenotype and functionality. The data analysis revealed that different vaccination strategies can result in similar immune responses. Vaccinated donors exhibited antigen-specific cells with a Th1 phenotype and a higher polyfunctional profile compared to recovered patients. Patients in the recovery phase displayed high percentages of memory B cells (MBCs) producing IgA, while donors showed high percentages of MBCs IgG-switched CD71⁺, indicating an activated profile with proliferative capabilities. The figure was created with *BioRender.com*.

5.3 Relapsing-remitting MS patients treated with FTY or natalizumab present a different vaccine-specific response compared to patients on other DMTs

The aim of this study was to ascertain whether COVID-19 vaccinated patients affected by the relapsing-remitting form of multiple sclerosis and receiving different MS-treatments would mount an effective T and B cell response against SARS-CoV-2. For this reason, we have used different approaches and techniques mainly based on flow cytometry, to carefully investigated cell phenotype and function.

Several observational studies evaluating the effectiveness of COVID-19 vaccines in MS patients treated with DMT showed that most of these drugs allow for mounting a protective immune response, at least in terms of antibody production and production of antigen-specific B and T cells, even if some patients can experience a reduced immune response. However, an immune signature associated with the phenotype and function of Ag⁺ T and B cells that could suggest the existence of a predisposition to breakthrough infection in MS patients has never been investigated.

Here, we show that nearly 6 months after the third SARS-CoV-2 vaccine dose, the overall SARS-CoV-2-specific T and B cell response in relapsing-remitting MS patients treated with different drugs was similar among all patients and healthy donors, except for those treated with FTY or natalizumab, whose cells displayed totally different immunological features.

In the case of FTY-treated patients, we saw that phenotype and function of Ag⁺ T and B cells seemed to mimic the characteristic of an aged immune system. Indeed, these patients were characterized by high proportions of effector memory T cells expressing PD-1 and CD57; CD4⁺ T cells producing granzyme; Ag⁺ T cells with low polyfunctional profile; decreased percentages of Ag⁺ B cells.

The immune system of MS patients is characterized by a premature aging [275], and DMT can cause drastic changes that worsen or even accelerate immune senescence long after the drug has been stopped [276]. The effects of cell depleting agents are not readily reversible, and even those of therapies primarily targeting cell migration such as natalizumab and FTY may long lasting effects. Aging of the immune system involves not only a decreased production of naïve T cells, but also an increase in terminally differentiated late effector memory T cells determining a narrowing of the T cell repertoire [277,278], with an increase in the level of activation and cytotoxicity [221]. Aging decreases B cell differentiation in the bone marrow and the output of mature B cells, induces a redistribution of B cell subsets in the periphery with a significant increase in frequencies and numbers of proinflammatory B cells, decreases the expression of molecules involved in Ig class-switch

recombination and somatic hypermutation, two processes leading to the generation of high-affinity protective antibodies as well as germinal center formation, and decreases B cell repertoire diversity [141,279].

We found that MS patients treated with different DMT display a different phenotype of Ag⁺ T and B cells. It has been shown that some effects of FTY, DMF and aCD20 resemble immunosenescence, as they cause a decrease in total B and T cells and induce a negative regulation of Th1 and Th17 differentiation while promoting Th2 differentiation [280]. FTY not only modulates lymphocyte trafficking, but also modulates the composition of B and T cells subsets, with an increase of circulating effector memory T cells and decrease of naïve T cells. On the contrary, natalizumab induces an increase in total T cells (including Th1 and Th17), total B cells, memory B cells, but alter the proportion of plasmablasts which have high expression of CD49d [276,281].

Assessing the molecular and cellular state of the immune system after vaccination, by adopting data-driven models, could be used to predict pathogen-specific immune responses or the prevention of breakthrough infection. The goal is to identify key immune signatures that are responsible for the creation of an effective immune response. Systems-biology analyses of influenza virus vaccination have identified antibody response predictors, these have been based on post-vaccination parameters, such as the magnitude of plasmablast increases on day 7, and changes in blood host-derived transcripts on days 1–3 after vaccination [282,283]. Moreover, certain immune signatures can predict not only the response to malaria vaccination, but the clinical outcomes of acute infection [284]. Questions regarding how much the immune signature before vaccination influence the creation of a protective immune response needs to be elucidated and how much these immunological signatures are similar across different populations (young, elderly, pregnant, different ethnicities) need to be investigated.

Even if we acknowledge some study limitations (*i.e.*, the number of patients per group and the cross-sectional investigation), we show, for the first time, that only FTY and natalizumab modify significantly (in terms of phenotype and functionality) the SARS-CoV-2-specific B and T cell composition after vaccination.

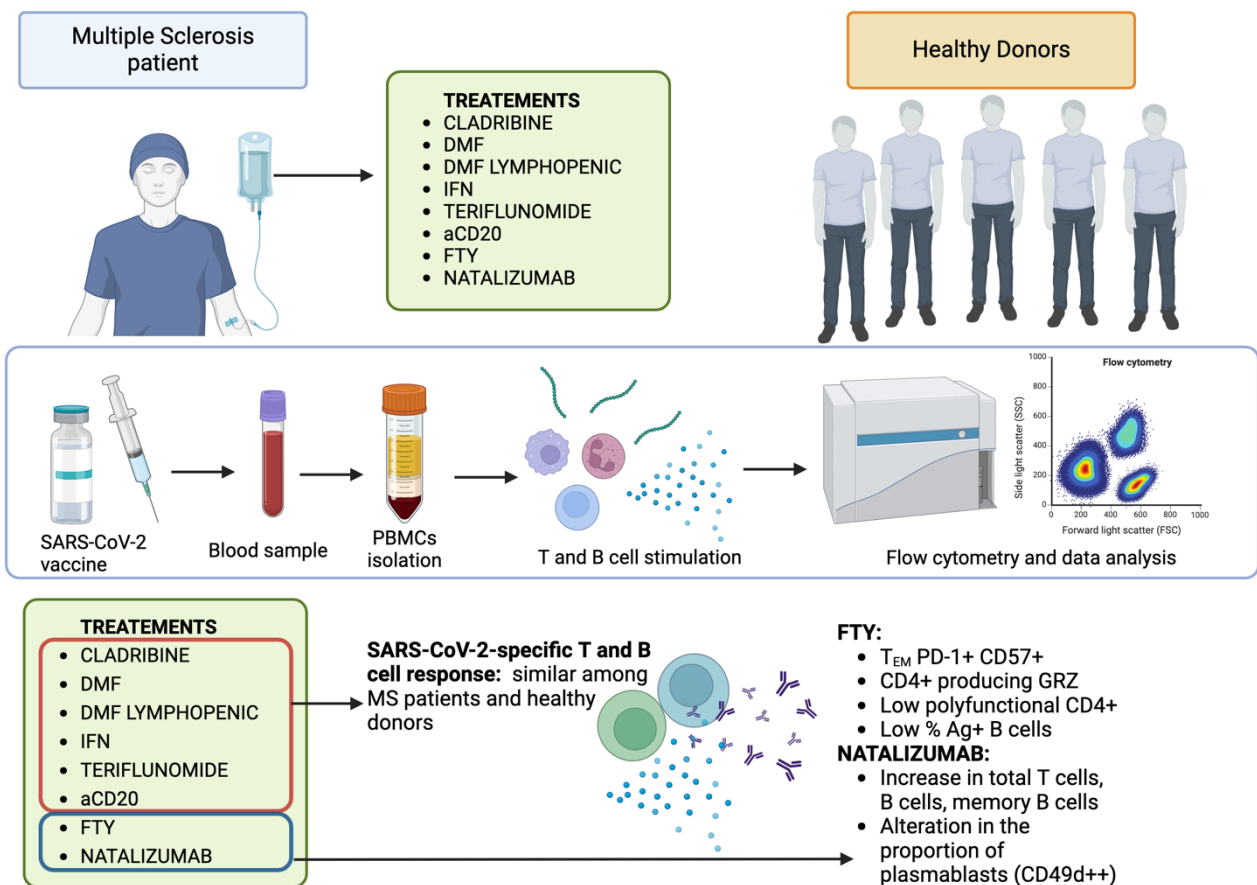


Figure 43. Investigation of SARS-CoV-2 specific response in multiple sclerosis patients under different disease modifying therapies. SARS-CoV-2 T and B cell response was studied in patients with Multiple Sclerosis (MS) undergoing different treatments and compared with those of a group of Healthy Donors (HD). The immune response was examined nearly 6 months after receiving the third dose of the SARS-CoV-2 vaccine. Blood samples were collected from patients and donors, and peripheral blood mononuclear cells (PBMCs) were isolated. T and B cells were then separately analyzed to characterize their phenotype and functionality. By using sophisticated data analysis approaches, it was observed that the overall SARS-CoV-2-specific T and B cell response in MS patients treated with different drugs was similar to that of healthy donors, except for those treated with FTY or natalizumab. These medications significantly alter the composition (in terms of phenotype and functionality) of SARS-CoV-2-specific B and T cells following vaccination. The figure was created with *BioRender.com*.

6. CONCLUSION

COVID-19 pandemic has undeniably been a life-changing event for people all over the world. There was a high urge to clear the mechanisms of infection and the pathways leading to the deleterious immune system activation. Scientists and clinicians worked relentlessly with the same objective for more than one year and still continue to ensure that such a dangerous pandemic will not happen again. We tried to participate and contribute in expanding the scientific knowledge by using innovative technique for the investigation of the immune response.

Firstly, we deepened the effects of infection on the adaptive immune system by comparing the ability of CD4⁺ and CD8⁺ T cells to produce cytokines and to be polyfunctional in infected and recovered patients. We also deepened the effects of different antigenic portion of SARS-CoV-2 by using peptides that mimic various structural proteins. We categorized patients in experiencing or recovering from a moderate or severe infection. We observe that during a severe infection the functionality of CD4⁺ and CD8⁺ T cells is importantly impaired but at the time of recovery these cells regain all the fundamental characteristics to mount a sustained immune response against SARS-CoV-2 antigens.

As vaccines became available worldwide, campaigns emphasizing the importance of vaccination in this global situation began to gain momentum. Different types of vaccines were available, *i.e.* RNA but also replication-deficient adenovirus based vaccines. Thus, as population received different combination of vaccine, we wanted to deepen the immune protection provided by these different vaccination scheme in comparison to individuals recovering from the infection. Overall, the immune response given by the different combination of vaccines was similar. However, this response was stronger if compared to recovered patients. The power of vaccination was seen in terms of percentage of antigen-specific as well as activated and highly polyfunctional T and B cells.

During the vaccination campaign, priority was given to immunocompromised individuals, recognizing them as the first in need. Due to their immune condition, however, the efficacy of vaccination was questioned. For this reason we wanted to deepen the ability to mount an immune response in patients with Multiple Sclerosis (MS) on different disease modifying therapies (DMTs). To gain a wide overview of the phenomenon, we compared patients on 8 different therapies with healthy donors (HDs). After an in-depth investigation, we observed that only patients treated with fingolimod and natalizumab exhibited a modified immune response, distinct from the one observed in HDs.

As of today, COVID-19 is a virus with which we can cohabit. Nevertheless, it is crucial to remain vigilant concerning vulnerable patients and potential dangerous virus variants. The overall

picture that can be obtained by our results is that a deepen investigation of the quality and quantity of the immune response help in gain information about the potential duration. If implemented in clinical analysis, this method would facilitate more personalized and targeted decision for re-vaccination schemes or the definition of new medical approaches.

7. REFERENCES

1. Sofi, M.S., A. Hamid, and S.U. Bhat, *SARS-CoV-2: A critical review of its history, pathogenesis, transmission, diagnosis and treatment*. Biosaf Health, 2020. **2**(4): p. 217-225.
2. Dietz, L., et al., *2019 Novel Coronavirus (COVID-19) Pandemic: Built Environment Considerations To Reduce Transmission*. mSystems, 2020. **5**(2).
3. Zhu, N., et al., *A Novel Coronavirus from Patients with Pneumonia in China, 2019*. N Engl J Med, 2020. **382**(8): p. 727-733.
4. Liu, Y.C., R.L. Kuo, and S.R. Shih, *COVID-19: The first documented coronavirus pandemic in history*. Biomed J, 2020. **43**(4): p. 328-333.
5. Dos Santos, W.G., *Natural history of COVID-19 and current knowledge on treatment therapeutic options*. Biomed Pharmacother, 2020. **129**: p. 110493.
6. Cucinotta, D. and M. Vanelli, *WHO Declares COVID-19 a Pandemic*. Acta Biomed, 2020. **91**(1): p. 157-160.
7. Cossarizza, A., et al., *SARS-CoV-2, the Virus that Causes COVID-19: Cytometry and the New Challenge for Global Health*. Cytometry A, 2020. **97**(4): p. 340-343.
8. Cossarizza, A., et al., *Handling and Processing of Blood Specimens from Patients with COVID-19 for Safe Studies on Cell Phenotype and Cytokine Storm*. Cytometry A, 2020. **97**(7): p. 668-673.
9. Petrosillo, N., et al., *COVID-19, SARS and MERS: are they closely related?* Clin Microbiol Infect, 2020. **26**(6): p. 729-734.
10. Cherry, J.D. and P. Krogstad, *SARS: the first pandemic of the 21st century*. Pediatr Res, 2004. **56**(1): p. 1-5.
11. Rabaan, A.A., et al., *SARS-CoV-2, SARS-CoV, and MERS-COV: A comparative overview*. Infez Med, 2020. **28**(2): p. 174-184.
12. Lessler, J., et al., *Incubation periods of acute respiratory viral infections: a systematic review*. Lancet Infect Dis, 2009. **9**(5): p. 291-300.
13. Riley, S., et al., *Transmission dynamics of the etiological agent of SARS in Hong Kong: impact of public health interventions*. Science, 2003. **300**(5627): p. 1961-6.
14. Lipsitch, M., et al., *Transmission dynamics and control of severe acute respiratory syndrome*. Science, 2003. **300**(5627): p. 1966-70.
15. Khan, M., et al., *COVID-19: A Global Challenge with Old History, Epidemiology and Progress So Far*. Molecules, 2020. **26**(1).

16. Who Mers-Cov Research, G., *State of Knowledge and Data Gaps of Middle East Respiratory Syndrome Coronavirus (MERS-CoV) in Humans*. PLoS Curr, 2013. **5**.
17. Chathappady House, N.N., S. Palissery, and H. Sebastian, *Corona Viruses: A Review on SARS, MERS and COVID-19*. Microbiol Insights, 2021. **14**: p. 11786361211002481.
18. Shirato, K., M. Kawase, and S. Matsuyama, *Middle East respiratory syndrome coronavirus infection mediated by the transmembrane serine protease TMPRSS2*. J Virol, 2013. **87**(23): p. 12552-61.
19. de Wit, E., et al., *Middle East respiratory syndrome coronavirus (MERS-CoV) causes transient lower respiratory tract infection in rhesus macaques*. Proc Natl Acad Sci U S A, 2013. **110**(41): p. 16598-603.
20. Pustake, M., et al., *SARS, MERS and CoVID-19: An overview and comparison of clinical, laboratory and radiological features*. J Family Med Prim Care, 2022. **11**(1): p. 10-17.
21. Naqvi, A.A.T., et al., *Insights into SARS-CoV-2 genome, structure, evolution, pathogenesis and therapies: Structural genomics approach*. Biochim Biophys Acta Mol Basis Dis, 2020. **1866**(10): p. 165878.
22. Walls, A.C., et al., *Structure, Function, and Antigenicity of the SARS-CoV-2 Spike Glycoprotein*. Cell, 2020. **183**(6): p. 1735.
23. Wang, M.Y., et al., *SARS-CoV-2: Structure, Biology, and Structure-Based Therapeutics Development*. Front Cell Infect Microbiol, 2020. **10**: p. 587269.
24. Salamanna, F., et al., *Body Localization of ACE-2: On the Trail of the Keyhole of SARS-CoV-2*. Front Med (Lausanne), 2020. **7**: p. 594495.
25. Xiao, F., et al., *Evidence for Gastrointestinal Infection of SARS-CoV-2*. Gastroenterology, 2020. **158**(6): p. 1831-1833 e3.
26. Yan, C.H., et al., *Association of chemosensory dysfunction and COVID-19 in patients presenting with influenza-like symptoms*. Int Forum Allergy Rhinol, 2020. **10**(7): p. 806-813.
27. Wrapp, D., et al., *Cryo-EM structure of the 2019-nCoV spike in the prefusion conformation*. Science, 2020. **367**(6483): p. 1260-1263.
28. Raj, V.S., et al., *Dipeptidyl peptidase 4 is a functional receptor for the emerging human coronavirus-EMC*. Nature, 2013. **495**(7440): p. 251-4.
29. Chu, H., et al., *Productive replication of Middle East respiratory syndrome coronavirus in monocyte-derived dendritic cells modulates innate immune response*. Virology, 2014. **454-455**: p. 197-205.
30. Wang, C., et al., *Alveolar macrophage dysfunction and cytokine storm in the pathogenesis of two severe COVID-19 patients*. EBioMedicine, 2020. **57**: p. 102833.

31. Wolfel, R., et al., *Virological assessment of hospitalized patients with COVID-2019*. Nature, 2020. **581**(7809): p. 465-469.
32. Lauer, S.A., et al., *The Incubation Period of Coronavirus Disease 2019 (COVID-19) From Publicly Reported Confirmed Cases: Estimation and Application*. Ann Intern Med, 2020. **172**(9): p. 577-582.
33. Galmiche, S., et al., *SARS-CoV-2 incubation period across variants of concern, individual factors, and circumstances of infection in France: a case series analysis from the ComCor study*. Lancet Microbe, 2023. **4**(6): p. e409-e417.
34. Paderno, A., et al., *Smell and taste alterations in COVID-19: a cross-sectional analysis of different cohorts*. Int Forum Allergy Rhinol, 2020. **10**(8): p. 955-962.
35. Sedaghat, A.R., I. Gengler, and M.M. Speth, *Olfactory Dysfunction: A Highly Prevalent Symptom of COVID-19 With Public Health Significance*. Otolaryngol Head Neck Surg, 2020. **163**(1): p. 12-15.
36. Zhang, R., et al., *CT features of SARS-CoV-2 pneumonia according to clinical presentation: a retrospective analysis of 120 consecutive patients from Wuhan city*. Eur Radiol, 2020. **30**(8): p. 4417-4426.
37. Inui, S., et al., *Chest CT Findings in Cases from the Cruise Ship Diamond Princess with Coronavirus Disease (COVID-19)*. Radiol Cardiothorac Imaging, 2020. **2**(2): p. e200110.
38. Osuchowski, M.F., et al., *The COVID-19 puzzle: deciphering pathophysiology and phenotypes of a new disease entity*. Lancet Respir Med, 2021. **9**(6): p. 622-642.
39. Siswanto, et al., *Possible silent hypoxemia in a COVID-19 patient: A case report*. Ann Med Surg (Lond), 2020. **60**: p. 583-586.
40. Dhont, S., et al., *The pathophysiology of 'happy' hypoxemia in COVID-19*. Respir Res, 2020. **21**(1): p. 198.
41. Manning, H.L. and D.A. Mahler, *Pathophysiology of dyspnea*. Monaldi Arch Chest Dis, 2001. **56**(4): p. 325-30.
42. Guan, W.J., et al., *Clinical Characteristics of Coronavirus Disease 2019 in China*. N Engl J Med, 2020. **382**(18): p. 1708-1720.
43. Duffin, J., *Measuring the ventilatory response to hypoxia*. J Physiol, 2007. **584**(Pt 1): p. 285-93.
44. Cantuti-Castelvetri, L., et al., *Neuropilin-1 facilitates SARS-CoV-2 cell entry and infectivity*. Science, 2020. **370**(6518): p. 856-860.
45. Hellman, U., et al., *Presence of hyaluronan in lung alveoli in severe Covid-19: An opening for new treatment options?* J Biol Chem, 2020. **295**(45): p. 15418-15422.

46. Carsana, L., et al., *Pulmonary post-mortem findings in a series of COVID-19 cases from northern Italy: a two-centre descriptive study*. Lancet Infect Dis, 2020. **20**(10): p. 1135-1140.
47. Yao, X.H., et al., *Pathological evidence for residual SARS-CoV-2 in pulmonary tissues of a ready-for-discharge patient*. Cell Res, 2020. **30**(6): p. 541-543.
48. Ackermann, M., et al., *Pulmonary Vascular Endothelialitis, Thrombosis, and Angiogenesis in Covid-19*. N Engl J Med, 2020. **383**(2): p. 120-128.
49. Sorbello, M., et al., *The Italian coronavirus disease 2019 outbreak: recommendations from clinical practice*. Anaesthesia, 2020. **75**(6): p. 724-732.
50. Gattinoni, L., J.J. Marini, and L. Camporota, *The Respiratory Drive: An Overlooked Tile of COVID-19 Pathophysiology*. Am J Respir Crit Care Med, 2020. **202**(8): p. 1079-1080.
51. Wilson, M.S. and T.A. Wynn, *Pulmonary fibrosis: pathogenesis, etiology and regulation*. Mucosal Immunol, 2009. **2**(2): p. 103-21.
52. Quartuccio, L., et al., *Urgent avenues in the treatment of COVID-19: Targeting downstream inflammation to prevent catastrophic syndrome*. Joint Bone Spine, 2020. **87**(3): p. 191-193.
53. Chen, W., *A potential treatment of COVID-19 with TGF-beta blockade*. Int J Biol Sci, 2020. **16**(11): p. 1954-1955.
54. Eapen, M.S., et al., *Endothelial to mesenchymal transition: a precursor to post-COVID-19 interstitial pulmonary fibrosis and vascular obliteration?* Eur Respir J, 2020. **56**(4).
55. Yu, M., et al., *Prediction of the Development of Pulmonary Fibrosis Using Serial Thin-Section CT and Clinical Features in Patients Discharged after Treatment for COVID-19 Pneumonia*. Korean J Radiol, 2020. **21**(6): p. 746-755.
56. Klok, F.A., et al., *Incidence of thrombotic complications in critically ill ICU patients with COVID-19*. Thromb Res, 2020. **191**: p. 145-147.
57. Burkhard-Koren, N.M., et al., *Higher prevalence of pulmonary macrothrombi in SARS-CoV-2 than in influenza A: autopsy results from 'Spanish flu' 1918/1919 in Switzerland to Coronavirus disease 2019*. J Pathol Clin Res, 2021. **7**(2): p. 135-143.
58. Jirak, P., et al., *Myocardial injury in severe COVID-19 is similar to pneumonias of other origin: results from a multicentre study*. ESC Heart Fail, 2021. **8**(1): p. 37-46.
59. Thachil, J., et al., *ISTH interim guidance on recognition and management of coagulopathy in COVID-19*. J Thromb Haemost, 2020. **18**(5): p. 1023-1026.
60. Leisman, D.E., et al., *Cytokine elevation in severe and critical COVID-19: a rapid systematic review, meta-analysis, and comparison with other inflammatory syndromes*. Lancet Respir Med, 2020. **8**(12): p. 1233-1244.

61. Wu, C., et al., *Risk Factors Associated With Acute Respiratory Distress Syndrome and Death in Patients With Coronavirus Disease 2019 Pneumonia in Wuhan, China*. JAMA Intern Med, 2020. **180**(7): p. 934-943.
62. Zhou, F., et al., *Clinical course and risk factors for mortality of adult inpatients with COVID-19 in Wuhan, China: a retrospective cohort study*. Lancet, 2020. **395**(10229): p. 1054-1062.
63. Chen, T., et al., *Clinical characteristics of 113 deceased patients with coronavirus disease 2019: retrospective study*. BMJ, 2020. **368**: p. m1091.
64. Goyal, P., et al., *Clinical Characteristics of Covid-19 in New York City*. N Engl J Med, 2020. **382**(24): p. 2372-2374.
65. Mazzone, A., et al., *Impaired immune cell cytotoxicity in severe COVID-19 is IL-6 dependent*. J Clin Invest, 2020. **130**(9): p. 4694-4703.
66. Buja, L.M., et al., *The emerging spectrum of cardiopulmonary pathology of the coronavirus disease 2019 (COVID-19): Report of 3 autopsies from Houston, Texas, and review of autopsy findings from other United States cities*. Cardiovasc Pathol, 2020. **48**: p. 107233.
67. Sadegh Beigee, F., et al., *Diffuse alveolar damage and thrombotic microangiopathy are the main histopathological findings in lung tissue biopsy samples of COVID-19 patients*. Pathol Res Pract, 2020. **216**(10): p. 153228.
68. Arachchilage, D.J., et al., *Thrombolysis restores perfusion in COVID-19 hypoxia*. Br J Haematol, 2020. **190**(5): p. e270-e274.
69. Grasselli, G., et al., *Pathophysiology of COVID-19-associated acute respiratory distress syndrome: a multicentre prospective observational study*. Lancet Respir Med, 2020. **8**(12): p. 1201-1208.
70. Botta, M., et al., *Ventilation management and clinical outcomes in invasively ventilated patients with COVID-19 (PRoVENT-COVID): a national, multicentre, observational cohort study*. Lancet Respir Med, 2021. **9**(2): p. 139-148.
71. Sinha, P., et al., *Prevalence of phenotypes of acute respiratory distress syndrome in critically ill patients with COVID-19: a prospective observational study*. Lancet Respir Med, 2020. **8**(12): p. 1209-1218.
72. Ragab, D., et al., *The COVID-19 Cytokine Storm; What We Know So Far*. Front Immunol, 2020. **11**: p. 1446.
73. Grasselli, G., et al., *Pathophysiology of COVID-19-associated acute respiratory distress syndrome - Authors' reply*. Lancet Respir Med, 2021. **9**(1): p. e5-e6.
74. Liu, Q., Y.H. Zhou, and Z.Q. Yang, *The cytokine storm of severe influenza and development of immunomodulatory therapy*. Cell Mol Immunol, 2016. **13**(1): p. 3-10.

75. Cardone, M., et al., *Lessons Learned to Date on COVID-19 Hyperinflammatory Syndrome: Considerations for Interventions to Mitigate SARS-CoV-2 Viral Infection and Detrimental Hyperinflammation*. *Front Immunol*, 2020. **11**: p. 1131.
76. de Jesus, A.A., et al., *Molecular mechanisms in genetically defined autoinflammatory diseases: disorders of amplified danger signaling*. *Annu Rev Immunol*, 2015. **33**: p. 823-74.
77. Domingo, P., et al., *The four horsemen of a viral Apocalypse: The pathogenesis of SARS-CoV-2 infection (COVID-19)*. *EBioMedicine*, 2020. **58**: p. 102887.
78. Barton, L.M., et al., *COVID-19 Autopsies, Oklahoma, USA*. *Am J Clin Pathol*, 2020. **153**(6): p. 725-733.
79. Huang, C., et al., *Clinical features of patients infected with 2019 novel coronavirus in Wuhan, China*. *Lancet*, 2020. **395**(10223): p. 497-506.
80. Del Valle, D.M., et al., *An inflammatory cytokine signature predicts COVID-19 severity and survival*. *Nat Med*, 2020. **26**(10): p. 1636-1643.
81. Ryabkova, V.A., L.P. Churilov, and Y. Shoenfeld, *Influenza infection, SARS, MERS and COVID-19: Cytokine storm - The common denominator and the lessons to be learned*. *Clin Immunol*, 2021. **223**: p. 108652.
82. Chomarat, P., et al., *IL-6 switches the differentiation of monocytes from dendritic cells to macrophages*. *Nat Immunol*, 2000. **1**(6): p. 510-4.
83. Dienz, O. and M. Rincon, *The effects of IL-6 on CD4 T cell responses*. *Clin Immunol*, 2009. **130**(1): p. 27-33.
84. Darif, D., et al., *The pro-inflammatory cytokines in COVID-19 pathogenesis: What goes wrong?* *Microb Pathog*, 2021. **153**: p. 104799.
85. Chen, L.Y.C., et al., *Assessing the importance of interleukin-6 in COVID-19*. *Lancet Respir Med*, 2021. **9**(2): p. e13.
86. Lee, D.W., et al., *Current concepts in the diagnosis and management of cytokine release syndrome*. *Blood*, 2014. **124**(2): p. 188-95.
87. Group, R.C., *Tocilizumab in patients admitted to hospital with COVID-19 (RECOVERY): a randomised, controlled, open-label, platform trial*. *Lancet*, 2021. **397**(10285): p. 1637-1645.
88. Guaraldi, G., et al., *Tocilizumab in patients with severe COVID-19: a retrospective cohort study*. *Lancet Rheumatol*, 2020. **2**(8): p. e474-e484.
89. Investigators, R.-C., et al., *Interleukin-6 Receptor Antagonists in Critically Ill Patients with Covid-19*. *N Engl J Med*, 2021. **384**(16): p. 1491-1502.
90. De Biasi, S., et al., *Prognostic immune markers identifying patients with severe COVID-19 who respond to tocilizumab*. *Front Immunol*, 2023. **14**: p. 1123807.

91. Galvan-Roman, J.M., et al., *IL-6 serum levels predict severity and response to tocilizumab in COVID-19: An observational study*. J Allergy Clin Immunol, 2021. **147**(1): p. 72-80 e8.
92. Liu, Y., et al., *Effects of Tocilizumab Therapy on Circulating B Cells and T Helper Cells in Patients With Neuromyelitis Optica Spectrum Disorder*. Front Immunol, 2021. **12**: p. 703931.
93. Kikuchi, J., et al., *Peripheral blood CD4(+)CD25(+)CD127(low) regulatory T cells are significantly increased by tocilizumab treatment in patients with rheumatoid arthritis: increase in regulatory T cells correlates with clinical response*. Arthritis Res Ther, 2015. **17**(1): p. 10.
94. Pesce, B., et al., *Effect of interleukin-6 receptor blockade on the balance between regulatory T cells and T helper type 17 cells in rheumatoid arthritis patients*. Clin Exp Immunol, 2013. **171**(3): p. 237-42.
95. Samson, M., et al., *Brief report: inhibition of interleukin-6 function corrects Th17/Treg cell imbalance in patients with rheumatoid arthritis*. Arthritis Rheum, 2012. **64**(8): p. 2499-503.
96. Sette, A. and S. Crotty, *Adaptive immunity to SARS-CoV-2 and COVID-19*. Cell, 2021. **184**(4): p. 861-880.
97. Soy, M., et al., *Cytokine storm in COVID-19: pathogenesis and overview of anti-inflammatory agents used in treatment*. Clin Rheumatol, 2020. **39**(7): p. 2085-2094.
98. Ziegler-Heitbrock, L., et al., *Nomenclature of monocytes and dendritic cells in blood*. Blood, 2010. **116**(16): p. e74-80.
99. Jose, R.J. and A. Manuel, *COVID-19 cytokine storm: the interplay between inflammation and coagulation*. Lancet Respir Med, 2020. **8**(6): p. e46-e47.
100. Cheng, S.C., et al., *Broad defects in the energy metabolism of leukocytes underlie immunoparalysis in sepsis*. Nat Immunol, 2016. **17**(4): p. 406-13.
101. Vergis, N., et al., *Defective monocyte oxidative burst predicts infection in alcoholic hepatitis and is associated with reduced expression of NADPH oxidase*. Gut, 2017. **66**(3): p. 519-529.
102. McBride, M.A., et al., *The Metabolic Basis of Immune Dysfunction Following Sepsis and Trauma*. Front Immunol, 2020. **11**: p. 1043.
103. Gibellini, L., et al., *Altered bioenergetics and mitochondrial dysfunction of monocytes in patients with COVID-19 pneumonia*. EMBO Mol Med, 2020. **12**(12): p. e13001.
104. Silvin, A., et al., *Elevated Calprotectin and Abnormal Myeloid Cell Subsets Discriminate Severe from Mild COVID-19*. Cell, 2020. **182**(6): p. 1401-1418 e18.
105. Giamarellos-Bourboulis, E.J., et al., *Complex Immune Dysregulation in COVID-19 Patients with Severe Respiratory Failure*. Cell Host Microbe, 2020. **27**(6): p. 992-1000 e3.

106. Kratofil, R.M., P. Kubes, and J.F. Deniset, *Monocyte Conversion During Inflammation and Injury*. *Arterioscler Thromb Vasc Biol*, 2017. **37**(1): p. 35-42.
107. Sanchez-Cerrillo, I., et al., *COVID-19 severity associates with pulmonary redistribution of CD1c+ DCs and inflammatory transitional and nonclassical monocytes*. *J Clin Invest*, 2020. **130**(12): p. 6290-6300.
108. Marsh, S.A., H.M. Arthur, and I. Spyridopoulos, *The secret life of nonclassical monocytes*. *Cytometry A*, 2017. **91**(11): p. 1055-1058.
109. Soudja, S.M., et al., *Inflammatory monocytes activate memory CD8(+) T and innate NK lymphocytes independent of cognate antigen during microbial pathogen invasion*. *Immunity*, 2012. **37**(3): p. 549-62.
110. Zhang, Y., et al., *PD-L1 blockade improves survival in experimental sepsis by inhibiting lymphocyte apoptosis and reversing monocyte dysfunction*. *Crit Care*, 2010. **14**(6): p. R220.
111. Zasada, M., et al., *Analysis of PD-1 expression in the monocyte subsets from non-septic and septic preterm neonates*. *PLoS One*, 2017. **12**(10): p. e0186819.
112. Tai, H., et al., *Monocyte Programmed Death Ligand-1, A Predictor for 28-Day Mortality in Septic Patients*. *Am J Med Sci*, 2018. **355**(4): p. 362-367.
113. Mantovani, A., et al., *Neutrophils in the activation and regulation of innate and adaptive immunity*. *Nat Rev Immunol*, 2011. **11**(8): p. 519-31.
114. Mortaz, E., et al., *Update on Neutrophil Function in Severe Inflammation*. *Front Immunol*, 2018. **9**: p. 2171.
115. Pelletier, M., et al., *Evidence for a cross-talk between human neutrophils and Th17 cells*. *Blood*, 2010. **115**(2): p. 335-43.
116. Injarabian, L., et al., *Neutrophil Metabolic Shift during their Lifecycle: Impact on their Survival and Activation*. *Int J Mol Sci*, 2019. **21**(1).
117. Rodriguez-Espinosa, O., et al., *Metabolic requirements for neutrophil extracellular traps formation*. *Immunology*, 2015. **145**(2): p. 213-24.
118. Borella, R., et al., *Metabolic reprogramming shapes neutrophil functions in severe COVID-19*. *Eur J Immunol*, 2022. **52**(3): p. 484-502.
119. Veras, F.P., et al., *SARS-CoV-2-triggered neutrophil extracellular traps mediate COVID-19 pathology*. *J Exp Med*, 2020. **217**(12).
120. Leppkes, M., et al., *Vascular occlusion by neutrophil extracellular traps in COVID-19*. *EBioMedicine*, 2020. **58**: p. 102925.
121. Middleton, E.A., et al., *Neutrophil extracellular traps contribute to immunothrombosis in COVID-19 acute respiratory distress syndrome*. *Blood*, 2020. **136**(10): p. 1169-1179.

122. Ouwendijk, W.J.D., et al., *High Levels of Neutrophil Extracellular Traps Persist in the Lower Respiratory Tract of Critically Ill Patients With Coronavirus Disease 2019*. *J Infect Dis*, 2021. **223**(9): p. 1512-1521.
123. Kawabata, K., T. Hagio, and S. Matsuoka, *The role of neutrophil elastase in acute lung injury*. *Eur J Pharmacol*, 2002. **451**(1): p. 1-10.
124. Khan, A.A., M.A. Alsahli, and A.H. Rahmani, *Myeloperoxidase as an Active Disease Biomarker: Recent Biochemical and Pathological Perspectives*. *Med Sci (Basel)*, 2018. **6**(2).
125. Schurink, B., et al., *Viral presence and immunopathology in patients with lethal COVID-19: a prospective autopsy cohort study*. *Lancet Microbe*, 2020. **1**(7): p. e290-e299.
126. Cavalcante-Silva, L.H.A., et al., *Neutrophils and COVID-19: The road so far*. *Int Immunopharmacol*, 2021. **90**: p. 107233.
127. Hazeldine, J. and J.M. Lord, *Neutrophils and COVID-19: Active Participants and Rational Therapeutic Targets*. *Front Immunol*, 2021. **12**: p. 680134.
128. Van der Sluis, R.M., C.K. Holm, and M.R. Jakobsen, *Plasmacytoid dendritic cells during COVID-19: Ally or adversary?* *Cell Rep*, 2022. **40**(4): p. 111148.
129. Tao, X., et al., *Strength of TCR signal determines the costimulatory requirements for Th1 and Th2 CD4+ T cell differentiation*. *J Immunol*, 1997. **159**(12): p. 5956-63.
130. Luckheeram, R.V., et al., *CD4(+)T cells: differentiation and functions*. *Clin Dev Immunol*, 2012. **2012**: p. 925135.
131. Crotty, S., *T Follicular Helper Cell Biology: A Decade of Discovery and Diseases*. *Immunity*, 2019. **50**(5): p. 1132-1148.
132. Juno, J.A., et al., *Humoral and circulating follicular helper T cell responses in recovered patients with COVID-19*. *Nat Med*, 2020. **26**(9): p. 1428-1434.
133. Martonik, D., et al., *The Role of Th17 Response in COVID-19*. *Cells*, 2021. **10**(6).
134. Wang, H., et al., *Regulatory T cells in COVID-19*. *Aging Dis*, 2021. **12**(7): p. 1545-1553.
135. Rydzynski Moderbacher, C., et al., *Antigen-Specific Adaptive Immunity to SARS-CoV-2 in Acute COVID-19 and Associations with Age and Disease Severity*. *Cell*, 2020. **183**(4): p. 996-1012 e19.
136. Betts, M.R. and R.A. Koup, *Detection of T-cell degranulation: CD107a and b*. *Methods Cell Biol*, 2004. **75**: p. 497-512.
137. De Biasi, S., et al., *Marked T cell activation, senescence, exhaustion and skewing towards TH17 in patients with COVID-19 pneumonia*. *Nat Commun*, 2020. **11**(1): p. 3434.
138. Chen, S., et al., *The role of B cells in COVID-19 infection and vaccination*. *Front Immunol*, 2022. **13**: p. 988536.

139. Nie, Y., et al., *Neutralizing antibodies in patients with severe acute respiratory syndrome-associated coronavirus infection*. J Infect Dis, 2004. **190**(6): p. 1119-26.
140. Blanco, E., et al., *Age-associated distribution of normal B-cell and plasma cell subsets in peripheral blood*. J Allergy Clin Immunol, 2018. **141**(6): p. 2208-2219 e16.
141. De Biasi, S., et al., *Expansion of plasmablasts and loss of memory B cells in peripheral blood from COVID-19 patients with pneumonia*. Eur J Immunol, 2020. **50**(9): p. 1283-1294.
142. Mansourabadi, A.H., et al., *B lymphocytes in COVID-19: a tale of harmony and discordance*. Arch Virol, 2023. **168**(5): p. 148.
143. Rossi, M.A., et al., *Evaluation of the risk of SARS-CoV-2 infection and hospitalization in vaccinated and previously infected subjects based on real world data*. Sci Rep, 2023. **13**(1): p. 2018.
144. Sadoff, J., et al., *Interim Results of a Phase 1-2a Trial of Ad26.COV2.S Covid-19 Vaccine*. N Engl J Med, 2021. **384**(19): p. 1824-1835.
145. Folegatti, P.M., et al., *Safety and immunogenicity of the ChAdOx1 nCoV-19 vaccine against SARS-CoV-2: a preliminary report of a phase 1/2, single-blind, randomised controlled trial*. Lancet, 2020. **396**(10249): p. 467-478.
146. Polack, F.P., et al., *Safety and Efficacy of the BNT162b2 mRNA Covid-19 Vaccine*. N Engl J Med, 2020. **383**(27): p. 2603-2615.
147. Baden, L.R., et al., *Efficacy and Safety of the mRNA-1273 SARS-CoV-2 Vaccine*. N Engl J Med, 2021. **384**(5): p. 403-416.
148. Dunkle, L.M., et al., *Efficacy and Safety of NVX-CoV2373 in Adults in the United States and Mexico*. N Engl J Med, 2022. **386**(6): p. 531-543.
149. Heath, P.T., et al., *Safety and Efficacy of NVX-CoV2373 Covid-19 Vaccine*. N Engl J Med, 2021. **385**(13): p. 1172-1183.
150. Mascellino, M.T., et al., *Overview of the Main Anti-SARS-CoV-2 Vaccines: Mechanism of Action, Efficacy and Safety*. Infect Drug Resist, 2021. **14**: p. 3459-3476.
151. Rydyznski Moderbacher, C., et al., *NVX-CoV2373 vaccination induces functional SARS-CoV-2-specific CD4+ and CD8+ T cell responses*. J Clin Invest, 2022. **132**(19).
152. Fiolet, T., et al., *Comparing COVID-19 vaccines for their characteristics, efficacy and effectiveness against SARS-CoV-2 and variants of concern: a narrative review*. Clin Microbiol Infect, 2022. **28**(2): p. 202-221.
153. Hoffmann, M., L. Zhang, and S. Pohlmann, *Omicron: Master of immune evasion maintains robust ACE2 binding*. Signal Transduct Target Ther, 2022. **7**(1): p. 118.

154. Andrews, N., et al., *Covid-19 Vaccine Effectiveness against the Omicron (B.1.1.529) Variant*. N Engl J Med, 2022. **386**(16): p. 1532-1546.
155. Shaw, R.H., et al., *Heterologous prime-boost COVID-19 vaccination: initial reactogenicity data*. Lancet, 2021. **397**(10289): p. 2043-2046.
156. Boyarsky, B.J., et al., *Antibody Response to 2-Dose SARS-CoV-2 mRNA Vaccine Series in Solid Organ Transplant Recipients*. JAMA, 2021. **325**(21): p. 2204-2206.
157. Werbel, W.A., et al., *Safety and Immunogenicity of a Third Dose of SARS-CoV-2 Vaccine in Solid Organ Transplant Recipients: A Case Series*. Ann Intern Med, 2021. **174**(9): p. 1330-1332.
158. Kang, S.W., et al., *Characteristics and risk factors of prolonged viable virus shedding in immunocompromised patients with COVID-19: a prospective cohort study*. J Infect, 2023. **86**(4): p. 412-414.
159. Shoham, S., et al., *Vaccines and therapeutics for immunocompromised patients with COVID-19*. EClinicalMedicine, 2023. **59**: p. 101965.
160. Galimiche, S., et al., *Immunological and clinical efficacy of COVID-19 vaccines in immunocompromised populations: a systematic review*. Clin Microbiol Infect, 2022. **28**(2): p. 163-177.
161. McGinley, M.P., C.H. Goldschmidt, and A.D. Rae-Grant, *Diagnosis and Treatment of Multiple Sclerosis: A Review*. JAMA, 2021. **325**(8): p. 765-779.
162. Tornatore, C., et al., *Vaccine Response in Patients With Multiple Sclerosis Receiving Teriflunomide*. Front Neurol, 2022. **13**: p. 828616.
163. Filipi, M. and S. Jack, *Interferons in the Treatment of Multiple Sclerosis: A Clinical Efficacy, Safety, and Tolerability Update*. Int J MS Care, 2020. **22**(4): p. 165-172.
164. Centonze, D., et al., *Disease-modifying therapies and SARS-CoV-2 vaccination in multiple sclerosis: an expert consensus*. J Neurol, 2021. **268**(11): p. 3961-3968.
165. Moss, P., *The T cell immune response against SARS-CoV-2*. Nat Immunol, 2022. **23**(2): p. 186-193.
166. Gratama, J.W., et al., *Monitoring cytomegalovirus IE-1 and pp65-specific CD4+ and CD8+ T-cell responses after allogeneic stem cell transplantation may identify patients at risk for recurrent CMV reactivations*. Cytometry B Clin Cytom, 2008. **74**(4): p. 211-20.
167. Newell, E.W., et al., *Simultaneous detection of many T-cell specificities using combinatorial tetramer staining*. Nat Methods, 2009. **6**(7): p. 497-9.
168. De Biasi, S., et al., *Analysis of Antigen-Specific T and B Cells for Monitoring Immune Protection Against SARS-CoV-2*. Curr Protoc, 2023. **3**(1): p. e636.

169. Havenar-Daughton, C., et al., *Cytokine-Independent Detection of Antigen-Specific Germinal Center T Follicular Helper Cells in Immunized Nonhuman Primates Using a Live Cell Activation-Induced Marker Technique*. J Immunol, 2016. **197**(3): p. 994-1002.
170. Reiss, S., et al., *Comparative analysis of activation induced marker (AIM) assays for sensitive identification of antigen-specific CD4 T cells*. PLoS One, 2017. **12**(10): p. e0186998.
171. Grifoni, A., et al., *Targets of T Cell Responses to SARS-CoV-2 Coronavirus in Humans with COVID-19 Disease and Unexposed Individuals*. Cell, 2020. **181**(7): p. 1489-1501 e15.
172. Bacher, P. and A. Scheffold, *Flow-cytometric analysis of rare antigen-specific T cells*. Cytometry A, 2013. **83**(8): p. 692-701.
173. Chattopadhyay, P.K., M. Roederer, and D.A. Price, *OMIP-002: Phenotypic analysis of specific human CD8⁺ T-cells using peptide-MHC class I multimers for any of four epitopes*. Cytometry A, 2010. **77**(9): p. 821-2.
174. Elgueta, R., et al., *Molecular mechanism and function of CD40/CD40L engagement in the immune system*. Immunol Rev, 2009. **229**(1): p. 152-72.
175. Cascino, K., M. Roederer, and T. Liechti, *OMIP-068: High-Dimensional Characterization of Global and Antigen-Specific B Cells in Chronic Infection*. Cytometry A, 2020. **97**(10): p. 1037-1043.
176. Boonyaratanakornkit, J. and J.J. Taylor, *Techniques to Study Antigen-Specific B Cell Responses*. Front Immunol, 2019. **10**: p. 1694.
177. Brummelman, J., et al., *Development, application and computational analysis of high-dimensional fluorescent antibody panels for single-cell flow cytometry*. Nat Protoc, 2019. **14**(7): p. 1946-1969.
178. Lugli, E., et al., *Subject classification obtained by cluster analysis and principal component analysis applied to flow cytometric data*. Cytometry A, 2007. **71**(5): p. 334-44.
179. Becht, E., et al., *Dimensionality reduction for visualizing single-cell data using UMAP*. Nat Biotechnol, 2018.
180. Huang, H., et al., *Towards a comprehensive evaluation of dimension reduction methods for transcriptomic data visualization*. Commun Biol, 2022. **5**(1): p. 719.
181. Bange, E.M., et al., *CD8⁺ T cells contribute to survival in patients with COVID-19 and hematologic cancer*. Nat Med, 2021. **27**(7): p. 1280-1289.
182. Sekine, T., et al., *Robust T Cell Immunity in Convalescent Individuals with Asymptomatic or Mild COVID-19*. Cell, 2020. **183**(1): p. 158-168 e14.
183. Le Bert, N., et al., *Highly functional virus-specific cellular immune response in asymptomatic SARS-CoV-2 infection*. J Exp Med, 2021. **218**(5).

184. Reynolds, C.J., et al., *Discordant neutralizing antibody and T cell responses in asymptomatic and mild SARS-CoV-2 infection*. *Sci Immunol*, 2020. **5**(54).
185. Bonifacius, A., et al., *COVID-19 immune signatures reveal stable antiviral T cell function despite declining humoral responses*. *Immunity*, 2021. **54**(2): p. 340-354 e6.
186. Peng, Y., et al., *Broad and strong memory CD4(+) and CD8(+) T cells induced by SARS-CoV-2 in UK convalescent individuals following COVID-19*. *Nat Immunol*, 2020. **21**(11): p. 1336-1345.
187. Le Bert, N., et al., *SARS-CoV-2-specific T cell immunity in cases of COVID-19 and SARS, and uninfected controls*. *Nature*, 2020. **584**(7821): p. 457-462.
188. Nelde, A., et al., *SARS-CoV-2-derived peptides define heterologous and COVID-19-induced T cell recognition*. *Nat Immunol*, 2021. **22**(1): p. 74-85.
189. Gangaev, A., et al., *Identification and characterization of a SARS-CoV-2 specific CD8(+) T cell response with immunodominant features*. *Nat Commun*, 2021. **12**(1): p. 2593.
190. Pera, A., et al., *CMV latent infection improves CD8+ T response to SEB due to expansion of polyfunctional CD57+ cells in young individuals*. *PLoS One*, 2014. **9**(2): p. e88538.
191. Betts, M.R., et al., *HIV nonprogressors preferentially maintain highly functional HIV-specific CD8+ T cells*. *Blood*, 2006. **107**(12): p. 4781-9.
192. Valverde-Villegas, J.M., et al., *New Insights about Treg and Th17 Cells in HIV Infection and Disease Progression*. *J Immunol Res*, 2015. **2015**: p. 647916.
193. Zambrano-Zaragoza, J.F., et al., *Th17 cells in autoimmune and infectious diseases*. *Int J Inflam*, 2014. **2014**: p. 651503.
194. Frank, K. and S. Paust, *Dynamic Natural Killer Cell and T Cell Responses to Influenza Infection*. *Front Cell Infect Microbiol*, 2020. **10**: p. 425.
195. Chen, X., et al., *Host Immune Response to Influenza A Virus Infection*. *Front Immunol*, 2018. **9**: p. 320.
196. Hornick, E.E., Z.R. Zacharias, and K.L. Legge, *Kinetics and Phenotype of the CD4 T Cell Response to Influenza Virus Infections*. *Front Immunol*, 2019. **10**: p. 2351.
197. Rha, M.S., et al., *PD-1-Expressing SARS-CoV-2-Specific CD8(+) T Cells Are Not Exhausted, but Functional in Patients with COVID-19*. *Immunity*, 2021. **54**(1): p. 44-52 e3.
198. Jung, J.H., et al., *SARS-CoV-2-specific T cell memory is sustained in COVID-19 convalescent patients for 10 months with successful development of stem cell-like memory T cells*. *Nat Commun*, 2021. **12**(1): p. 4043.
199. Paolini, A., et al., *Patients Recovering from Severe COVID-19 Develop a Polyfunctional Antigen-Specific CD4+ T Cell Response*. *Int J Mol Sci*, 2022. **23**(14).

200. Cohen, K.W., et al., *Longitudinal analysis shows durable and broad immune memory after SARS-CoV-2 infection with persisting antibody responses and memory B and T cells*. Cell Rep Med, 2021. **2**(7): p. 100354.
201. Dan, J.M., et al., *Immunological memory to SARS-CoV-2 assessed for up to 8 months after infection*. Science, 2021. **371**(6529).
202. Adamo, S., et al., *Signature of long-lived memory CD8(+) T cells in acute SARS-CoV-2 infection*. Nature, 2022. **602**(7895): p. 148-155.
203. Kousathanas, A., et al., *Whole-genome sequencing reveals host factors underlying critical COVID-19*. Nature, 2022. **607**(7917): p. 97-103.
204. Long, Q.X., et al., *Clinical and immunological assessment of asymptomatic SARS-CoV-2 infections*. Nat Med, 2020. **26**(8): p. 1200-1204.
205. Hartley, G.E., et al., *Rapid generation of durable B cell memory to SARS-CoV-2 spike and nucleocapsid proteins in COVID-19 and convalescence*. Sci Immunol, 2020. **5**(54).
206. Jeffery-Smith, A., et al., *SARS-CoV-2-specific memory B cells can persist in the elderly who have lost detectable neutralizing antibodies*. J Clin Invest, 2022. **132**(2).
207. Oberhardt, V., et al., *Rapid and stable mobilization of CD8(+) T cells by SARS-CoV-2 mRNA vaccine*. Nature, 2021. **597**(7875): p. 268-273.
208. Sahin, U., et al., *BNT162b2 vaccine induces neutralizing antibodies and poly-specific T cells in humans*. Nature, 2021. **595**(7868): p. 572-577.
209. Skelly, D.T., et al., *Two doses of SARS-CoV-2 vaccination induce robust immune responses to emerging SARS-CoV-2 variants of concern*. Nat Commun, 2021. **12**(1): p. 5061.
210. Agrati, C., et al., *Persistent Spike-specific T cell immunity despite antibody reduction after 3 months from SARS-CoV-2 BNT162b2-mRNA vaccine*. Sci Rep, 2022. **12**(1): p. 6687.
211. Goel, R.R., et al., *mRNA vaccines induce durable immune memory to SARS-CoV-2 and variants of concern*. Science, 2021. **374**(6572): p. abm0829.
212. Ciabattini, A., et al., *Evidence of SARS-CoV-2-Specific Memory B Cells Six Months After Vaccination With the BNT162b2 mRNA Vaccine*. Front Immunol, 2021. **12**: p. 740708.
213. Guerrero, G., et al., *BNT162b2 vaccination induces durable SARS-CoV-2-specific T cells with a stem cell memory phenotype*. Sci Immunol, 2021. **6**(66): p. eabl5344.
214. Parry, H., et al., *Differential immunogenicity of BNT162b2 or ChAdOx1 vaccines after extended-interval homologous dual vaccination in older people*. Immun Ageing, 2021. **18**(1): p. 34.

215. Parry, H., et al., *Immunogenicity of single vaccination with BNT162b2 or ChAdOx1 nCoV-19 at 5-6 weeks post vaccine in participants aged 80 years or older: an exploratory analysis*. *Lancet Healthy Longev*, 2021. **2**(9): p. e554-e560.
216. Stuart, A.S.V., et al., *Immunogenicity, safety, and reactogenicity of heterologous COVID-19 primary vaccination incorporating mRNA, viral-vector, and protein-adjuvant vaccines in the UK (Com-COV2): a single-blind, randomised, phase 2, non-inferiority trial*. *Lancet*, 2022. **399**(10319): p. 36-49.
217. Pozzetto, B., et al., *Immunogenicity and efficacy of heterologous ChAdOx1-BNT162b2 vaccination*. *Nature*, 2021. **600**(7890): p. 701-706.
218. Goldberg, Y., et al., *Protection and Waning of Natural and Hybrid Immunity to SARS-CoV-2*. *N Engl J Med*, 2022. **386**(23): p. 2201-2212.
219. Mazzone, A., et al., *First-dose mRNA vaccination is sufficient to reactivate immunological memory to SARS-CoV-2 in subjects who have recovered from COVID-19*. *J Clin Invest*, 2021. **131**(12).
220. De Biasi, S., et al., *Endogenous control of inflammation characterizes pregnant women with asymptomatic or paucisymptomatic SARS-CoV-2 infection*. *Nat Commun*, 2021. **12**(1): p. 4677.
221. Lo Tartaro, D., et al., *Molecular and cellular immune features of aged patients with severe COVID-19 pneumonia*. *Commun Biol*, 2022. **5**(1): p. 590.
222. Lo Tartaro, D., et al., *Detailed characterization of SARS-CoV-2-specific T and B cells after infection or heterologous vaccination*. *Front Immunol*, 2023. **14**: p. 1123724.
223. Gibellini, L., et al., *Plasma Cytokine Atlas Reveals the Importance of TH2 Polarization and Interferons in Predicting COVID-19 Severity and Survival*. *Front Immunol*, 2022. **13**: p. 842150.
224. Fox, R.J., et al., *Characterizing absolute lymphocyte count profiles in dimethyl fumarate-treated patients with MS: Patient management considerations*. *Neurol Clin Pract*, 2016. **6**(3): p. 220-229.
225. Bar-Or, A., et al., *Teriflunomide effect on immune response to influenza vaccine in patients with multiple sclerosis*. *Neurology*, 2013. **81**(6): p. 552-8.
226. Kaufman, M., et al., *Natalizumab treatment shows no clinically meaningful effects on immunization responses in patients with relapsing-remitting multiple sclerosis*. *J Neurol Sci*, 2014. **341**(1-2): p. 22-7.
227. Olberg, H.K., et al., *Immunotherapies influence the influenza vaccination response in multiple sclerosis patients: an explorative study*. *Mult Scler*, 2014. **20**(8): p. 1074-80.

228. Olberg, H.K., et al., *Antibody response to seasonal influenza vaccination in patients with multiple sclerosis receiving immunomodulatory therapy*. Eur J Neurol, 2018. **25**(3): p. 527-534.
229. Kappos, L., et al., *Onset of clinical and MRI efficacy occurs early after fingolimod treatment initiation in relapsing multiple sclerosis*. J Neurol, 2016. **263**(2): p. 354-360.
230. Kelly, H., B. Sokola, and H. Abboud, *Safety and efficacy of COVID-19 vaccines in multiple sclerosis patients*. J Neuroimmunol, 2021. **356**: p. 577599.
231. Bar-Or, A., et al., *Effect of ocrelizumab on vaccine responses in patients with multiple sclerosis: The VELOCE study*. Neurology, 2020. **95**(14): p. e1999-e2008.
232. Achiron, A., et al., *COVID-19 vaccination in patients with multiple sclerosis: What we have learnt by February 2021*. Mult Scler, 2021. **27**(6): p. 864-870.
233. Achiron, A., et al., *Humoral immune response to COVID-19 mRNA vaccine in patients with multiple sclerosis treated with high-efficacy disease-modifying therapies*. Ther Adv Neurol Disord, 2021. **14**: p. 17562864211012835.
234. Buttari, F., et al., *COVID-19 vaccines in multiple sclerosis treated with cladribine or ocrelizumab*. Mult Scler Relat Disord, 2021. **52**: p. 102983.
235. Gallo, A., et al., *Preliminary evidence of blunted humoral response to SARS-CoV-2 mRNA vaccine in multiple sclerosis patients treated with ocrelizumab*. Neurol Sci, 2021. **42**(9): p. 3523-3526.
236. Gadani, S.P., et al., *Discordant humoral and T cell immune responses to SARS-CoV-2 vaccination in people with multiple sclerosis on anti-CD20 therapy*. EBioMedicine, 2021. **73**: p. 103636.
237. Tortorella, C., et al., *Humoral- and T-Cell-Specific Immune Responses to SARS-CoV-2 mRNA Vaccination in Patients With MS Using Different Disease-Modifying Therapies*. Neurology, 2022. **98**(5): p. e541-e554.
238. Kister, I., et al., *Hybrid and vaccine-induced immunity against SAR-CoV-2 in MS patients on different disease-modifying therapies*. Ann Clin Transl Neurol, 2022. **9**(10): p. 1643-1659.
239. Maniscalco, G.T., et al., *Humoral efficacy of the third SARS-CoV-2 vaccine dose in Multiple Sclerosis subjects undergoing different disease-modifying therapies*. Mult Scler Relat Disord, 2022. **68**: p. 104371.
240. Disanto, G., et al., *Longitudinal Postvaccine SARS-CoV-2 Immunoglobulin G Titers, Memory B-Cell Responses, and Risk of COVID-19 in Multiple Sclerosis Over 1 Year*. Neurol Neuroimmunol Neuroinflamm, 2023. **10**(1).

241. Achiron, A., et al., *In-depth characterization of long-term humoral and cellular immune responses to COVID-19m-RNA vaccination in multiple sclerosis patients treated with teriflunomide or alemtuzumab*. *Mult Scler Relat Disord*, 2023. **72**: p. 104616.
242. Apostolidis, S.A., et al., *Cellular and humoral immune responses following SARS-CoV-2 mRNA vaccination in patients with multiple sclerosis on anti-CD20 therapy*. *Nat Med*, 2021. **27**(11): p. 1990-2001.
243. Dominelli, F., et al., *Multiple sclerosis-disease modifying therapies affect humoral and T-cell response to mRNA COVID-19 vaccine*. *Front Immunol*, 2022. **13**: p. 1050183.
244. WHO Working Group on the Clinical Characterisation and Management of COVID-19 infection, *A minimal common outcome measure set for COVID-19 clinical research*. *Lancet Infect Dis*, 2020. **20**(8): p. e192-e197.
245. Cossarizza, A., et al., *Guidelines for the use of flow cytometry and cell sorting in immunological studies (third edition)*. *Eur J Immunol*, 2021. **51**(12): p. 2708-3145.
246. Roederer, M., J.L. Nozzi, and M.C. Nason, *SPICE: exploration and analysis of post-cytometric complex multivariate datasets*. *Cytometry A*, 2011. **79**(2): p. 167-74.
247. Hahne, F., et al., *flowCore: a Bioconductor package for high throughput flow cytometry*. *BMC Bioinformatics*, 2009. **10**: p. 106.
248. Nowicka, M., et al., *CyTOF workflow: differential discovery in high-throughput high-dimensional cytometry datasets*. *F1000Res*, 2017. **6**: p. 748.
249. Weber, L.M., et al., *diffcyt: Differential discovery in high-dimensional cytometry via high-resolution clustering*. *Commun Biol*, 2019. **2**: p. 183.
250. Damsker, J.M., A.M. Hansen, and R.R. Caspi, *Th1 and Th17 cells: adversaries and collaborators*. *Ann N Y Acad Sci*, 2010. **1183**: p. 211-21.
251. Schmidt, M.E. and S.M. Varga, *The CD8 T Cell Response to Respiratory Virus Infections*. *Front Immunol*, 2018. **9**: p. 678.
252. Turner, J.S., et al., *SARS-CoV-2 infection induces long-lived bone marrow plasma cells in humans*. *Nature*, 2021. **595**(7867): p. 421-425.
253. Sutton, H.J., et al., *Atypical B cells are part of an alternative lineage of B cells that participates in responses to vaccination and infection in humans*. *Cell Rep*, 2021. **34**(6): p. 108684.
254. Meckiff, B.J., et al., *Primary EBV Infection Induces an Acute Wave of Activated Antigen-Specific Cytotoxic CD4(+) T Cells*. *J Immunol*, 2019. **203**(5): p. 1276-1287.
255. Casazza, J.P., et al., *Acquisition of direct antiviral effector functions by CMV-specific CD4+ T lymphocytes with cellular maturation*. *J Exp Med*, 2006. **203**(13): p. 2865-77.

256. Nemes, E., et al., *Cytotoxic granule release dominates gag-specific CD4+ T-cell response in different phases of HIV infection*. AIDS, 2010. **24**(7): p. 947-57.
257. Betts, M.R., et al., *Sensitive and viable identification of antigen-specific CD8+ T cells by a flow cytometric assay for degranulation*. J Immunol Methods, 2003. **281**(1-2): p. 65-78.
258. Tan, A.T., et al., *Early induction of functional SARS-CoV-2-specific T cells associates with rapid viral clearance and mild disease in COVID-19 patients*. Cell Rep, 2021. **34**(6): p. 108728.
259. Diao, B., et al., *Reduction and Functional Exhaustion of T Cells in Patients With Coronavirus Disease 2019 (COVID-19)*. Front Immunol, 2020. **11**: p. 827.
260. Snell, L.M., et al., *Overcoming CD4 Th1 Cell Fate Restrictions to Sustain Antiviral CD8 T Cells and Control Persistent Virus Infection*. Cell Rep, 2016. **16**(12): p. 3286-3296.
261. Ferretti, A.P., et al., *Unbiased Screens Show CD8(+) T Cells of COVID-19 Patients Recognize Shared Epitopes in SARS-CoV-2 that Largely Reside outside the Spike Protein*. Immunity, 2020. **53**(5): p. 1095-1107 e3.
262. Reuter, M.A., C. Pombo, and M.R. Betts, *Cytokine production and dysregulation in HIV pathogenesis: lessons for development of therapeutics and vaccines*. Cytokine Growth Factor Rev, 2012. **23**(4-5): p. 181-91.
263. Carvalho-Gomes, A., et al., *Cytomegalovirus specific polyfunctional T-cell responses expressing CD107a predict control of CMV infection after liver transplantation*. Cell Immunol, 2022. **371**: p. 104455.
264. Pan, K., et al., *Mass spectrometric identification of immunogenic SARS-CoV-2 epitopes and cognate TCRs*. Proc Natl Acad Sci U S A, 2021. **118**(46).
265. Troyano-Hernaez, P., R. Reinoso, and A. Holguin, *Evolution of SARS-CoV-2 Envelope, Membrane, Nucleocapsid, and Spike Structural Proteins from the Beginning of the Pandemic to September 2020: A Global and Regional Approach by Epidemiological Week*. Viruses, 2021. **13**(2).
266. Sheikh-Mohamed, S., et al., *Systemic and mucosal IgA responses are variably induced in response to SARS-CoV-2 mRNA vaccination and are associated with protection against subsequent infection*. Mucosal Immunol, 2022. **15**(5): p. 799-808.
267. Montague, B.T., et al., *Elevated serum IgA following vaccination against SARS-CoV-2 in a cohort of high-risk first responders*. Sci Rep, 2022. **12**(1): p. 14932.
268. Sette, A. and S. Crotty, *Immunological memory to SARS-CoV-2 infection and COVID-19 vaccines*. Immunol Rev, 2022. **310**(1): p. 27-46.

269. De Rosa, S.C., et al., *Vaccination in humans generates broad T cell cytokine responses*. J Immunol, 2004. **173**(9): p. 5372-80.
270. Precopio, M.L., et al., *Immunization with vaccinia virus induces polyfunctional and phenotypically distinctive CD8(+) T cell responses*. J Exp Med, 2007. **204**(6): p. 1405-16.
271. Ellebedy, A.H., et al., *Defining antigen-specific plasmablast and memory B cell subsets in human blood after viral infection or vaccination*. Nat Immunol, 2016. **17**(10): p. 1226-34.
272. Wrammert, J., et al., *Rapid and massive virus-specific plasmablast responses during acute dengue virus infection in humans*. J Virol, 2012. **86**(6): p. 2911-8.
273. Wrammert, J., et al., *Human immune memory to yellow fever and smallpox vaccination*. J Clin Immunol, 2009. **29**(2): p. 151-7.
274. Borobia, A.M., et al., *Immunogenicity and reactogenicity of BNT162b2 booster in ChAdOx1-S-primed participants (CombiVacS): a multicentre, open-label, randomised, controlled, phase 2 trial*. Lancet, 2021. **398**(10295): p. 121-130.
275. Dema, M., et al., *Immunosenescence in multiple sclerosis: the identification of new therapeutic targets*. Autoimmun Rev, 2021. **20**(9): p. 102893.
276. Mills, E.A. and Y. Mao-Draayer, *Aging and lymphocyte changes by immunomodulatory therapies impact PML risk in multiple sclerosis patients*. Mult Scler, 2018. **24**(8): p. 1014-1022.
277. Wack, A., et al., *Age-related modifications of the human alphabeta T cell repertoire due to different clonal expansions in the CD4+ and CD8+ subsets*. Int Immunol, 1998. **10**(9): p. 1281-8.
278. Cossarizza, A., et al., *Highly active antiretroviral therapy restores CD4+ Vbeta T-cell repertoire in patients with primary acute HIV infection but not in treatment-naive HIV+ patients with severe chronic infection*. J Acquir Immune Defic Syndr, 2004. **35**(3): p. 213-22.
279. Frasca, D., et al., *B Cell Immunosenescence*. Annu Rev Cell Dev Biol, 2020. **36**: p. 551-574.
280. Sica, F., D. Centonze, and F. Buttari, *Fingolimod Immune Effects Beyond Its Sequestration Ability*. Neurol Ther, 2019. **8**(2): p. 231-240.
281. Cuculiza Henriksen, A., et al., *Natalizumab differentially affects plasmablasts and B cells in multiple sclerosis*. Mult Scler Relat Disord, 2021. **52**: p. 102987.
282. Nakaya, H.I., et al., *Systems biology of vaccination for seasonal influenza in humans*. Nat Immunol, 2011. **12**(8): p. 786-95.
283. Bucasas, K.L., et al., *Early patterns of gene expression correlate with the humoral immune response to influenza vaccination in humans*. J Infect Dis, 2011. **203**(7): p. 921-9.

284. Tran, T.M., et al., *A Molecular Signature in Blood Reveals a Role for p53 in Regulating Malaria-Induced Inflammation*. *Immunity*, 2019. **51**(4): p. 750-765 e10.

ACKNOWLEDGEMENTS

I would like to express my gratitude to my supervisor, Prof. Andrea Cossarizza, for providing me with the opportunity to work in his laboratory and team. Your mentorship and sharing of expertise and knowledge have been instrumental in shaping my academic and research journey.

I am also grateful to my co-supervisor, Dr. Sara De Biasi, for her insightful feedback and mentorship. Your expertise has significantly enriched my research and contributed to its depth and quality.

I extend my thanks to Prof. Lara Gibellini and all the people who have worked alongside me. Your collaboration and support have been precious for my scientific and personal growth.

Furthermore, I would like to thank all the clinicians who generously shared their time, expertise, and resources in advancing the scope and impact of our research endeavors.

I would also like to express my heartfelt appreciation to my family and friends for their unwavering support, encouragement, and understanding throughout this endeavor. Your love, patience, and belief in me have been a constant source of motivation and strength. A special acknowledgment goes to Pietro, who has been there for the entire journey, always supporting and helping me.

This thesis would not have been possible without the collective efforts and support of all those mentioned above. Thank you for being an integral part of this journey.



Article

Patients Recovering from Severe COVID-19 Develop a Polyfunctional Antigen-Specific CD4+ T Cell Response

Annamaria Paolini ¹, Rebecca Borella ¹, Anita Neroni ¹, Domenico Lo Tartaro ¹, Marco Mattioli ¹, Lucia Fidanza ¹, Alessia Di Nella ¹, Elena Santacroce ¹, Licia Gozzi ², Stefano Busani ^{3,4}, Tommaso Trenti ⁵, Marianna Meschiari ², Giovanni Guaraldi ^{2,3}, Massimo Girardis ^{3,4}, Cristina Mussini ^{2,3}, Lara Gibellini ¹, Sara De Biasi ^{1,*} and Andrea Cossarizza ^{1,6}

- ¹ Department of Medical and Surgical Sciences for Children and Adults, University of Modena and Reggio Emilia School of Medicine, Via Campi 287, 41125 Modena, Italy; annamaria.paolini@unimore.it (A.P.); rebecca.borella@unimore.it (R.B.); anneroni@unimore.it (A.N.); domenico.lotartaro@unimore.it (D.L.T.); mattioli.marco@gmail.com (M.M.); lucia.fidanza@unimore.it (L.F.); adinella@unimore.it (A.D.N.); 239216@studenti.unimore.it (E.S.); lara.gibellini@unimore.it (L.G.); andrea.cossarizza@unimore.it (A.C.)
- ² Infectious Diseases Clinics, AOU Policlinico di Modena, Via del Pozzo 71, 41124 Modena, Italy; licia.gozzi@gmail.com (L.G.); mariannameschiari1209@gmail.com (M.M.); giovanni.guaraldi@unimore.it (G.G.); cristina.mussini@unimore.it (C.M.)
- ³ Department of Surgery, Medicine, Dentistry and Morphological Sciences, University of Modena and Reggio Emilia, Via del Pozzo 71, 41124 Modena, Italy; stefano.busani@unimore.it (S.B.); massimo.girardis@unimore.it (M.G.)
- ⁴ Department of Anesthesia and Intensive Care, AOU Policlinico and University of Modena and Reggio Emilia, Via del Pozzo 71, 41124 Modena, Italy
- ⁵ Department of Laboratory Medicine and Pathology, Diagnostic Hematology and Clinical Genomics, AUSL/AOU Policlinico, 41124 Modena, Italy; t.trenti@ausl.mo.it
- ⁶ National Institute for Cardiovascular Research, Via Irnerio 48, 40126 Bologna, Italy
- * Correspondence: sara.debiasi@unimore.it



Citation: Paolini, A.; Borella, R.; Neroni, A.; Lo Tartaro, D.; Mattioli, M.; Fidanza, L.; Di Nella, A.; Santacroce, E.; Gozzi, L.; Busani, S.; et al. Patients Recovering from Severe COVID-19 Develop a Polyfunctional Antigen-Specific CD4+ T Cell Response. *Int. J. Mol. Sci.* **2022**, *23*, 8004. <https://doi.org/10.3390/ijms23148004>

Academic Editors: Vincenzo Barnaba, Manlio Ferrarini and Jeffrey L. Platt

Received: 30 June 2022

Accepted: 18 July 2022

Published: 20 July 2022

Publisher's Note: MDPI stays neutral with regard to jurisdictional claims in published maps and institutional affiliations.



Copyright: © 2022 by the authors. Licensee MDPI, Basel, Switzerland. This article is an open access article distributed under the terms and conditions of the Creative Commons Attribution (CC BY) license (<https://creativecommons.org/licenses/by/4.0/>).

Abstract: Specific T cells are crucial to control SARS-CoV-2 infection, avoid reinfection and confer protection after vaccination. We have studied patients with severe or moderate COVID-19 pneumonia, compared to patients who recovered from a severe or moderate infection that had occurred about 4 months before the analyses. In all these subjects, we assessed the polyfunctionality of virus-specific CD4+ and CD8+ T cells by quantifying cytokine production after in vitro stimulation with different SARS-CoV-2 peptide pools covering different proteins (M, N and S). In particular, we quantified the percentage of CD4+ and CD8+ T cells simultaneously producing interferon- γ , tumor necrosis factor, interleukin (IL)-2, IL-17, granzyme B, and expressing CD107a. Recovered patients who experienced a severe disease display high proportions of antigen-specific CD4+ T cells producing Th1 and Th17 cytokines and are characterized by polyfunctional SARS-CoV-2-specific CD4+ T cells. A similar profile was found in patients experiencing a moderate form of COVID-19 pneumonia. No main differences in polyfunctionality were observed among the CD8+ T cell compartments, even if the proportion of responding cells was higher during the infection. The identification of those functional cell subsets that might influence protection can thus help in better understanding the complexity of immune response to SARS-CoV-2.

Keywords: COVID-19; antigen-specific T cells; cytokine production; polyfunctionality; flow cytometry

1. Introduction

The characterization of the immune response mounted against Severe Acute Respiratory Syndrome-Coronavirus-2 (SARS-CoV-2) infection is crucial to understanding and predicting short- and long-term protection. Both innate and adaptive immunity has been well described during severe cases as well as in recovered patients [1–10] and it has been reported that an integrated response can limit COVID-19 disease severity [11]. Developing

SARS-CoV-2 antigen-specific CD4⁺ and CD8⁺ T cells besides antibodies is crucial to prevent severe outcomes and protect against reinfections [11,12]. This explains, at least in part, why: (i) immunocompromised patients with reduced humoral response and deficient B cells can develop a SARS-CoV-2 specific T cell response [13]; (ii) patients experiencing mild COVID-19 can successfully control the virus thanks to a robust SARS-CoV-2 T cell response even in the absence of antibodies [11,14–17].

SARS-CoV-2 T cell response in patients recovered from COVID-19 is multi-specific as T cells recognize several epitopes, by using a heterogenous T cell receptor (TCR) [18–21]. Functional studies using peptide pools covering most of SARS-CoV-2 encoded proteome demonstrated that T cell response to structural proteins such as the membrane (M), spike (S) or nucleocapsid (N) is co-dominant and that a significant reactivity is also developed against other targets, such as Open Reading Frames (ORFs) and nonstructural proteins (NSPs) [5,18,19]. However, whether this multi-specificity is the key to long-term protection is still uncertain.

CD4⁺ and CD8⁺ T cell polyfunctionality indicate the ability of cells to simultaneously produce more than one cytokine and to exert multiple functions. This is a crucial feature in antigen-specific responses as, in some cases, the quality of the response can be more important than the quantity in conferring protection against reinfection or pathogen reactivation [22,23]. In this scenario, CD4⁺ T helper type 1 (Th1) and Th17 are fundamental in inducing CD8⁺ T and B cells activity and promoting a pro-inflammatory response [12,24,25]. For example, Th1 and Th17 CD4⁺ T and CD8⁺ T cells dominate the influenza A virus-specific response, so inducing both a highly inflammatory environment and viral clearance [26–28].

For these reasons, given the role and capability of these cells, the aim of the study is to characterize the polyfunctional profile of SARS-CoV-2-specific T cells. Moreover, we aimed to investigate possible differences in the specific response between patients experiencing and recovering from moderate or severe infection, deepening at the same time the immunogenic capacity of M, N and S SARS-CoV-2 structural proteins.

2. Results

2.1. Characteristics of the Patients

We studied a total of 28 patients with COVID-19 pneumonia admitted into the Infectious Diseases Clinics or to the Intensive Care Unit (ICU) of the University Hospital in Modena over the period of March 2020–May 2020, and 10 healthy donors.

Characteristics of patients are reported in Table 1. COVID-19 moderate and COVID-severe presented higher levels of LDH when compared to recovered moderate and recovered severe, respectively. Regarding SARS-CoV-2-specific IgM and IgG, even if IgM were more represented among patients with moderate disease, no statistically significant differences were found between those with COVID-19 and the recovered, while HD tested negative for both assays. One patient from the COVID-19 severe group and one from the recovered severe group presented with type 2 diabetes. Recovered moderate and recovered severe were hospitalized and diagnosed with SARS-CoV-2 infection 120 ± 18 (mean \pm SD) days and 128 ± 3 (mean \pm SD) days, respectively, before blood withdrawal.

An example of the gating strategy for the identification of cells able to exert one or more functions is reported in Figure S1. Peripheral blood mononuclear cells (PBMCs) were stimulated or not with M, N or S peptide pool, cultured and stained. PBMCs were first gated according to their physical parameters, and the aggregates were electronically removed from the analysis by using a gate designed for singlets. Living (Live/Dead, L/D-) cells and CD3⁺ T cells were identified. Among CD3⁺ cells, CD4⁺ and CD8⁺ T cell subpopulations were identified. In each subpopulation, the percentage of cells producing interferon (IFN)- γ , Tumor Necrosis Factor (TNF), Interleukin (IL)-2, IL-17, and granzyme B (GRZB), as well as expression of CD107a, was then quantified.

Table 1. Demographic and clinical characteristics of healthy donors (HD), COVID-19 and recovered patients.

Variable	Healthy Donor (n = 10)	COVID-19 Moderate (n = 7)	COVID-19 Severe (n = 6)	Recovered Moderate (n = 9)	Recovered Severe (n = 6)	p-Value COVID-19 Moderate vs. COVID-19 Severe	p-Value COVID-19 Moderate vs. Recovered Moderate	p-Value Recovered Moderate vs. Recovered Severe	p-Value COVID-19 Severe vs. Recovered Severe
Demographic characteristics									
Age (median years, range) ¹	49.5 (37–70)	55.0 (43–65)	63.0 (53–68)	56.0 (36–63)	56.5 (43–61)	ns	ns	ns	ns
Sex (M, %) ²	5 (50)	6 (85.7)	6 (100)	5 (55.6)	4 (66.7)	ns	ns	ns	ns
Clinical characteristics									
<i>Coexisting conditions</i>									
Type 2 diabetes, N (%) ²	/	0 (0)	1 (16.7)	0 (0)	1 (16.7)	ns	ns	ns	ns
Cardiovascular Dis., N (%) ²	/	0 (0)	0 (0)	0 (0)	0 (0)	NA	NA	NA	NA
Chronic Kidney Dis., N (%) ²	/	0 (0)	0 (0)	0 (0)	0 (0)	NA	NA	NA	NA
Cancer, N (%) ²	/	0 (0)	0 (0)	0 (0)	0 (0)	NA	NA	NA	NA
Clinical Blood parameters									
Total bilirubin, mg/dL (median, range) ¹	/	1.0(0.6–1.4)	0.8(0.3–0.9)	0.7(0.3–0.9)	0.4(0.3–0.8)	ns	ns	ns	ns
CK, U/L (median, range) ¹	/	81.0 (56.0–154.0)	34.5 (23.0–259.0)	102.0 (87.0–139.0)	139.0 (12.0–282.0)	ns	ns	ns	ns
Creatinine, mg/dL (median, range) ¹	/	0.8 (0.6–1.0)	0.6 (0.5–0.8)	0.9 (0.7–1.1)	0.9 (0.8–1.2)	ns	ns	ns	ns
D-dimer, ng/mL (median, range) ¹	/	495 (230–7810)	750 (190–5820)	180 (100.0–340.0)	255 (140.0–780.0)	ns	ns	ns	ns
LDH, U/L (median, range) ¹	/	591 (580–886)	581 (507.0–1521)	361 (244–450)	384 (337–430)	ns	0.0272	ns	0.0272
CRP, mg/dL (median, range) ¹	/	0.3 (0.2–0.9)	0.35 (0.2–12.1)	0.2 (0.2–0.3)	0.2 (0.2–0.4)	ns	ns	ns	ns
Blood cell count									
White blood cells, N/μL (median, range) ¹	/	7500 (2888–10,880)	6305 (4800–15,300)	6480 (4420.0–7160)	6985 (6340.0–7680)	ns	ns	ns	ns
Lymphocytes, N/μL (median, range) ¹	/	2898 (2698–3098)	1642 (629–2460)	2240 (1600–7160)	2615 (2120–3740)	ns	ns	ns	ns
Neutrophils, N/μL (median, range) ¹	/	6390 (5545–7235)	3818 (1906–14,560)	3120 (2430–2980)	3755 (3060.0–3900)	ns	ns	ns	ns
Detection of SARS-CoV-2 IgM, IgG									
IgM, Index (median, range) ¹	0.0	28.7 (5.7–59.1)	6.4 (1.2–66.3)	4.7 (0.3–28.6)	4.5 (0.5–20.0)	ns	ns	ns	ns
IgG, Index (median, range) ¹	0.0	7.3 (6.3–9.0)	6.2 (1.5–8.6)	6.1 (2.0–9.4)	3.9(1.2–7.0)	ns	ns	ns	ns

NA; not applicable. ns; not significant, p -Value > 0.05. ¹ Kruskal–Wallis test with original FDR method of Benjamini and Hochberg. ² Chi-square test.

2.2. Recovered Patients Who Experienced a Severe Disease Display High Percentage of Antigen-Specific CD4+ T Cells Producing Th1 and Th17 Cytokines

Cytokine production was assessed following 16 h of *in vitro* stimulation with SARS-CoV-2 peptide pools covering the sequence of different proteins (N, M or S). The percentage of CD4+ and CD8+ T cells producing IFN- γ , TNF, IL-2, IL-17, and GRZB was quantified along with the percentage of cells able to express CD107a. The identification of these cytokines allows us to recognize different subsets of helper CD4+ and CD8+ T cells, such as: (i) Th1, defined as cells producing IFN- γ , TNF, IL-2; (ii) Th17 identified as cells producing IL-17; (iii) cytotoxic T cells, which are positive for GRZB and CD107a [29,30].

Individuals who recovered from a severe form of COVID-19 disease showed a higher percentage of CD4+ T cells responding to N and S compared to healthy donors (HD) (Figure 1a). Moreover, taking into consideration all the stimuli used, patients who recovered from a severe disease exhibited a higher percentage of CD4+ T cells producing IFN- γ , TNF and IL-2 compared to either HD or individuals who recovered from moderate disease (Figure 1b). This was also observed when COVID-19 patients with a moderate disease were compared to HD. Furthermore, recovered individuals who experienced a severe disease also displayed a higher percentage of CD4+ T cells producing IL-17 compared to recovered moderate, regardless of the stimulus used (Figure 1b). On the other hand, COVID-19 patients with severe infection were characterized by higher proportions of cells expressing CD107a compared to HD after M and S stimulation, indicating a more enhanced cytotoxic phenotype (Figure 1b).

Regarding CD8+ T cell response, the percentage of CD8+ T cells responding to peptide pool stimulation was higher in COVID-19 patients with a moderate disease compared to either HD or recovered individuals who experienced a moderate infection. In addition, COVID-19 patients with severe form exhibited a higher percentage of responding CD8+ T cells compared to those who recovered from a severe form (Figure 2a). Furthermore, after *in vitro* stimulation with M, COVID-19 severe patients displayed a higher percentage of CD8+ T cells expressing CD107a compared to individuals who recovered from severe infection (Figure 2b). Thus, antigen-specific CD8+ T cells are more abundant among COVID-19 patients and present a more pronounced cytotoxic phenotype in line with their role in mediating clearance during viral infections [31].

2.3. Recovered Patients Who Experienced a Severe Disease Are Characterized by Polyfunctional SARS-CoV-2 Antigen-Specific CD4+ T cells

In vitro stimulation with the M peptide pool induced a different polyfunctional profile between COVID-19 moderate and severe patients, COVID-19 severe patients and those who recovered from severe disease. Moreover, the polyfunctional response was different when compared to HD in either patients with moderate COVID-19 or those who recovered from severe disease. In particular, COVID-19 moderate patients and recovered individuals from severe disease, when compared to HD, reported higher percentages of IFN- γ +IL-2+TNF+, IFN- γ +TNF+ and IL-2+TNF+ within CD4+ T cells. Patients experiencing COVID-19 moderate also displayed a high percentage of IFN- γ +IL-2+ within CD4+ T cells. The percentage of the latest population was higher in COVID-19 severe and recovered moderate if compared to recovered severe and HD (Figure 3a).

Stimulation with N induced differences in the overall polyfunctionality of CD4+ T cells between patients who recovered (moderate vs. severe) and between COVID-19 severe patients and those who recovered from severe disease. Finally, COVID-19 moderate patients and recovered displayed a different cytokine profile when compared to HD. Regarding the subsets of polyfunctional CD4+ T cells, individuals who recovered from the severe disease exhibited the same cytokine production as seen with M stimulation. In addition, this group of patients presented a small population of TNF+, IL-17+ cells. COVID-19 moderate patients, compared to HD, also presented a high percentage of IFN- γ +IL-2+TNF+ and IL-2+TNF+ (Figure 3b).

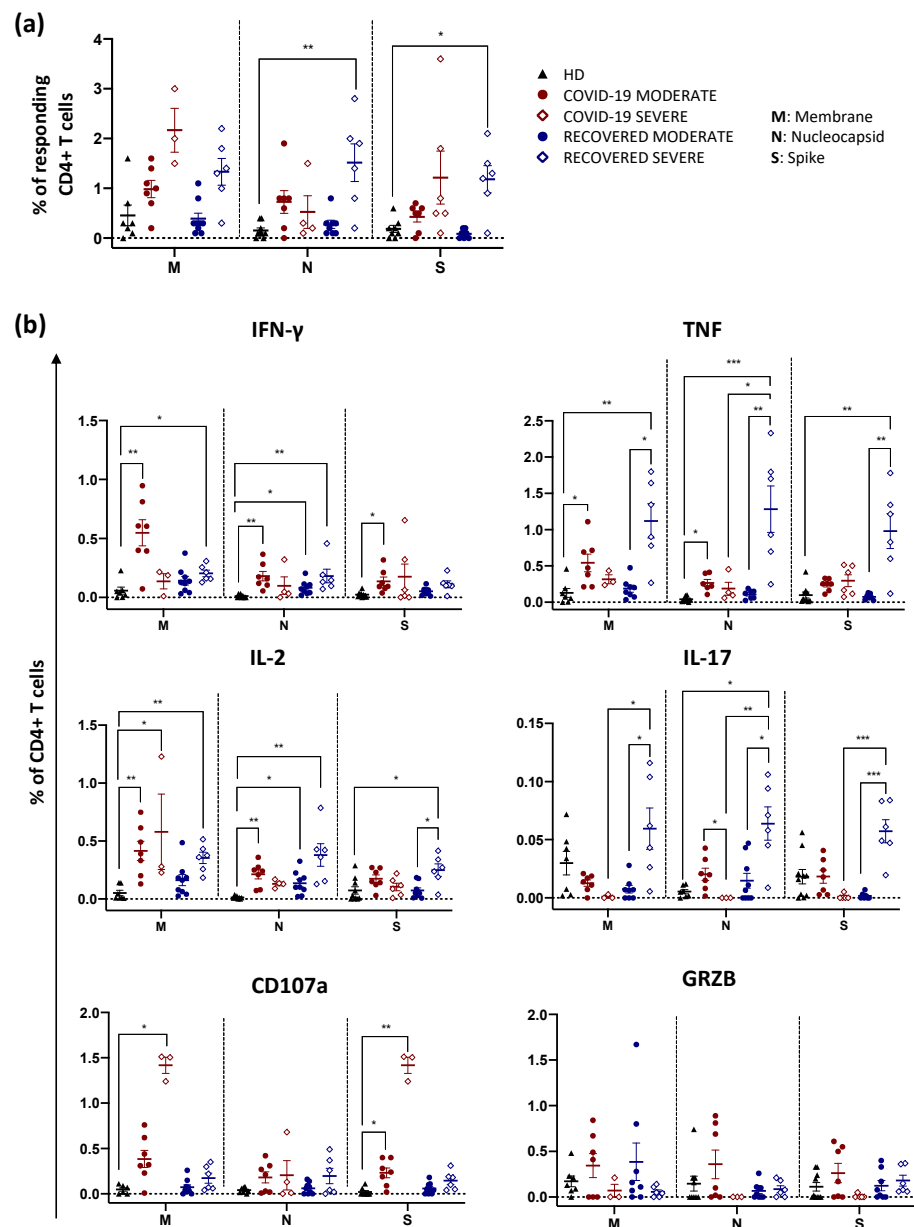


Figure 1. Total cytokine production by CD4+ T cells after in vitro stimulation. (a) Percentage of responding CD4+ T cells after stimulation with M, N or S. Data represent individual values from healthy donors (HD, $n = 10$), COVID-19 moderate ($n = 7$), COVID-19 severe ($n = 6$), recovered moderate ($n = 9$) and recovered severe ($n = 6$). Mean (center bar) \pm standard error of the mean (SEM, upper and lower bars) is represented. Statistical analysis was performed using Kruskal–Wallis non-parametric test corrected for multiple comparisons by controlling the False Discovery Rate (FDR), method of Benjamini and Hochberg. * $q < 0.05$; ** $q < 0.01$. Background was subtracted from each sample. (b) Representation of the total production of each cytokine after stimulation of CD4+ T cells. We evaluated the percentage of CD4+ T cells producing IFN- γ , TNF, IL-2, IL-17, GRZB as well as expressing CD107a among HD ($n = 10$), COVID-19 moderate ($n = 7$), COVID-19 severe ($n = 6$), recovered moderate ($n = 9$) and recovered severe ($n = 6$). Data are represented as individual values, mean (center bar) \pm standard error of the mean (SEM, upper and lower bars) is represented. Statistical analysis was performed using Kruskal–Wallis non-parametric test corrected for multiple comparisons by controlling the False Discovery Rate (FDR), method of Benjamini and Hochberg. * $q < 0.05$; ** $q < 0.01$; *** $q < 0.001$. Background (i.e., the value determined in unstimulated controls) was subtracted from each sample.

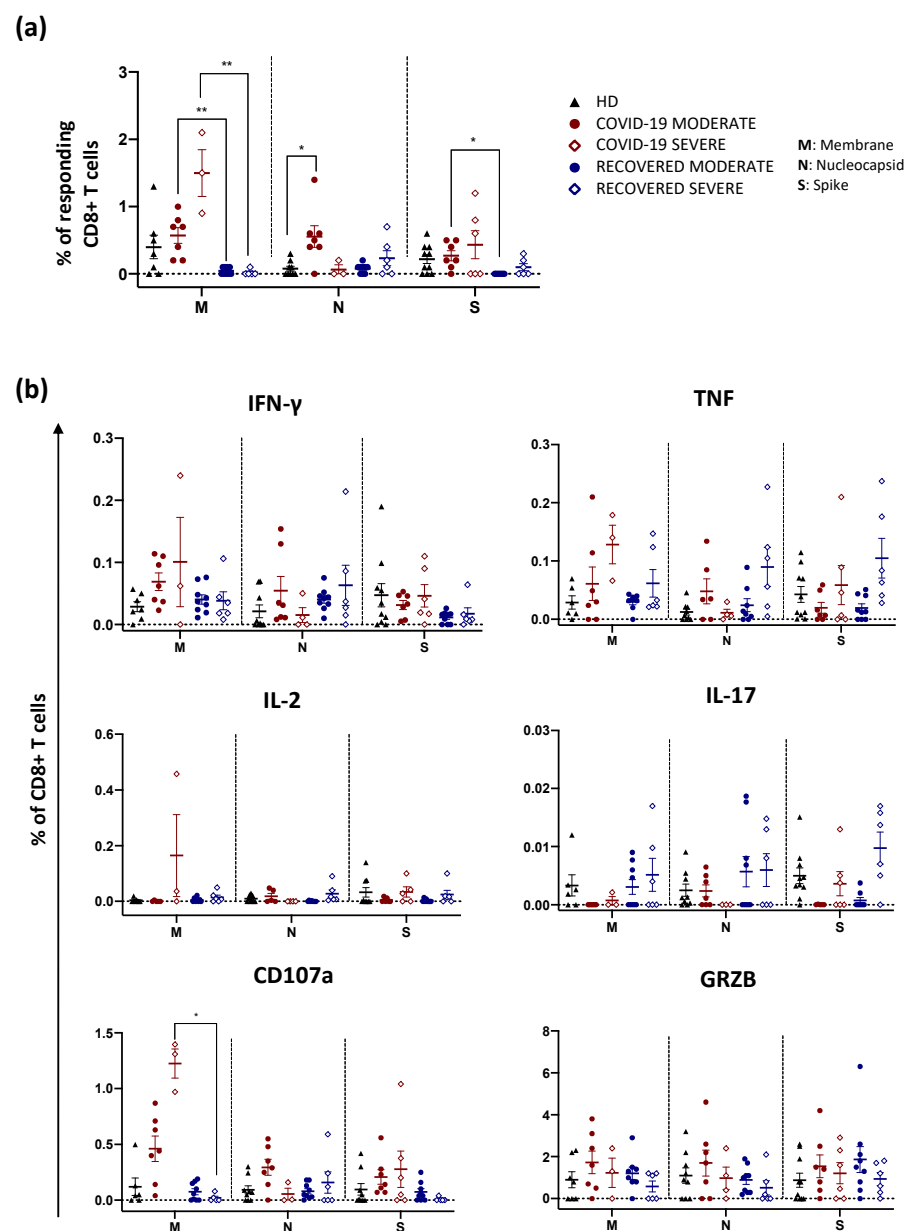


Figure 2. Total cytokine production by CD8+ T cells after in vitro stimulation. (a) Percentage of responding CD8+ T cells after stimulation with M, N or S. Data represent individual values from HD ($n = 10$), COVID-19 moderate ($n = 7$), COVID-19 severe ($n = 6$), recovered moderate ($n = 9$) and recovered severe ($n = 6$). Mean (center bar) \pm standard error of the mean (SEM, upper and lower bars) is represented. Statistical analysis was performed using Kruskal–Wallis non-parametric test corrected for multiple comparisons by controlling the False Discovery Rate (FDR), method of Benjamini and Hochberg. * $q < 0.05$; ** $q < 0.01$. Background was subtracted from each sample. (b) Representation of the total production of cytokines after stimulation of CD8+ T cells. We evaluated the percentage of CD8+ T cells producing IFN- γ , TNF, IL-2, IL-17, GRZB as well as expressing CD107a among HD ($n = 10$), COVID-19 moderate ($n = 7$), COVID-19 severe ($n = 6$), recovered moderate ($n = 9$) and recovered severe ($n = 6$). Data are represented as individual values, mean (center bar) \pm standard error of the mean (SEM, upper and lower bars) is represented. Statistical analysis was performed using Kruskal–Wallis non-parametric test corrected for multiple comparisons by controlling the False Discovery Rate (FDR), method of Benjamini and Hochberg. * $q < 0.05$. Background (i.e., the value determined in unstimulated controls) was subtracted from each sample.

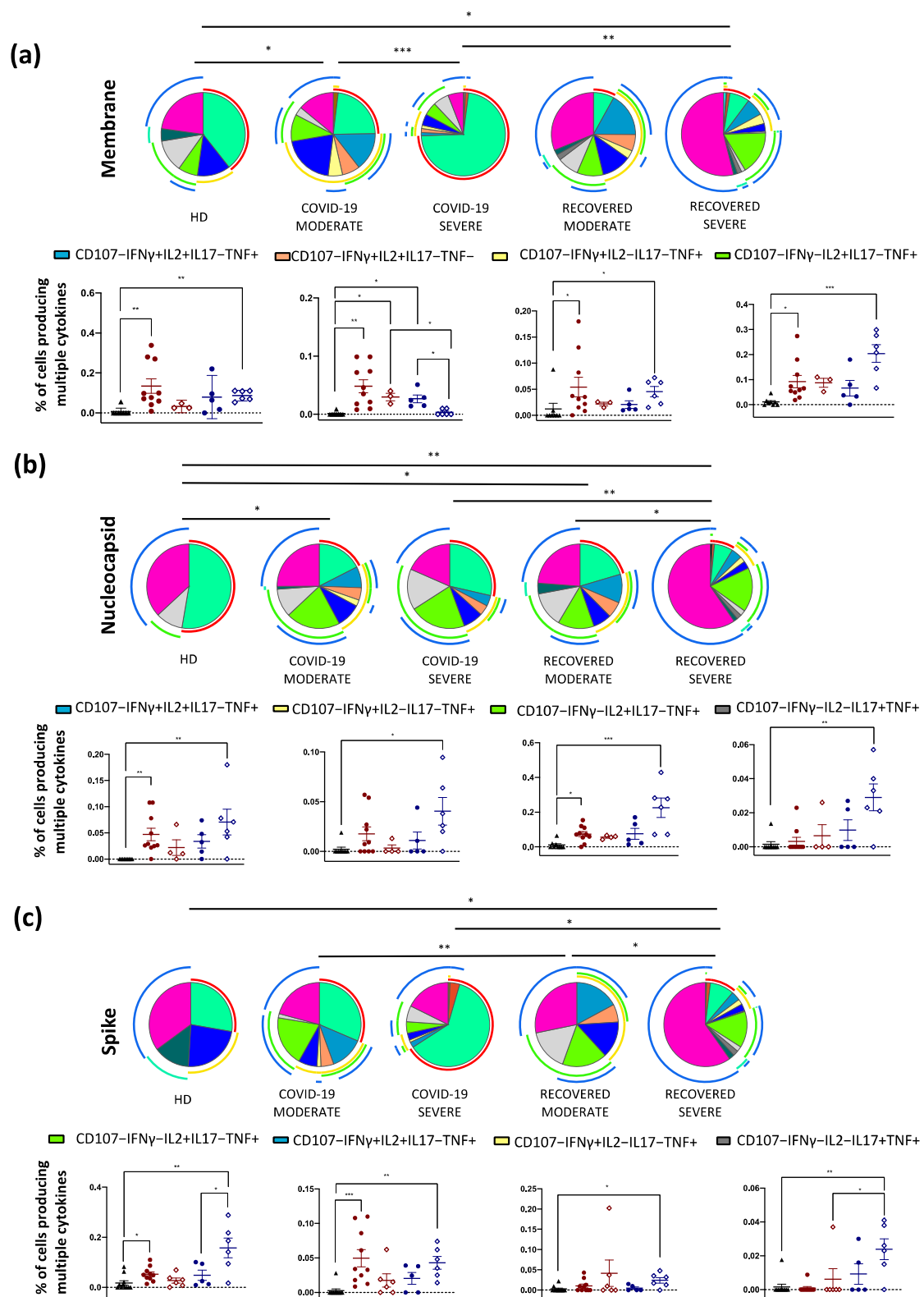


Figure 3. Cont.

(d)

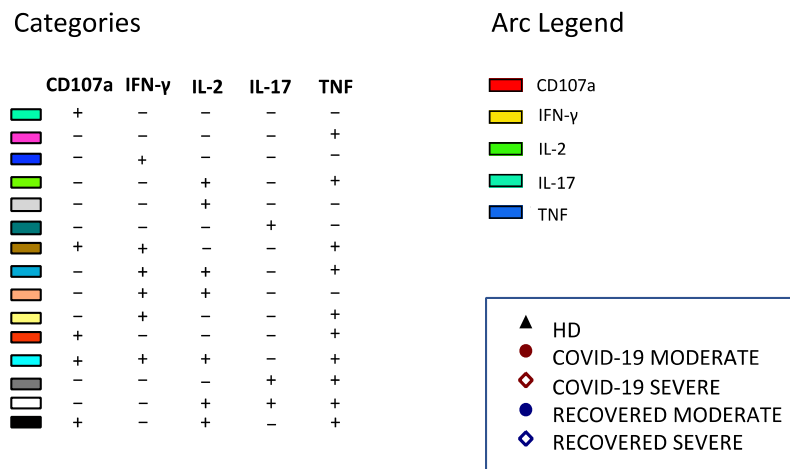


Figure 3. Polyfunctionality of CD4+ T cells after in vitro stimulation. Pie charts representing the proportion of CD4+ T cells producing different combinations of IFN- γ TNF, IL-2, IL-17, GRZB as well as expressing CD107a after stimulation with (a) M; (b) N; or (c) S peptide pools from HD ($n = 10$), COVID-19 moderate ($n = 7$), COVID-19 severe ($n = 6$), recovered moderate ($n = 9$) and recovered severe ($n = 6$) patients. For clarity, panel (d) reports the legend for the colors and the symbols used in panels (a–c). Data in pie charts are represented as median values. Frequencies were corrected by background subtraction as determined in non-stimulated controls using SPICE software. Statistical analysis between pie charts was performed using permutation test (* $p < 0.05$; ** $p < 0.01$; *** $p < 0.001$). Pie arches represent the total production of different cytokines. Comparison between the production of different combinations of cytokines by CD4+ T cells is represented. Data are represented as individual values, mean (center bar) \pm standard error of the mean (SEM, upper and lower bars) is represented. Statistical analysis was performed using Kruskal–Wallis non-parametric test corrected for multiple comparisons by controlling the False Discovery Rate (FDR), method of Benjamini and Hochberg. * $q < 0.05$; ** $q < 0.01$; *** $q < 0.001$.

Finally, after stimulation with S, individuals who recovered from different disease severity showed a different polyfunctionality as well as COVID-19 moderate patients and recovered from the moderate disease. In addition, recovered from severe disease displayed a distinct polyfunctional asset compared to COVID-19 severe and HD. Individuals who recovered from severe disease presented almost overlapping results as those observed after stimulation with N and M. Moreover, they also displayed a higher percentage of TNF+IL-17+ within CD4+ T cells if compared to COVID-19 severe and HD. Regarding COVID-19 moderate, the cell distribution after stimulation is the same as the one measured after N stimulation (Figure 3c). For clarity, Figure 3d shows the legend of the colors and symbols of the previous Figure 3 panels.

The polyfunctional profile of CD8+ T cells after in vitro stimulation with M or N was similar among the groups. Only the S peptide pool induced a slightly different profile in COVID-19 moderate patients when compared to HD (Figure 4).

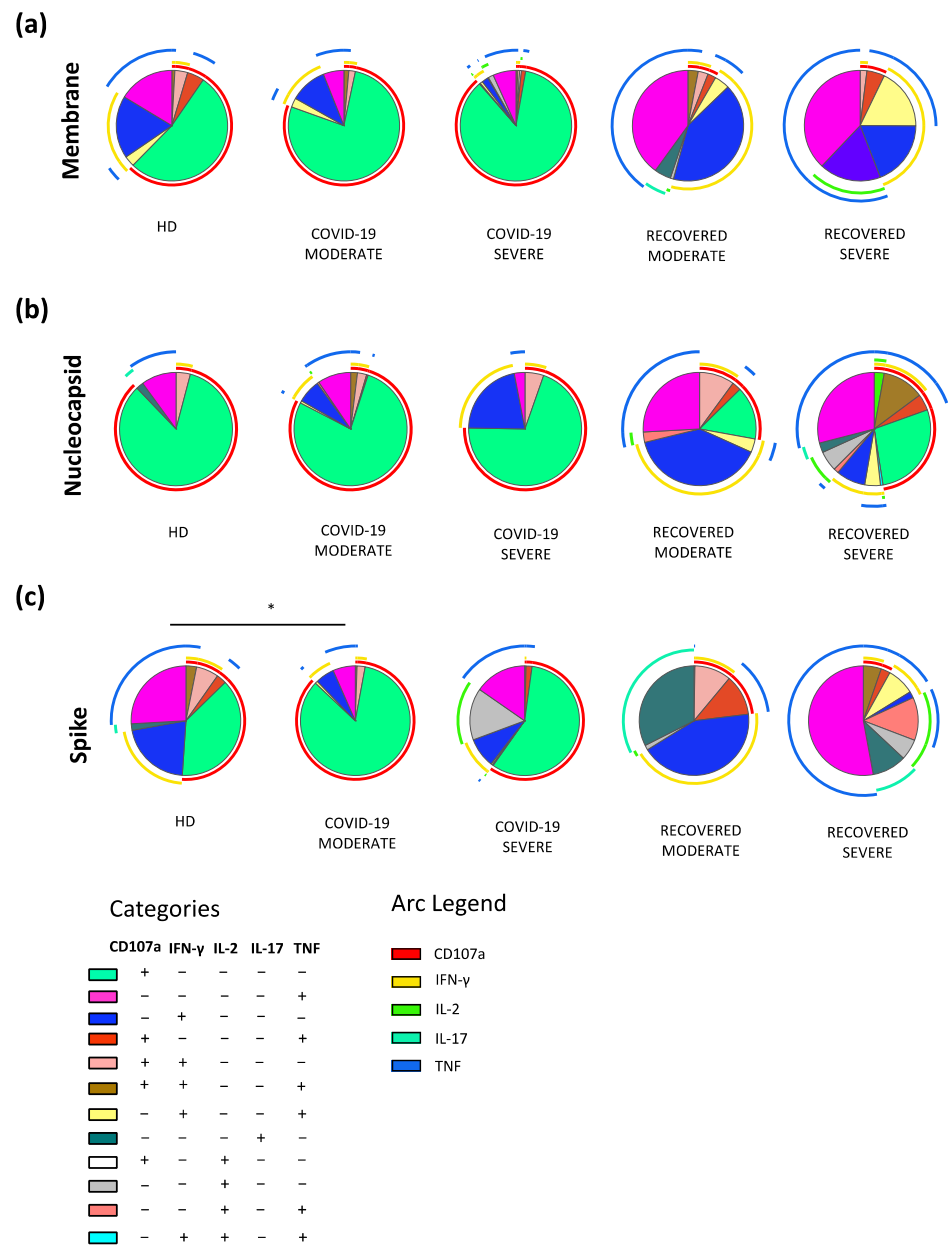


Figure 4. Polyfunctionality of CD8+ T cells after in vitro stimulation. Pie charts representing the proportion of CD8+ T cells producing different combinations of IFN- γ , TNF, IL-2, IL-17, GRZB as well as expressing CD107a after stimulation with (a) M; (b) N; or (c) S peptide pools from HD ($n = 10$), COVID-19 moderate ($n = 7$), COVID-19 severe ($n = 6$), recovered moderate ($n = 9$) and recovered severe ($n = 6$) patients. Data in pie charts are represented as median values. Frequencies were corrected by background subtraction as determined in non-stimulated controls using SPICE software. Statistical analysis between pie charts was performed using permutation test ($* p < 0.05$). Pie arches represent the total production of different cytokines.

3. Discussion

In this study, we describe the differences in the production of cytokines by SARS-CoV-2-specific T cells from patients with COVID-19 (severe or moderate) and in recovered individuals after in vitro stimulation with different peptide pools. Our aim was to measure not only the magnitude but also the characteristics, in qualitative terms, of such antigen-specific response. We found that COVID-19 moderate patients develop polyfunctional CD4+ T cells compared to patients experiencing a severe infection, that in turn display a higher percentage of CD107a+ cells. Besides their helper capability, CD4+ T cells can

exert cytotoxicity, and this has been described during persistent infections such as those by Epstein–Barr virus [32], cytomegalovirus [33], and Human Immunodeficiency Virus (HIV) [34]. Cytotoxic potential can be measured, detecting the expression of the degranulation marker CD107a [35]. This result is in line with other studies demonstrating that patients experiencing severe COVID-19 usually mount an impaired SARS-CoV-2 T cell-specific response [11,36]. It is known that the expression of exhaustion markers such as Programmed Death-1 (PD-1) and T-cell immunoglobulin and mucin domain-3 (Tim-3) is associated with disease progression [37,38]. This might reinforce the concept that patients experiencing a more severe infection present impaired CD4+ and CD8+ T cell functionality due to an exhausted phenotype. However, whether the expression of such markers reflects functional exhaustion rather than ongoing activation is still debated [37].

During the infection, Th1 cytokines such as IFN- γ , IL-2 and TNF are essential for supporting the expansion and maturation of CD8+ T lymphocytes and B cells [12]. The loss of CD4+ Th1 leads to a progressive CD8+ T cell decline and dysfunction with important implications for controlling the infection [39]. In addition, Th17 cells are responsible for the recruitment of several different cell populations at the site of the infection, inducing the inflammatory process necessary for the immediate protective response against a pathogen [24,25]. We found that, if compared to patients experiencing severe COVID-19, those recovering from severe COVID-19 display SARS-CoV-2-specific, highly polyfunctional CD4+ T cells with a Th1 and Th17 phenotype. No differences were reported in the CD8+ T cell compartment, reflecting the T cell kinetics of the immune response contraction according to which 2 weeks after onset symptoms, when circulating CD8+ T cells progressively decline, CD4+ T cells remain stable and eventually increase in the initial recovery phase (1–2 months after infection), more than immediately after infection [11,40].

T cells are able to both proliferate and secrete cytokines that in turn can influence other cell functions as well as induce cytolysis of infected cells. Polyfunctionality is the ability of cells to simultaneously perform more than one function, and it can be measured at a single cell level by flow cytometry [41]. In CD4+ T cells, such property is a correlate for protection against different pathogens. As an example, comparing the profile (more than the amount) of T cell cytokine production in different groups of HIV-infected individuals such as in those who control the infection to that of patients with a chronic progression of the infection revealed the presence of several key molecules involved in controlling the infection. This approach suggested that in some cases the quality of the T cell response, not the quantity, is correlated with immune protection [23]. During cytomegalovirus (CMV) infection, the development of polyfunctional T cells correlates with a better prognosis and confers an immunological advantage against other pathogens [22]. In addition, polyfunctional CD4+ T cells represent a marker for spontaneous control of viral replication in CMV-seropositive patients undergoing liver transplantation [42]. On the whole, this indicates the importance of measuring representative functions of T cells to identify and define correlates of immune protection.

The identification of the most immunogenic epitopes is key to the study and understanding of cellular immune response to gain insights into virus-induced infection mechanisms. An immunogenic peptide is one that is presented by a self-major histocompatibility complex (MHC) and is able to elicit a T cell response [43]. Thus, the identification of such epitopes is also of importance in the context of future therapies. M, N and S are SARS-CoV-2 structural proteins that constitute different portions of the virus. These proteins have different interactions with the other parts of the virion, and during the infection, they interact differently and in different moments with the host cell. This may define a different level of immunogenicity for each protein. For these reasons, we deepened the SARS-CoV-2 specific response to M, N and S. Overall, in our study we observed that M, N and S induced a similar response among the categories considered, confirming their co-dominance [18,44].

We are aware that this study has a main limitation since the number of individuals that we could study is relatively small, because of the difficulties to obtain biological

material from patients admitted to the hospital. However, even if we could study a relatively low number of patients, we could define the polyfunctionality profile of CD4+ and CD8+ T cells during and after SARS-CoV-2 infection in patients experiencing different severities of COVID-19. Global knowledge of the complex interaction during the cellular response to infection, as well as SARS-CoV-2-induced changes, is helping in understanding mechanisms beyond the immune response toward protective phenotype. In addition, the identification of unique cell subsets involved in immune protection could allow us to develop and use more and more sophisticated techniques that accurately measure the outcome of new therapies. Thus, the successful use of functional T cell analyses will likely help to significantly advance the field of SARS-CoV-2 therapy as well as vaccine efficacy, and hopefully, aid in reducing the global burden of the pandemic.

4. Materials and Methods

4.1. Patients

Four groups of patients were enrolled in this study, along with a group of healthy donors (HD). We enrolled 13 COVID-19 patients admitted into the Infectious Diseases Clinics or Intensive Care Unit (ICU) of the University Hospital in Modena between March and May 2020. Patients tested positive for the SARS-CoV-2 PCR test. Within this group, 7 patients (median age: 55.0 years) were classified as moderate and 6 (63.0 years) as severe, according to World Health Organization guidelines [45]. We also studied 15 COVID-19 recovered patients, enrolled during follow-up visits between June and August 2020. Within this group, 9 patients (56.0 years) were classified as moderate and 6 (56.5 years) as severe. COVID-19 and recovered patients were subdivided for the analysis according to disease severity. Moreover, 10 HD (49.5 years) were included in this study. HD presented neither symptoms nor prior diagnosis of SARS-CoV-2 and had negative serology. Informed consent, according to Helsinki Declaration, was provided by each participant. All uses of human material have been approved by the local Ethical Committee (Comitato Etico dell'Area Vasta Emilia Nord, protocol number 177/2020, 11 March 2020) and by the University Hospital Committee (Direzione Sanitaria dell'Azienda Ospedaliero-Universitaria di Modena, protocol number 7531, 11 March 2020).

4.2. Blood Processing

Blood samples were obtained after informed consent. For COVID-19 patients, blood was obtained after diagnosis of SARS-CoV-2 infection during hospitalization. For recovered patients, blood was collected during a follow-up visit within 120–128 days after hospital admission and SARS-CoV-2 diagnosis. Up to 20 mL of blood were collected from each patient in vacuettes containing ethylenediamine-tetraacetic acid. Peripheral blood mononuclear cells (PBMCs) were isolated according to standard procedures and stored in liquid nitrogen until use [46].

Plasma was collected and stored at $-80\text{ }^{\circ}\text{C}$ until the quantification of IgM and IgG, performed according to standard methods by SARS-CoV-2 IgM or IgG Quant Reagent Kit for use with Alinity (Abbott, Abbott Park, IL, USA).

4.3. In Vitro Stimulation and Intracellular Cytokine Staining (ICS)

For functional assays on cytokine production by T cells, isolated PBMCs were thawed and rested for 6 h. PBMCs were cultured in the presence of 15-mer peptides with 11-amino acids overlap, covering the sequence of different proteins of SARS-CoV-2: Nucleocapsid phosphoprotein ("N") (PepTivator SARS-CoV-2 Prot_N), Membrane glycoprotein ("M") (PepTivator SARS-CoV-2 Prot_M) and Spike glycoprotein (PepTivator SARS-CoV-2 Prot_S) (Miltenyi Biotec, Bergisch Gladbach, Germany). Each peptide was tested separately and $1\text{ }\mu\text{g/mL}$ of anti-CD28 (Miltenyi Biotec, Bergisch Gladbach, Germany) was added to each condition. PBMCs were stimulated for 16 h at $37\text{ }^{\circ}\text{C}$ in a 5% CO_2 atmosphere in a complete culture medium (RPMI 1640 supplemented with 10% fetal bovine serum and 1% each of l-glutamine, sodium pyruvate, nonessential amino acids, antibiotics, 0.1 M HEPES,

55 μM β -mercaptoethanol). A negative control with unstimulated cells was included in the experimental conditions. All samples were incubated with a protein transport inhibitor containing brefeldin A (Golgi Plug, BD Biosciences Pharmingen, San Diego, CA, USA), a protein transport inhibitor containing monensin (Golgi Stop, BD Biosciences Pharmingen, San Diego, CA, USA) and mAb CD107a-PE (Biolegend, San Diego, CA, USA) at a previously defined concentration. After stimulation, cells were stained with LIVE-DEAD Aqua (ThermoFisher Scientific, Eugene, OR, USA) and surface mAbs recognizing CD3 PE-Cy5, CD4 AF700, and CD8 APC-Cy7 (Biolegend, San Diego, CA, USA). Cells were washed with stain buffer, fixed and permeabilized with the Cytotfix/Cytoperm buffer set (BD Biosciences Pharmingen, San Diego, CA, USA) for cytokine detection [47]. Cells were stained with previously titrated directly conjugated mAbs: IL-17A-PE-Cy7, TNF-BV605, IFN- γ -FITC, IL-2-APC and GRZB-BV421 (all mAbs from Biolegend, San Diego, CA, USA). Cells were analyzed by an Attune NxT acoustic cytometer (ThermoFisher Scientific, Eugene, OR, USA). Table S1 reports mAb titers, producer, clone, catalog number, lot number and type of fluorochrome used in the panel.

4.4. Statistical Analysis

Quantitative variables were compared using the Kruskal–Wallis non-parametric test corrected for multiple comparisons by controlling the False Discovery Rate (FDR), method of Benjamini and Hochberg. Statistically significant q values are represented (* $q < 0.05$; ** $q < 0.01$; *** $q < 0.001$). T cell polyfunctionality was defined by using Simplified Presentation of Incredibly Complex Evaluation (SPICE) software (version 6, kindly provided by Dr. Mario Roederer, Vaccine Research Center, NIAID, NIH, Bethesda, MD, USA) [48]. Data from the total cytokine production are represented as individual values, means, and standard errors of the mean. Regarding polyfunctionality, data in pie charts are represented as median values; statistical analysis was performed using permutation test (* $p < 0.05$; ** $p < 0.01$; *** $p < 0.001$). Data in graphs are reported as individual values, means and standard errors of the mean. Statistical analyses were carried out using Prism 6.0 (GraphPad Software Inc., La Jolla, CA, USA). Background was subtracted from each sample.

Supplementary Materials: The following supporting information can be downloaded at: <https://www.mdpi.com/article/10.3390/ijms23148004/s1>.

Author Contributions: Conceptualization, A.P., L.G. (Lara Gibellini), S.D.B. and A.C.; Data curation, A.P. and L.G. (Licia Gozzi); Funding acquisition, A.C.; Methodology, R.B., A.N., D.L.T., M.M. (Marco Mattioli), L.F., A.D.N., E.S., T.T., L.G. (Lara Gibellini) and S.D.B.; Patients' recruitment, S.B., M.M. (Marianna Meschiari), G.G., M.G. and C.M.; Writing—original draft, A.P.; Writing—review & editing, A.P., S.D.B. and A.C. All authors have read and agreed to the published version of the manuscript.

Funding: This study was partially supported by “Bando ricerca COVID-19 grant number COVID-2020-12371808” from Ministero della Salute to AC and by unrestricted donations from Glem Gas spa (San Cesario, Modena, Italy), Sanfelice 1893 Banca Popolare (San Felice sul Panaro, Modena, Italy), Rotary Club Distretto 2072 (Clubs: Modena, Modena L.A. Muratori, Carpi, Sassuolo, and Castelvetro di Modena), C.O.F.I.M. spa & Gianni Gibellini, Franco Appari, Andrea Lucchi, Federica Vagnarelli, Biogas Europa Service & Massimo Faccia, Pierangelo Bertoli Fans Club and Alberto Bertoli, Maria Santoro, Valentina Spezzani and BPER Banca. Finally, special thanks to the patients who donated blood to participate in this study.

Institutional Review Board Statement: All uses of human material have been approved by the local Ethical Committee (Comitato Etico dell'Area Vasta Emilia Nord, protocol number 177/2020, 11 March 2020) and by the University Hospital Committee (Direzione Sanitaria dell'Azienda Ospedaliero-Universitaria di Modena, protocol number 7531, 11 March 2020).

Informed Consent Statement: Informed consent was obtained from all subjects involved in the study.

Data Availability Statement: All flow cytometry data files are available on request.

Acknowledgments: S.D.B. and L.G. are Marylou Ingram Scholar of the International Society for Advancement of Cytometry (ISAC) for the period 2015–2020 and 2020–2025, respectively. Paola Paglia (ThermoFisher Scientific, Monza, Italy) is kindly acknowledged for precious technical advice.

Conflicts of Interest: The authors declare no conflict of interest. The funders had no role in the design of the study; in the collection, analyses, or interpretation of data; in the writing of the manuscript, or in the decision to publish the results.

References

1. De Biasi, S.; Meschiari, M.; Gibellini, L.; Bellinazzi, C.; Borella, R.; Fidanza, L.; Gozzi, L.; Iannone, A.; Lo Tartaro, D.; Mattioli, M.; et al. Marked T cell activation, senescence, exhaustion and skewing towards TH17 in patients with COVID-19 pneumonia. *Nat. Commun.* **2020**, *11*, 3434. [[CrossRef](#)] [[PubMed](#)]
2. De Biasi, S.; Lo Tartaro, D.; Meschiari, M.; Gibellini, L.; Bellinazzi, C.; Borella, R.; Fidanza, L.; Mattioli, M.; Paolini, A.; Gozzi, L.; et al. Expansion of plasmablasts and loss of memory B cells in peripheral blood from COVID-19 patients with pneumonia. *Eur. J. Immunol.* **2020**, *50*, 1283–1294. [[CrossRef](#)] [[PubMed](#)]
3. Gibellini, L.; De Biasi, S.; Paolini, A.; Borella, R.; Boraldi, F.; Mattioli, M.; Lo Tartaro, D.; Fidanza, L.; Caro-Maldonado, A.; Meschiari, M.; et al. Altered bioenergetics and mitochondrial dysfunction of monocytes in patients with COVID-19 pneumonia. *EMBO Mol. Med.* **2020**, *12*, e13001. [[CrossRef](#)]
4. Dan, J.M.; Mateus, J.; Kato, Y.; Hastie, K.M.; Yu, E.D.; Faliti, C.E.; Grifoni, A.; Ramirez, S.I.; Haupt, S.; Frazier, A.; et al. Immunological memory to SARS-CoV-2 assessed for up to 8 months after infection. *Science* **2021**, *371*, eabf4063. [[CrossRef](#)]
5. Gangaev, A.; Ketelaars, S.L.C.; Isaeva, O.I.; Patiwaal, S.; Dopler, A.; Hoefakker, K.; De Biasi, S.; Gibellini, L.; Mussini, C.; Guaraldi, G.; et al. Identification and characterization of a SARS-CoV-2 specific CD8(+) T cell response with immunodominant features. *Nat. Commun.* **2021**, *12*, 2593. [[CrossRef](#)]
6. Borella, R.; De Biasi, S.; Paolini, A.; Boraldi, F.; Lo Tartaro, D.; Mattioli, M.; Fidanza, L.; Neroni, A.; Caro-Maldonado, A.; Meschiari, M.; et al. Metabolic reprogramming shapes neutrophil functions in severe COVID-19. *Eur. J. Immunol.* **2022**, *52*, 484–502. [[CrossRef](#)] [[PubMed](#)]
7. Gibellini, L.; De Biasi, S.; Meschiari, M.; Gozzi, L.; Paolini, A.; Borella, R.; Mattioli, M.; Lo Tartaro, D.; Fidanza, L.; Neroni, A.; et al. Plasma Cytokine Atlas Reveals the Importance of TH2 Polarization and Interferons in Predicting COVID-19 Severity and Survival. *Front. Immunol.* **2022**, *13*, 842150. [[CrossRef](#)] [[PubMed](#)]
8. Osuchowski, M.F.; Winkler, M.S.; Skirecki, T.; Cajander, S.; Shankar-Hari, M.; Lachmann, G.; Monneret, G.; Venet, F.; Bauer, M.; Brunkhorst, F.M.; et al. The COVID-19 puzzle: Deciphering pathophysiology and phenotypes of a new disease entity. *Lancet Respir. Med.* **2021**, *9*, 622–642. [[CrossRef](#)]
9. Wiech, M.; Chrosicki, P.; Swatler, J.; Stepnik, D.; De Biasi, S.; Hampel, M.; Brewinska-Olchowik, M.; Maliszewska, A.; Sklinda, K.; Durlik, M.; et al. Remodeling of T Cell Dynamics During Long COVID Is Dependent on Severity of SARS-CoV-2 Infection. *Front. Immunol.* **2022**, *13*, 886431. [[CrossRef](#)]
10. Lo Tartaro, D.; Neroni, A.; Paolini, A.; Borella, R.; Mattioli, M.; Fidanza, L.; Quong, A.; Petes, C.; Awong, G.; Douglas, S.; et al. Molecular and cellular immune features of aged patients with severe COVID-19 pneumonia. *Commun. Biol.* **2022**, *5*, 590. [[CrossRef](#)]
11. Rydzynski Moderbacher, C.; Ramirez, S.I.; Dan, J.M.; Grifoni, A.; Hastie, K.M.; Weiskopf, D.; Belanger, S.; Abbott, R.K.; Kim, C.; Choi, J.; et al. Antigen-Specific Adaptive Immunity to SARS-CoV-2 in Acute COVID-19 and Associations with Age and Disease Severity. *Cell* **2020**, *183*, 996–1012.e19. [[CrossRef](#)] [[PubMed](#)]
12. Bertoletti, A.; Tan, A.; Le Bert, N. The T-cell response to SARS-CoV-2: Kinetic and quantitative aspects and the case for their protective role. *Oxf. Open Immunol.* **2021**, *2*, iqab006. [[CrossRef](#)]
13. Bange, E.M.; Han, N.A.; Wileyto, P.; Kim, J.Y.; Gouma, S.; Robinson, J.; Greenplate, A.R.; Hwee, M.A.; Porterfield, F.; Owoyemi, O.; et al. CD8(+) T cells contribute to survival in patients with COVID-19 and hematologic cancer. *Nat. Med.* **2021**, *27*, 1280–1289. [[CrossRef](#)] [[PubMed](#)]
14. Sekine, T.; Perez-Potti, A.; Rivera-Ballesteros, O.; Stralin, K.; Gorin, J.B.; Olsson, A.; Llewellyn-Lacey, S.; Kamal, H.; Bogdanovic, G.; Muschiol, S.; et al. Robust T Cell Immunity in Convalescent Individuals with Asymptomatic or Mild COVID-19. *Cell* **2020**, *183*, 158–168.e14. [[CrossRef](#)]
15. Le Bert, N.; Clapham, H.E.; Tan, A.T.; Chia, W.N.; Tham, C.Y.L.; Lim, J.M.; Kunasegaran, K.; Tan, L.W.L.; Dutertre, C.A.; Shankar, N.; et al. Highly functional virus-specific cellular immune response in asymptomatic SARS-CoV-2 infection. *J. Exp. Med.* **2021**, *218*, e20202617. [[CrossRef](#)]
16. Reynolds, C.J.; Swadling, L.; Gibbons, J.M.; Pade, C.; Jensen, M.P.; Diniz, M.O.; Schmidt, N.M.; Butler, D.K.; Amin, O.E.; Bailey, S.N.L.; et al. Discordant neutralizing antibody and T cell responses in asymptomatic and mild SARS-CoV-2 infection. *Sci. Immunol.* **2020**, *5*, eabf3698. [[CrossRef](#)]
17. Bonifacius, A.; Tischer-Zimmermann, S.; Dragon, A.C.; Gussarow, D.; Vogel, A.; Krettek, U.; Godecke, N.; Yilmaz, M.; Kraft, A.R.M.; Hoepfer, M.M.; et al. COVID-19 immune signatures reveal stable antiviral T cell function despite declining humoral responses. *Immunity* **2021**, *54*, 340–354.e6. [[CrossRef](#)]

18. Grifoni, A.; Weiskopf, D.; Ramirez, S.I.; Mateus, J.; Dan, J.M.; Moderbacher, C.R.; Rawlings, S.A.; Sutherland, A.; Premkumar, L.; Jadi, R.S.; et al. Targets of T Cell Responses to SARS-CoV-2 Coronavirus in Humans with COVID-19 Disease and Unexposed Individuals. *Cell* **2020**, *181*, 1489–1501.e15. [[CrossRef](#)]
19. Peng, Y.; Mentzer, A.J.; Liu, G.; Yao, X.; Yin, Z.; Dong, D.; Dejnirattisai, W.; Rostron, T.; Supasa, P.; Liu, C.; et al. Broad and strong memory CD4(+) and CD8(+) T cells induced by SARS-CoV-2 in UK convalescent individuals following COVID-19. *Nat. Immunol.* **2020**, *21*, 1336–1345. [[CrossRef](#)]
20. Le Bert, N.; Tan, A.T.; Kunasegaran, K.; Tham, C.Y.L.; Hafezi, M.; Chia, A.; Chng, M.H.Y.; Lin, M.; Tan, N.; Linster, M.; et al. SARS-CoV-2-specific T cell immunity in cases of COVID-19 and SARS, and uninfected controls. *Nature* **2020**, *584*, 457–462. [[CrossRef](#)]
21. Nelde, A.; Bilich, T.; Heitmann, J.S.; Maringer, Y.; Salih, H.R.; Roerden, M.; Lubke, M.; Bauer, J.; Rieth, J.; Wacker, M.; et al. SARS-CoV-2-derived peptides define heterologous and COVID-19-induced T cell recognition. *Nat. Immunol.* **2021**, *22*, 74–85. [[CrossRef](#)] [[PubMed](#)]
22. Pera, A.; Campos, C.; Corona, A.; Sanchez-Correa, B.; Tarazona, R.; Larbi, A.; Solana, R. CMV latent infection improves CD8+ T response to SEB due to expansion of polyfunctional CD57+ cells in young individuals. *PLoS ONE* **2014**, *9*, e88538. [[CrossRef](#)] [[PubMed](#)]
23. Betts, M.R.; Nason, M.C.; West, S.M.; De Rosa, S.C.; Migueles, S.A.; Abraham, J.; Lederman, M.M.; Benito, J.M.; Goepfert, P.A.; Connors, M.; et al. HIV nonprogressors preferentially maintain highly functional HIV-specific CD8+ T cells. *Blood* **2006**, *107*, 4781–4789. [[CrossRef](#)]
24. Valverde-Villegas, J.M.; Matte, M.C.; de Medeiros, R.M.; Chies, J.A. New Insights about Treg and Th17 Cells in HIV Infection and Disease Progression. *J. Immunol. Res.* **2015**, *2015*, 647916. [[CrossRef](#)] [[PubMed](#)]
25. Zambrano-Zaragoza, J.F.; Romo-Martinez, E.J.; Duran-Avelar Mde, J.; Garcia-Magallanes, N.; Vibanco-Perez, N. Th17 cells in autoimmune and infectious diseases. *Int. J. Inflamm.* **2014**, *2014*, 651503. [[CrossRef](#)]
26. Frank, K.; Paust, S. Dynamic Natural Killer Cell and T Cell Responses to Influenza Infection. *Front. Cell. Infect. Microbiol.* **2020**, *10*, 425. [[CrossRef](#)]
27. Chen, X.; Liu, S.; Goraya, M.U.; Maarouf, M.; Huang, S.; Chen, J.L. Host Immune Response to Influenza A Virus Infection. *Front. Immunol.* **2018**, *9*, 320. [[CrossRef](#)]
28. Hornick, E.E.; Zacharias, Z.R.; Legge, K.L. Kinetics and Phenotype of the CD4 T Cell Response to Influenza Virus Infections. *Front. Immunol.* **2019**, *10*, 2351. [[CrossRef](#)]
29. Damsker, J.M.; Hansen, A.M.; Caspi, R.R. Th1 and Th17 cells: Adversaries and collaborators. *Ann. N. Y. Acad. Sci.* **2010**, *1183*, 211–221. [[CrossRef](#)]
30. Betts, M.R.; Koup, R.A. Detection of T-cell degranulation: CD107a and b. *Methods Cell Biol.* **2004**, *75*, 497–512. [[CrossRef](#)]
31. Schmidt, M.E.; Varga, S.M. The CD8 T Cell Response to Respiratory Virus Infections. *Front. Immunol.* **2018**, *9*, 678. [[CrossRef](#)] [[PubMed](#)]
32. Meckiff, B.J.; Ladell, K.; McLaren, J.E.; Ryan, G.B.; Leese, A.M.; James, E.A.; Price, D.A.; Long, H.M. Primary EBV Infection Induces an Acute Wave of Activated Antigen-Specific Cytotoxic CD4+ T Cells. *J. Immunol.* **2019**, *203*, 1276–1287. [[CrossRef](#)] [[PubMed](#)]
33. Casazza, J.P.; Betts, M.R.; Price, D.A.; Precopio, M.L.; Ruff, L.E.; Brenchley, J.M.; Hill, B.J.; Roederer, M.; Douek, D.C.; Koup, R.A. Acquisition of direct antiviral effector functions by CMV-specific CD4+ T lymphocytes with cellular maturation. *J. Exp. Med.* **2006**, *203*, 2865–2877. [[CrossRef](#)] [[PubMed](#)]
34. Nemes, E.; Bertocelli, L.; Lugli, E.; Pinti, M.; Nasi, M.; Manzini, L.; Manzini, S.; Prati, F.; Borghi, V.; Cossarizza, A.; et al. Cytotoxic granule release dominates gag-specific CD4+ T-cell response in different phases of HIV infection. *Aids* **2010**, *24*, 947–957. [[CrossRef](#)]
35. Betts, M.R.; Brenchley, J.M.; Price, D.A.; De Rosa, S.C.; Douek, D.C.; Roederer, M.; Koup, R.A. Sensitive and viable identification of antigen-specific CD8+ T cells by a flow cytometric assay for degranulation. *J. Immunol. Methods* **2003**, *281*, 65–78. [[CrossRef](#)]
36. Tan, A.T.; Linster, M.; Tan, C.W.; Le Bert, N.; Chia, W.N.; Kunasegaran, K.; Zhuang, Y.; Tham, C.Y.L.; Chia, A.; Smith, G.J.D.; et al. Early induction of functional SARS-CoV-2-specific T cells associates with rapid viral clearance and mild disease in COVID-19 patients. *Cell Rep.* **2021**, *34*, 108728. [[CrossRef](#)]
37. Moss, P. The T cell immune response against SARS-CoV-2. *Nat. Immunol.* **2022**, *23*, 186–193. [[CrossRef](#)]
38. Diao, B.; Wang, C.; Tan, Y.; Chen, X.; Liu, Y.; Ning, L.; Chen, L.; Li, M.; Liu, Y.; Wang, G.; et al. Reduction and Functional Exhaustion of T Cells in Patients With Coronavirus Disease 2019 (COVID-19). *Front. Immunol.* **2020**, *11*, 827. [[CrossRef](#)] [[PubMed](#)]
39. Snell, L.M.; Osokine, I.; Yamada, D.H.; De la Fuente, J.R.; Elsaesser, H.J.; Brooks, D.G. Overcoming CD4 Th1 Cell Fate Restrictions to Sustain Antiviral CD8 T Cells and Control Persistent Virus Infection. *Cell Rep.* **2016**, *16*, 3286–3296. [[CrossRef](#)] [[PubMed](#)]
40. Ferretti, A.P.; Kula, T.; Wang, Y.; Nguyen, D.M.V.; Weinheimer, A.; Dunlap, G.S.; Xu, Q.; Nabils, N.; Perullo, C.R.; Cristofaro, A.W.; et al. Unbiased Screens Show CD8(+) T Cells of COVID-19 Patients Recognize Shared Epitopes in SARS-CoV-2 that Largely Reside outside the Spike Protein. *Immunity* **2020**, *53*, 1095–1107.e3. [[CrossRef](#)]
41. Reuter, M.A.; Pombo, C.; Betts, M.R. Cytokine production and dysregulation in HIV pathogenesis: Lessons for development of therapeutics and vaccines. *Cytokine Growth Factor Rev.* **2012**, *23*, 181–191. [[CrossRef](#)] [[PubMed](#)]

42. Carvalho-Gomes, A.; Cubells, A.; Pallares, C.; Corpas-Burgos, F.; Berenguer, M.; Aguilera, V.; Lopez-Labrador, F.X. Cytomegalovirus specific polyfunctional T-cell responses expressing CD107a predict control of CMV infection after liver transplantation. *Cell. Immunol.* **2022**, *371*, 104455. [[CrossRef](#)] [[PubMed](#)]
43. Pan, K.; Chiu, Y.; Huang, E.; Chen, M.; Wang, J.; Lai, I.; Singh, S.; Shaw, R.M.; MacCoss, M.J.; Yee, C. Mass spectrometric identification of immunogenic SARS-CoV-2 epitopes and cognate TCRs. *Proc. Natl. Acad. Sci. USA* **2021**, *118*, e2111815118. [[CrossRef](#)] [[PubMed](#)]
44. Troyano-Hernández, P.; Reinoso, R.; Holguín, Á. Evolution of SARS-CoV-2 Envelope, Membrane, Nucleocapsid, and Spike Structural Proteins from the Beginning of the Pandemic to September 2020: A Global and Regional Approach by Epidemiological Week. *Viruses* **2021**, *13*, 243. [[CrossRef](#)] [[PubMed](#)]
45. WHO Working Group on the Clinical Characterisation and Management of COVID-19 infection. A minimal common outcome measure set for COVID-19 clinical research. *Lancet Infect. Dis.* **2020**, *20*, e192–e197. [[CrossRef](#)]
46. Cossarizza, A.; Chang, H.D.; Radbruch, A.; Abrignani, S.; Addo, R.; Akdis, M.; Andra, I.; Andreato, F.; Annunziato, F.; Arranz, E.; et al. Guidelines for the use of flow cytometry and cell sorting in immunological studies (third edition). *Eur. J. Immunol.* **2021**, *51*, 2708–3145. [[CrossRef](#)]
47. De Biasi, S.; Tartaro, D.L.; Gibellini, L.; Paolini, A.; Quong, A.; Petes, C.; Awong, G.; Douglas, S.; Lin, D.; Nieto, J.; et al. Endogenous control of inflammation characterizes pregnant women with asymptomatic or paucisymptomatic SARS-CoV-2 infection. *Nat. Commun.* **2021**, *12*, 4677. [[CrossRef](#)]
48. Roederer, M.; Nozzi, J.L.; Nason, M.C. SPICE: Exploration and analysis of post-cytometric complex multivariate datasets. *Cytometry Part A* **2011**, *79*, 167–174. [[CrossRef](#)]



OPEN ACCESS

EDITED BY

Silvia Piconese,
Sapienza University of Rome, Italy

REVIEWED BY

Antonino Cassotta,
Institute for Research in Biomedicine
(IRB), Switzerland
Kyra Zens,
University of Zurich, Switzerland

*CORRESPONDENCE

Sara De Biasi
✉ sara.debiasi@unimore.it

[†]These authors share senior authorship

SPECIALTY SECTION

This article was submitted to
T Cell Biology,
a section of the journal
Frontiers in Immunology

RECEIVED 14 December 2022

ACCEPTED 23 January 2023

PUBLISHED 09 February 2023

CITATION

Lo Tartaro D, Paolini A, Mattioli M,
Swatler J, Neroni A, Borella R,
Santacroce E, Di Nella A, Gozzi L, Busani S,
Cuccorese M, Trenti T, Meschiari M,
Guaraldi G, Girardis M, Mussini C,
Piwocka K, Gibellini L, Cossarizza A
and De Biasi S (2023) Detailed
characterization of SARS-CoV-2-specific
T and B cells after infection or
heterologous vaccination.
Front. Immunol. 14:1123724.
doi: 10.3389/fimmu.2023.1123724

COPYRIGHT

© 2023 Lo Tartaro, Paolini, Mattioli, Swatler,
Neroni, Borella, Santacroce, Di Nella, Gozzi,
Busani, Cuccorese, Trenti, Meschiari,
Guaraldi, Girardis, Mussini, Piwocka, Gibellini,
Cossarizza and De Biasi. This is an open-
access article distributed under the terms of
the [Creative Commons Attribution License
\(CC BY\)](https://creativecommons.org/licenses/by/4.0/). The use, distribution or
reproduction in other forums is permitted,
provided the original author(s) and the
copyright owner(s) are credited and that
the original publication in this journal is
cited, in accordance with accepted
academic practice. No use, distribution or
reproduction is permitted which does not
comply with these terms.

Detailed characterization of SARS-CoV-2-specific T and B cells after infection or heterologous vaccination

Domenico Lo Tartaro¹, Annamaria Paolini¹, Marco Mattioli¹, Julian Swatler^{1,2}, Anita Neroni¹, Rebecca Borella¹, Elena Santacroce¹, Alessia Di Nella¹, Licia Gozzi³, Stefano Busani^{4,5}, Michela Cuccorese⁶, Tommaso Trenti⁶, Marianna Meschiari³, Giovanni Guaraldi^{3,4}, Massimo Girardis^{4,5}, Cristina Mussini^{3,4}, Katarzyna Piwocka², Lara Gibellini¹, Andrea Cossarizza^{1,7†} and Sara De Biasi^{1*†}

¹Department of Medical and Surgical Sciences for Children and Adults, University of Modena and Reggio Emilia School of Medicine, Modena, Italy, ²Laboratory of Cytometry, Nencki Institute of Experimental Biology, Warsaw, Poland, ³Infectious Diseases Clinics, Azienda Ospedaliero-Universitaria (AOU) Policlinico di Modena, Modena, Italy, ⁴Department of Surgery, Medicine, Dentistry and Morphological Sciences, University of Modena and Reggio Emilia, Modena, Italy, ⁵Department of Anesthesia and Intensive Care, Azienda Ospedaliero-Universitaria (AOU) Policlinico and University of Modena and Reggio Emilia, Modena, Italy, ⁶Department of Laboratory Medicine and Pathology, Diagnostic Hematology and Clinical Genomics, Azienda Unità Sanitaria Locale AUSL/AOU Policlinico, Modena, Italy, ⁷National Institute for Cardiovascular Research, Bologna, Italy

The formation of a robust long-term antigen (Ag)-specific memory, both humoral and cell-mediated, is created following severe acute respiratory syndrome coronavirus 2 (SARS-CoV-2) infection or vaccination. Here, by using polychromatic flow cytometry and complex data analyses, we deeply investigated the magnitude, phenotype, and functionality of SARS-CoV-2-specific immune memory in two groups of healthy subjects after heterologous vaccination compared to a group of subjects who recovered from SARS-CoV-2 infection. We find that coronavirus disease 2019 (COVID-19) recovered patients show different long-term immunological profiles compared to those of donors who had been vaccinated with three doses. Vaccinated individuals display a skewed T helper (Th)1 Ag-specific T cell polarization and a higher percentage of Ag-specific and activated memory B cells expressing immunoglobulin (Ig)G compared to those of patients who recovered from severe COVID-19. Different polyfunctional properties characterize the two groups: recovered individuals show higher percentages of CD4⁺ T cells producing one or two cytokines simultaneously, while the vaccinated are distinguished by highly polyfunctional populations able to release four molecules, namely, CD107a, interferon (IFN)- γ , tumor necrosis factor (TNF), and interleukin (IL)-2. These data suggest that functional and phenotypic properties of SARS-CoV-2 adaptive immunity differ in recovered COVID-19 individuals and vaccinated ones.

KEYWORDS

SARS-CoV-2, antigen-specific response, polyfunctionality, T cells, B cells, cytokine

Introduction

Memory is the main characteristic of the immune system, being at the basis of its efficacy and functionality, and indeed the activation of secondary response is the crucial strategy utilized by vaccination. Natural infection and vaccines induce the formation and subsequent expansion of antigen (Ag)-specific cells that can block pathogens as soon as they try to invade the host. The creation of a pool of long-living memory T and B cells able to respond to future *stimuli* is crucial for vaccine efficacy, as well as the plasma level of antibodies (1).

During natural infection, typically after a couple of weeks, the magnitude of the severe acute respiratory syndrome coronavirus 2 (SARS-CoV-2)-specific CD4⁺ and CD8⁺ memory T-cell response peaks at the maximum and is of the order of 0.5% and 0.2% of the repertoire, respectively (2). CD4⁺ T cells display a memory profile (including a specific subset formed by stem cell memory) and are able to produce high levels of both IL-2 and T helper (Th)1 cytokines (3–5). CD4⁺ T-cell response is greater than the CD8⁺ counterpart (2). Robust immunity is certainly maintained by more than 6 months, but the duration of SARS-CoV-2-specific T cells could depend also on the clinical severity of the initial infection (6). Long-lived T-cell responses and efficient response to SARS-CoV-2 are characterized by a CD45RA⁺ effector-memory phenotype and a potent activation of the interferon (IFN) transcriptomic signature whose magnitude is largely due to the genetic background of the host (7–10).

Regarding B-cell response, which is highly altered during coronavirus disease 2019 (COVID-19) (11), in the plasma of most individuals, anti-SARS-CoV-2 antibodies (Abs) persist for more than 6 months after primary infection, but some patients rapidly lose their specific Abs (6, 12, 13). However, specific memory B cells (MBCs) predominantly express immunoglobulin (Ig)M⁺ or IgG1⁺ and rise until 150 days after infection (14), regardless of age (15). Receptor-binding domain (RBD)-specific IgG⁺ MBCs are predominantly CD27⁺, and their number significantly correlates with circulating follicular helper T-cell numbers (14).

Vaccination against SARS-CoV-2 induces a robust specific immune response. CD8⁺ T-cell response can be detected as early as 11 days after the first vaccination (16), and such cells can recognize immunodominant peptides from ORF1ab (17). Two-dose vaccination with BNT162b2 leads to strong generation of virus-specific CD4⁺ T-cell responses with a Th1 profile, and it is detectable 6 months after vaccination (18–21). Spike-specific antibodies peak after 7 days, and titers and *Angiotensin-converting enzyme 2* (ACE2)/RBD binding-inhibiting activity is still observed after 6 months, despite a progressive decline over time. Concomitant to antibody reduction, spike-specific MBCs, mostly switched to IgG, increase and persist 6 months after vaccination (22). T-cell responses after vaccination are of similar magnitude to those seen after natural infection, although they seem to be more differentiated with the presence of T stem cell memory (T_{SCM}) subsets (23). An adenovirus-based vaccine generates a higher magnitude of spike-specific T cells (24, 25), while mRNA vaccines develop higher antibody titers. For this reason, heterologous vaccines have been used in clinical practice (26, 27).

As vaccination and natural infection increase across the world, there is growing interest in predicting the risk of primary infection or reinfection. Observational and limited comparison between natural and vaccine-induced immunity showed that the protection against SARS-CoV-2 infection was significantly higher in COVID-19 recovered individuals if compared to that of those vaccinated who additionally

received a booster vaccine (28). Antibodies decline more rapidly following vaccination in naive individuals than those in individuals who have recovered from COVID-19, but they display the same frequencies of spike-specific B and CD4⁺ T cells at 8 months after vaccination (29). However, besides the magnitude of the spike-specific antibody response or neutralizing titer, the percentage, phenotypic identity, and functional profile of specific cellular immune responses have not been taken into account as immune correlates of protection.

Here, by using high-parameter polychromatic flow cytometry and sophisticated data analyses, we deeply investigated the magnitude, phenotype, and functionality of SARS-CoV-2-specific immune memory in two groups of healthy subjects after heterologous vaccination compared to those of a group of subjects who recovered from SARS-CoV-2 infection.

Results

Study design

Three groups of donors were enrolled in this study. The first one was composed of nine COVID-19 recovered patients (hereafter called REC; mean age of 35.1 ± 11.1 years), with a mean of 131.1 days (range 64–165 days) from last infection during follow-up visits at the Infectious Diseases Clinics of the Azienda Ospedaliero-Universitaria Policlinico di Modena. All REC had symptoms consistent with COVID-19 and positive PCR-based testing for SARS-CoV-2 over the period of March 2020–August 2020. Within this group, four patients were classified as severe (35.3 ± 5.68 years) while five patients were moderate (35.0 ± 7.4) according to World Health Organization guidelines (30). Given that there were no differences between moderate and severe recovered individuals and their low number, they were considered as a unique group for the statistical analysis. Twenty-three vaccinated donors were enrolled in this study, and they were divided into two groups: one was composed of 11 donors with a mean of 31.1 days (range 30–35 days) after the third dose of SARS-CoV-2 vaccine (hereafter defined MIX; 27.0 ± 4.5 years); these subjects were vaccinated with three different vaccines (first dose: ChAdOx1; second dose: BNT162b2; third dose: mRNA-1273). The second group was composed of 12 donors with a mean of 33.9 days (range 26–44 days, hereafter defined RNA; 35.3 ± 11.3 years) after being vaccinated with two different RNA vaccines (first and second doses: BNT162b2; third dose: mRNA-1273). Each participant, including healthy donors, provided informed consent according to the Helsinki Declaration, and all uses of human material have been approved by the local Ethics Committee (Comitato Etico dell'Area Vasta Emilia Nord, protocol number 177/2020, 11 March 2020) and by the University Hospital Committee (Direzione Sanitaria dell'Azienda Ospedaliero Universitaria di Modena, protocol number 7531, 11 March 2020). The clinical characteristics of all participants are reported in Table 1 and in the *Methods* section.

MIX showed a skewed Th1 Ag-specific CD4⁺ T-cell polarization compared to that of recovered ones

To investigate the percentage of Ag-specific T cells, we used T-cell receptor (TCR)-dependent activation-induced marker (AIM) assays to identify and quantify SARS-CoV-2-specific CD4⁺ T cells (31–34). We

TABLE 1 Demographic and clinical characteristics of COVID-19 recovered patients and vaccinated donors.

Variable	REC (n=9)	MIX (n=11)	RNA (n=12)	p-value (RECvsMIX)	p-value (RECvsRNA)	p-value (MIXvsRNA)
Demographic characteristics						
Age (mean years, range) ¹	35.1 (22.0-41.0)	27.0 (22.0-39.0)	35.3 (23.0-62.0)	0.0177	ns	ns
Sex (Male, %) ²	88.9	27.3	45.5	0.0098	ns	ns
Race/Ethnicity						
White: Non-Hispanic or Latino (%) ³	66.7	100	100	ns	ns	ns
White: Hispanic or Latino (%) ³	11.1	0	0	/	/	/
Black (%) ³	22.2	0	0	/	/	/
Hospitalization status						
Never hospitalized (%)	11.1	/	/	/	/	/
Hospitalized (%)	88.9	/	/	/	/	/
Days of hospitalization (mean days, range)	11.6 (4.0-17.0)	/	/	/	/	/
Sample Collection						
Sample Collection Dates	March 2020-August 2020	December 2021-January 2022	December 2021-January 2022	/	/	/
Days post symptom onset or third dose vaccine (mean days, range) ¹	131.1 (64.0-165.0)	31.8 (30.0-35.0)	33.9 (26.0-44.0)	0.0004	0.0009	ns
Disease Severity						
Moderate (%)	55.6% (5/9)	/	/	/	/	/
Severe (%)	44.4% (4/9)	/	/	/	/	/
Vaccine type						
First dose	/	ChAdOx1	BNT162b2	/	/	/
Second dose	/	BNT162b2	BNT162b2	/	/	/
Third dose	/	mRNA-1273	mRNA-1273	/	/	/
Detection of SARS-CoV-2 IgG						
IgG, Index mean value AU/mL (± SD) ¹	1,344.2 (±663.4)	12,205.4 (±9,457.4)	6,422.1 (±2,496.1)	0.0001	0.0011	ns

¹Kruskal-Wallis test with Original FDR methods of Benjamini and Hochberg;

²Fisher's exact test;

³Chi-squared test;

ns, not significant; SD, standard deviation; AU, arbitrary unit.

stimulated peripheral blood mononuclear cells (PBMCs) from nine REC patients and 11 MIX and 12 RNA donors overnight with 15-mer peptides with 11-amino acid overlap, covering the complete sequence of Wuhan SARS-CoV-2 spike glycoprotein (see *Methods* for details).

The phenotype of Ag-specific T cells (i.e., those CD137⁺CD69⁺) within CD4⁺ T cells, hereafter termed Ag⁺CD4⁺ T cells, was first analyzed by manual gating and compared with the non-Ag-specific CD4⁺ T cell counterparts (CD137⁻CD69⁻, hereafter called Ag⁻CD4⁺). Ag⁺CD4⁺ T cells showed different cell subset distributions (in terms of the expression of differentiation markers such as CD45RA, CCR7, CD28, and CD95) and Th cell polarization (evaluated by the expression of CCR6 and CXCR3). Ag⁺CD4⁺ T displayed a low percentage of naive (N, CD45RA⁺CCR7⁺CD28⁺CD95⁻) and higher frequencies of memory compartment such as central memory (CM; CD45RA⁻CCR7⁺CD28⁺CD95⁺), transitional memory (TM; CD45RA⁻CCR7⁻CD

28⁺CD95⁺), effector memory (EM; CD45RA⁻CCR7⁻CD28⁻CD95⁺), and T_{SCM} (CD45RA⁺CCR7⁺CD28⁺CD95⁺) and a similar percentage of terminally differentiated effector memory (EMRA; CD45RA⁺CCR7⁻CD28⁻CD95⁺) (Supplementary Figures S1A, B). Considering T-cell polarization, in comparison with Ag⁻CD4⁺ T cells, those Ag-specific displayed a higher percentage of Th1 (CXCR3⁺CCR6⁻), Th17 (CXCR3⁻CCR6⁺), and Th1/Th17 (CXCR3⁺CCR6⁺) and a lower percentage of Th0/Th2 (CXCR3⁻CCR6⁻) (Supplementary Figure S1C).

To gain a more detailed overview on the differentiation status and Th-polarization, we took advantage of unsupervised FlowSOM clustering. This analysis revealed a total of 19 clusters, and within these, six clusters represented SARS-CoV-2-reactive CD4⁺ T cells expressing CD69 and CD137 (Figures 1A, B; Supplementary Figure S2).

The frequencies of the different clusters of T cells within Ag⁻CD4⁺ T cells were similar in the three groups of individuals as

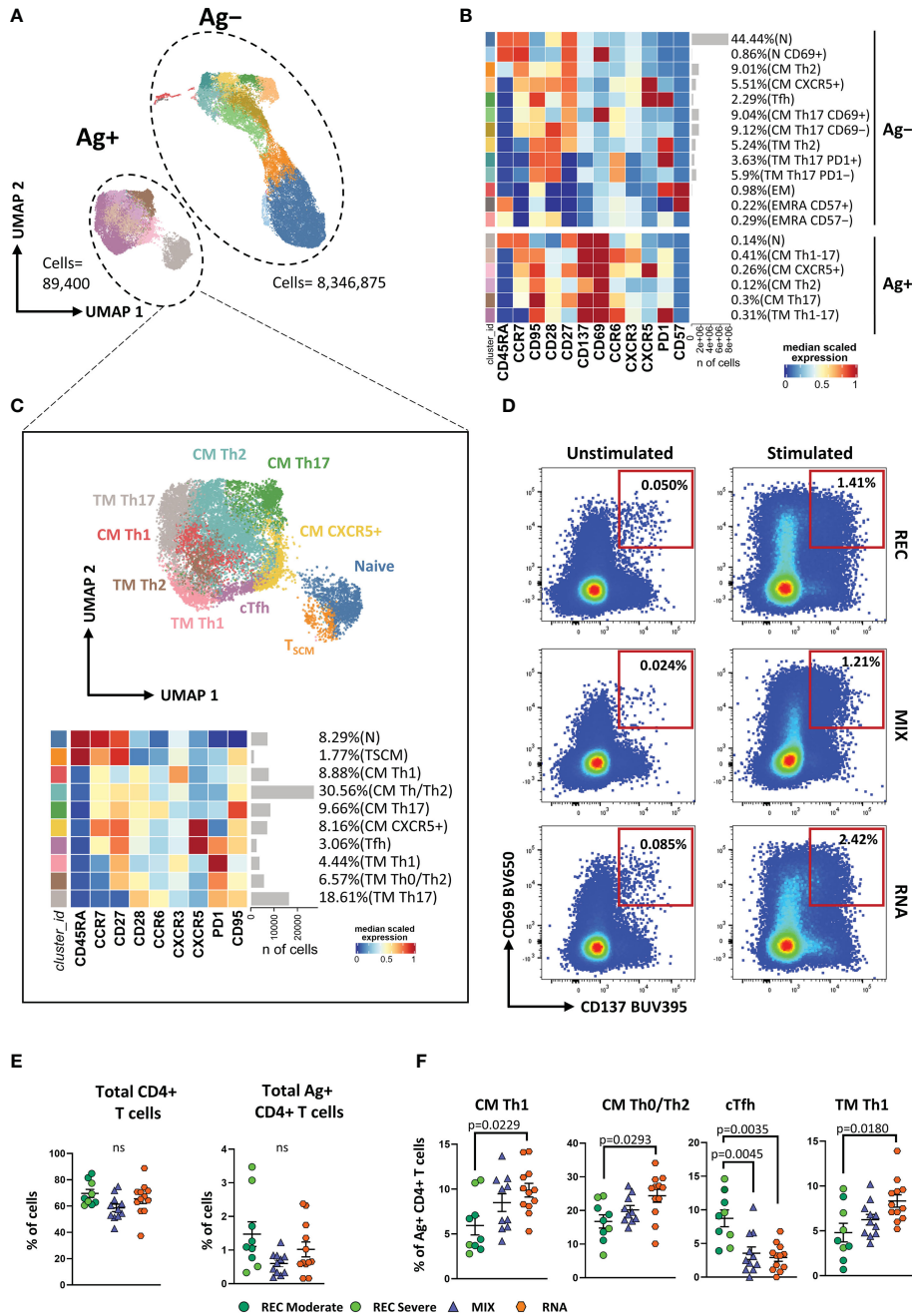


FIGURE 1

Immune phenotyping of antigen-specific CD4⁺ T cells. (A) Uniform Manifold Approximation and Projection (UMAP) plot shows the 2D spatial distribution of 8,436,275 cells from nine donors who recovered from SARS-CoV-2 infection (REC, severe = 4 and moderate = 5) and 23 vaccinated donors (MIX = 11 and RNA = 12) embedded with FlowSOM clusters. Ag⁺, antigen-specific CD4⁺ T cells; Ag⁻, non-antigen-specific CD4⁺ T cells. (B) Heatmap of the median marker intensities of the 12 lineage markers across the 19 cell populations obtained with FlowSOM algorithm after the manual metacluster merging. The colors of cluster_id column correspond to the colors used to label the UMAP plot clusters. The color in the heatmap is referred to the median of the *arcsinh* marker expression (0–1 scaled) calculated over cells from all of the samples. Blue represents lower expression, while red represents higher expression. Light gray bar along the rows (clusters) and values in brackets indicate the relative sizes of the clusters. N, naive; T_{SCM}, T stem cell memory; CM, central memory; TM, transitional memory; EM, effector memory; EMRA, effector memory reexpressing the CD45RA; cTfh, circulating T follicular helper cells. The black bar on the right is used to group Ag⁺ or Ag⁻ subpopulations. (C) UMAP and heatmap visualization of 10 manually merged antigen-specific CD4⁺ T-cell clusters. (D) Representative dot plots showing manual gating analysis of Ag-specific (CD137⁺CD69⁺) CD4⁺ T cells after overnight stimulation with spike protein compared to unstimulated control [activation-induced marker assay (AIM assay)]. Numbers in the dot plots indicate the percentage of cells identified by manual gating. (E) Dot plots show the total percentage of antigen-specific CD4⁺ T cells. Kruskal–Wallis test with Benjamini–Hochberg correction for multiple comparisons was used to test the differences among the three groups. (F) Dot plots show the cell percentage of the antigen-specific CD4⁺ T cells. The central bar represents the mean ± SEM. Generalized linear mixed model (GLMM) test was used for the statistical analysis. Adjusted P-values are reported in the figure. ns, not significant.

shown in [Supplementary Figure S3](#). We focused our attention on Ag^+CD4^+ T cells that were selected and reclustered. We obtained 10 clusters, representing different subpopulations of Ag^+ T cells. We found naive T cells that were defined as $CD45RA^+CCR7^+CD27^+CD95^-$, T_{SCM} as $CD45RA^+CCR7^+CD27^+CD95^+$, CM Th1 as $CCR7^+CD45RA^-CCR6^-CXCR3^+$ (CM Th1), CM Th0/Th2 as $CCR7^+CD45RA^-CCR6^-CXCR3^-$, CM Th17 as $CCR7^+CD45RA^-CCR6^+CXCR3^-$, CM CXCR5⁺ as $CCR7^+CD45RA^-CXCR5^+PD-1^-$, circulating T follicular helper as $CCR7^+CD45RA^-CXCR5^+PD-1^+$ (cTfh), TM Th1 as $CCR7^-CD45RA^-CD28^+CXCR3^+$ (TM Th1), TM Th0/Th2 as $CCR7^-CD45RA^-CD28^+CCR6^-CXCR3^-$, and TM Th17 as $CCR7^-CD45RA^-CD28^+CCR6^+CXCR3^-$ ([Figure 1C](#)).

The percentage of total $CD4^+$ and Ag^+CD4^+ T cells was similar among the three groups ([Figures 1D, E](#)). Despite that, within the latter, we observed a different distribution of the populations among REC and vaccinated groups (both MIX and RNA). RNA displayed higher percentages of CM Th1, CM Th0/Th2, and TM Th1 if compared to those in REC subjects. Moreover, both MIX and RNA showed a lower percentage of cTfh cells ([Figure 1F](#)). No differences were found between Ag^+CD4^+ T-cell clusters of MIX and RNA. Similar percentages of all other clusters were present in REC, MIX, and RNA subjects ([Supplementary Figure S4](#)).

Vaccinated individuals showed a higher percentage of Tc1-like Ag-specific $CD8^+$ T cells compared to that of recovered subjects

The AIM assay was used for $CD8^+$ T-cell analysis to identify and quantify SARS-CoV-2-specific (see *Methods*). We first manually gated different subpopulations of T cells on the basis of differentiation markers and cytotoxic-polarization markers (Tc-polarization). We observed that Ag^+CD8^+ T cells, if compared to Ag^-CD8^+ T lymphocytes, displayed lower percentages of N and higher percentages of T_{SCM} , CM, and TM; similar percentages of both EM and EMRA were found ([Supplementary Figures S5A, B](#)). In terms of Tc-polarization, similar percentages of Tc1 cells were found within Ag^+ and Ag^-CD8^+ T cells. However, Ag^+CD8^+ T cells were characterized by higher percentages of both Tc17 and Tc1/Tc17 and lower percentages of Tc0/Tc2 ([Supplementary Figure S5C](#)).

As for $CD4^+$ T-cell analysis, we applied unsupervised analysis and found 21 clusters, of which six were SARS-CoV-2-reactive $CD8^+$ T cells ([Figures 2A, B](#); [Supplementary Figure S6A](#)). Considering Ag^-CD8^+ T cells, both MIX and RNA showed increased levels of TM Tc17 $CD69^+$, TM Tc0/Tc2, and TM Th0/Th2 $PD1^+CXCR5^+$ if compared to those of REC subjects. Furthermore, RNA showed a higher percentage of TM Tc1 $PD1^+CXCR5^+$ compared to those of REC and MIX ([Supplementary Figure S7](#)). Ag^+CD8^+ T cells were selected and after reclustering, 11 clusters were identified. Besides naive T cells and T_{SCM} , defined as $CD45RA^+CCR7^+CD27^+CD28^+CD95^-$ and $CD45RA^+CCR7^+CD27^+CD28^+CD95^+$, respectively, we found two clusters of CM T cells defined as follows: CM Tc1 $PD-1^-$ that were $CD45RA^-CCR7^+CD28^+CXCR3^+PD-1^-$ and CM Tc1 $PD-1^+$ that were $CD45RA^-CCR7^+CD28^+CXCR3^+PD-1^+$.

Among effector Ag^+CD8^+ T cells, we found five clusters defined as TM Tc1 $PD-1^-$ ($CCR7^-CD45RA^-CD28^+CXCR3^+PD-1^-$), TM Tc1 $PD-1^+$ ($CCR7^-CD45RA^-CD28^+CXCR3^+PD-1^+$), TM Tc0/Tc2

($CCR7^-CD45RA^-CD28^+CCR6^-CXCR3^-$), TM Tc17 ($CCR7^-CD45RA^-CD28^+CCR6^+CXCR3^-$), and EM Tc1 $CD57^+PD-1^+$ ($CCR7^-CD45RA^-CD28^+CD57^+PD-1^+$). Moreover, three populations of effector memory cells reexpressing $CD45RA$ (EMRA) were detected, i.e., EMRA Tc1 $CD57^-PD-1^+$ ($CCR7^-CD45RA^+CXCR3^+CD57^-PD-1^+$), EMRA Tc1 $CD57^+PD-1^+$ ($CCR7^-CD45RA^+CXCR3^+CD57^+PD-1^+$), and EMRA Tc1 $CD57^+PD-1^-$ ($CCR7^-CD45RA^+CXCR3^+CD57^+PD-1^-$) ([Figure 2C](#)).

Similar percentages of total $CD8^+$ and Ag^+CD8^+ T cells were found among the three groups ([Figures 2D, E](#)). However, within the Ag^+ population, we observed increased percentages of EM Tc1 $CD57^+PD-1^+$ in both vaccinated groups if compared to that in the recovered ones ([Figure 2F](#)). Furthermore, MIX and RNA showed increased levels of EMRA Tc1 $CD57^+PD-1^+$ terminal effector $CD8^+$ T cells compared to that in REC. Finally, we observed that the percentage of EMRA Tc1 $CD57^+PD-1^-$ terminal effector $CD8^+$ T cells was higher in MIX compared to those of both REC and RNA ([Figure 2E](#)). Similar percentages of all other subpopulations were found among REC, MIX, and RNA ([Supplementary Figure S8](#)).

Patients who recovered from COVID-19 display more polyfunctional antigen-specific $CD4^+$ T cells compared to those in vaccinated donors

Besides Th-polarization, the functional properties of Ag^+ -specific T cells were investigated by measuring the percentages of cells producing IFN- γ , tumor necrosis factor (TNF), interleukin (IL)-2, IL-17, and granzyme B (GZMB), along with the expression of the degranulation marker CD107a. The percentages of cells producing cytokines were assessed following 16 h of *in vitro* stimulation with SARS-CoV-2 peptide pool covering the complete sequence of Wuhan SARS-CoV-2 spike glycoprotein. The gating strategy is reported in [Supplementary Figure S9](#).

REC displayed a higher percentage of $CD4^+$ T cells producing TNF, IL-2, and IL-17 than that in the MIX group, but not with respect to that of the RNA group. Furthermore, a higher percentage of $CD4^+$ T cells producing IL-2 and TNF was observed in RNA compared to that in MIX subjects. Similar percentages of IFN- γ , CD107a, and GZMB were found among the three groups ([Figure 3A, B](#)).

Polyfunctional properties were investigated in $CD4^+$ and $CD8^+$ T cells by analyzing the simultaneous production of TNF, CD107a, IFN- γ , IL-2, and IL-17 using the bioinformatic Simplified Presentation of Incredibly Complex Evaluation (SPICE) tool. Among $CD4^+$ T cells, REC exhibited a different polyfunctionality profile from those who had been vaccinated ([Figure 3C](#)). In particular, REC displayed a higher percentage of $CD4^+$ T cells simultaneously producing IL-2 and TNF compared to those in MIX and RNA. The percentage of $CD4^+$ T cells producing TNF or IL-17 was higher in REC compared to those in both vaccinated groups. Moreover, RNA exhibited higher percentages of $CD4^+$ T cells simultaneously producing IL-2 and TNF or IL-2 alone compared to those in MIX. Furthermore, we found that both vaccinated groups displayed higher percentages of cells defined as “highly polyfunctional” as simultaneously producing CD107a, IFN- γ , IL-2, and TNF compared to those in REC ([Figure 3D](#)). The functional properties of $CD8^+$ T were similar between the three groups ([Supplementary Figure S10](#)).

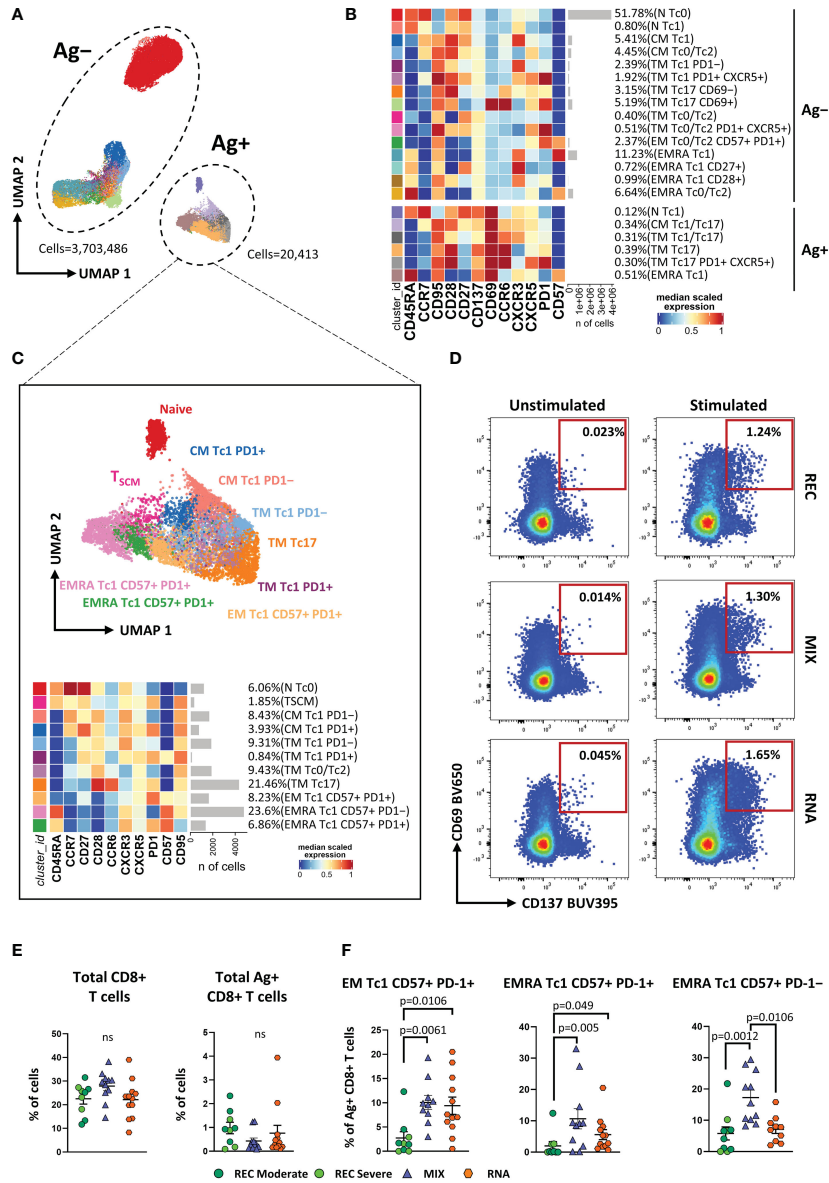


FIGURE 2
 Immune phenotyping of antigen-specific CD8⁺ T cells. **(A)** UMAP plot shows the 2D spatial distribution of 3,723,899 cells from nine donors who recovered from SARS-CoV-2 infection (REC, severe = 4 and moderate = 5) and 23 vaccinated donors (MIX = 11 and RNA = 12) embedded with FlowSOM clusters. Ag⁺, antigen-specific CD8⁺ T cells; Ag⁻, non-antigen-specific CD8⁺ T cells. **(B)** Heatmap of the median marker intensities of the 12 lineage markers across the 21 cell populations obtained with FlowSOM algorithm after the manual metacluster merging. The colors of cluster_id column correspond to the colors used to label the UMAP plot clusters. The color in the heatmap is referred to the median of the *arcsinh* marker expression (0–1 scaled) calculated over cells from all of the samples. Blue represents lower expression, while red represents higher expression. Light gray bar along the rows (clusters) and values in brackets indicate the relative sizes of the clusters. N, naive; CM, central memory; TM, transitional memory; EM, effector memory; EMRA, effector memory reexpressing the CD45RA. The black bar on the right is used to group Ag⁺ or Ag⁻ subpopulations. **(C)** Uniform Manifold Approximation and Projection UMAP and heatmap visualization of 11 manually merged antigen-specific CD8⁺ T cell clusters. **(D)** Representative dot plots showing manual gating analysis of Ag-specific (CD137⁺CD69⁺) CD8⁺ T cells after overnight stimulation with spike protein compared to unstimulated control (activation-induced marker assay (AIM assay)). Numbers in the dot plots indicate the percentage of cells identified by manual gating. **(E)** Dot plots show the total percentage of antigen-specific CD8⁺ T cells. Kruskal–Wallis test with Benjamini–Hochberg correction for multiple comparisons was used to test the differences among the three groups. **(F)** Dot plots show the relative cell percentage of the antigen-specific CD8⁺ T-cell clusters of nine donors who recovered from SARS-CoV-2 infection (REC, severe = 4 and moderate = 5) and 23 vaccinated donors (MIX = 11 and RNA = 12). The central bar represents the mean ± SEM. Generalized linear mixed model GLMM test was used for the statistical analysis. Adjusted P-values are reported in the figure. ns, not significant.

Vaccinated donors showed a higher percentage of antigen-specific and activated memory B cells expressing IgG compared to that in REC

SARS-CoV-2 antibodies decline already as early as 21 days after infection or vaccination (6). However, long-lived MBCs constitute a

lasting long-term memory and provide a rapid recall response differentiating into high-affinity matured plasma cells (35). For this reason, we measured the frequencies of circulating SARS-CoV-2 spike-specific B cells (Ag⁺ B cells) (see *Methods*).

Similar percentages of total B cells were found among the three groups (Figure 4A). However, both MIX and RNA showed a higher percentage of Ag⁺ B cells (defined as CD45⁺CD19⁺decoy⁻Spike-

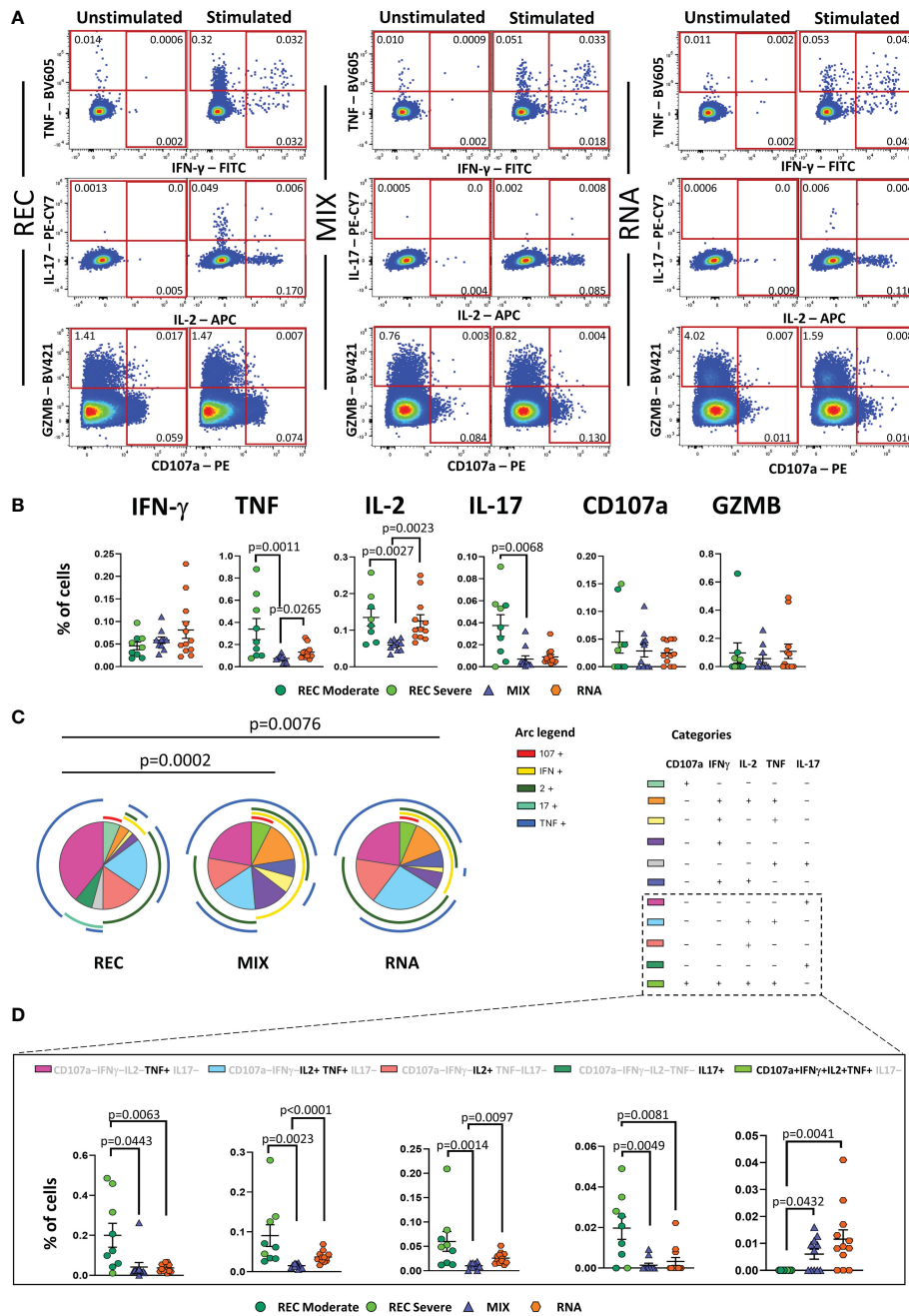


FIGURE 3

Cytokine production and polyfunctionality of antigen-specific CD4⁺ T cells. **(A)** Representative dot plots showing manual gating analysis of intracellular cytokine production of CD4⁺ T lymphocytes after overnight stimulation with spike protein compared to unstimulated control. Numbers in the dot plots indicate the percentage of cells identified by the gates. **(B)** Comparison between the total production of IFN-γ, TNF, IL-17, IL-2, CD107a, and GZMB by CD4⁺ T cells after *in vitro* stimulation with 15-mer peptides, covering the complete sequence of Wuhan SARS-CoV-2 spike glycoprotein. Data represent individual values from nine healthy subjects who recovered from SARS-CoV-2 infection (REC, severe = 4 and moderate = 5) and 23 vaccinated donors (MIX = 11 and RNA = 12). Mean (center bar) ± SEM (upper and lower bars). Kruskal–Wallis test with Benjamini–Hochberg correction for multiple comparisons was used to test the differences among the three groups. **(C)** Pie charts representing the proportion of responding CD4⁺ T cells producing different combinations of CD107a, IL-2, IL-17, IFN-γ, and TNF after *in vitro* stimulation with 15-mer peptides, covering the complete sequence of Wuhan SARS-CoV-2 spike glycoprotein. Frequencies were corrected by background subtraction as determined in non-stimulated controls using SPICE software. Pie arches represent the total production of different cytokines. **(D)** Percentage of polyfunctional population within CD4⁺ T cells. Kruskal–Wallis test with Benjamini–Hochberg correction for multiple comparisons was used to test the differences among the three groups. Adjusted P-values are indicated in the figure.

BUV661⁺Spike-BV650⁺) when compared to that in REC (Figure 4B).

By applying manual gating, we observed that Ag⁺ B cells compared to its Ag⁻ counterpart displayed a lower percentage of naive B cells and an increased percentage of memory switched,

memory unswitched and of CD27⁻IgD⁻ B cells (Supplementary Figure S11A). Moreover, after vaccination or SARS-CoV-2 infection, ~42%–96% of Ag⁺ B cells were IgG⁺. This percentage decreased to ~5%–22% in the Ag⁻ B cells, where ~69%–90% of cells were IgD⁺IgM⁺ (Supplementary Figure S11B). Furthermore, the

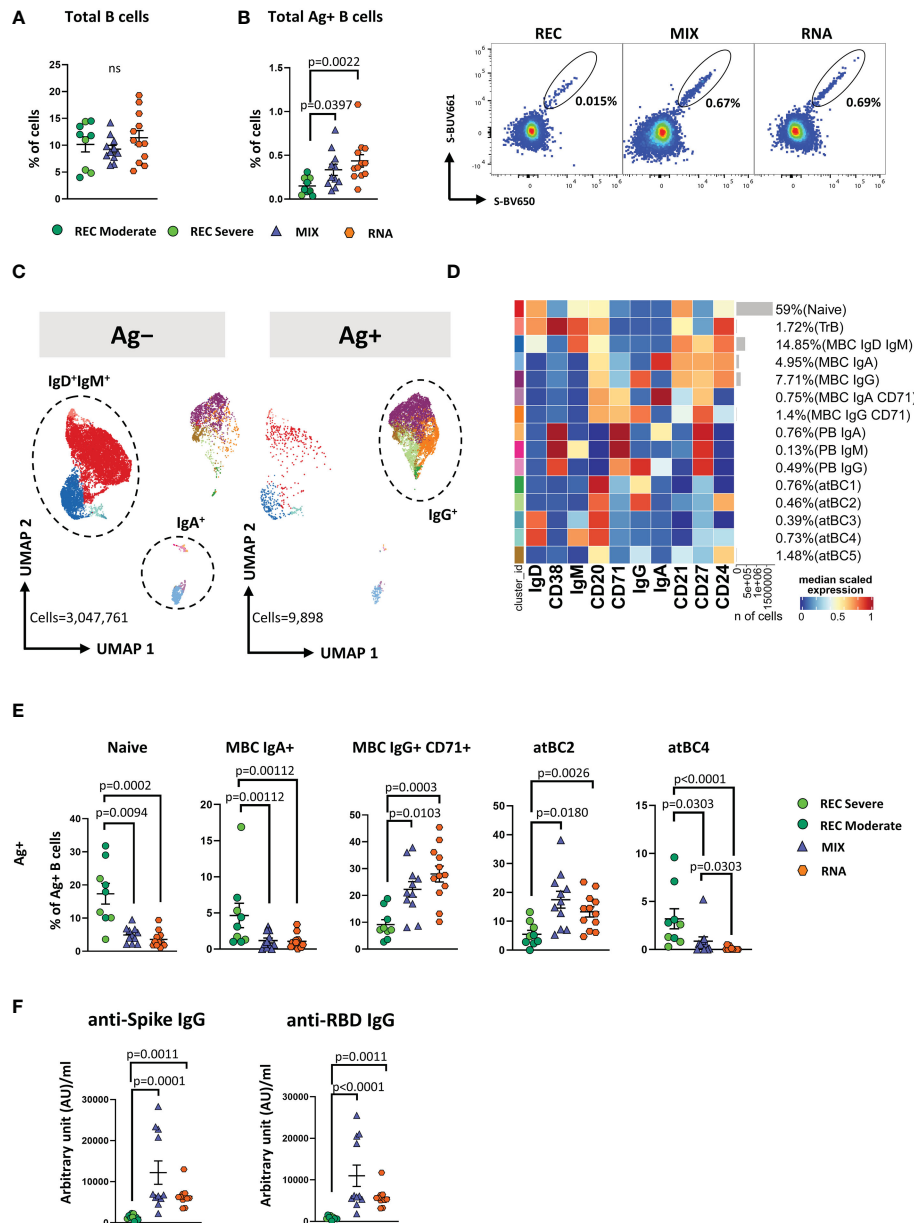


FIGURE 4

Immune phenotyping of antigen-specific $CD19^+$ B cells. (A) Dot plots show the total percentage of $CD19^+$ B cells. Kruskal–Wallis test with Benjamini–Hochberg correction for multiple comparisons was used to test the differences among the three groups. (B) Dot plots show the total percentage of antigen-specific $CD19^+$ B cells (left); representative dot plots showing manual gating analysis of Ag^+ B cells from REC, MIX, and RNA. Numbers in the dot plots indicate the percentage of cells identified by the gates (right). Kruskal–Wallis test with Benjamini–Hochberg correction for multiple comparisons was used to test the differences among the three groups. (C) UMAP plot shows the 2D spatial distribution of 3,057,659 cells from nine donors who recovered from SARS-CoV-2 infection (REC, severe = 4 and moderate = 5) and 23 vaccinated donors (MIX = 11 and RNA = 12) embedded with FlowSOM clusters. Ag^+ , antigen-specific $CD19^+$ B cells; Ag^- , non-antigen-specific $CD19^+$ B cells. (D) Heatmap of the median marker intensities of the 10 lineage markers across the 15 cell populations obtained with FlowSOM algorithm after the manual metacluster merging. The colors of cluster_id column correspond to the colors used to label the UMAP plot clusters. The color in the heatmap is referred to the median of the *arcsinh* marker expression (0–1 scaled) calculated over cells from all of the samples. Blue represents lower expression, while red represents higher expression. Light gray bar along the rows (clusters) and values in brackets indicate the relative sizes of the clusters. N, naive; TrB, transitional B cells; MBC, memory B cell; atBC, atypical B cell. (E) Dot plots show the percentage of 15 Ag^+ B cell clusters among nine donors who recovered from SARS-CoV-2 infection (REC, severe = 4 and moderate = 5) and 23 vaccinated donors (MIX = 11 and RNA = 12). The central bar represents the mean \pm SEM. GLMM test was used for the statistical analysis. Adjusted P-values are reported in the figure. (F) Anti-spike and anti-RBD IgG concentrations in plasma samples from REC, MIX, and RNA individuals. Kruskal–Wallis test with Benjamini–Hochberg correction for multiple comparisons was used to test the differences among the three groups. Adjusted P-values are indicated in the figure.

percentage of IgA^+ B cells was higher in the Ag^- compartment (Supplementary Figure S11B).

To deeply characterize both Ag^- and Ag^+ B cells, we took advantage of unsupervised clustering. The analysis revealed 15 clusters, spanning

from naive to atypical B cells (atBCs; $CD21^-CD27^-CD38^-$) (36) (Figures 4C, D; Supplementary Figure S12A).

Besides naive and transitional B cells (TrB), respectively defined as naive: $CD20^+CD21^+CD24^+CD38^-IgD^+IgM^+$ and TrB: $CD20^+CD21^+$

CD24⁺CD38⁺IgD⁺IgM⁺, we found five clusters of MBCs defined as follows: MBC IgD⁺ IgM⁺ (CD20⁺CD21⁺CD24⁺CD27⁺IgD⁺IgM⁺), MBC IgA⁺ (CD20⁺CD21⁺CD24⁺CD27⁺IgA⁺), MBC IgG⁺ (CD20⁺CD21⁺CD24⁺CD27⁺IgG⁺), MBC IgA⁺ CD71⁺ (CD20⁺CD21⁺CD24⁺CD27⁺IgA⁺CD71⁺), and MBC IgG⁺ CD71⁺ (CD20⁺CD21⁺CD24⁺CD27⁺IgG⁺CD71⁺). Among plasmablasts (PBs), we found the following three clusters: PB IgA⁺ as CD27⁺CD71⁺CD38⁺⁺IgA⁺, PB IgM⁺ as CD27⁺CD71⁺CD38⁺⁺IgM⁺, and PB IgG⁺ as CD27⁺CD71⁺CD38⁺⁺IgG⁺. Together with naive, TrBs, MBCs, and PBs, we identified five clusters of atBCs, i.e., atBC1 as CD21⁻CD27⁻CD20⁺IgG⁺, atBC2 as CD21⁻CD27⁻CD24⁺CD20⁺IgG⁺, atBC3 as CD21⁻CD27⁻CD20⁺IgD⁺, atBC4 as CD21⁻CD27⁻CD20⁺IgD⁺IgM⁺, and atBC5 as CD21⁻CD27⁻CD20⁺CD24⁺.

Within Ag⁻ B cells, MIX and RNA showed higher levels of MBC IgD⁺IgM⁺ and lower levels of atBC5 compared to those in REC (Supplementary Figure S13). Within Ag⁺ B cells, MIX and RNA displayed lower percentages of naive, MBC IgA⁺, and atBC4 B cells if compared to those in REC, while the percentages of MBC IgG⁺ CD71⁺ and atBC2 were significantly higher (Figure 4E). Moreover, REC displayed a higher percentage of atBC4 cells if compared to those in MIX and RNA (Figure 4E). Similar percentages of all other subpopulations were found among REC, MIX, and RNA subjects (Supplementary Figure S14).

In addition, we measured IgG antibodies able to bind the spike and the RBD of the S1 subunit of the spike protein (the latter known as neutralizing antibodies). We observed that both vaccinated groups had higher levels of anti-spike and anti-RBD-binding IgG compared to those in REC subjects (Figure 4F).

Recovered patients show different immunological profiles compared to those of vaccinated donors

The principal component analysis (PCA) computed using the complete phenotype of Ag⁺ B and T cells, CD4⁺ T cell polyfunctionality, plasmatic anti-spike, and anti-RBD antibodies showed that the group of REC clusters in a different position of the two-dimensional PCA space if compared to MIX and RNA, which are almost entirely overlapping (Figure 5A, left). Immune features related to the amount of MBC IgA, CD107a⁻IFN- γ ⁻IL2⁻TNF⁺IL17⁻, CD107a⁻IFN- γ ⁻IL2⁺TNF⁺IL17⁻, CD107a⁻IFN- γ ⁻IL2⁻TNF⁻IL17⁺, and naive B cells (more abundant in REC subjects) were the main drivers of the clusterization of samples in two different areas (Figure 5A, right). Moreover, the picture of PCA contribution also reveals that both vaccinated groups were characterized by increased levels of MBC IgG CD71⁺, anti-spike, and anti-RBD IgG antibodies (Figure 5A, right).

By using the same parameters used to perform the PCA, we assessed the existence of immunological correlations between the variables within the REC, MIX, and RNA groups. It is to note that in REC, but not in the MIX and RNA groups, a strong positive correlation was present among the percentages of MBC IgA CD71⁺ and all polyfunctional CD4⁺ T-cell subsets (Figure 5B, Supplementary Figure S15). The percentages of MBC IgD⁺ IgM⁺, transitional, and naive B cells inversely correlate with all polyfunctional CD4⁺ T-cell subsets (Figure 5B, Supplementary Figure S15).

Discussion

Vaccines are designed to induce a long-term adaptive immune response that confers durable protection. In this study, as revealed by PCA, we report that COVID-19 recovered patients show different long-term immunological profiles compared to those of donors who had been vaccinated with three doses (either with adenovirus or mRNA technologies). Vaccinated individuals display a skewed Th1 Ag-specific T-cell polarization and a higher percentage of Ag-specific and activated MBCs expressing IgG compared to those of patients who recovered from severe COVID-19. Different polyfunctional properties characterize the two groups: recovered individuals show higher percentages of CD4⁺ T cells producing one or two cytokines simultaneously, while vaccinated donors are distinguished by highly polyfunctional populations able to release four molecules such as CD107a, IFN- γ , TNF, and IL-2.

SARS-CoV-2 entry route shapes the innate immune response, as major players such as macrophages and neutrophils contribute to recruit T and B cells that should mount a local specific immune response, with the consequent production of mucosal antibodies. This means that different adaptive mechanisms are involved in the protective immunity generated by the infection or vaccination. Indeed, we found that recovered individuals are characterized by higher percentages of MBCs producing IgA if compared to those of vaccinated ones. However, systemic and mucosal IgA responses are variably induced in response to vaccination and are associated with protection against subsequent infection (37, 38).

SARS-CoV-2-specific cells wane more slowly than do antibodies [reviewed in (39)], and T cells able to exert an efficient protection are those capable of exerting many functions simultaneously. Polyfunctional T-cell responses have been documented also in HIV-1 (40), hepatitis B virus vaccine (41), and vaccinia-induced responses (42), indicating that highly functional T-cell responses are commonly found in response to other viral infections and vaccination and are effectively controlled by cellular immunity. The functional population able to produce four cytokines or more is likely of significant immunologic importance because it could directly eliminate virally infected cells (assuming that such cells express or upregulate CD107a) and suppress viral replication while maintaining itself without CD4⁺ T-cell help through autocrine production of IL-2.

We found that vaccinated donors are characterized by MBCs IgG-switched that express CD71. Ag-specific B cells can be divided into antibody-secreting cells (or PBs) and MBCs after infection or vaccination. A particular subset of B cells, called activated B cells, is distinct from antibody-secreting cells and is committed to the MBC lineage. Activated B cells are characterized by the expression of CD71, which is the transferrin receptor and indicates higher activation status and proliferative capabilities (43). This population is also typically found in blood after infection with Ebola or influenza virus and also after vaccination (44–46).

As far as vaccination strategy is concerned, the ChAdOx1 vaccine uses a nonreplicating adenovirus as a vector to introduce into the cells of the recipient's DNA coding for the spike protein of SARS-CoV-2. BNT162b2 instead uses messenger RNA (mRNA) coding for spike, which cells take up and use to synthesize the protein. mRNA vaccines are good at inducing antibody responses, and the vector-based

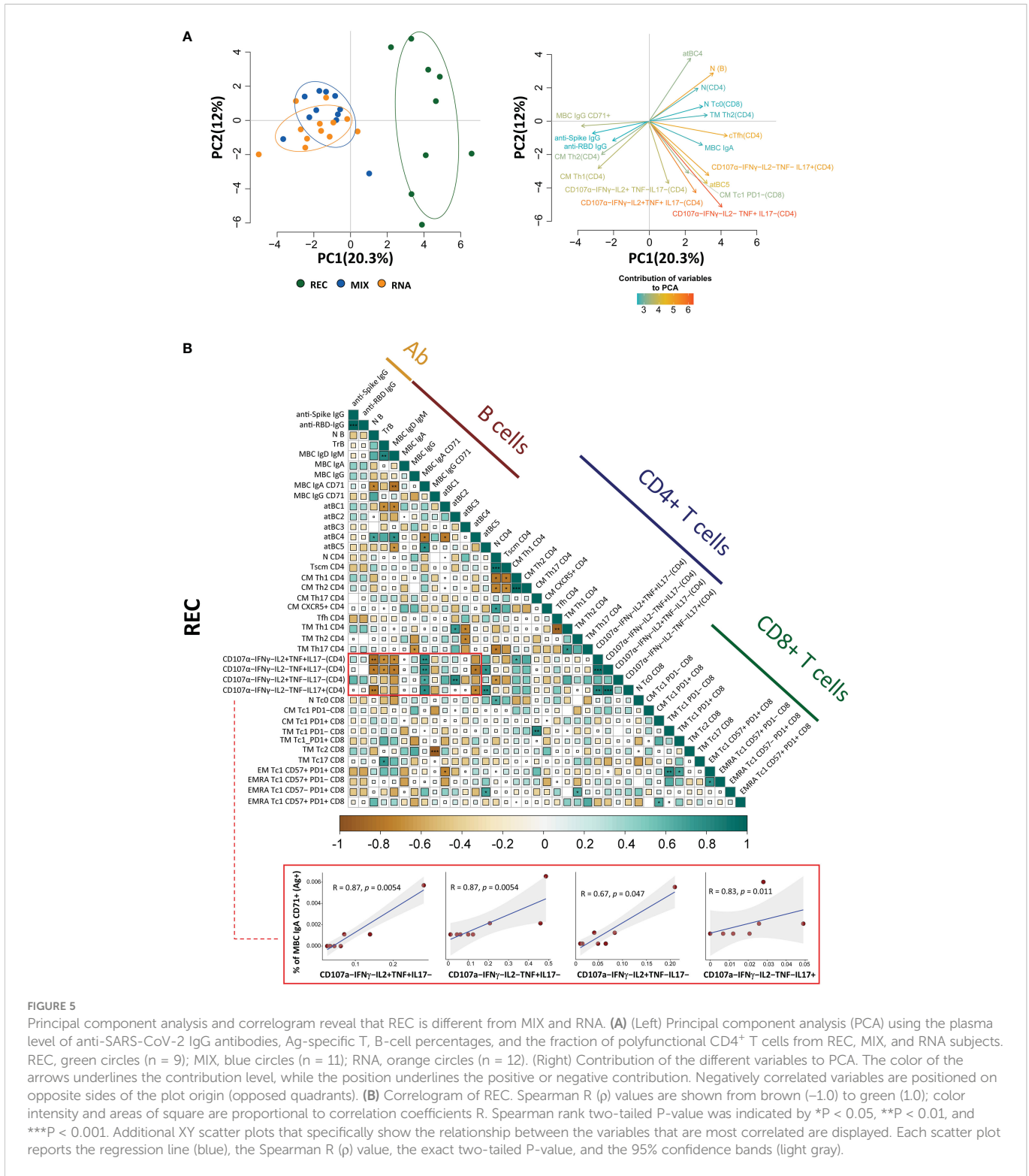


FIGURE 5
 Principal component analysis and correlogram reveal that REC is different from MIX and RNA. **(A)** (Left) Principal component analysis (PCA) using the plasma level of anti-SARS-CoV-2 IgG antibodies, Ag-specific T, B-cell percentages, and the fraction of polyfunctional CD4⁺ T cells from REC, MIX, and RNA subjects. REC, green circles (n = 9); MIX, blue circles (n = 11); RNA, orange circles (n = 12). (Right) Contribution of the different variables to PCA. The color of the arrows underlines the contribution level, while the position underlines the positive or negative contribution. Negatively correlated variables are positioned on opposite sides of the plot origin (opposed quadrants). **(B)** Correlogram of REC. Spearman R (p) values are shown from brown (-1.0) to green (1.0); color intensity and areas of square are proportional to correlation coefficients. Spearman rank two-tailed P-value was indicated by *P < 0.05, **P < 0.01, and ***P < 0.001. Additional XY scatter plots that specifically show the relationship between the variables that are most correlated are displayed. Each scatter plot reports the regression line (blue), the Spearman R (p) value, the exact two-tailed P-value, and the 95% confidence bands (light gray).

vaccines are better at triggering T-cell responses. In a Spanish study, people who received a dose of the Pfizer-BioNTech vaccine 8 weeks after an initial AstraZeneca dose had few side effects and a robust antibody response 2 weeks after the second shot, suggesting that mixing the two types of vaccine may give the immune system multiple ways to recognize a pathogen (47). However, in our small cohort of vaccinated individuals, the immunological response was not different in the two groups of individuals who received different vaccination

strategies likely because the immune response has been investigated after the third dose.

We are well aware that this study has some limitations. First of all, the number of patients studied is low, but the B- and T-cell compartments were investigated in-depth in terms of phenotype and functionality. Second, the number of days post symptom onset (for recovered individuals) or after the third dose of the vaccine (for vaccinated ones) is different. This could be relevant when interpreting

the results regarding SARS-CoV-2-specific antibodies or the percentage of Ag-specific B cells and cTfh cells in recovered patients. Third, a group of donors who developed hybrid immunity characterized by immunity developed by natural infection and vaccination.

However, our study can provide a novel characterization of the humoral and cellular immune responses upon COVID-19 vaccination or infection by including the fine phenotypic and functional analysis of Ag-specific B and T cells together with the comparison between different vaccination strategies (after the third dose of vaccination) and natural infection.

Methods

Blood collection and isolation of mononuclear cells

Up to 30 ml of blood was collected from each patient in vacuettes containing ethylenediaminetetraacetic acid (EDTA). Blood was immediately processed. Isolation of PBMCs was performed using Ficoll-Hypaque according to standard procedures (48). PBMCs were stored in liquid nitrogen in fetal bovine serum (FBS) supplemented with 10% dimethyl sulfoxide (DMSO). Plasma was stored at -80°C until use.

Activation-induced cell marker assay and T-cell phenotype

Isolated PBMCs were thawed and rested for 6 h. After resting, CD40-blocking antibody (0.5 µg/ml final concentration) (Miltenyi Biotec, Bergisch Gladbach, Germany) was added to the cultures 15 min before stimulation. PBMCs were cultured in a 96-well plate in the presence of 15-mer peptides with 11-amino acid overlap, covering the complete sequence of Wuhan SARS-CoV-2 spike glycoprotein (PepTivator SARS-CoV-2 Prot_S complete, Miltenyi Biotec, Bergisch Gladbach, Germany) together with 1 µg/ml of anti-CD28 (Miltenyi Biotec, Germany). PBMCs were stimulated for 18 h at 37°C in a 5% CO₂ atmosphere in complete culture medium (RPMI 1640 supplemented with 10% FBS and 1% each of L-glutamine, sodium pyruvate, nonessential amino acids, antibiotics, 0.1 M 4-(2-hydroxyethyl)-1-piperazineethanesulfonic acid (HEPES), and 55 µM β-mercaptoethanol) (33, 34). For each stimulated sample, an unstimulated one was prepared as a negative control. After stimulation, cells were washed with Phosphate buffer saline (PBS) and stained with PromoFluor IR-840 (Promokine, PromoCell, Heidelberg, Germany) for 20 min at room temperature (RT). Next, cells were washed with FACS buffer (PBS added with 2% FBS) and stained with the following fluorochrome-labeled monoclonal antibodies (mAbs) for 30 min at 37°C: CXCR5-BUV661, CCR6-BUV496, and CXCR3-BV785. Finally, cells were washed with FACS buffer and stained for 20 min at RT with Duraclone IM T-cell panel (Beckman Coulter, Brea, CA, USA) containing CD45-Krome Orange, CD3-APC-A750, CD4-APC, CD8-AF700, CD27-PC7, CD57-Pacific Blue, CD279 (PD1)-PC5.5, CD28-ECD, CCR7-PE, and CD45RA-FITC and added with three other fluorescent mAbs, i.e., CD69-BV650, CD137-BUV395, and CD95-BV605. Samples were acquired

on a CytoFLEX LX flow cytometer (Beckman Coulter). All reagents used for T-cell phenotype are reported in [Supplementary Table S1](#). All mAbs added to DuraClone IM T cells were previously titrated on human PBMCs and used at the concentration giving the best signal-to-noise ratio. The gating strategy used to identify CD4⁺ and CD8⁺ T cells is reported in [Supplementary Figure S16](#).

Intracellular cytokine staining

Isolated PBMCs were thawed and rested for 6 h. PBMCs were then cultured in the presence of 15-mer peptides with 11-amino acid overlap, covering the complete sequence of Wuhan SARS-CoV-2 spike glycoprotein (PepTivator SARS-CoV-2 Prot_S complete, Miltenyi Biotec, Bergisch Gladbach, Germany) together with 1 µg/ml of anti-CD28 (Miltenyi Biotec, Germany). PBMCs were stimulated for 16 h at 37°C in a 5% CO₂ atmosphere in complete culture medium (RPMI 1640 supplemented with 10% FBS and 1% each of L-glutamine, sodium pyruvate, nonessential amino acids, antibiotics, 0.1 M HEPES, and 55 µM β-mercaptoethanol). For each stimulated sample, an unstimulated one was prepared as a negative control. All samples were incubated with protein transport inhibitor containing brefeldin A (Golgi Plug, Becton Dickinson) and monensin (Golgi Stop, Becton Dickinson) and previously titrated concentration of CD107a-PE (BioLegend, San Diego, CA, USA). After stimulation, cells were washed with PBS and stained with LIVE/DEAD fixable Aqua (ThermoFisher Scientific, USA) for 20 min at RT. Next, cells were washed with FACS buffer and stained with surface mAbs recognizing CD3-PE.Cy5, CD4-AF700, and CD8-APC.Cy7 (BioLegend, San Diego, CA, USA). Cells were washed with FACS buffer and fixed and permeabilized with the Cytofix/Cytoperm buffer set (Becton Dickinson Bioscience, San Jose, CA, USA) for cytokine detection. Then, cells were stained with previously titrated mAbs recognizing IL-17-PE-Cy7, TNF-BV605, IFN-γ-FITC, IL-2-APC, and GZMB BV421 (all mAbs from BioLegend). Samples were acquired on an Attune NxT acoustic cytometer (ThermoFisher Scientific, USA). [Supplementary Table S1](#) reports mAb titers, clones, catalog numbers, and type of fluorochrome used in the panel. Gating strategy used to identify and analyze the intracellular cytokine production of CD4⁺ and CD8⁺ T lymphocytes is reported in [Supplementary Figure S9](#).

Detection of SARS-CoV-2-specific B cells

Thawed PBMCs were washed twice with RPMI 1640 supplemented with 10% FBS and 1% each of L-glutamine, sodium pyruvate, nonessential amino acids, antibiotics, 0.1 M HEPES, 55 µM β-mercaptoethanol, and 0.02 mg/ml DNase. PBMCs were washed with PBS and stained using viability marker PromoFluor IR-840 (Promokine, PromoCell, Heidelberg, Germany) for 20 min at RT in PBS. Next, cells were washed with PBS and stained for 15 min at RT with streptavidin-AF700 (decoy channel; ThermoFisher Scientific, USA) to remove false-positive SARS-CoV-2-specific B cells. After washing with FACS buffer, cells were stained with biotinylated full-length SARS-CoV-2 spike protein (R&D Systems, Minneapolis, USA) labeled with different streptavidin-fluorophore conjugates. Full-length biotinylated spike protein was mixed and incubated with streptavidin-BUV661 (Becton Dickinson) or

streptavidin-BV650 (BioLegend) at a 6:1 mass ratio for 15 min at RT. All samples were stained with both fluorescent biotinylated spike protein for 1 h at 4°C. Then, cells were washed with FACS buffer and stained for 20 min at RT with DuraClone IM B cells (Beckman Coulter, Brea, CA, USA) containing the following lyophilized directly conjugated mAbs: anti-IgD-FITC, CD21-PE, CD19-ECD, CD27-PC7, CD24-APC, CD38-AF750, anti-IgM-PB, and CD45-KrO to which the following drop-in antibodies were added: CD71-BUV395, CD20-BV785, anti-IgG-BUV496, and anti-IgA-PerCP-Vio700. Samples were acquired on a CytoFLEX LX flow cytometer (Beckman Coulter). A minimum of 1,000,000 cells per sample were acquired. All reagents used for B-cell phenotype are reported in [Supplementary Table S1](#). All mAbs added to DuraClone IM B cells were previously titrated on human PBMCs and used at the concentration giving the best signal-to-noise ratio. The gating strategy used to identify Ag⁻ and Ag⁺ B cells is reported in [Supplementary Figure S17](#).

Computational analysis of flow cytometry data

T-cell analysis

Compensated Flow Cytometry Standard (FCS) 3.0 files were imported into FlowJo software version v10.7.1 and analyzed by standard gating to remove doublets, aggregates, and dead cells. For *ex vivo* immunophenotyping of non-antigen-specific (Ag⁻) and antigen-specific (Ag⁺) T cells of both CD4⁺ and CD8⁺, we analyzed only the data of stimulated samples. For each sample, we therefore selected data from all living CD4⁺ or CD8⁺ T cells and imported them in R using flowCore package v2.4.0 (49) for a total of 8,436,275 CD4⁺ T cells (of which 89,400 were SARS-CoV-2-specific) and 3,723,899 CD8⁺ T cells (of which 20,413 were SARS-CoV-2-specific). Further analysis was performed using CATALYST v1.17.3 (50). All data obtained by flow cytometry were transformed in R using hyperbolic arcsine “ $\text{arcsinh}(x/\text{cofactor})$ ” applying manually defined cofactors (where x is the fluorescence-measured intensity value). Clustering and dimensional reduction were performed using FlowSOM (version 2.4.0) and Uniform Manifold Approximation and Projection (UMAP) (version 0.2.8.0) algorithms, respectively. The Ag⁺ CD4⁺ and CD8⁺ T-cell clusters have been reanalyzed more in-depth by performing a new step of clustering using the following markers: CD45RA, CCR7, CD27, CD28, PD-1, CCR6, CXCR3, CXCR5, and CD95. Starting from 15 clusters of either CD4⁺ T cells or CD8⁺ T cells, reclustering gave origin to 10 clusters of CD4⁺ T cells and 11 of CD8⁺ T lymphocytes. The quality control (QC) of clustering for CD4⁺ and CD8⁺ T cells is reported in [Supplementary Figures S2 and S6](#), respectively.

B-cell analysis

Compensated FCS 3.0 files were imported into FlowJo software version v10.7.1 and analyzed by standard gating to remove doublets, aggregates, and dead cells and identify CD19⁺ B cells. Then, from the total CD19⁺ B cells, we excluded decoy-positive B cells to remove false-positive SARS-CoV-2-specific B cells. For each sample, we selected the SARS-CoV-2-specific B cells as positive cells for both Spike_streptavidin-BUV661 and Spike_streptavidin-BV650 (we referred to as Ag⁺ B cells). The remaining double-negative cells were non-SARS-CoV-2-specific B cells (we referred to as Ag⁻ B cells). Then, we exported for each sample

separately both Ag⁺ and Ag⁻ B cells and imported them in R using flowCore package v2.4.0 for a total of 3,057,659 CD19⁺ B cells (of which 9,898 were SARS-CoV-2-specific). The unsupervised analysis was performed using CATALYST v1.17.3. All data were transformed in R using hyperbolic arcsin ($\text{arcsinh}(x/\text{cofactor})$) applying manually defined cofactors (where x is the fluorescence-measured intensity value). Clustering and dimensional reduction were performed using FlowSOM and UMAP algorithms, respectively. The QC of clustering for B cells is reported in [Supplementary Figure S12](#).

Measuring anti-SARS-CoV-2 anti-spike and anti-RBD IgG antibodies

Anti-spike antibody levels were measured by qualitative and semiquantitative chemiluminescent microparticle immunoassay (CMIA). AdviseDx SARS-CoV-2 IgG II assay (Abbott) was used to detect plasmatic IgG antibodies able to bind the RBD of the S1 subunit of the spike protein. Plasma, SARS-CoV-2 Ag-coated paramagnetic microparticles, and assay diluent are combined and incubated. The anti-spike IgG antibodies present in the sample bind to the SARS-CoV-2 Ag-coated paramagnetic microparticles. The mixture was then washed. Anti-human IgG acridinium-labeled conjugate was added and incubated to create a reaction mixture. The resulting chemiluminescent reaction was measured as a relative light unit (RLU). There is a direct relationship between the amount of IgG antibodies to SARS-CoV-2 in the sample and the RLU detected by the system optics. Results from the anti-spike AdviseDx SARS-CoV-2 IgG II assay are reported as arbitrary units per milliliter (AU/ml). As recommended, we applied a cutoff of 50 AU/ml as a positive threshold. Every measurement was performed on Abbott “Alinity I” platform. The level of anti-RBD IgG antibodies was calculated by using NAB Neutralizing Antibody kit (SGM Italia).

Principal component analysis and correlation plot

PCA was performed and visualized in R using prcomp and pca3d package. To perform PCA, we used a matrix containing the level of plasmatic anti-SARS-CoV-2 IgG antibodies, Ag-specific T, B-cell percentages, and the fraction of polyfunctional CD4⁺ T cells ([Supplementary Table S2](#)). The total contribution of a given variable retained by PC1 and PC2 is equal to $[(C1 * \text{Eig1}) + (C2 * \text{Eig2})]/(\text{Eig1} + \text{Eig2})$, where $C1$ and $C2$ are the contributions of the variable on PC1 and PC2; Eig1 and Eig2 are the eigenvalues of PC1 and PC2.

Correlation analysis was performed on the same parameters used to run the PCA (see above) except the following features that were not used for the correlation analysis of REC donors because they were not available: PB IgA, PB, and CD107a⁺IFN- γ ⁺IL2⁺TNF⁺IL17⁺. Pairwise correlations between variables were calculated and visualized as a correlogram using R packages stats (version 3.6.2) and corrplot (version 0.90). Spearman’s rank correlation coefficient (ρ) was indicated by color scale; significance was indicated by asterisks (* $P < 0.05$; ** $P < 0.005$; *** $P < 0.0005$).

Statistical analysis

Differential cell population abundance analysis was performed using generalized linear mixed model (GLMM) implemented within diffcyt package (51) applying FDR cutoff = 0.05; each P-value was reported in the figure. Quantitative variables were compared using Kruskal–Wallis nonparametric test corrected for multiple comparisons by controlling the false discovery rate (FDR), method

of Benjamini and Hochberg. Statistically significant adjusted P-values are represented. Statistical analysis of cytokine production was performed using GraphPad Prism version 8 (GraphPad Software Inc., La Jolla, USA). The total percentage of Ag-specific (Ag⁺CD4⁺ and Ag⁺CD8⁺) T-cell data has been calculated as background subtracted data. SPICE software (version 6, kindly provided by Dr. Mario Roederer, Vaccine Research Center, NIAID, NIH, Bethesda, MD, USA) was used to analyze flow cytometry data on T-cell polyfunctionality (52). Data from the total cytokine production are represented as individual values, means, and standard errors of the mean. Regarding polyfunctionality, data in pie charts are represented as median values, and statistical analysis was performed using the permutation test. Data in graphs are represented as individual values, means, and standard errors of the mean.

Data availability statement

The original contributions presented in the study are included in the article/**Supplementary Material**. Further inquiries can be directed to the corresponding author.

Ethics statement

The studies involving human participants were reviewed and approved by Each participant, including healthy donors, provided informed consent according to Helsinki Declaration, and all uses of human material have been approved by the local Ethical Committee (Comitato Etico dell'Area Vasta Emilia Nord, protocol number 177/2020, March 11th, 2020) and by the University Hospital Committee (Direzione Sanitaria dell'Azienda Ospedaliero Universitaria di Modena, protocol number 7531, March 11th, 2020). The patients/participants provided their written informed consent to participate in this study.

Author contributions

DT, AP, AN, RB, JS, LGi, ES, AD, MC carried out experiments. DT and AP drafted the figures. DT and AN drafted and revised the tables. MMe, MMa, MG, GG, SB, CM, TT followed patients. LGo drafted and revised the clinical tables. AP performed ICS analysis. DT and KP performed bioinformatic and statistical analyses. DT, SB and AC conceived the study. SB and AC wrote the manuscript. All authors contributed to the article and approved the submitted version.

References

1. Moss P. The T cell immune response against SARS-CoV-2. *Nat Immunol* (2022) 23(2):186–93. doi: 10.1038/s41590-021-01122-w
2. Cohen KW, Linderman SL, Moodie Z, Czartoski J, Lai L, Mantus G, et al. Longitudinal analysis shows durable and broad immune memory after SARS-CoV-2 infection with persisting antibody responses and memory B and T cells. *Cell Rep Med* (2021) 2(7):100354. doi: 10.1016/j.xcrm.2021.100354
3. Rha MS, Jeong HW, Ko JH, Choi SJ, Seo IH, Lee JS, et al. PD-1-Expressing SARS-CoV-2-Specific CD8(+) T cells are not exhausted, but functional in patients

Acknowledgments

SB and LGi are Marylou Ingram Scholar of the International Society for Advancement of Cytometry (ISAC) for the period 2015–2020 and 2020–2025, respectively. Drs. Paola Paglia (ThermoFisher Scientific, Monza, Italy), Leonardo Beretta (Beckman Coulter, Milan, Italy) are acknowledged for their support in providing reagents and materials in this study, and for precious technical suggestions. JS was supported by EMBO Scientific Exchange Grant (Short-Term Fellowship) STF-8905. This study was partially supported by unrestricted donations from Glem Gas spa (San Cesario, Modena, Italy), Sanfelice 1893 Banca Popolare (San Felice sul Panaro, Modena, Italy), Rotary Club Distretto 2072 (Clubs: Modena, Modena L.A. Muratori, Carpi, Sassuolo, and Castelvetro di Modena), BPER Banca and FAR 2022 by the University of Modena and Reggio Emilia (“Features and magnitude of long- and short-term immune memory against smallpox and COVID-19”). AD has been supported by a 2021 FAR fellowship from the University of Modena and Reggio Emilia. Finally, we gratefully acknowledge the subjects who donated blood to participate in this study.

Conflict of interest

The authors declare that the research was conducted in the absence of any commercial or financial relationships that could be construed as a potential conflict of interest.

The reviewer AC declared a past co-authorship with some of the authors to the handling editor.

Publisher's note

All claims expressed in this article are solely those of the authors and do not necessarily represent those of their affiliated organizations, or those of the publisher, the editors and the reviewers. Any product that may be evaluated in this article, or claim that may be made by its manufacturer, is not guaranteed or endorsed by the publisher.

Supplementary material

The Supplementary Material for this article can be found online at: <https://www.frontiersin.org/articles/10.3389/fimmu.2023.1123724/full#supplementary-material>

with COVID-19. *Immunity* (2021) 54(1):44–52 e43. doi: 10.1016/j.immuni.2020.12.002

4. Jung JH, Rha MS, Sa M, Choi HK, Jeon JH, Seok H, et al. SARS-CoV-2-specific T cell memory is sustained in COVID-19 convalescent patients for 10 months with successful development of stem cell-like memory T cells. *Nat Commun* (2021) 12(1):4043. doi: 10.1038/s41467-021-24377-1

5. Paolini A, Borella R, Neroni A, Lo Tartaro D, Mattioli M, Fidanza L, et al. Patients recovering from severe COVID-19 develop a polyfunctional antigen-


- specific CD4+ T cell response. *Int J Mol Sci* (2022) 23(14):8004. doi: 10.3390/ijms23148004
6. Dan JM, Mateus J, Kato Y, Hastie KM, Yu ED, Faliti CE, et al. Immunological memory to SARS-CoV-2 assessed for up to 8 months after infection. *Science* (2021) 371(6529):eabf4063. doi: 10.1126/science.abf4063
 7. Adamo S, Michler J, Zurbuchen Y, Cervia C, Taeschler P, Raebler ME, et al. Signature of long-lived memory CD8(+) T cells in acute SARS-CoV-2 infection. *Nature* (2022) 602(7895):148–55. doi: 10.1038/s41586-021-04280-x
 8. Niemi ME, Karjalainen J, Liao RG, Neale BM, Daly M, Ganna A, et al. Initiative c-HG: Mapping the human genetic architecture of COVID-19. *Nature* (2021) 600(7889):472–7. doi: 10.1038/s41586-021-03767-x
 9. Kousathanas A, Pairo-Castineira E, Rawlik K, Stuckey A, Odhams CA, Walker S, et al. Whole-genome sequencing reveals host factors underlying critical COVID-19. *Nature* (2022) 607(7917):97–103. doi: 10.1038/s41586-022-04576-6
 10. Pathak GA, Karjalainen J, Stevens C, Neale BM, Daly M, Ganna A, et al. Initiative c-HG: A first update on mapping the human genetic architecture of COVID-19. *Nature* (2022) 608(7921):E1–E10. doi: 10.1038/s41586-022-04826-7
 11. De Biasi S, Lo Tartaro D, Meschiaro M, Gibellini L, Bellinazzi C, Borella R, et al. Expansion of plasmablasts and loss of memory B cells in peripheral blood from COVID-19 patients with pneumonia. *Eur J Immunol* (2020) 50(9):1283–94. doi: 10.1002/eji.202048838
 12. Long QX, Tang XJ, Shi QL, Li Q, Deng HJ, Yuan J, et al. Clinical and immunological assessment of asymptomatic SARS-CoV-2 infections. *Nat Med* (2020) 26(8):1200–4. doi: 10.1038/s41591-020-0965-6
 13. Sekine T, Perez-Potti A, Rivera-Ballesteros O, Stralin K, Gorin JB, Olsson A, et al. Robust T cell immunity in convalescent individuals with asymptomatic or mild COVID-19. *Cell* (2020) 183(1):158–168 e114. doi: 10.1016/j.cell.2020.08.017
 14. Hartley GE, Edwards ESJ, Aui PM, Varese N, Stojanovic S, McMahon J, et al. Rapid generation of durable B cell memory to SARS-CoV-2 spike and nucleocapsid proteins in COVID-19 and convalescence. *Sci Immunol* (2020) 5(54):eabf8891. doi: 10.1126/sciimmunol.abf8891
 15. Jeffery-Smith A, Burton AR, Lens S, Rees-Spear C, Davies J, Patel M, et al. SARS-CoV-2-specific memory B cells can persist in the elderly who have lost detectable neutralizing antibodies. *J Clin Invest* (2022) 132(2):e152042. doi: 10.1172/JCI152042
 16. Oberhardt V, Luxenburger H, Kemming J, Schulien I, Ciminski K, Giese S, et al. Rapid and stable mobilization of CD8(+) T cells by SARS-CoV-2 mRNA vaccine. *Nature* (2021) 597(7875):268–73. doi: 10.1038/s41586-021-03841-4
 17. Gangaev A, Khetlaars SLC, Isaeva OI, Patiwael S, Dopler A, Hoefakker K, et al. Identification and characterization of a SARS-CoV-2 specific CD8(+) T cell response with immunodominant features. *Nat Commun* (2021) 12(1):2593. doi: 10.1038/s41467-021-22811-y
 18. Sahin U, Muik A, Vogler I, Derhovanessian E, Kranz LM, Vormehr M, et al. BNT162b2 vaccine induces neutralizing antibodies and poly-specific T cells in humans. *Nature* (2021) 595(7868):572–7. doi: 10.1038/s41586-021-03653-6
 19. Skelly DT, Harding AC, Gilbert-Jaramillo J, Knight ML, Longet S, Brown A, et al. Two doses of SARS-CoV-2 vaccination induce robust immune responses to emerging SARS-CoV-2 variants of concern. *Nat Commun* (2021) 12(1):5061. doi: 10.1038/s41467-021-25167-5
 20. Agrati C, Castilletti C, Goletti D, Sacchi A, Bordoni V, Mariotti D, et al. Persistent spike-specific T cell immunity despite antibody reduction after 3 months from SARS-CoV-2 BNT162b2-mRNA vaccine. *Sci Rep* (2022) 12(1):6687. doi: 10.1038/s41598-022-07741-z
 21. Goel RR, Painter MM, Apostolidis SA, Mathew D, Meng W, Rosenfeld AM, et al. mRNA vaccines induce durable immune memory to SARS-CoV-2 and variants of concern. *Science* (2021) 374(6572):abm0829. doi: 10.1126/science.abm0829
 22. Ciabattini A, Pastore G, Fiorino F, Polvere J, Lucchesi S, Pettini E, et al. Evidence of SARS-CoV-2-specific memory B cells six months after vaccination with the BNT162b2 mRNA vaccine. *Front Immunol* (2021) 12:740708. doi: 10.3389/fimmu.2021.740708
 23. Guerrero G, Picozza M, D'Orso S, Placido R, Pirronello M, Verdiani A, et al. BNT162b2 vaccination induces durable SARS-CoV-2-specific T cells with a stem cell memory phenotype. *Sci Immunol* (2021) 6(66):eab15344. doi: 10.1126/sciimmunol.ab15344
 24. Parry H, Bruton R, Stephens C, Brown K, Amirthalingam G, Otter A, et al. Differential immunogenicity of BNT162b2 or ChAdOx1 vaccines after extended-interval homologous dual vaccination in older people. *Immun Ageing* (2021) 18(1):34. doi: 10.1186/s12979-021-00246-9
 25. Parry H, Bruton R, Tut G, Ali M, Stephens C, Greenwood D, et al. Immunogenicity of single vaccination with BNT162b2 or ChAdOx1 nCoV-19 at 5–6 weeks post vaccine in participants aged 80 years or older: An exploratory analysis. *Lancet Healthy Longev* (2021) 2(9):e554–60. doi: 10.1016/S2666-7568(21)00169-0
 26. Stuart ASV, Shaw RH, Liu X, Greenland M, Aley PK, Andrews NJ, et al. Immunogenicity, safety, and reactogenicity of heterologous COVID-19 primary vaccination incorporating mRNA, viral-vector, and protein-adjuvant vaccines in the UK (Com-COV2): A single-blind, randomised, phase 2, non-inferiority trial. *Lancet* (2022) 399(10319):36–49. doi: 10.1016/S0140-6736(21)02718-5
 27. Pozzetto B, Legros V, Djebali S, Barateau V, Guibert N, Villard M, et al. Immunogenicity and efficacy of heterologous ChAdOx1-BNT162b2 vaccination. *Nature* (2021) 600(7890):701–6. doi: 10.1038/s41586-021-04120-y
 28. Goldberg Y, Mandel M, Bar-On YM, Bodenheimer O, Freedman LS, Ash N, et al. Protection and waning of natural and hybrid immunity to SARS-CoV-2. *N Engl J Med* (2022) 386(23):2201–12. doi: 10.1056/NEJMoa2118946
 29. Mazzoni A, Di Lauria N, Maggi L, Salati L, Vanni A, Capone M, et al. First-dose mRNA vaccination is sufficient to reactivate immunological memory to SARS-CoV-2 in subjects who have recovered from COVID-19. *J Clin Invest* (2021) 131(12):e149150. doi: 10.1172/JCI149150
 30. Marshall JC, Murthy S, Diaz J, Adhikari NK, Angus DC, Arabi YM, et al. Characterisation of WHO GotC, management of c-i: A minimal common outcome measure set for COVID-19 clinical research. *Lancet Infect Dis* (2020) 20(8):e192–7. doi: 10.1016/S1473-3099(20)30483-7
 31. Bacher P, Scheffold A. Flow-cytometric analysis of rare antigen-specific T cells. *Cytometry A* (2013) 83(8):692–701. doi: 10.1002/cyto.a.22317
 32. Reiss S, Baxter AE, Cirelli KM, Dan JM, Morou A, Daigneault A, et al. Comparative analysis of activation induced marker (AIM) assays for sensitive identification of antigen-specific CD4 T cells. *PLoS One* (2017) 12(10):e0186998. doi: 10.1371/journal.pone.0186998
 33. Grifoni A, Weiskopf D, Ramirez SI, Mateus J, Dan JM, Moderbacher CR, et al. Targets of T cell responses to SARS-CoV-2 coronavirus in humans with COVID-19 disease and unexposed individuals. *Cell* (2020) 181(7):1489–1501 e1415. doi: 10.1016/j.cell.2020.05.015
 34. De Biasi S, Paolini A, Lo Tartaro D, Gibellini L, Cossarizza A. Analysis of antigen-specific T and B cells for monitoring immune protection against SARS-CoV-2. *Curr Protoc* (2023) 3(1):e636. doi: 10.1002/cpz1.636
 35. Turner JS, Kim W, Kalaidina E, Goss CW, Rauseo AM, Schmitz AJ, et al. SARS-CoV-2 infection induces long-lived bone marrow plasma cells in humans. *Nature* (2021) 595(7867):421–5. doi: 10.1038/s41586-021-03647-4
 36. Sutton HJ, Aye R, Idris AH, Vistein R, Nduati E, Kai O, et al. Atypical B cells are part of an alternative lineage of B cells that participates in responses to vaccination and infection in humans. *Cell Rep* (2021) 34(6):108684. doi: 10.1016/j.celrep.2020.108684
 37. Sheikh-Mohamed S, Isho B, Chao GYC, Zuo M, Cohen C, Lustig Y, et al. Systemic and mucosal IgA responses are variably induced in response to SARS-CoV-2 mRNA vaccination and are associated with protection against subsequent infection. *Mucosal Immunol* (2022) 15(5):799–808. doi: 10.1038/s41385-022-00511-0
 38. Montague BT, Wiperman MF, Chio E, Crow R, Hooper AT, O'Brien MP, et al. Elevated serum IgA following vaccination against SARS-CoV-2 in a cohort of high-risk first responders. *Sci Rep* (2022) 12(1):14932. doi: 10.1038/s41598-022-19095-7
 39. Sette A, Crotty S. Immunological memory to SARS-CoV-2 infection and COVID-19 vaccines. *Immunol Rev* (2022) 310(1):27–46. doi: 10.1111/imr.13089
 40. Betts MR, Nason MC, West SM, De Rosa SC, Migueles SA, Abraham J, et al. HIV Nonprogressors preferentially maintain highly functional HIV-specific CD8+ T cells. *Blood* (2006) 107(12):4781–9. doi: 10.1182/blood-2005-12-4818
 41. De Rosa SC, Lu FX, Yu J, Peretto SP, Falloon J, Moser S, et al. Vaccination in humans generates broad T cell cytokine responses. *J Immunol* (2004) 173(9):5372–80. doi: 10.4049/jimmunol.173.9.5372
 42. Precopio ML, Betts MR, Parrino J, Price DA, Gostick E, Ambrozak DR, et al. Immunization with vaccinia virus induces polyfunctional and phenotypically distinctive CD8(+) T cell responses. *J Exp Med* (2007) 204(6):1405–16. doi: 10.1084/jem.20062363
 43. Ellebedy AH, Jackson KJ, Kissick HT, Nakaya HI, Davis CW, Roskin KM, et al. Defining antigen-specific plasmablast and memory B cell subsets in human blood after viral infection or vaccination. *Nat Immunol* (2016) 17(10):1226–34. doi: 10.1038/ni.3533
 44. Wrammert J, Onlamoon N, Akondy RS, Perng GC, Polsrila K, Chandele A, et al. Rapid and massive virus-specific plasmablast responses during acute dengue virus infection in humans. *J Virol* (2012) 86(6):2911–8. doi: 10.1128/JVI.06075-11
 45. Wrammert J, Miller J, Akondy R, Ahmed R. Human immune memory to yellow fever and smallpox vaccination. *J Clin Immunol* (2009) 29(2):151–7. doi: 10.1007/s10875-008-9267-3
 46. Wrammert J, Ahmed R. Maintenance of serological memory. *Biol Chem* (2008) 389(5):537–9. doi: 10.1515/bc.2008.066
 47. Borobia AM, Carcas AJ, Perez-Olmeda M, Castano L, Bertran MJ, Garcia-Perez J, et al. Immunogenicity and reactogenicity of BNT162b2 booster in ChAdOx1-s-primed participants (CombiVacS): A multicentre, open-label, randomised, controlled, phase 2 trial. *Lancet* (2021) 398(10295):121–30. doi: 10.1016/S0140-6736(21)01420-3
 48. Cossarizza A, Chang HD, Radbruch A, Abignano S, Addo R, Akdis M, et al. Guidelines for the use of flow cytometry and cell sorting in immunological studies (third edition). *Eur J Immunol* (2021) 51(12):2708–3145. doi: 10.1002/eji.202170126
 49. Hahne F, LeMeur N, Brinkman RR, Ellis B, Haaland P, Sarkar D, et al. flowCore: A bioconductor package for high throughput flow cytometry. *BMC Bioinf* (2009) 10:106. doi: 10.1186/1471-2105-10-106
 50. Nowicka M, Krieg C, Crowell HL, Weber LM, Hartmann FJ, Guglietta S, et al. CyTOF workflow: Differential discovery in high-throughput high-dimensional cytometry datasets. *F1000Res* (2017) 6:748. doi: 10.12688/f1000research.11622.3
 51. Weber LM, Nowicka M, Sonesson C, Robinson MD. Diffcyt: Differential discovery in high-dimensional cytometry via high-resolution clustering. *Commun Biol* (2019) 2:183. doi: 10.1038/s42003-019-0415-5
 52. Roederer M, Nozzi JL, Nason MC. SPICE: exploration and analysis of post-cytometric complex multivariate datasets. *Cytometry A* (2011) 79(2):167–74. doi: 10.1002/cyto.a.21015

Immunosenescence and vaccine efficacy revealed by immunometabolic analysis of SARS-CoV-2-specific cells in multiple sclerosis patients

Received: 13 November 2023

Accepted: 11 March 2024

Published online: 29 March 2024

 Check for updates

Sara De Biasi^{1,8}  , Domenico Lo Tartaro^{1,8}, Anita Neroni¹, Moritz Rau^{1,2}, Nikolaos Paschalidis³ , Rebecca Borella¹, Elena Santacroce¹, Annamaria Paolini¹, Lara Gibellini¹ , Alin Liviu Ciobanu¹ , Michela Cuccorese⁴, Tommaso Trenti⁴, Ignacio Rubio² , Francesca Vitetta⁵, Martina Cardi⁵ , Rafael José Argüello⁶ , Diana Ferraro⁵ & Andrea Cossarizza^{1,7}  


Disease-modifying therapies (DMT) administered to patients with multiple sclerosis (MS) can influence immune responses to SARS-CoV-2 and vaccine efficacy. However, data on the detailed phenotypic, functional and metabolic characteristics of antigen (Ag)-specific cells following the third dose of mRNA vaccine remain scarce. Here, using flow cytometry and 45-parameter mass cytometry, we broadly investigate the phenotype, function and the single-cell metabolic profile of SARS-CoV-2-specific T and B cells up to 8 months after the third dose of mRNA vaccine in a cohort of 94 patients with MS treated with different DMT, including cladribine, dimethyl fumarate, fingolimod, interferon, natalizumab, teriflunomide, rituximab or ocrelizumab. Almost all patients display functional immune response to SARS-CoV-2. Different metabolic profiles characterize antigen-specific-T and -B cell response in fingolimod- and natalizumab-treated patients, whose immune response differs from all the other MS treatments.

The immunosuppressive and immunomodulatory disease-modifying therapies (DMT) used for multiple sclerosis (MS) act at different levels, i.e., inhibiting the expansion of activated lymphocytes (teriflunomide), redirecting pathological immune cells away from the central nervous system [natalizumab, fingolimod (FTY)] or depleting immune cell subsets (B and T cells; anti-CD20, cladribine)¹. In treated patients, DMT can introduce risk for increased infections, reduced vaccine

effectiveness or reduce the duration of specific immunity. These aspects are of critical importance, especially in the course of a pandemic such as that due to SARS-CoV-2, where the host immune response is crucial^{2–12}, and that was effectively fought by several different vaccines.

In patients with MS, DMT such as interferon (IFN)- β , glatiramer acetate and dimethyl fumarate (DMF) are not expected to compromise

¹Department of Medical and Surgical Sciences for Children and Adults, University of Modena and Reggio Emilia School of Medicine, Modena, Italy.

²Department of Anesthesiology and Intensive Care Medicine, Jena University Hospital, Jena, Germany. ³Biomedical Research Foundation Academy of Athens, Athens, Greece. ⁴Department of Laboratory Medicine and Pathology, Diagnostic Hematology and Clinical Genomics, Azienda Unità Sanitaria Locale AUSL/AOU Policlinico, Modena, Italy. ⁵Neurology Unit, Department of Biomedical, Metabolic and Neurosciences, Nuovo Ospedale Civile Sant'Agostino Estense, University of Modena and Reggio Emilia, Modena, Italy. ⁶Aix Marseille Univ, CNRS, INSERM, CIML, Centre d'Immunologie de Marseille-Luminy, Marseille, France. ⁷National Institute for Cardiovascular Research, Bologna, Italy. ⁸These authors contributed equally: Sara De Biasi, Domenico Lo Tartaro.  e-mail: sara.debiasi@unimore.it; andrea.cossarizza@unimore.it

vaccine efficacy¹³, although the effect of DMF-induced lymphopenia on vaccine efficacy is unknown, and attenuated vaccine responses in patients with moderate or severe lymphopenia is conceivable¹⁴. A modestly diminished rate of immune response to vaccines was described in patients treated with teriflunomide, even if this did not compromise the achievement of seroprotective antibody levels¹⁵. Valid immune response to diphtheria-tetanus toxoid and to Keyhole limpet hemocyanin (KLH) was found in natalizumab-treated patients¹⁶, while H1N1 and seasonal influenza vaccination provided evidence that an adequate response to the immunization may not occur in some patients^{17,18}. Adequate immune responses to seasonal influenza vaccine and tetanus toxoid booster were detected in patients receiving FTY¹⁹. On the other hand, MS patients treated with cell-depleting agents (such as ocrelizumab, rituximab, ofatumumab, alemtuzumab, and cladribine) displayed attenuated vaccine responses, especially if they were vaccinated during the maximum cell depletion period. Peripherally B cell-depleted ocrelizumab recipients mounted attenuated humoral responses to clinically relevant vaccines and the neoantigen KLH, suggesting that use of standard non-live vaccines while on ocrelizumab treatment requires careful considerations²⁰. It is nevertheless recommended to vaccinate patients for seasonal influenza because a potentially protective humoral response, even if attenuated, can be expected²¹.

How different DMT affect vaccination effectiveness and safety in patients with MS was highlighted during the outbreak of coronavirus diseases (COVID-19). In particular, therapies with anti-CD20 (rituximab/ocrelizumab) monoclonal antibodies or with the sphingosine-phosphate receptor modulator (FTY) have been shown to weaken the formation of immune response after SARS-CoV-2 vaccination^{22–31}. MS patients treated with teriflunomide or alemtuzumab achieved effective humoral and cellular immune responses up to 6 months following the second COVID-19 vaccination. Immune responses were reinforced following the third vaccine booster³². However, the response to vaccination was mainly measured by humoral responses (in term of antibody titers in plasma) and/or production of interferon (IFN)- γ by T cells as correlate for a protective response. However, the protective capacity of the adaptive immune response to SARS-CoV-2 depends not only on virus-specific antibodies, but also on the cellular response³³. The phenotype of antigen-specific (Ag⁺) T cells of patients treated with rituximab/ocrelizumab displayed a skewed response, mostly compromising circulating follicular helper T (T_{fh}) cell responses and augmenting the induction of CD8⁺ T cell³³. Moreover, when compared to healthy donors (HD), MS patients showed lower percentages in Ag-specific cells able to produce IFN- γ , interleukin (IL)-2 and tumor necrosis factor (TNF)³⁴.

A detailed overview of different functional and metabolic features of the long-term immune response after vaccination in relapsing-remitting (RR) MS patients treated with different DMT is still missing. Here, we broadly interrogate SARS-CoV-2 antigen-specific T and B cells 6 months after the third dose of mRNA vaccine in a cohort of 94 MS patients treated with different DMT such as cladribine, DMF, FTY, IFN- β , natalizumab, teriflunomide or rituximab/ocrelizumab. By using 21-parameter flow cytometry, we investigate the phenotype and function of antigen-specific T and B cells. In addition, the metabolic profile of such cells is examined using 45-parameter mass cytometry, allowing profiling of the metabolic regulome at the single-cell level (scMEP)^{9,35,36}. We find that almost all patients develop a detectable and functional SARS-CoV-2 immune response. In particular, we show that a diverse metabolic profile characterizes antigen-specific T and B cell response in FTY- and natalizumab-treated MS patients, who generate a unique immune response that differs from all other MS treatments. Finally, using our own approach of prediction analysis, we identify a SARS-CoV-2 specific immunological signature that could likely predict protection from breakthrough SARS-CoV-2 infection.

Results

Demographic and clinical characteristics of the patients

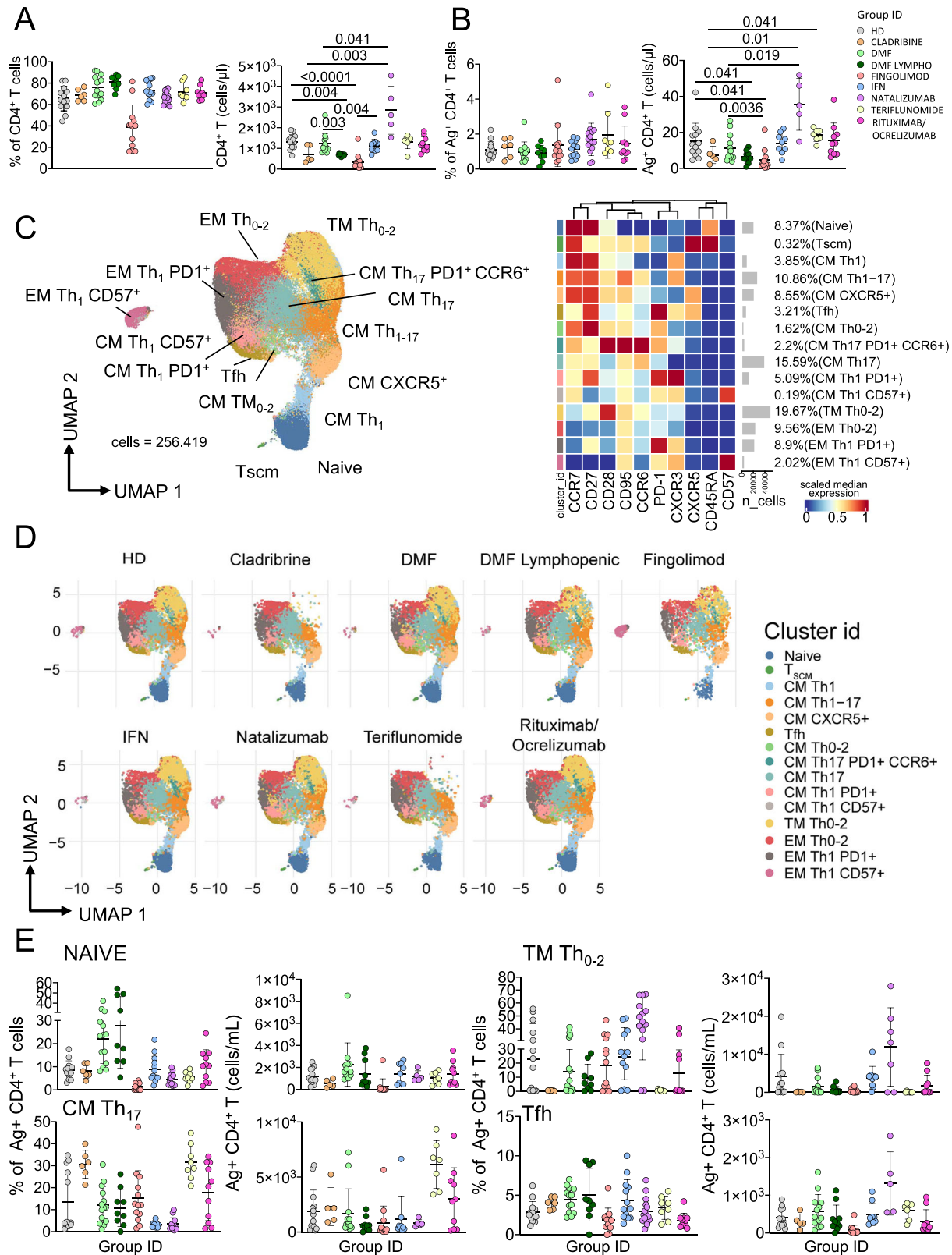
MS patients and healthy donors had a median age of 44.0 (interquartile range, IQR: 41.5–48.5), were mostly female (71.7%), with a median disease duration of 14.3 years (IQR: 10.0–17.1). The most common anti-COVID-19 vaccine used was Pfizer-BioNTech (Comirnaty): 69 persons (64.2%), followed by Moderna (Spikevax): 38 persons (35.8%). Median time from the last dose of vaccine to sample collection was 4.4 months (IQR: 3.8–5.3). Demographic and clinical characteristics of 94 MS patients and 13 healthy donors (HD), the type of DMT at the time of vaccination, the type of third dose vaccine and median range of time to last administration, prior COVID-19 infection status, and relevant comorbidities are shown in Supplementary Data 1. Patients were eligible for inclusion if they met the following criteria: (a) a confirmed diagnosis of Relapsing-Remitting Multiple Sclerosis (RRMS), and (b) a history of treatment with FTY, dimethyl fumarate, natalizumab, or teriflunomide for a minimum of 6 months, or having undergone at least two infusion cycles with rituximab or ocrelizumab or completed at least one full cycle of cladribine. Patients on ocrelizumab or rituximab, as per routine clinical practice, underwent SARS-CoV-2 vaccination at least six weeks before subsequent infusion or at least three months after the last infusion. Exclusion criteria comprised treatment with steroids during the preceding 6 weeks and a history of COVID-19 before vaccination. Patients treated with different DMT were enrolled such as: natalizumab ($n = 15$; 15.9%), DMF ($n = 18$; 19.1%), DMF patients with decreased absolute lymphocyte counts ($<800/\mu\text{L}$) at the time of sampling, defined “DMF lymphopenic” ($n = 10$; 10.6%), interferon IFN ($n = 12$; 12.8%), FTY ($n = 14$; 14.9%), rituximab/ocrelizumab [$n = 11$; 11.7%, which included those treated with ocrelizumab ($n = 7$; 63.6%) or rituximab ($n = 4$; 36.4%)], cladribine ($n = 6$; 6.4%), and teriflunomide ($n = 8$; 8.6%).

MS patients treated with different DMT develop similar percentages of Ag⁺ CD4⁺ T cells, but these cells display a different phenotype compared to healthy donors

First, we investigated by manual gating the percentage of CD4⁺ T cells. Figure 1A shows that lymphopenic patients treated with DMF displayed higher percentage of CD4⁺ T cells if compared to HD, while all other MS patients treated with different therapies showed similar percentages of CD4⁺ T cells. The absolute number of CD4⁺ T cells was lower in patients treated with cladribine, FTY- and lymphopenic-DMF treated patients and higher in those treated with natalizumab if compared to HD.

Then, we identified Ag⁺ T cells, defined as cells expressing CD137 and CD69 after 18 h of in vitro stimulation with SARS-CoV-2 peptides (Supplementary Fig. 1)^{9,35}. As shown in Fig. 1B, the percentage of Ag⁺ T cells within CD4⁺ T cells was similar in all MS patients and HD, confirming that MS patients treated with different drugs mount a detectable specific T cell response. The absolute number of Ag⁺ CD4⁺ T cells was lower in FTY-treated patients if compared to HD and DMF-, IFN-, natalizumab-, teriflunomide- or rituximab/ocrelizumab-treated patients.

Then, the pool of Ag⁺ CD4⁺ T cells was analyzed by an unsupervised method, i.e., FlowSOM, to better depict their phenotype in terms of differentiation and T helper polarization towards circulating follicular helper (T_{fh}), Th0/Th2, Th1 or Th17 (Fig. 1C, Supplementary Fig. 2). Cell clustering resulted in 15 different populations that represent the entire differentiation spectrum, from the most undifferentiated cell type (i.e., naïve) to the most differentiated one, such as effector memory T cells (EM). The expression of antigens such as CD45RA, CCR7, CD27, CD28 and CD95 was used to identify the differentiation status to define naïve (CD45RA⁺CCR7⁺CD27⁺CD28⁺CD95⁻), stem memory cell (T_{SCM}, CD45RA⁺CCR7⁺CD27⁺CD28⁺CD95⁺), central memory (CM, CD45RA⁺CCR7⁺CD27⁺CD28⁺CD95⁺), transitional memory (TM, CD45RA⁺CCR7⁺CD27⁺CD28⁺CD95⁺), and effector memory (EM) (CD45RA⁺CCR7⁺CD27⁺CD28⁺CD95⁺). Surface molecules such as



CXCR3, CCR6, CXCR5 and PD1 were used for a classification regarding Th polarization, i.e., Th0/Th2 defined as CXCR3⁻CCR6⁻, Th1 as CXCR3⁺CCR6⁻, Th17 as CXCR3⁻CCR6⁺, Th1/Th17 as CXCR3⁺CCR6⁺ and Tfh as CXCR3⁻CCR6⁻CXCR5⁺PD1⁺. Senescent T cells were characterized by the expression of CD57 (Fig. 1C).

Even if MS patients mount a CD4⁺ Ag⁺ T cell response whose frequency was similar among HD and MS patients treated with different

drugs, cellular composition was phenotypically different. Differences were evident for the percentage of naïve cells and the Th1 compartment as far as DMF- or teriflunomide-treated patients are concerned (Fig. 1D), but these differences were lost when absolute numbers were considered (Fig. 1E). Natalizumab-treated patients displayed the highest percentage of Ag⁺ TM Th0-2 cells if compared to healthy donors or to the other treatments; this difference was maintained also

Fig. 1 | Ag⁺ CD4⁺ T cell landscape. **A** Percentage and absolute number of CD4⁺ T cells. Dot plots show the percentage and absolute number of CD4⁺ T cells. The central bar represents the mean \pm SD. Kruskal–Wallis test (one-sided) with Benjamini–Hochberg correction for multiple comparisons. Significant adjusted *q*-values are reported in the figure. **B** Percentage and absolute number of Ag⁺ CD4⁺ T cells. Dot plots show the percentage and absolute number of Ag⁺ CD4⁺ T cells. The central bar represents the mean \pm SD. Kruskal–Wallis test (one-sided) with Benjamini–Hochberg correction for multiple comparisons. Significant adjusted *q*-values are reported in the figure. **C** Ag⁺ CD4⁺ T cells phenotype UMAP and Heatmap. Uniform Manifold Approximation and Projection (UMAP) plot shows the 2D spatial distribution of 256,419 cells from healthy donors (HD) and MS patients treated with different DMT embedded with FlowSOM clusters. Heatmap of the median marker intensities of the 10 lineage markers across the 15 cell populations obtained with FlowSOM algorithm after the manual metacluster merging. The colors of cluster_id column correspond to the colors used to label the UMAP plot

clusters. The color in the heatmap is referred to the median of the *arcsinh* marker expression (0–1 scaled) calculated over cells from all the samples. Blue represents lower expression, while red represents higher expression. Light gray bar along the rows (clusters) and values in brackets indicate the relative sizes of the clusters. N naive, T_{SCM} T stem cell memory, CM central memory, TM transitional memory, EM effector memory, EMRA effector memory reexpressing the CD45RA, cTfh circulating T follicular helper cells. **D** UMAP graphs stratified by therapy: healthy donors (HD); Cladribine; Dimethyl Fumarate (DMF); DMF Lymphopenic; Fingolimod; interferon β (IFN); Natalizumab; Teriflunomide; Rituximab/Ocrelizumab. **E** Dot plots of different subpopulation of Ag⁺ T cells in patients treated with different DMT. The central bar represents the mean \pm SD. Kruskal–Wallis test with Benjamini–Hochberg correction for multiple **A–E**: HD: *n* = 13; Cladribine: *n* = 6; DMF: *n* = 14; DMF Lymphopenic: *n* = 9; Fingolimod: *n* = 12; IFN: *n* = 13; Natalizumab: *n* = 15; Teriflunomide: *n* = 8; Rituximab/Ocrelizumab: *n* = 11.

for the absolute numbers. A detailed representation of all statistical differences among therapies for each cluster is reported in detail in the Supplementary Fig. 3.

Patients treated with teriflunomide develop higher percentage of Ag⁺ CD8⁺ T cells if compared to healthy donors

Next, we aimed to investigate Ag⁺ CD8⁺ T cells. Figure 2A shows that lymphopenic MS patients treated with DMF showed lower percentage of CD8⁺ T cells if compared to HD. Absolute number of CD8⁺ T cells was lower in cladribine-, DMF- (both groups of patients) or FTY-treated patients if compared to HD. Natalizumab-treated patients displayed the highest absolute number when compared to cladribine-, DMF-, FTY- or IFN-treated patients. Lymphopenic DMF-treated patients showed the lowest absolute number of CD8⁺ T cells when compared to the other treatments. Figure 2B indicates that, as far as the percentage of Ag⁺ CD8⁺ T cells is considered (gating strategy is shown in Supplementary Fig. 4), teriflunomide-treated patients displayed the highest percentage. DMF- or FTY-treated patients showed the lowest absolute number if compared to HD.

Then, we applied the aforementioned unsupervised method of analysis, *i.e.*, FlowSOM, for the identification of the phenotype of Ag⁺ CD8⁺ T cells (Fig. 2C, Supplementary Fig. 5). We could identify 12 different clusters, spanning from that of naïve Tc0 cells to terminally differentiated effector memory T cells re-expressing CD45RA (EMRA), that were also CD57⁺ and/or PD-1⁺. More in detail, FlowSOM revealed one cluster of CM Tc0/2 (CD45RA⁻CCR7⁺CD27⁺CD28⁺PD-1⁺), one cluster of TM Tc1 expressing CXCR5 (CD45RA⁻CCR7⁺CD27⁺CD28⁺PD-1⁺CXCR5⁺CXCR3⁺), five clusters of EM (mainly Tc0/2, Tc17 or Tc1 expressing or not CD57 and PD-1) and four clusters of EMRA (mainly Tc0/2, Tc17 or Tc1 expressing or not CD57 and PD-1). The phenotype of Ag⁺ CD8⁺ T cells of DMT-treated patients was quite different not only from that of HD, but also among different therapies (Fig. 2D). Natalizumab-treated patients displayed the highest percentage of CM Tc0/2 cells, while FTY-treated patients displayed the lowest percentage of TM Tc1 CXCR5⁺ cells. Natalizumab-treated patients showed the highest percentage and absolute numbers of CM Tc0-2 and TM Tc1 CXCR5⁺, (Fig. 2E). All differences in the phenotype are reported in detail in the Supplementary Fig. 6.

MS patients treated with different DMT reveal polyfunctional profiles

The functional properties of Ag⁺-specific T cells were investigated by measuring the percentages of cells producing IFN- γ , tumor necrosis factor (TNF), interleukin (IL)–2, IL-17, and/or granzyme B (GRZB), along with the expression of the degradation marker CD107a. The percentages of cells producing cytokines were assessed after 16 h of *in vitro* stimulation with a SARS-CoV-2 peptide pool covering the complete sequence of SARS-CoV-2 spike glycoprotein (Supplementary Figs. 7–10).

MS patients treated with FTY showed the highest percentage of CD4⁺ T cells producing GRZB and the lowest percentage of CD4⁺ T cells producing IL-2, displaying a more cytotoxic profile, that is typically found in autoimmune diseases and, in particular, during MS (Fig. 3A). Polyfunctional properties were investigated in CD4⁺ and CD8⁺ T cells by analyzing the simultaneous production of TNF, CD107a, IFN- γ , IL-2, and IL-17 using the bioinformatic Simplified Presentation of Incredibly Complex Evaluation (SPICE) tool. Healthy donors displayed a different polyfunctional profile if compared to FTY-, natalizumab-, teriflunomide- or rituximab/ocrelizumab-treated MS patients. The polyfunctional profile of natalizumab-treated patients was different. These differences were mainly due to the percentage of CD4⁺ T cells producing CD107a⁺IFN- γ ⁺IL2⁺IL17⁺TNF⁺, CD107a⁺IFN- γ ⁺IL2⁺IL17⁺TNF⁺ and CD107a⁺IFN- γ ⁺IL2⁺IL17⁺TNF⁺ (Fig. 3B).

Regarding Ag⁺ CD8⁺ T cell, FTY-treated patients showed a higher percentage of CD8⁺ T cells producing GRZB if compared to those treated with DMF, natalizumab or IFN (Fig. 3C). The polyfunctional profile of CD8⁺ T cells of HD was then different from those of rituximab/ocrelizumab-treated patients. The percentage of CD8⁺ T cells that were CD107a⁺IFN- γ ⁺IL2⁺IL17⁺TNF⁺ was higher in teriflunomide-treated patients if compared to those treated with DMF (Fig. 3D).

Fingolimod- or rituximab/ocrelizumab-treated-patients displayed low or undetectable levels of Ag⁺ B cells

Natalizumab-treated MS patients were characterized by highest percentage and absolute number of B cells if compared to all groups (Fig. 4A). Consistent with expectations, patients treated with rituximab/ocrelizumab exhibited markedly reduced, but detectable levels of circulating B cells. Subsequently, the percentage of Ag⁺ B cells was quantified, revealing that rituximab/ocrelizumab-treated patients displayed the lowest proportion and absolute count of these cells (Fig. 4B, Supplementary Fig. 11). Furthermore, patients treated with FTY showed a reduced percentage and absolute count of these cells compared to HD. Moreover, the phenotype of Ag⁺ B cells was extensively characterized using the aforementioned unsupervised methods. (Supplementary Fig. 12). Ag⁺ B cells were composed by 11 clusters, such as: naïve (CD20⁺CD21⁺CD24⁺CD38⁺IgD⁺IgM⁺); transitional B cells (TrB; CD20⁺CD21⁺CD27⁺CD24⁺CD38⁺IgD⁺IgM⁺); immature TrB (CD20⁺CD21⁺CD24⁺CD27⁺CD38⁺IgD⁺IgM⁺); six clusters of memory B cell MBCs defined as follows: MBC unswitched (CD20⁺CD21⁺CD24⁺CD27⁺IgD⁺IgM⁺), MBC IgA⁺ (CD20⁺CD21⁺CD24⁺CD27⁺IgA⁺IgD⁺IgM⁺), MBC IgG⁺ CD21^{low} (CD20⁺CD21^{low}CD24⁺CD27⁺IgG⁺), MBC IgG⁺ CD20⁻ (CD21⁺CD24⁺CD27⁺), and MBC IgG⁺ CD71⁺ (CD20⁺CD21⁺CD24⁺CD27⁺IgG⁺) and MBC IgG⁺ (CD20⁺CD21⁺CD24⁺CD27⁺CD71⁺IgG⁺); plasmablasts (PB) were defined as PB CD27⁺CD71⁺CD38⁺⁺; atypical B cells (atBCs) as CD21⁻CD27⁻CD20⁺IgG⁺ (Fig. 4C). Ag⁺ B cells were phenotypically very similar in all groups except for rituximab/ocrelizumab treated patients (Fig. 4D and Supplementary Fig. 13). The highest percentage of naïve Ag⁺ B cells was found in FTY-treated MS patients and the lowest in

Fig. 2 | Ag⁺ CD8⁺ T cell landscape. **A** Percentage and absolute number of CD8⁺ T cells. Dot plots show the percentage and absolute number of CD8⁺ T cells. The central bar represents the mean \pm SD. Kruskal–Wallis test (one-sided) with Benjamini–Hochberg correction for multiple comparisons. Significant adjusted *q*-values are reported in the figure. **B** Percentage and absolute number of Ag⁺ CD8⁺ T cells. Dot plots show the percentage and absolute number of Ag⁺ CD8⁺ T cells. The central bar represents the mean \pm SD. Kruskal–Wallis test (one-sided) with Benjamini–Hochberg correction for multiple comparisons. Significant adjusted *q*-values are reported in the figure. **C** Ag⁺ CD8⁺ T cells phenotype UMAP and Heatmap. Uniform Manifold Approximation and Projection (UMAP) plot shows the 2D spatial distribution of 93,757 cells from healthy donors (HD) and MS patients treated with different DMT embedded with FlowSOM clusters. Heatmap of the median marker intensities of the 10 lineage markers across the 12 cell populations obtained with FlowSOM algorithm after the manual metacluster merging. The colors of cluster_id column correspond to the colors used to label the UMAP plot

clusters. The color in the heatmap is referred to the median of the *arcsinh* marker expression (0–1 scaled) calculated over cells from all of the samples. Blue represents lower expression, while red represents higher expression. Light gray bar along the rows (clusters) and values in brackets indicate the relative sizes of the clusters. N naive, T_{SCM} T stem cell memory, CM central memory, TM transitional memory, EM effector memory, EMRA effector memory reexpressing the CD45RA, cTfh circulating T follicular helper cells. **D** UMAP graphs stratified by therapy: healthy donors (HD); Cladribine; Dimethyl Fumarate (DMF); DMF Lymphopenic; Fingolimod; interferon 1 β (IFN); Natalizumab; Teriflunomide; Rituximab/Ocrelizumab. **E** Dot plots of different subpopulation of Ag⁺ T cells in patients treated with different DMT. The central bar represents the mean \pm SD. Kruskal–Wallis test with Benjamini–Hochberg correction for multiple. In **A–E** plots: HD: *n* = 13; Cladribine: *n* = 6; DMF: *n* = 14; DMF Lymphopenic: *n* = 9; Fingolimod: *n* = 12; IFN: *n* = 13; Natalizumab: *n* = 15; Teriflunomide: *n* = 8; Rituximab/Ocrelizumab: *n* = 11.

Ag⁺ T cells from MS patients treated with different DMT switch on different metabolic features

After *in vitro* stimulation with the SARS-CoV-2 peptide pool, the metabolism of cells expressing CD69 and CD137 within CD4⁺ and CD8⁺ T cells was investigated by using single-cell metabolic regulome profiling (scMEP), a technique that quantifies proteins that regulate metabolic pathway activity by 45-parameter mass cytometry [adapted from ref. 36]. PBMC from patients treated with different DMT were stained with 22 mAbs recognizing cell phenotype and 23 mAbs recognizing molecules involved in different metabolic pathways (see Supplementary Table 5) and analyzed by mass cytometry. We identified all major cell lineages of Ag⁺ T cells (Supplementary Figs. 14–16), and then we focused on their metabolic states (Fig. 5).

Along with their distinct functions, Ag⁺ T cell lineages also possess unique metabolic profiles which are essential for their function and maintenance. T cell activation is indeed accompanied by a switch from a metabolism mainly based upon mitochondrial respiration to a metabolism where the glycolytic flux is prevalent³⁷.

Clustering cells on the basis of the expression of proteins involved in different metabolic pathways (*i.e.*, GLUT1, MCT1, GAPDH, LDHA, HK2, PFKB4, G6PD, CytC, CS, IDH1, ATP5A, CD98, GLUT1/2, CD36, CPT1A, VDACL1, pACC, pPGC1 α , pS6, pPDK1, HIF1 α , pNRF2, pH3), we identified 10 scMEP states (Supplementary Figs. 17–19). These metabolic states spanned from cells with a quiescent or exhausted metabolism (scMEP1, 2, 3) to those with high activation of different metabolic pathways (scMEP6, 9, 10) (Fig. 5A–C). In particular, 20% of Ag⁺ T cells were characterized by the scMEP1 state, a basal level of metabolic activation (low expression of all metabolic features, except from MCT1 and CS), while 44% of Ag⁺ T cells was grouped into scMEP2 state, a metabolic quiescent/exhausted state (with very low levels of all markers except PFKB4 and CPT1A). Cells in scMEP3 state displayed high levels of GLUT1/2 and CD36, meaning that amino acid metabolism as well as fatty acid oxidation (FAO) were activated; scMEP4 state described a metabolic phenotype of pentose pathway activation (high expression of G6PD), activation of tricarboxylic acid (TCA) cycle (IDH1, ATP5A), involvement of amino acid pathway (high expression of GLUT1/2) and enhanced mitochondrial dynamics (phosphorylation of VDACL1). scMEP5 and scMEP7 states grouped cells characterized by low activation of mainly glycolysis, pentose, oxidative phosphorylation (OXPHOS) and FAO (high expression of MCT1, HK2, PFKB4, CytC, CS, CD98, GLUT1/2). A total of 20% of Ag⁺ T cells was grouped into scMEP6 (4.96%) and scMEP9 (14.88%) states, characterized by a glycolytic profile (high protein expression of HK2 and PFK4) and cell growth (pPDK1). scMEP8 represented 0.33% of Ag⁺ T cells, characterized by glycolytic activation (high expression of GLUT1, MCT1, HK2) as well as activation of amino acid pathway (CD98) and mTOR activation (pS6). Finally, 0.46% of Ag⁺ T cells clustered into scMEP10, a highly activated metabolic state where all metabolic pathways taken into account are switched on.

As far as different therapies were considered, the distribution of Ag⁺ T cell on the basis of metabolic states was different (Fig. 5D). In particular, FTY-treated patients were characterized by the lowest percentages of Ag⁺ T cells in scMEP4 and scMEP9 states, meaning that these cells do not rely on glycolysis and pentose pathway. When compared to HD, Ag⁺ T cells from DMF-treated patients (the non-lymphopenic ones) and IFN-treated ones displayed a low proportion of scMEP2, suggesting that the drug is able to reprogram metabolism.

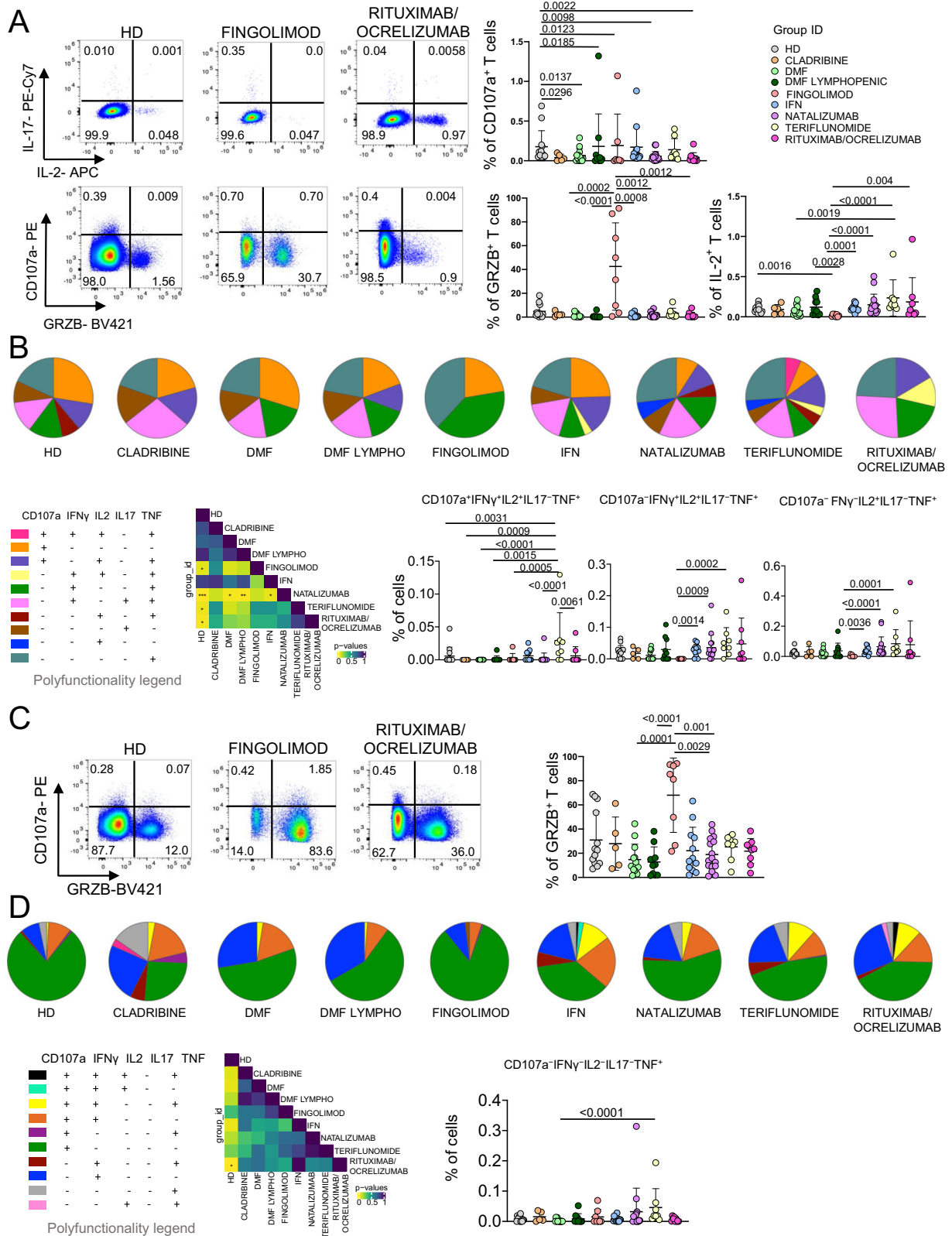
Because Ag⁺ T cell scMEP states were defined using exclusively metabolic features, we tried to associate their metabolic features with phenotypic properties (Fig. 5E). As expected, scMEP metabolic states were clearly linked to immunological phenotypes. scMEP2 state was composed by terminally differentiated (EMRA) CD8⁺ T cells expressing low level of CD27, high level of CD57 and medium level of PD-1. scMEP4 state was mainly represented by effector memory CD4⁺ T cells expressing CD27, while scMEP 9 state was composed by a small cluster of cycling. We found that a few cells were present in scMEP10, which is formed by activated (HLA-DR⁺CD38⁺) Ag⁺ CD8^{dim} T cells expressing CD57 and CD11c; such population is typically present in autoimmune diseases, is expanded in an Ag-dependent manner and mainly produce IFN- γ ³⁸.

To determine the pattern of the dynamic development of scMEP states, trajectory inference analysis has been applied (Fig. 5F). After *in vitro* stimulation, Ag⁺ T cells acquire different metabolic states starting from scMEP5, passing through highly metabolic activated state (scMEP5, 7 and 9), and reaching the final state of metabolic quiescence (scMEP1, 2 and 3).

Finally, on freshly isolated PBMC from a small subgroup of patients, we could profile the global metabolic capacities and dependencies of Ag⁺ T cells by the SCENITH assay³⁹. We found that Ag⁺ CD4⁺ T cells from IFN-treated patients displayed a higher glucose dependence when compared to HD, while natalizumab-treated patients displayed the highest glycolytic capacity (Supplementary Fig. 20).

Ag⁺ plasmablasts from FTY-treated MS patients are fully glycolytic while those from the rituximab/ocrelizumab group display a quiescent/senescent metabolism

Metabolic demands of Ag⁺ B cells are related to their functional activity. Upon stimulation, Ag⁺ B cells have a balanced increase in lactate production and oxygen consumption, with proportionally increased GLUT1 expression leading to enhance glucose uptake and mitochondrial mass⁴⁰. Moreover, their proliferation and function are regulated by HIF-1 α expression. Here, we found that Ag⁺ B cells displayed 8 different metabolic states (Fig. 6A–C and Supplementary Figs. 21–23). Approximately 5.26% of cells were classified into scMEP1, a metabolic state marked by the upregulation of GLUT1. Another 16.91% exhibited activation in TCA, ECT, signaling, and transcription, categorizing them as scMEP2. The majority, comprising over 60% of cells, fell into scMEP3, scMEP4, and scMEP6 groups. These states displayed



similar metabolic activities, excluding glycolysis. Notably, cells in the scMEP4 state exhibited elevated CD36 expression, indicating heightened activity in the fatty acid pathway. About 6.42% of Ag⁺ B cells clustered into scMEP5, characterized by reduced glycolytic activation but increased engagement in the pentose pathway, ETC, TCA, fatty acid metabolism, mitochondrial dynamics, proliferation, and signal transduction. Additionally, less than 2% of non-proliferating cells were

distributed into scMEP7 and scMEP8 states. These states exhibited low mTOR and pentose pathway activation but demonstrated glycolytic, TCA, ECT activation.

The distribution of metabolic states changed significantly across different groups, including HD and MS patients treated with DMTs (Fig. 6D). In particular, patients treated with FTY and rituximab/ocrelizumab exhibited the highest proportion of Ag⁺ B cells in scMEP1 state.

Fig. 3 | Ag⁺ CD4⁺ and CD8⁺ T cell functionality. **A** Percentage of Ag⁺ CD4⁺ T cells producing different cytokines after in vitro stimulation with SARS-CoV-2 peptides. Representative dot plots showing the percentages of CD4⁺ Ag⁺ cells producing IL-2, IL-17, CD107a and granzyme B (GRZB). Plots show mean (center bar) ± SD. Kruskal–Wallis (one-sided) test with Benjamini–Hochberg correction for multiple comparisons. **B** Polyfunctional profile of Ag⁺ CD4⁺ T cells. (Upper) Pie charts representing the proportion of Ag⁺ CD4⁺ T cells producing different combinations of CD107a, IL2, IL17, IFN γ , and TNF. Each color refers to specific polyfunctional CD4 T subpopulation as reported in the ‘polyfunctionality legend’. The far-left heatmap illustrates the statistical variances among the 9 distinct pie charts; Kruskal–Wallis test (one-sided) with Benjamini–Hochberg correction for multiple comparisons. (far-right) Dot plot reporting the percentages of Ag⁺ CD4⁺ producing different combination of cytokines. Kruskal–Wallis (one-sided) test with Benjamini–Hochberg correction for multiple comparisons. **C** Percentage of Ag⁺ CD8⁺ T cells producing different cytokines after in vitro stimulation with SARS-CoV-2 peptides. Representative dot plots of Ag⁺ CD8⁺ cells

producing CD107a and GRZB. Dot plot representing the percentage of Ag⁺ CD8⁺ T cells producing GRZB is shown, mean (center bar) ± SD. Kruskal–Wallis test (one-sided) with Benjamini–Hochberg correction for multiple comparisons.

D Polyfunctional profile of Ag⁺ CD8⁺ T cells. (Upper) Pie charts representing the percentage of Ag⁺ CD8⁺ T cells producing different combinations of CD107a, IL2, IL17, IFN γ , and TNF. Each color refers to specific polyfunctional CD8 T subpopulation as reported in the ‘polyfunctionality legend’. The far-left heatmap illustrates the statistical variances among the 9 distinct pie charts; Kruskal–Wallis test (one-sided) with Benjamini–Hochberg correction for multiple comparisons (Right) Dot plot reporting the percentage of Ag⁺ CD8⁺ CD107a IFN γ IL2 IL17 TNF population. The central bar represents the mean ± SEM. Kruskal–Wallis test with Benjamini–Hochberg correction for multiple comparisons was used to test the differences among the nine groups. In **A–C** plots: HD healthy donors ($N=13$); Cladribine ($N=6$); DMF Dimethyl Fumarate ($N=14$); DMF Lymphopenic: Dimethyl Fumarate Lymphopenic ($N=9$); Fingolimod ($N=12$); IFN Interferon 1β ($N=13$); Natalizumab ($N=15$); Teriflunomide ($N=8$); rituximab/ocrelizumab ($N=11$).

However, they showed a lower percentage of cells in scMEP3 compared to patients treated with natalizumab. Those treated with rituximab/ocrelizumab displayed the lowest percentage of cells in scMEP4. As far as the phenotype of these B cells is concerned, plasmablasts constituted most of cells in scMEP1, scMEP7 and scMEP8; memory B cells were grouped in scMEP3 and scMEP4; recently activated Ag⁺ B cells were in scMEP2 while atypical B cells (atBC) were in scMEP5 (Fig. 6E). These results are in line with the clustering performed by using both lineage and metabolic markers (Supplementary Figs. 24–25).

As for Ag⁺ T cell, we determined the dynamic development of scMEP states by using trajectory inference analysis (Fig. 6F). After in vitro stimulation, Ag⁺ B cells acquired different metabolic states starting from scMEP2, passing through mid-metabolic activated state (scMEP3, 4 and 5), reaching the final state of highly metabolic activation (scMEP7, 8 and 1).

Finally, due to limited cell number, we could use the SCENITH assay on freshly isolated PBMC only from a limited number of patients treated with different DMT. We found that Ag⁺ B cells from natalizumab-treated patients displayed a trend of higher glycolytic capacity when compared to HD (Supplementary Fig. 26). Even the results are not statistically significant, this observed trend seems to confirm what we have found by the scMEP.

FTY- and natalizumab-treated patients develop a different antigen-specific immune response

In order to describe an immunological signature indicating how different DMT could shape Ag-specific immunity and protection against SARS-CoV-2, we took advantage of the use of the principal component analysis (PCA)⁷. Based on the first two PCs, PCA revealed that only FTY- and natalizumab-treated patients develop a clearly different quality of the Ag-specific immune response ($p < 0.05$, Fig. 7A), forming separate clusters, while all other groups (also including the rituximab/ocrelizumab one) displayed similar immunological features even when compared to HD.

As shown in Fig. 7A, FTY-treated patients form a cluster on the left side of PC1 (whose weight was 13.9%) while natalizumab-treated patients are on the right side. Figure 7B reveals that the main responsible of this division were the immunological features more represented in FTY-treated patients, such as: Ag⁺ cytotoxic CD4⁺ and CD8⁺ T cells (expressing CD107a and Granzyme), cells in scMEP2 (quiescent metabolic state), Ag⁺ T cells expressing of CD57 and PD-1 (indicating senescence and exhaustion/activation). On the contrary, the main features responsible for the clusterization of natalizumab-treated patients were the absolute number of Ag⁺ B and Ag⁺ CD4⁺ T cells, the number of B and CD8⁺ T cells, the marked shift of Ag⁺ T cell towards Th1 phenotype, and more marked metabolic status in B cells (scMEP3).

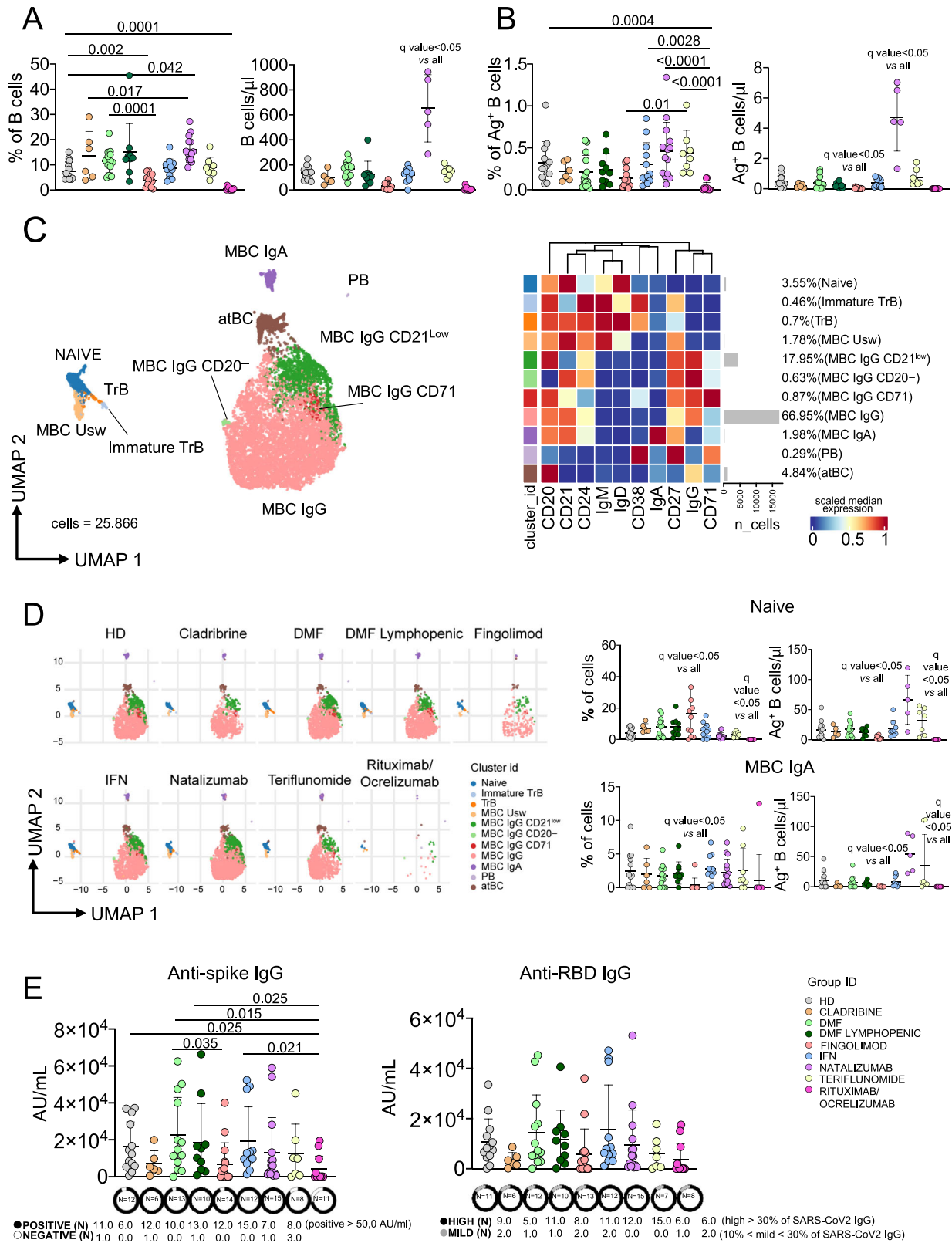
To better point out the distinctive features of the immune response in patients undergoing treatment with natalizumab or FTY, we employed PCA specifically on these patient groups (Fig. 7C, left panel). FTY patients are divided from patients treated with natalizumab according to PC1 (26.5%). Besides the aforementioned immunological features responsible for the different clusterization, also that different metabolic engagement by Ag⁺ B cells was responsible for the division (Fig. 7C, right panel). Indeed, FTY-treated patients displayed higher percentage of glycolytic Ag⁺ B cells in scMEP1 and scMEP7 states together with higher percentage of Ag⁺ T cells in scMEP2, characterized by low level of all metabolic markers, except from PFKFB4 and CPT1A.

High percentage of Ag⁺ T cells in scMEP10 and scMEP7 as well as a high percentage of Ag⁺ B cells in scMEP1, scMEP2 and scMEP5 predict protection from SARS-CoV2-breakthrough infection

Accurate identification of phenotype-relevant subsets from heterogeneous cell populations is crucial to delineate an immunological signature that could predict protection from breakthrough infections. To pursue this, and to identify subpopulations that could be associated with categorical or continuous phenotypes from single-cell data, we used a supervised learning framework called ‘‘phenotype-associated subpopulations from single-cell data’’ (PENCIL), based on rejection strategy learning⁴¹. Using this classification mode, we interrogated subpopulations of Ag⁺ T and B cells that were associated with individuals that experienced symptomatic SARS-CoV-2 infection after the third dose of vaccine.

A total of 18 individuals (MS patients and HD, as reported in Supplementary Data 1) experienced SARS-CoV-2 infection within 6 months from the last dose of vaccine. Taking into consideration data from Ag⁺ T cells analyzed with scMEP, we performed the prediction analysis (see Methods). PENCIL revealed that high percentages of Ag⁺ T cells grouped into scMEP7 (effector memory CD4⁺CD27⁺PD-1^{dim}CD57^{dim}) and scMEP10 (mainly formed by CD8^{dim}CD11c⁺ T cells with almost all metabolic pathways activated and by T cell, also expressing PD-1 and CD57) were associated with absence of SARS-CoV-2 infection, meaning that these clusters of cells can confer high immune protection. On the contrary, a high percentage of cells grouped into scMEP9 (CD4⁺ TM) and scMEP2 (either CD4 or CD8, either EM or EMRA, expressing PD-1 and CD57 with a metabolically resting phenotype) were associated with the onset of a SARS-CoV-2 breakthrough infection (Fig. 8A, B). To validate this prediction, patients and HD were stratified by therapy and we observed that high percentage of scMEP2 (in the case of HD and IFN-treated individuals) and scMEP9 (in rituximab/ocrelizumab group) were associated with breakthrough infection (Supplementary Fig. 27).

Then, Ag⁺ B cells that underwent scMEP analysis were interrogated by PENCIL (see Methods). PENCIL indicated that a high percentage of scMEP1 (not proliferating plasmablasts, highly glycolytic),



scMEP2 cells (i.e., recently activated naïve B cells with activated mitochondrial metabolism), and scMEP5 cells (atypical B cells, coupled with activation of all metabolic pathways) predict protection from SARS-CoV-2 infection. On the contrary, a high percentage of cells grouped into scMEP3 (memory B cells, PD-1^{dim}) predict SARS-CoV-2 infection (Fig. 8C, D). We validate this prediction as performed with Ag⁺ T cells. Even if not significant for the low number of cells and

patients, high percentage of scMEP3 (as in the case of HD, Natalizumab and rituximab/ocrelizumab) can predict breakthrough infection (Supplementary Fig. 27).

Discussion

The aim of this study was to ascertain whether COVID-19 vaccinated patients affected by the relapsing-remitting form of multiple sclerosis

Fig. 4 | Ag⁺ B cell landscape. **A** Dot plot shows the total percentage and the absolute number of CD19⁺ B cells. The central bar represents the mean \pm SD. Kruskal–Wallis test (one-sided) with Benjamini–Hochberg correction for multiple comparisons. **B** Dot plot shows the percentage and absolute number of antigen-specific CD19⁺ B cells. The central bar represents the mean \pm SD. Kruskal–Wallis test (one-sided) with Benjamini–Hochberg correction for multiple comparisons was used to test the differences among the nine groups. **C** UMAP plot shows the 2D spatial distribution of 25,866 antigen-specific B cells from healthy controls (HD) and patients with Multiple Sclerosis embedded with FlowSOM clusters. Heatmap of the median marker intensities of the 10 lineage markers across the 11 cell populations obtained with FlowSOM algorithm after the manual metacluster merging. The colors of cluster_id column on the left correspond to the colors used to label the UMAP plot clusters. Each color in the heatmap is referred to the median of the arcsinh marker expression (0–1 scaled) calculated over cells from samples. Blue represents lower expression, while red represents higher expression. Light gray

histogram bar and values indicate the relative sizes of the clusters. Naive; TrB, transitional B cells; MBC Unsw, memory B cell unswitched; MBC memory B cell, PB plasmablasts, atBC atypical B cell. **D** (Left) UMAP graphs stratified by therapy. (Right) Dot plot showing the percentages and absolute numbers of naive and MBC IgA B cells. The central bar represents the mean \pm SD. Kruskal–Wallis test (one-sided) with Benjamini–Hochberg correction for multiple comparisons was used to test the differences among the nine groups. **E** Anti-spike and anti-RBD IgG concentrations in plasma samples from HD and MS treated groups. The central bar represents the mean \pm SD. Kruskal–Wallis test (one-sided) with Benjamini–Hochberg correction for multiple comparisons. Adjusted *P*-values are indicated in the figure. Plots **A–E** HD healthy controls (*N* = 13); Cladribine (*N* = 6); DMF: Dimethyl Fumarate (*N* = 14); DMF Lymphopenic: Dimethyl Fumarate Lymphopenic (*N* = 9); Fingolimod (*N* = 12); IFN: Interferon β (*N* = 13); Natalizumab (*N* = 15); Teriflunomide (*N* = 8); Rituximab/Ocrelizumab (*N* = 11).

and receiving different MS-treatments would mount an effective T and B cell response against SARS-CoV-2. For this reason, we have used different approaches and techniques mainly based on flow and mass cytometry, to carefully investigated cell phenotype, function and metabolism.

Several observational studies evaluating the effectiveness of COVID-19 vaccines in MS patients treated with DMT showed that most of these drugs allow for mounting a protective immune response, at least in terms of antibody production and production of antigen-specific B and T cells, even if some patients can experience a reduced immune response. However, an immune signature associated with the phenotype and function of Ag⁺ T and B cells that could suggest the existence of a predisposition to breakthrough infection in MS patients has never been investigated.

Here, we show that nearly 6 months after the third SARS-CoV-2 vaccine dose, the overall SARS-CoV-2-specific T and B cell response in relapsing-remitting MS patients treated with different drugs was similar among all patients and healthy donors, except for those treated with FTY or natalizumab, whose cells displayed totally different immunological features as well as a diverse immunometabolic engagement.

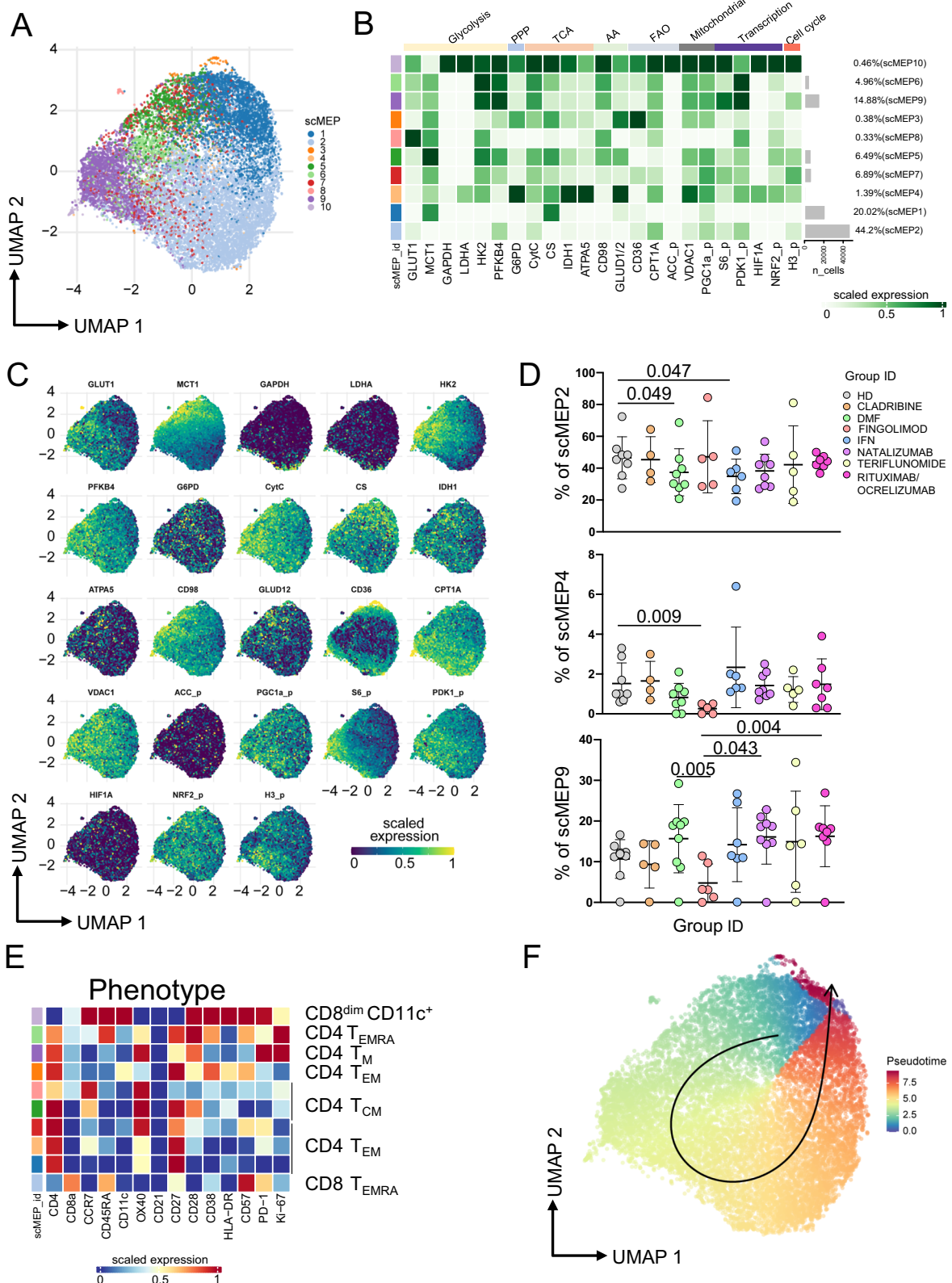
In the case of FTY-treated patients, we saw that phenotype, function, and metabolism of Ag⁺ T and B cells seemed to mimic the characteristic of an aged immune system. Indeed, these patients were characterized by high proportions of effector memory T cells expressing PD-1 and CD57; CD4⁺ T cells producing granzyme; Ag⁺ T cells with low polyfunctional profile; decreased percentages of Ag⁺ B cells. Moreover, most Ag⁺ T and B cells display a glycolytic metabolism which might constitute a rescue mechanism to maintain an activated and functional phenotype when metabolism is skewed due to the possible, well known age-dependent mitochondrial impairment^{42,43}.

The immune system of MS patients is characterized by a premature aging⁴⁴, and DMT can cause drastic changes that worsen or even accelerate immune senescence long after the drug has been stopped⁴⁵. The effects of cell depleting agents are not readily reversible, and even those of therapies primarily targeting cell migration such as natalizumab and FTY may long lasting effects. Aging of the immune system involves not only a decreased production of naive T cells, but also an increase in terminally differentiated late effector memory T cells determining a narrowing of the T cell repertoire^{46,47}, with an increase in the level of activation and cytotoxicity⁸. Aging decreases B cell differentiation in the bone marrow and the output of mature B cells, induces a redistribution of B cell subsets in the periphery with a significant increase in frequencies and numbers of proinflammatory B cells, decreases the expression of molecules involved in Ig class-switch recombination and somatic hypermutation, two processes leading to the generation of high-affinity protective antibodies as well as germinal center formation, and decreases B cell repertoire diversity^{5,48}. These phenotypic and functional alterations

are strictly connected to age-associated metabolic changes that impact the bioenergetic program of T and B cells at discrete phases of development and activation⁴⁹. Glycolysis and LDH activity are reduced in aged T cells⁵⁰ and mitochondrial dysfunction is one of the main hallmarks of aged T cells, that are characterized by smaller or dysfunctional mitochondria characterized by a decreased respiration rate and ATP production³⁷.

We found that MS patients treated with different DMT display a different phenotype of Ag⁺ T and B cells. It has been shown that some effects of FTY, DMF and rituximab/ocrelizumab resemble immunosenescence, as they cause a decrease in total B and T cells and induce a negative regulation of Th1 and Th17 differentiation while promoting Th2 differentiation⁵¹. FTY not only modulates lymphocyte trafficking, but also modulates the composition of B and T cells subsets, with an increase of circulating effector memory T cells and decrease of naive T cells. On the contrary, natalizumab induces an increase in total T cells (including Th1 and Th17), total B cells, memory B cells, but alter the proportion of plasmablasts which have high expression of CD49d^{45,52}. Moreover, most Ag⁺ B cells of natalizumab-treated patients were metabolically quiescent. Natalizumab binds CD49d (integrin $\alpha 4$) which is also a molecule expressed during cell activation⁵³. Given that natalizumab prevents this phenomenon, likely it also prevents metabolic activation of B cells and their capability to differentiate and produce antibodies. The metabolic pathways within immune cells regulate the formation of antigen-specific immune and its cell function. Indeed, metabolic pathways can influence the development of various T helper subsets. For example, Treg cells predominantly depend on OXPHOS and mitochondrial FAO for development and survival, whereas the generation of Th17 cells requires glycolysis⁵⁴. Here, for the first time, by applying a method based upon mass cytometry, we confirm how different therapies are able to modify the metabolic profiles of circulating antigen-specific cells.

Assessing the molecular and cellular state of the immune system after vaccination, by adopting data-driven models, could be used to predict pathogen-specific immune responses or the prevention of breakthrough infection. The goal is to identify key immune signatures that are responsible for the creation of an effective immune response. Systems-biology analyses of influenza virus vaccination have identified antibody response predictors, these have been based on post-vaccination parameters, such as the magnitude of plasmablast increases on day 7, and changes in blood host-derived transcripts on days 1–3 after vaccination^{55,56}. Moreover, certain immune signatures can predict not only the response to malaria vaccination, but the clinical outcomes of acute infection^{57,58}. Then, we applied for the first time to mass cytometry data a prediction approach like PENCIL, that is typically used to analyze single cell transcriptome. We found that predominance of metabolically active Ag⁺ CD4⁺, CD27⁺, PD-1^{dim} CD57^{dim} T cells and CD8^{dim}, CD11c⁺ Ag⁺ T cells correlates with the absence of breakthrough infection and may thus confer high immune protection.



In addition, high percentage of non-proliferating, Ki67⁺ plasmablasts, highly glycolytic, recently activated naïve B cells with activated mitochondrial metabolism and metabolically activated atypical B cells predict protection from SARS-CoV-2 infection. This may indicate these cells are able to recognize antigens but do not to properly react and mount a specific response, paving the way to approaches to increase the effectiveness of vaccination.

Questions regarding how much the immune signature before vaccination influence the creation of a protective immune response needs to be elucidated and how much these immunological signatures are similar across different populations (young, elderly, pregnant, different ethnicities) need to be investigated.

The study has some limitations. First, the number of patients per group is relatively small, and the investigation is cross-sectional.

Fig. 5 | Ag⁺ T cell metabolic states. **A** Uniform Manifold Approximation and Projection (UMAP) plot shows the 2D spatial distribution of 107,522 cells from HD and MS patients. UMAP dimensionality reduction is calculated using sampled data from all cells and all available metabolic features; through FlowSOM clustering are identified 10 different clusters, defined as scMEP. Cells are colored by their scMEP state. **B** Heatmap of the median marker intensities of the 23 metabolic markers across the 10 cell populations, obtained with FlowSOM algorithm. The colors of cluster_id column correspond to the colors used to label the UMAP plot clusters/scMEP. The color in the heatmap is referred to the median of the arcsinh marker expression (0–1 scaled): white represents a lower expression, while dark green represents a higher expression. Light gray bar along the rows (clusters/scMEP) and values in percentages indicate the relative sizes of the clusters. **C** Projection of UMAP graphs stratified by HD and all different MS patients. **D** Representative dot

plots showing percentages of scMEP2, scMEP4 and scMEP9 among different Group_IDs. The central bar represents the mean \pm SD. Kruskal–Wallis test (one-sided) with Benjamini–Hochberg correction for multiple comparisons is used to test the differences among groups. Adjusted *q*-values are reported in the figure, if significant. healthy donors (HD, *n* = 8), multiple sclerosis patients treated with Cladribine (*n* = 4), Dimethyl Fumarate (DMF, *n* = 8), Fingolimod (*n* = 5), interferon β (IFN, *n* = 6), Natalizumab (*n* = 8), Teriflunomide (*n* = 5), Rituximab/Ocrelizumab (*n* = 7). **E** Heatmap of 14 immunological markers enrichment modeling (not used for metabolic clustering) across different scMEP states, showing the relationship between metabolic states and functional properties. Light gray bar along the rows (clusters/scMEP) and values in percentages indicate the relative sizes of the clusters/scMEP. **F** Pseudotime visualization of scMEP development based on the estimated trajectory and envisaged in UMAP space.

However, considering the parameters that we have investigated, all groups were homogeneous and there were no outliers. Second, given that the exposure to SARS-CoV-2 was not controlled, the results from prediction analysis should therefore be considered preliminary and subject to further validation. However, our findings suggest that only FTY and natalizumab modify significantly (in terms of phenotype and metabolic status) the SARS-CoV-2-specific B and T cell composition after vaccination.

Methods

Patient's selection

Demographic and clinical characteristics of 93 MS patients and 13 healthy donors (HD), the type of DMT at the time of vaccination, the type of third dose vaccine and median range of time to last administration, prior COVID-19 infection status, and relevant comorbidities are shown in Supplementary Data 1. Patients were eligible for inclusion if they met the following criteria: (a) a confirmed diagnosis of Relapsing-Remitting Multiple Sclerosis (RRMS), and (b) a history of treatment with FTY, dimethyl fumarate, natalizumab, or teriflunomide for a minimum of six months, or having undergone at least two infusion cycles with rituximab or ocrelizumab or completed at least one full cycle of cladribine. Patients on ocrelizumab or rituximab, as per routine clinical practice, underwent SARS-CoV-2 vaccination at least 6 weeks before subsequent infusion or at least 3 months after the last infusion. Exclusion criteria comprised treatment with steroids during the preceding six weeks and a history of COVID-19 before vaccination.

Blood collection and isolation of mononuclear cells

Up to 30 mL of blood were collected from each patient in vacuettes containing ethylenediamine-tetraacetic acid (EDTA). Blood was immediately processed. Isolation of peripheral blood mononuclear cells (PBMC) was performed using ficoll-hypaque according to standard procedures. For all experiments, except those related to metabolic investigation, PBMC were stored in liquid nitrogen in fetal bovine serum (FBS) supplemented with 10% dimethyl sulfoxide (DMSO). For metabolic investigation, PBMC were used immediately after isolation. Plasma was stored at -80°C until use. The study was reviewed and approved by each participant, including healthy donors, provided informed consent according to Helsinki Declaration, and all uses of human material have been approved by the local Ethical Committee (Comitato Etico dell'Area Vasta Emilia Nord, protocol number 199/2022, May 24th, 2020) and by the University Hospital Committee (Direzione Sanitaria dell'Azienda Ospedaliero Universitaria di Modena, protocol number 5974, February 24th, 2023). The patients/participants provided their written informed consent to participate in this study.

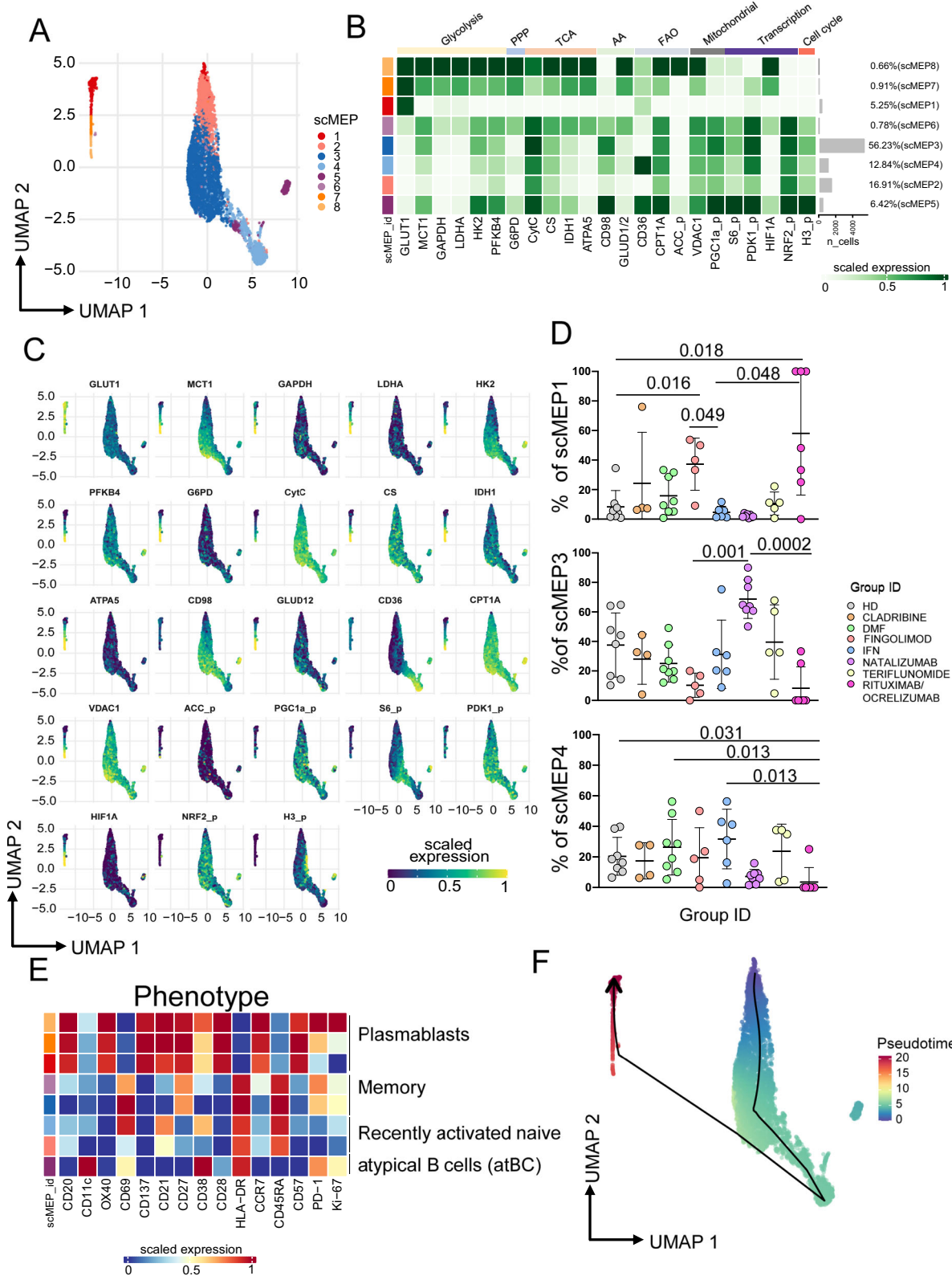
Activation induced cell marker assay (AIM) and T cell phenotype

Isolated PBMCs were thawed and rested for 6 h. After resting, CD40-blocking antibody (0.5 mg/ml final concentration) (Miltenyi Biotec,

Bergisch Gladbach, Germany) was added to the cultures 15 min before stimulation. PBMCs were cultured in 96-well plate in the presence of 15-mer peptides with 11-amino acids overlap, covering the complete sequence of Wuhan SARS-CoV-2 Spike glycoprotein (PepTivator SARS-CoV-2 Prot_S complete, Miltenyi Biotec, Bergisch Gladbach, Germany) together with 1 $\mu\text{g}/\text{mL}$ of anti-CD28 (Miltenyi Biotec, Germany). PBMCs were stimulated for 18 h at 37°C in a 5% CO_2 atmosphere in complete culture medium (RPMI 1640 supplemented with 10% fetal bovine serum and 1% each of L-glutamine, sodium pyruvate, nonessential amino acids, antibiotics, 0.1 M HEPES, 55 μM β -mercaptoethanol). For each stimulated sample, an unstimulated one was prepared, as negative control. After stimulation, cells were washed with PBS and stained with PromoFluor IR-840 (Promokine, PromoCell, Heidelberg, Germany) for 20 min at room temperature (RT). Next, cells were washed with FACS buffer (PBS supplemented with 2% FBS) and stained with the following fluorochrome-labeled mAbs: CXCR5-BUV661, CCR6-BUV496, CXCR3-BV785 for 30 min at 37°C . Finally, cells were washed with FACS buffer and stained for 20 min at RT with Duraclone IM T cell panel (Beckman Coulter, Brea, CA) containing CD45-Krome Orange, CD3-APC-A750, CD4-APC, CD8-AF700, CD27-PC7, CD57-Pacific Blue, CD279 (PD1)-PC5.5, CD28-ECD, CCR7-PE, CD45RA-FITC and added with other three fluorescent mAbs i.e., CD69-BV650, CD137-BUV395 and CD95-BV605. Samples were acquired on a CytoFLEX LX flow cytometer (Beckman Coulter). All reagents used for T cell phenotyping are listed in Supplementary Table 1. All mAbs added to DuraClone IM T cells were previously titrated on human PBMCs and used at the concentration giving the best signal-to-noise ratio. The gating strategies used to identify $\text{CD}4^{+}$ and $\text{CD}8^{+}$ T cells are reported in the Supplementary Figs. 1 and 4.

Detection of SARS-CoV-2-specific B cells

Thawed PBMC were washed twice with RPMI 1640 supplemented with 10% fetal bovine serum and 1% each of L-glutamine, sodium pyruvate, nonessential amino acids, anti-biotics, 0.1 M HEPES, 55 μM β -mercaptoethanol and 0.02 mg/ml DNase. PBMC were washed with PBS and stained using viability marker PromoFluor IR-840 (Promokine, PromoCell, Heidelberg, Germany) for 20 min at RT in PBS. Next, cells were washed with PBS and stained for 15 min at RT with streptavidin-AF700 (decoy channel; ThermoFisher Scientific, USA) to remove false positive SARS-CoV-2-specific B cells. After washing with FACS buffer, cells were stained with biotinylated full-length SARS-CoV-2 spike protein (R&D Systems, Minneapolis) labeled with different streptavidin-fluorophore conjugates. Full-length biotinylated spike protein was mixed and incubated with streptavidin-BUV661 (Becton Dickinson) or streptavidin-BV650 (BioLegend) at a 6:1 mass ratio for 15 min at RT. All samples were stained with both biotinylated streptavidin for 1 h at 4°C . Then, cells were washed with FACS buffer and stained for 20 min at RT with DuraClone IM B cells (Beckman Coulter, Brea, CA) containing the following lyophilized directly conjugated mAbs: anti-IgD-FITC, CD21-PE, CD19-ECD, CD27-PC7, CD24-APC, CD38-AF750, anti-IgM-PB, CD45-KrO to which following drop-in antibodies were added: CD71-BUV395,



CD20-BV785, anti-IgG-BUV496 and anti-IgA-PerCP-Vio700. Samples were acquired on a CytoFLEX LX flow cytometer (Beckman Coulter). A minimum of 1,000,000 cells per sample were acquired. All reagents used for B cell phenotype are reported in Supplementary Table 3. All mAbs added to DuraClone IM B cells were previously titrated on human PBMCs and used at the concentration giving the best signal-to-

noise ratio. The gating strategy used to identify Ag⁻ and Ag⁺ B cells is reported in the Supplementary Fig. 11.

Intracellular cytokine staining (ICS)

Isolated PBMCs were thawed and rested for 6 h. PBMCs were stimulated in the presence of a pool of lyophilized peptides covering

Fig. 6 | Ag⁺ B cell metabolic states. **A** Uniform Manifold Approximation and Projection (UMAP) plot shows the 2D spatial distribution of 9,780 cells from HD and MS patients. UMAP dimensionality reduction is calculated using sampled data from all cells and all available metabolic features; through FlowSOM clustering are identified 8 different clusters, defined as scMEP. Cells are colored by their scMEP state. **B** Heatmap of the median marker intensities of the 23 metabolic markers across the 8 cell populations, obtained with FlowSOM algorithm. The colors of cluster_id column correspond to the colors used to label the UMAP plot clusters/scMEP. The color in the heatmap is referred to the median of the arcsinh marker expression (0–1 scaled): white represents a lower expression, while dark green represents a higher expression. Light gray bar along the rows (clusters/scMEP) and values in percentages indicate the relative sizes of the clusters. **C** Projection of UMAP graphs stratified by HD and all different MS patients. **D** Representative dot plots showing percentages of scMEP1, scMEP3 and scMEP4 among different

Group_IDs. The central bar represents the mean \pm SD. Kruskal–Wallis test (one-sided) with Benjamini–Hochberg correction for multiple comparisons is used to test the differences among groups. Adjusted *q*-values are reported in the figure, if significant. healthy donors (HD, *n* = 8), multiple sclerosis patients treated with Cladribine (*n* = 4), Dimethyl Fumarate (DMF, *n* = 8), Fingolimod (*n* = 5), IFN (*n* = 6), Natalizumab (*n* = 8), Teriflunomide (*n* = 5), Rituximab/Ocrelizumab (*n* = 7). **E** Heatmap of 15 immunological markers enrichment modeling (not used for metabolic clustering) across different scMEP states, showing the relationship between metabolic states and functional properties. Light gray bar along the rows (clusters/scMEP) and values in percentages indicate the relative sizes of the clusters/scMEP. **F** Pseudotime visualization of scMEP development based on the estimated trajectory and envisaged in UMAP space. Colors are representative of the different distribution of cells population: blue represents less active metabolic state, while red represents an increased/enhanced metabolic state.

the complete protein coding sequence (aa 5–1273) of spike glycoprotein (“S”) of SARS-CoV-2 (PepTivator SARS-CoV-2 Prot_S Complete Miltenyi Biotec, Bergisch Gladbach, Germany) together with 1 μ g/ml of anti-CD28/49d (Becton Dickinson). PBMCs were stimulated for 16 h at 37 °C in a 5% CO₂ atmosphere in complete culture medium (RPMI 1640 supplemented with 10% FBS and 1% each of L-glutamine, sodium pyruvate, non-essential amino acids, antibiotics, 0.1 M HEPES, 55 mM β -mercaptoethanol, and 0.02 mg/mL DNase I). For each stimulated sample, an unstimulated one was prepared as a negative control. All samples were incubated with protein transport inhibitors brefeldin A (Golgi Plug, Becton Dickinson Bioscience, San Jose, CA, USA) and monensin (Golgi Stop, Becton Dickinson Bioscience, San Jose, CA, USA) and previously titrated concentration of CD107a-PE (BioLegend, San Diego, CA, USA). After stimulation, cells were washed with PBS and stained with LIVE/DEAD fixable Aqua (ThermoFisher Scientific, USA) for 20 min at RT. Next, cells were washed with FACS buffer and stained with surface mAbs recognizing CD3-PE.Cy5, CD4-AF700, and CD8-APC.Cy7 (BioLegend, San Diego, CA, USA). Cells were washed with FACS buffer and fixed and permeabilized with the Cytofix/Cytoperm buffer set (Becton Dickinson Bioscience, San Jose, CA, USA) for cytokine detection. Then, cells were stained with previously titrated mAbs recognizing IL-17-PE-Cy7, TNF-BV605, IFN- γ -FITC, IL-2-APC, and GRZB-BV421 (all mAbs from BioLegend, San Diego, CA, USA). Samples were acquired on an Attune NxT acoustic cytometer (ThermoFisher Scientific, USA). Supplementary Table 2 reports mAb titers, clones, catalog numbers, and type of fluorochrome used in the panel.

Gating strategy used to identify and analyze the intracellular cytokine production of CD4⁺ and CD8⁺ T lymphocytes is reported in Supplementary Fig. 7.

Computational analysis of flow cytometry data

T cell analysis. Compensated Flow Cytometry Standard (FCS) 3.0 files were imported into FlowJo software version v10.7.1 and analyzed by standard gating to remove doublets, aggregates and dead cells. For ex vivo immunophenotyping of non-antigen-specific (Ag⁻) and antigen-specific (Ag⁺) T cells of both CD4⁺ and CD8⁺ we analyzed only the data of stimulated samples. For each sample, we therefore selected data from all living CD4⁺ or CD8⁺ T cells and imported them in R using flowCore package v2.4.0 for a total of 37,397,203 CD4⁺ T cells (of which 465,729 were SARS-CoV-2 specific) and 12,758,008 CD8⁺ T cells (of which 180,267 were SARS-CoV-2 specific). The further analysis was performed using CATALYST v1.17.3. All data obtained by flow cytometry were transformed in R using hyperbolic arcsine “arcsinh (x/cofactor)” applying manually defined cofactors (where x is the fluorescence measured intensity value). Clustering and dimensional reduction were performed using FlowSOM (version 2.4.0) and UMAP (version 0.2.8.0) algorithms, respectively. The Ag⁺ CD4⁺ and CD8⁺ T cell clusters have been analyzed using the following markers: CD45RA, CCR7, CD27, CD28, PD-1, CCR6, CXCR3, CXCR5 and CD95. The quality

control (QC) of clustering for CD4⁺ and CD8⁺ T cells is reported in the respective Supplementary Figs. 2 and 5.

B cell analysis. Compensated Flow Cytometry Standard (FCS) 3.0 files were imported into FlowJo software version v10.7.1 and analysed by standard gating to remove doublets, aggregates, dead cells, and identify CD19⁺ B cells. From total CD19⁺ B cells, to remove false positive SARS-CoV-2-specific B cells we eliminated decoy-positive B cells. For each sample, we selected the SARS-CoV-2-specific B cells as positive cells for both Spike_streptavidin-BUV661 and Spike_streptavidin-BV650 and now referred to as Ag⁺ B cells. The remaining double negative cells were non-SARS-CoV-2-specific B cells and mentioned to as Ag⁻ B cells. Then, we exported for each sample separately both Ag⁺ and Ag⁻ B cells and imported them in R using flowCore package v2.4.0. The unsupervised analysis was performed using CATALYST v1.17.3. All data were transformed in R using hyperbolic arcsin (arcsinh x/cofactor) applying manually defined cofactors. Clustering and dimensional reduction were performed using FlowSOM and UMAP algorithms, respectively. For each day of acquisition at CytoFLEX LX, we had a sample used as quality control (QC).

Mass cytometry

scMEP staining protocol. Thawed PBMCs were washed twice with RPMI 1640 supplemented with 10% fetal bovine serum and 1% each of L-glutamine, sodium pyruvate, nonessential amino acids, antibiotics, 0.1 M HEPES, 55 μ M β -mercaptoethanol and 0.02 mg/ml DNase. PBMCs were washed with Maxpar PBS and stained for 5 min at 37 °C with a working solution of the pre-titrated Cell-ID Cisplatin-195Pt in Maxpar PBS. For quenching the cisplatin stain, PBMCs were washed twice with Maxpar Cell Staining Buffer, using at least 5x the volume of the cell suspension. After that, PBMCs were stained with 100 μ l of 1x Surface mAb Mix (see Supplementary Table 5 for all reagents used) at room temperature for 15 min. Samples were gently vortexed and incubated at room temperature for additional 15 min. Following the incubation, cells were washed twice by adding 2 mL Maxpar Cell Staining Buffer to each tube, centrifuged at 300 \times g for 5 min, and supernatant was removed by aspiration, leaving a residual volume about 100 μ L. For each sample, the pellet was thoroughly disrupted by pulse vortex. Cells were prepared for nuclear staining, 1 mL of Foxp3 Fixation/Permeabilization working solution was added to each sample, and they were incubated for 30 min at 4 °C, protected by light. Then, 2 mL of 1X Permeabilization Buffer were added to each samples' tube and centrifuged at 400–600 \times g for 5 min at room temperature. PBMCs were stained with 100 μ l of 1x Nuclear mAb Mix and incubate for at least 30 min at 4 °C. Cells were subsequently washed twice; a first time with 2 mL of 1X Permeabilization Buffer and a second time with 2 mL of Maxpar Cell Staining Buffer. Samples were placed on ice for 10 min to chill. Then, 1 mL of 4 °C methanol was added, samples were mixed gently, and incubated on ice for further 15 min. PBMCs were washed twice with 2 mL of Maxpar Cell Staining

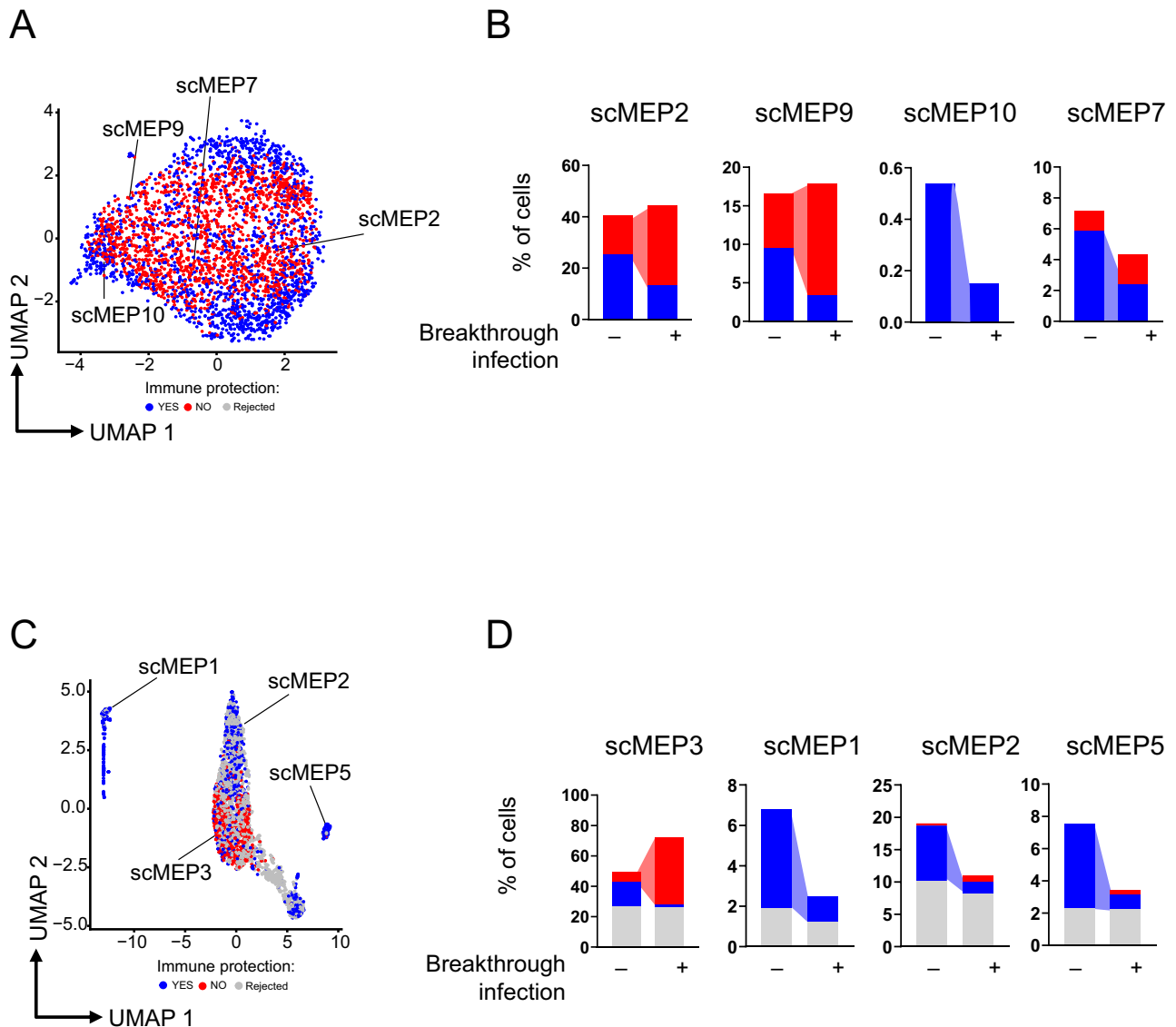


Fig. 8 | PENCIL prediction of Ag⁺ T and B cell subpopulations associated with SARS-CoV-2 breakthrough infection. A UMAP visualization displaying the Ag⁺ T cells from specific scMEP clusters. **B** Bar plot illustrating the percentage of cells within the scMEP clusters, whether associated or not with immune protection, among patients experiencing or not SARS-CoV-2 breakthrough infections. **C** UMAP visualization displaying the Ag⁺ B cells from specific scMEP clusters. **D** Bar plot

illustrating the percentage of cells within the scMEP clusters, whether associated or not with immune protection, among patients experiencing or not SARS-CoV-2 breakthrough infections. In gray: not assigned cells (Rejected); in blue: cells associated with immune protection (YES); in red: cells not associated with immune protection (NO).

Buffer, centrifuged at $800 \times g$ for 5 min, and supernatants were removed by aspiration. PBMCs were then stained with 100 μ l of 1x Phospho-Mix and incubated for 30 min at room temperature. Cells were washed twice by adding 2 mL Maxpar Cell Staining Buffer to each tube, centrifuged at $800 \times g$ for 5 min, and supernatants were removed by aspiration, leaving a residual volume about 100 μ l. It was essential to thoroughly disrupt the pellet by pulse vortex, before adding 1 mL of the 1.6% formaldehyde solution to each tube. After gently mixing, PBMCs were incubated at room temperature for 10 min. When incubation was completed, cells were centrifuged at $800 \times g$ for 5 min and supernatant was removed by aspiration. One mL of Cell-ID Intercalation solution was then added to each sample and gently vortex. Samples were incubated at 4 $^{\circ}$ C overnight. After centrifuging tube at $800 \times g$ for 5 min, each pellet was resuspended in the residual volume of iridium fix/perm solution and transferred into a labeled 1.5 mL microcentrifuge tube ready to be stored at -80° C.

After thawing in Maxpar cell staining buffer (CSB), cells were washed twice with CSB. Prior to acquisition cells were also washed with Maxpar cell acquisition solution (CAS). Immediately before acquisition, cells were resuspended to a final concentration of 10^6 /ml in CAS with EQ Passport beads (1:10 dilution) and acquired on the HeliosTM system (Standard Biotoools, South San Francisco, CA, USA). Acquisition rate was constantly monitored at 350 to 400 events/sec, to minimize ion cloud fusion and maximize data quality. Acquired data were normalized using Passport beads (Fluidigm/Standard Biotoools method) with CyTOF software (version 10.7.1014).

SCENITH assay on SARS-CoV-2-specific B cells. Freshly isolated PBMCs were rested overnight in RPMI 1640 supplemented with 10% FBS and 1% each of L-glutamine, sodium pyruvate, nonessential amino acids, antibiotics, 0.1 M HEPES, 55 mM β -mercaptoethanol. After resting, cells were washed with PBS and stained with biotinylated full-length SARS-CoV-2 spike protein (R&D Systems, Minneapolis, USA)

labeled with different streptavidin fluorophore conjugates. Full-length biotinylated spike protein was mixed and incubated with streptavidin-BUV661 (Becton Dickinson) or streptavidin-BV650 (BioLegend) at a 6:1 mass ratio for 15 min at room temperature (RT). PBMCs were stained with both biotinylated streptavidin at 4 °C for 1 h. Then, cells were washed at 1000 rpm for 7 min and resuspended in complete medium at a density of $1 \times 10^6/0.1$ ml and incubated at 37 °C for 4 h. After the incubation cells were washed at 1000 rpm for 7 min and resuspended in 340 μ l of complete medium and equally distributed in 4 tubes (one for each condition CO, DG, DGO, O) to proceed with SCENITH protocol. All the reagents were prepared the day of the experiment, empty tubes and 20X inhibitors CO; DG; O; P (stored at -20 °C in aliquots) were equilibrated at 37 °C for 30 min before cell treatment. 5 μ l of each 20X inhibitor and 10 μ l of 20X puromycin were added to the corresponding tube and incubated at 37 °C for 40 min. In the DGO tube, DG and O were added simultaneously. After incubation, tubes with cells were filled up with ice cold MACS Buffer, centrifuged at 400 \times g during 5 min at 4 °C and the supernatant was discarded by aspirating. Cells were resuspended in 100 μ l of PromoFluor IR-840 (Promokine, PromoCell, Heidelberg, Germany) and Fc Block (Becton Dickinson) and incubated for 15 min, at 4 °C, in the dark. Without washing, 100 μ l of 2X surface staining mix including the previously titrated mAbs CD19-PE, CD69-FITC, were added to cells and samples were incubated for 25 min at 4 °C in the dark. Tubes were filled up with FACS buffer, centrifuged at 400 \times g, during 5 min, at 4 °C and the supernatant was discarded by aspirating. Red blood cells lysis was avoided. The following intracellular staining with Invitrogen FOXP3 stain buffer was performed: cells were resuspended in 100 μ l of Foxp3 Fixation/Permeabilization solution, vortexed and incubated for 20 min at RT in the dark. Then 1X Permeabilization Buffer was added to cells and samples were centrifuged at 600 \times g for 5 min at RT. The supernatant was discarded by aspiration and cells were resuspended in 50 μ l of intracellular block (1X Permeabilization Buffer + 20% FCS) and incubate for 10 min at RT. Without washing 50 μ l of anti-puromycin-AF647 antibody solution 1/250 were added to cells and cells were incubated for 1 h at 4 °C in the dark. At the end of incubation cells were washed with 1X Permeabilization Buffer and centrifuged at 600 \times g for 5 min at 4 °C. The supernatant was discarded, and stained cells were resuspended in 400 μ l of FACS Buffer and acquired by flow cytometer CytoFLEX LX (Beckman Coulter, Hiialeah, FL). A minimum of 1,500,000 cells per sample were acquired. All reagents used for the staining of cells are reported in Supplementary Table 4.

SCENITH assay performed on SARS-CoV-2-specific T cells. Freshly isolated PBMCs were incubated at a density of $1 \times 10^6/0.1$ ml in complete medium (RPMI 1640 supplemented with 10% FBS and 1% each of L-glutamine, sodium pyruvate, nonessential amino acids, antibiotics, 0.1 M HEPES, 55 mM β -mercaptoethanol) with CD40-blocking antibody (0.5 μ g/ml final concentration) (Miltenyi Biotec, Bergisch Gladbach, Germany) for 15 min at 37 °C before stimulation. Then, cells were stimulated by adding in the medium PepTivator SARS-CoV-2 Prot_S complete (Miltenyi Biotec, Bergisch Gladbach, Germany) containing 15-mer peptides with 11-amino acid overlap, covering the complete sequence of Wuhan SARS-CoV-2 spike glycoprotein, together with CD28/CD49d (Becton Dickinson) and incubated for 18 h at 37 °C in a 5% CO₂ atmosphere. At the end of stimulation, cells were washed at 1000 rpm for 7 min and resuspended in 340 μ l of complete medium and equally divided into 4 FACS tubes (one for each condition CO, DG, DGO, O) to perform the SCENITH protocol. All the reagents were prepared the day of the experiment, empty tubes and 20X inhibitors CO; DG; O; P (stored at -20 °C in aliquots) were equilibrated at 37 °C for 30 min before cell treatment. 5 μ l of each 20X inhibitor and 10 μ l of 20X puromycin were added to the corresponding tube and incubated at 37 °C for 40 min. In the DGO tube, DG and O were added simultaneously. After incubation, tubes with cells were filled up with ice cold

MACS Buffer, centrifuged at 400 \times g during 5 min at 4 °C and the supernatant was aspirated. Cells were resuspended in 100 μ l of PromoFluor IR-840 (Promokine, PromoCell, Heidelberg, Germany) and Fc Block (Becton Dickinson) and incubated for 15 min at 4 °C, in the dark. Without washing, 100 μ l of 2X surface staining mix including the previously titrated mAbs CD4-FITC, CD8-PE, CD3-PB, CD69-BV650, CD137-BUV395 were added to cells and samples were incubated for 25 min at 4 °C in the dark. Tubes were filled up with FACS buffer, centrifuged at 400 \times g, during 5 min, at 4 °C and the supernatant was discarded by aspirating. Red blood cells lysis was avoided, and the following intracellular staining with Invitrogen FOXP3 stain buffer was performed: cells were resuspended in 100 μ l of Foxp3 Fixation/Permeabilization solution, vortexed and incubated for 20 min at RT in the dark. Then 1X Permeabilization Buffer was added to cells and samples were centrifuged at 600 \times g for 5 min at RT. The supernatant was discarded by aspirating and cells were resuspended in 50 μ l of intracellular block (1X Permeabilization Buffer + 20% FCS) and incubated for 10 min at RT. Without any washing step, 50 μ l of anti-puromycin-AF647 antibody solution 1/250 was added to cells and followed by incubation for 1 h at 4 °C in the dark. Cells were washed with 1X Permeabilization Buffer and centrifuged at 600 g for 5 min at 4 °C. The supernatant was discarded, and stained cells were resuspended in 400 μ l of FACS Buffer and acquired by flow cytometer CytoFLEX LX (Beckman Coulter, Hiialeah, FL). A minimum of 1,500,000 cells per sample were acquired. All reagents used for the staining of cells are reported in Supplementary Table 4.

Statistical analysis. Quantitative variables were compared using Kruskal-Wallis non-parametric test corrected for multiple comparisons by controlling the False Discovery Rate (FDR), method of Benjamini and Hochberg. Statistically significant q-values are represented. Statistical analysis of cytokines production was performed using GraphPad Prism version 8 (GraphPad Software Inc., La Jolla, USA). Total percentage of antigen-specific (Ag⁺CD4⁺ and Ag⁺CD8⁺) T cell data have been calculated as background subtracted data. Simplified Presentation of Incredibly Complex Evaluation (SPICE) software (version 6, Vaccine Research Center, NIAID, NIH, Bethesda, MD, USA) was used to analyze flow cytometry data on T cell polyfunctionality. Data from the total cytokine production are represented as individual values, means, and standard errors of the mean. Regarding polyfunctionality, data in pie charts are represented as median values and statistical analysis was performed using permutation test; data in graphs are represented as individual values, means, and standard errors of the mean.

Principal component analysis. Principal Component Analysis (PCA) was executed and visualized in R using the `prcomp` function (`stats` v3.6.2) and the `pca3d` package v0.1. The data used included the proportions, absolute number and scMEP metabolic state of Ag⁺ CD19⁺ B cells, CD4⁺, CD8⁺ T cells along with clinical parameters (reported in Source Data File). Missing values of dataset were imputed using `missMDA` package v1.18. The total impact of a specific variable resulting by PC1 and PC2 was computed as $[(C1 * Eig1) + (C2 * Eig2)] / (Eig1 + Eig2)$, where C1 and C2 represent the contributions of the variable to PC1 and PC2, and Eig1 and Eig2 denote the eigenvalues of PC1 and PC2, respectively. The Euclidean distance of MS-treated groups to HD in PCA space was calculated using the `phenoptr` v.0.3.2 package.

PENCIL prediction analysis. PENCIL v0.7 was used to predict cell clusters associated with absence of breakthrough infection in MS patients and HD⁴¹. As single cell input data we used our 45-parameter mass cytometry data (scMEP data) analyzed previously with R by using CATALYST v1.18.1 (see method above). We imported into Seurat v4.9.9 58 the expression matrix, containing hyperbolic arcsinh (cofactor 5) transformed data, and the metadata (also UMAP coordinates) of Ag⁺ T

or B lymphocytes. Cells from all individuals were divided in two groups on the basis of SARS-CoV-2 breakthrough infection and were used as input to run PENCIL. For T cells prediction, to reduce the number of rejected cells due to huge differences in cell number from who experienced SARS-CoV-2 breakthrough infection (10,591 cells) and who did not (96,931 cells), a downsampled dataset was used (a total of 21,591, whose 11,000 for who experienced SARS-CoV-2 breakthrough infection; 10,591 for who did not get COVID-19). Prediction displayed 68% accuracy. Then 5650 was used for Ag⁺ B cells prediction (2825 for each group); a total of 1047 cells were rejected. The precision of the prediction was 76%.

Reporting summary

Further information on research design is available in the Nature Portfolio Reporting Summary linked to this article.

Data availability

All data generated or analysed in this study are included in this published article (and its supplementary information files). Further inquiries can be directed to the corresponding authors. Source data are provided with this paper.

References

- Tornatore, C. et al. Vaccine response in patients with multiple sclerosis receiving teriflunomide. *Front. Neurol.* **13**, 828616 (2022).
- De Biasi, S. et al. Marked T cell activation, senescence, exhaustion and skewing towards TH17 in patients with COVID-19 pneumonia. *Nat. Commun.* **11**, 3434 (2020).
- Cossarizza, A. et al. Handling and processing of blood specimens from patients with COVID-19 for safe studies on cell phenotype and cytokine storm. *Cytom. A* **97**, 668–673 (2020).
- Cossarizza, A., De Biasi, S., Guaraldi, G., Girardis, M. & Mussini, C. Modena Covid-19 Working G. SARS-CoV-2, the virus that causes COVID-19: cytometry and the new challenge for global health. *Cytom. A* **97**, 340–343 (2020).
- De Biasi, S. et al. Expansion of plasmablasts and loss of memory B cells in peripheral blood from COVID-19 patients with pneumonia. *Eur. J. Immunol.* **50**, 1283–1294 (2020).
- De Biasi, S. et al. Endogenous control of inflammation characterizes pregnant women with asymptomatic or paucisymptomatic SARS-CoV-2 infection. *Nat. Commun.* **12**, 4677 (2021).
- De Biasi, S. et al. Prognostic immune markers identifying patients with severe COVID-19 who respond to tocilizumab. *Front Immunol.* **14**, 1123807 (2023).
- Lo Tartaro, D. et al. Molecular and cellular immune features of aged patients with severe COVID-19 pneumonia. *Commun. Biol.* **5**, 590 (2022).
- Lo Tartaro, D. et al. Detailed characterization of SARS-CoV-2-specific T and B cells after infection or heterologous vaccination. *Front Immunol.* **14**, 1123724 (2023).
- Paolini, A. et al. Patients recovering from severe COVID-19 develop a polyfunctional antigen-specific CD4⁺ T cell response. *Int. J. Mol. Sci.* **23**, 8004 (2022).
- Gibellini, L. et al. Plasma cytokine atlas reveals the importance of TH2 polarization and interferons in predicting COVID-19 severity and survival. *Front Immunol.* **13**, 842150 (2022).
- Borella, R. et al. Metabolic reprogramming shapes neutrophil functions in severe COVID-19. *Eur. J. Immunol.* **52**, 484–502 (2022).
- Centonze, D. et al. Disease-modifying therapies and SARS-CoV-2 vaccination in multiple sclerosis: an expert consensus. *J. Neurol.* **268**, 3961–3968 (2021).
- Fox, R. J. et al. Characterizing absolute lymphocyte count profiles in dimethyl fumarate-treated patients with MS: patient management considerations. *Neurol. Clin. Pract.* **6**, 220–229 (2016).
- Bar-Or, A. et al. Teriflunomide effect on immune response to influenza vaccine in patients with multiple sclerosis. *Neurology* **81**, 552–558 (2013).
- Kaufman, M. et al. Natalizumab treatment shows no clinically meaningful effects on immunization responses in patients with relapsing-remitting multiple sclerosis. *J. Neurol. Sci.* **341**, 22–27 (2014).
- Olberg, H. K. et al. Immunotherapies influence the influenza vaccination response in multiple sclerosis patients: an explorative study. *Mult. Scler.* **20**, 1074–1080 (2014).
- Olberg, H. K. et al. Antibody response to seasonal influenza vaccination in patients with multiple sclerosis receiving immunomodulatory therapy. *Eur. J. Neurol.* **25**, 527–534 (2018).
- Kappos, L. et al. Onset of clinical and MRI efficacy occurs early after fingolimod treatment initiation in relapsing multiple sclerosis. *J. Neurol.* **263**, 354–360 (2016).
- Kelly, H., Sokola, B. & Abboud, H. Safety and efficacy of COVID-19 vaccines in multiple sclerosis patients. *J. Neuroimmunol.* **356**, 577599 (2021).
- Bar-Or, A., Herman, A. & Stokmaier, D. Author Response: Effect of ocrelizumab on vaccine responses in patients with multiple sclerosis: the VELOCE study. *Neurology* **96**, 870 (2021).
- Achiron, A. et al. COVID-19 vaccination in patients with multiple sclerosis: What we have learnt by February 2021. *Mult. Scler.* **27**, 864–870 (2021).
- Achiron, A. et al. Humoral immune response to COVID-19 mRNA vaccine in patients with multiple sclerosis treated with high-efficacy disease-modifying therapies. *Ther. Adv. Neurol. Disord.* **14**, 17562864211012835 (2021).
- Buttari, F. et al. COVID-19 vaccines in multiple sclerosis treated with cladribine or ocrelizumab. *Mult. Scler. Relat. Disord.* **52**, 102983 (2021).
- Gallo, A. et al. Preliminary evidence of blunted humoral response to SARS-CoV-2 mRNA vaccine in multiple sclerosis patients treated with ocrelizumab. *Neurol. Sci.* **42**, 3523–3526 (2021).
- Gadani, S. P. et al. Discordant humoral and T cell immune responses to SARS-CoV-2 vaccination in people with multiple sclerosis on anti-CD20 therapy. *EBioMedicine* **73**, 103636 (2021).
- Tortorella, C. et al. Humoral- and T-cell-specific immune responses to SARS-CoV-2 mRNA vaccination in patients with MS using different disease-modifying therapies. *Neurology* **98**, e541–e554 (2022).
- Zabalza, A. et al. Is humoral and cellular response to SARS-CoV-2 vaccine modified by DMT in patients with multiple sclerosis and other autoimmune diseases? *Mult. Scler.* **28**, 1138–1145 (2022).
- Kister, I. et al. Hybrid and vaccine-induced immunity against SARS-CoV-2 in MS patients on different disease-modifying therapies. *Ann. Clin. Transl. Neurol.* **9**, 1643–1659 (2022).
- Maniscalco, G. T. et al. Humoral efficacy of the third SARS-CoV-2 vaccine dose in Multiple Sclerosis subjects undergoing different disease-modifying therapies. *Mult. Scler. Relat. Disord.* **68**, 104371 (2022).
- Disanto, G., et al. Longitudinal postvaccine SARS-CoV-2 immunoglobulin G titers, memory B-cell responses, and risk of COVID-19 in multiple sclerosis over 1 year. *Neurol. Neuroimmunol. Neuroinflamm.* **10**, e200043 (2023).
- Achiron, A. et al. In-depth characterization of long-term humoral and cellular immune responses to COVID-19m-RNA vaccination in multiple sclerosis patients treated with teriflunomide or alemtuzumab. *Mult. Scler. Relat. Disord.* **72**, 104616 (2023).

33. Apostolidis, S. A. et al. Cellular and humoral immune responses following SARS-CoV-2 mRNA vaccination in patients with multiple sclerosis on anti-CD20 therapy. *Nat. Med* **27**, 1990–2001 (2021).
34. Dominelli, F. et al. Multiple sclerosis-disease modifying therapies affect humoral and T-cell response to mRNA COVID-19 vaccine. *Front Immunol.* **13**, 1050183 (2022).
35. De Biasi, S., Paolini, A., Lo Tartaro, D., Gibellini, L. & Cossarizza, A. Analysis of antigen-specific T and B cells for monitoring immune protection against SARS-CoV-2. *Curr. Protoc.* **3**, e636 (2023).
36. Hartmann, F. J. et al. Single-cell metabolic profiling of human cytotoxic T cells. *Nat. Biotechnol.* **39**, 186–197 (2021).
37. De Biasi, S. et al. Mitochondrial functionality and metabolism in T cells from progressive multiple sclerosis patients. *Eur. J. Immunol.* **49**, 2204–2221 (2019).
38. Vinay, D. S. & Kwon, B. S. CD11c+CD8+ T cells: two-faced adaptive immune regulators. *Cell Immunol.* **264**, 18–22 (2010).
39. Arguello, R. J. et al. SCENITH: a flow cytometry-based method to functionally profile energy metabolism with single-cell resolution. *Cell Metab.* **32**, 1063–1075 e1067 (2020).
40. Caro-Maldonado, A. et al. Metabolic reprogramming is required for antibody production that is suppressed in anergic but exaggerated in chronically BAFF-exposed B cells. *J. Immunol.* **192**, 3626–3636 (2014).
41. Ren, T. et al. Supervised learning of high-confidence phenotypic subpopulations from single-cell data. *Nat. Mach. Intell.* **5**, 528–541 (2023).
42. Cottrell, D. A. & Turnbull, D. M. Mitochondria and ageing. *Curr. Opin. Clin. Nutr. Metab. Care* **3**, 473–478 (2000).
43. Sgarbi, G. et al. Mitochondria hyperfusion and elevated autophagic activity are key mechanisms for cellular bioenergetic preservation in centenarians. *Aging (Albany NY)* **6**, 296–310 (2014).
44. Dema, M., Eixarch, H., Villar, L. M., Montalban, X. & Espejo, C. Immunosenescence in multiple sclerosis: the identification of new therapeutic targets. *Autoimmun. Rev.* **20**, 102893 (2021).
45. Mills, E. A. & Mao-Draayer, Y. Aging and lymphocyte changes by immunomodulatory therapies impact PML risk in multiple sclerosis patients. *Mult. Scler.* **24**, 1014–1022 (2018).
46. Wack, A. et al. Age-related modifications of the human alphabeta T cell repertoire due to different clonal expansions in the CD4+ and CD8+ subsets. *Int Immunol.* **10**, 1281–1288 (1998).
47. Cossarizza, A. et al. Highly active antiretroviral therapy restores CD4+ Vbeta T-cell repertoire in patients with primary acute HIV infection but not in treatment-naive HIV+ patients with severe chronic infection. *J. Acquir Immune Defic. Syndr.* **35**, 213–222 (2004).
48. Frasca, D., Diaz, A., Romero, M., Garcia, D. & Blomberg, B. B. B Cell Immunosenescence. *Annu Rev. Cell Dev. Biol.* **36**, 551–574 (2020).
49. Han, S., Georgiev, P., Ringel, A. E., Sharpe, A. H. & Haigis, M. C. Age-associated remodeling of T cell immunity and metabolism. *Cell Metab.* **35**, 36–55 (2023).
50. Van de Griend, R. J. et al. Changes in human T lymphocytes after thymectomy and during senescence. *J. Clin. Immunol.* **2**, 289–295 (1982).
51. Sica, F., Centonze, D. & Buttari, F. Fingolimod immune effects beyond its sequestration ability. *Neurol. Ther.* **8**, 231–240 (2019).
52. Cuculiza Henriksen, A. et al. Natalizumab differentially affects plasmablasts and B cells in multiple sclerosis. *Mult. Scler. Relat. Disord.* **52**, 102987 (2021).
53. Zucchetto, A. et al. The CD49d/CD29 complex is physically and functionally associated with CD38 in B-cell chronic lymphocytic leukemia cells. *Leukemia* **26**, 1301–1312 (2012).
54. Michalek, R. D. et al. Cutting edge: distinct glycolytic and lipid oxidative metabolic programs are essential for effector and regulatory CD4+ T cell subsets. *J. Immunol.* **186**, 3299–3303 (2011).
55. Nakaya, H. I. et al. Systems biology of vaccination for seasonal influenza in humans. *Nat. Immunol.* **12**, 786–795 (2011).
56. Bucacas, K. L. et al. Early patterns of gene expression correlate with the humoral immune response to influenza vaccination in humans. *J. Infect. Dis.* **203**, 921–929 (2011).
57. Tran, T. M. et al. A molecular signature in blood reveals a role for p53 in regulating malaria-induced inflammation. *Immunity* **51**, 750–765 e710 (2019).
58. Hao, Y. et al. Integrated analysis of multimodal single-cell data. *Cell* **184**, 3573–3587 e3529 (2021).

Acknowledgements

This work was supported by grants from: Fondazione Italiana Sclerosi Multipla (FISM) to A.C., project “Unraveling the role and functionality of T cells in treated multiple sclerosis SARS-CoV-2 vaccinated patients,” protocol no. 2021/C19-R-Single/O11; Bando MIUR “Dipartimenti di Eccellenza 2023/2027”, Area CUN_06 Scienze Mediche, to A.C.; S.D.B. and L.Gi are Marylou Ingram Scholar of the International Society for Advancement of Cytometry (ISAC) for the period 2015–2020 and 2020–2025, respectively. Drs. Paola Paglia (ThermoFisher Scientific, Monza, Italy), Leonardo Beretta (Beckman Coulter, Milan, Italy), Dr. Paolo Santino, Ernesto Lopez, Gloria Martrus (Standard Biotech, San Francisco, CA, US), Dr. Marco Mattioli, Dr. Andrea De Fanti and Dr. Alessia Di Nella are acknowledged for their support in providing reagents and materials, for precious help and technical suggestions. Finally, we gratefully acknowledge the individuals who donated blood to participate in this study.

Author contributions

A.N., R.B., N.P., A.P., E.S., A.L.C. and T.T. performed experiments; M.Cu, T.T. quantified plasmatic antibodies; D.L.T., M.R. performed bioinformatic analysis; D.F., F.V., M.Ca enrolled the patients; L.G., R.J.A., I.R., A.C. discussed the data; S.D.B. and A.C. supervised experiments, bioinformatic analysis, and wrote the manuscript; A.C. and D.F. corrected and revised the manuscript.

Competing interests

There are restrictions to the commercial use of SCENITH due to a pending patent application by R.J.A. (PCT/EP2020/060486). A.N., R.B., N.P., A.P., E.S., M.Cu, A.L.C., M.C., T.T., D.L.T., M.R., D.F., F.V., M.Ca, L.G., I.R., A.C., S.D.B., D.F. declare that the research was conducted in the absence of any commercial or financial relationships that could be construed as a potential conflict of interest.

Additional information

Supplementary information The online version contains supplementary material available at <https://doi.org/10.1038/s41467-024-47013-0>.

Correspondence and requests for materials should be addressed to Sara De Biasi or Andrea Cossarizza.

Peer review information *Nature Communications* thanks the anonymous reviewer(s) for their contribution to the peer review of this work. A peer review file is available.

Reprints and permissions information is available at <http://www.nature.com/reprints>

Publisher's note Springer Nature remains neutral with regard to jurisdictional claims in published maps and institutional affiliations.

Open Access This article is licensed under a Creative Commons Attribution 4.0 International License, which permits use, sharing, adaptation, distribution and reproduction in any medium or format, as long as you give appropriate credit to the original author(s) and the source, provide a link to the Creative Commons licence, and indicate if changes were made. The images or other third party material in this article are included in the article's Creative Commons licence, unless indicated otherwise in a credit line to the material. If material is not included in the article's Creative Commons licence and your intended use is not permitted by statutory regulation or exceeds the permitted use, you will need to obtain permission directly from the copyright holder. To view a copy of this licence, visit <http://creativecommons.org/licenses/by/4.0/>.

© The Author(s) 2024